NATIONAL TECHNICAL UNIVERSITY OF ATHENS

SCHOOL OF APPLIED MATHEMATICAL

AND PHYSICAL SCIENCES

Triage Biodosimetry and Mechanistic Insights into Chromosomal Aberration Formation and Chromothripsis for Risk Assessment following Exposure to Radiation of Different Qualities

Thesis submitted for the degree of Doctor of Philosophy

Antonio Pantelias

ATHENS 2022

ΕΘΝΙΚΟ ΜΕΤΣΟΒΙΟ ΠΟΛΥΤΕΧΝΕΙΟ

ΣΧΟΛΗ ΕΦΑΡΜΟΣΜΕΝΩΝ ΜΑΘΗΜΑΤΙΚΩΝ

ΚΑΙ ΦΥΣΙΚΩΝ ΕΠΙΣΤΗΜΩΝ

Βιοδοσιμετρία και Διερεύνηση Μηχανισμών Επαγωγής Χρωμοσωμικών Αλλοιώσεων και Χρωμοθρύψης για Εκτίμηση Επικινδυνότητας μετά από Έκθεση σε Ακτινοβολίες Διαφορετικών Ποιοτήτων

ΔΙΔΑΚΤΟΡΙΚΗ ΔΙΑΤΡΙΒΗ

ΑΝΤΩΝΙΟΣ ΠΑΝΤΕΛΙΑΣ

ΑΘΗΝΑ 2022

ADVISORY COMMITTEE

Alexandros Georgakilas, Professor,
National Technical University of Athens

Georgia Terzoudi, Director of Research,
NCSR "Demokritos"

Marios Anagnostakis, Professor,
National Technical University of Athens

EXAMINATION COMMITTEE

Alexandros Georgakilas, Professor,
National Technical University of Athens

Georgia Terzoudi, Director of Research,
NCSR "Demokritos"

Marios Anagnostakis, Professor,
National Technical University of Athens

Michael Kokkoris, Professor,
National Technical University of Athens

Maria Paravatou, Director of Research,
NCSR "Demokritos"

Maria Diakaki, Assistant Professor,
National Technical University of Athens

Dimitris Emfietzoglou, Professor,
University of Ioannina

ΤΡΙΜΕΛΗΣ ΣΥΜΒΟΥΛΕΥΤΙΚΗ ΕΠΙΤΡΟΠΗ

Αλέξανδρος Γεωργακίλας, Καθηγητής,
Εθνικό Μετσόβιο Πολυτεχνείο

Γεωργία Τερζούδη, Ερευνήτρια Α',
ΕΚΕΦΕ «Δημόκριτος»

Μάριος Αναγνωστάκης, Καθηγητής,
Εθνικό Μετσόβιο Πολυτεχνείο

ΕΠΤΑΜΕΛΗΣ ΕΞΕΤΑΣΤΙΚΗ ΕΠΙΤΡΟΠΗ

Αλέξανδρος Γεωργακίλας, Καθηγητής,
Εθνικό Μετσόβιο Πολυτεχνείο

Γεωργία Τερζούδη, Ερευνήτρια Α',
ΕΚΕΦΕ «Δημόκριτος»

Μάριος Αναγνωστάκης, Καθηγητής,
Εθνικό Μετσόβιο Πολυτεχνείο

Μιχάλης Κόκκορης, Καθηγητής,
Εθνικό Μετσόβιο Πολυτεχνείο

Μαρία Παραβατού, Ερευνήτρια Α',
ΕΚΕΦΕ «Δημόκριτος»

Μαρία Διακάκη, Επίκουρη Καθηγήτρια,
Εθνικό Μετσόβιο Πολυτεχνείο

Δημήτρης Εμφιετζόγλου, Καθηγητής,
Πανεπιστήμιο Ιωαννίνων

Acknowledgements

I would like to thank my supervisors, Professor Alexandros Georgakilas and Dr Georgia Terzoudi, as well as the member of my Advisory Committee, Professor Marios Anagnostakis, for their guidance, encouragement and constant support. The research presented in this doctoral thesis was conducted in the framework of a collaboration between the Laboratory of Health Physics, Radiobiology & Cytogenetics at the National Centre for Scientific Research "Demokritos", and the DNA Damage Laboratory at the National Technical University of Athens. I would like, therefore, to thank all the scientific and technical staff for their kind assistance.

Moreover, I would like to acknowledge the productive collaboration with Dr Adayabalam Balajee and Dr Terri Ryan from the Cytogenetic Biodosimetry Laboratory, Oak Ridge Institute for Science and Education, USA, regarding the research work presented in Chapter 3 of this doctoral thesis. Similarly, I would like to thank Dr Demetre Zafiropoulos and Dr Roberto Cherubini for the assistance and beam time they offered us at the Italian Institute of Nuclear Physics (INFN), regarding the high-LET irradiation experiments described in Chapter 5.

Finally, I would like to express my gratitude to my family and friends for their patience and understanding. Dedicating this doctoral thesis to them is an understatement of their invaluable generosity.

Funding: This research work was supported by the Hellenic Foundation for Research and Innovation (H.F.R.I.) under the "2nd H.F.R.I. PhD Fellowship Grant" (Application: 1193; Fellowship: 469271; Contract: 61505500).

Χρηματοδότηση: Η ερευνητική εργασία υποστηρίχτηκε από το Ελληνικό Ίδρυμα Έρευνας και Καινοτομίας (ΕΛ.ΙΔ.Ε.Κ.) στο πλαίσιο της Δράσης «2η Προκήρυξη Υποτροφιών ΕΛ.ΙΔ.Ε.Κ. για Υποψήφιους Διδάκτορες» (Αίτηση: 1193; Υποτροφία 469271; Σύμβαση: 61505500).

ΕΛ.ΙΔ.Ε.Κ.
Ελληνικό Ίδρυμα Έρευνας & Καινοτομίας

Abstract

Human exposure to ionizing radiation, due to its extensive use in medical and industrial applications, may result in diverse biological effects depending on the radiation quality, absorbed dose and dose rate. In addition, accidental radiological exposure in the event of a major incident or act of nuclear terrorism can cause serious health effects to hundreds or thousands of people. Consequently, for mass-casualty medical management, there is a critical need for the development of suitable biomarkers of exposure that could enable high-throughput biodosimetry, in order to obtain individualized dose estimates. Moreover, the evaluation of the associated health consequences of an exposure could be greatly facilitated by the elucidation of the mechanisms underlying the biological action of different radiation qualities, as well as the genetic predisposition to radiation-induced adverse effects.

In the present doctoral thesis, all the above issues have been thoroughly examined. The research efforts have been focused on the prompt estimation of individualized absorbed dose, using cytogenetic endpoints, and on the assessment of the associated health risk based on the understanding of the mechanisms underlying genomic instability, following exposure to radiation of different qualities. Specifically, among the biomarkers of radiation exposure, we selected chromosome aberrations in peripheral blood lymphocytes that can be visualized and analyzed by means of the cell-fusion-mediated premature chromosome condensation (PCC). Improving on this assay, we have developed the rapid and minimally invasive micro-PCC assay that has the potential to automate absorbed dose estimation in large-scale radiological emergencies, since it requires only 100μl of blood and can be performed in 96-well plates. Furthermore, we have explored the advantages of applying DNA probes and the multicolor fluorescence in situ hybridization (mFISH) technique to prematurely condensed chromosomes, for the analysis of chromosomal rearrangements and the identification of predictive biomarkers for early and late health effects.

Additionally, emphasis has been given to the elucidation of the mechanisms underlying the formation of chromosome aberrations by different radiation qualities and the phenomenon of chromothripsis, which has been proposed as an alternative mutational process driving carcinogenesis. Using cytogenetic endpoints, we have provided, for the first time, experimental evidence for the induction of PCC in micronuclei as the mechanistic origin of chromothripsis. Moreover, we have demonstrated, for the first time, that high linear energy transfer (LET) radiation can induce localized chromosome shattering, which we have proposed as a fingerprint of exposure to high-LET radiation. This observation is considered of great significance, since localized chromosome shattering may lead to chromothripsis, resulting in chromosomal and genomic instability, and potentially carcinogenesis.

Finally, for the individualized assessment of intrinsic radiosensitivity, we have developed an enhanced G2-assay, which is expected to contribute substantially to radiation protection, personalized radiotherapy, as well as to the safety of personnel related to space exploration.

Keywords: premature chromosome condensation (PCC); PCC assay; micro-PCC assay; high-throughput biodosimetry; micronuclei; chromothripsis; chromosomal instability; RO-3306; high-LET radiation; protons; α-particles; C-ions; chromatin dynamics; localized chromosome shattering; chromothripsis-like chromosomal rearrangements; RBE values; fingerprint of exposure; radiation oncology; space exploration; individualized radiosensitivity.

Περίληψη

Η έκθεση του ανθρώπου στην ιοντίζουσα ακτινοβολία, λόγω της ευρείας χρήσης της σε ιατρικές και βιομηχανικές εφαρμογές, μπορεί να οδηγήσει σε ποικίλες βιολογικές επιπτώσεις ανάλογα με την ποιότητα της ακτινοβολίας, την απορροφούμενη δόση και τον ρυθμό δόσης. Επιπλέον, η έκθεση σε ακτινοβολία σε περίπτωση μεγάλου ατυχήματος ή πυρηνικής τρομοκρατικής ενέργειας μπορεί να προκαλέσει σοβαρές επιπτώσεις στην υγεία εκατοντάδων ή ακόμη και χιλιάδων ανθρώπων. Συνεπώς, για την διαχείριση ατυχημάτων μεγάλης κλίμακας, κρίνεται αναγκαία η ανάπτυξη κατάλληλων βιοδεικτών έκθεσης που θα μπορούσαν να επιτρέψουν τη βιοδοσιμετρία υψηλής απόδοσης, προκειμένου να ληφθούν εξατομικευμένες εκτιμήσεις δόσης. Επιπλέον, η αξιολόγηση των σχετικών επιπτώσεων μιας έκθεσης στην υγεία θα μπορούσε να διευκολυνθεί σημαντικά από την αποσαφήνιση των μηχανισμών που διέπουν τη βιολογική δράση ακτινοβολιών διαφορετικών ποιοτήτων, καθώς και τη γενετική προδιάθεση για δυσμενείς επιπτώσεις που προκαλούνται από την ακτινοβολία.

Στην παρούσα διδακτορική διατριβή έχουν εξεταστεί διεξοδικά όλα τα παραπάνω θέματα. Οι ερευνητικές προσπάθειες επικεντρώθηκαν στην έγκαιρη εκτίμηση της εξατομικευμένης απορροφούμενης δόσης, χρησιμοποιώντας κυτταρογενετικούς βιοδείκτες, και στην αξιολόγηση του σχετικού κινδύνου για την υγεία με βάση την κατανόηση των μηχανισμών που διέπουν τη γονιδιωματική αστάθεια, μετά από έκθεση σε ακτινοβολίες διαφορετικών ποιοτήτων. Συγκεκριμένα, μεταξύ των βιοδεικτών έκθεσης σε ακτινοβολία, επιλέξαμε τις χρωμοσωμικές ανωμαλίες στα λεμφοκύτταρα του περιφερικού αίματος οι οποίες μπορούν να απεικονιστούν και να αναλυθούν μέσω της πρόωρης χρωμοσωμικής συμπύκνωσης (PCC) που πραγματοποιείται με κυτταρικές συντήξεις. Βελτιώνοντας τη μέθοδο αυτή, αναπτύξαμε την ταχεία και ελάχιστα επεμβατική μέθοδο micro-PCC που έχει τη δυνατότητα να αυτοματοποιήσει την εκτίμηση απορροφούμενης δόσης σε μεγάλης κλίμακας ραδιολογικές καταστάσεις έκτακτης ανάγκης, καθώς απαιτεί μόνο 100 μl αίματος και μπορεί να εκτελεστεί σε τρυβλία 96 κοιλοτήτων. Επιπλέον, διερευνήσαμε τα πλεονεκτήματα της εφαρμογής ανιχνευτών DNA και της τεχνικής πολύχρωμου in situ υβριδισμού φθορισμού (mFISH) σε πρόωρα συμπυκνωμένα χρωμοσώματα, για την ανάλυση των χρωμοσωμικών αναδιατάξεων και τη διερεύνηση προγνωστικών βιοδεικτών για άμεσες και απώτερες επιπτώσεις στην υγεία.

Επιπρόσθετα, ιδιαίτερη έμφαση δόθηκε στη διαλεύκανση των μηχανισμών που διέπουν τον σχηματισμό χρωμοσωμικών ανωμαλιών από ακτινοβολίες διαφορετικών ποιοτήτων και το φαινόμενο της χρωμοθρύψης, το οποίο έχει προταθεί ως εναλλακτική οδός γονιδιωματικής αστάθειας και καρκινογένεσης. Χρησιμοποιώντας κυτταρογενετικούς βιοδείκτες, παρουσιάσαμε, για πρώτη φορά, πειραματικά δεδομένα για την επαγωγή PCC σε μικροπυρήνες ως τη μηχανιστική προέλευση της χρωμοθρύψης. Επιπλέον, τεκμηριώσαμε, για πρώτη φορά, πως η ακτινοβολία υψηλής γραμμικής μεταφοράς ενέργειας (high-LET) μπορεί να προκαλέσει τοπικό θρυμματισμό χρωμοσωμάτων, τον οποίο προτείναμε ως δακτυλικό αποτύπωμα έκθεσης σε ακτινοβολία high-LET. Αυτή η παρατήρηση είναι ιδιαίτερα σημαντική, καθώς ο τοπικός θρυμματισμός χρωμοσωμάτων μπορεί να οδηγήσει σε χρωμοθρύψη, με αποτέλεσμα την χρωμοσωμική και γονιδιωματική αστάθεια, και δυνητικά την καρκινογένεση.

Τέλος, για την εξατομικευμένη αξιολόγηση της εγγενούς ακτινοευαισθησίας, αναπτύξαμε μια ενισχυμένη χρωμοσωμική μέθοδο G2 (enhanced G2-assay) η οποία αναμένεται να συμβάλει ουσιαστικά στην ακτινοπροστασία, στην εξατομικευμένη ακτινοθεραπεία, καθώς και στην ασφάλεια του προσωπικού που σχετίζεται με την εξερεύνηση του διαστήματος.

Table of Contents

Doctoral Thesis Outline and Structure

Human beings and living organisms are continuously being exposed to ionizing radiation from cosmic rays, terrestrial radiation and naturally occurring radon. In addition, human exposure to radiation occurs because of its extensive use in medical and industrial applications. Although radiation can have potential health effects, it is at present a powerful tool in medical diagnostics and is the preferred treatment modality for most human cancers. Furthermore, occupational and accidental radiological or nuclear exposure can cause serious health issues and, in the event of a major incident or act of nuclear terrorism, hundreds or thousands of people may potentially get exposed to radiation. Particularly, the incidents of Chernobyl and Fukushima showed that the first responders to these radiation emergencies sustained high levels of radiation exposure. This clearly illustrates a critical need for the development of suitable automatable biomarkers of exposure for individualized radiation dose estimates, which are a prerequisite for risk assessments based on epidemiological studies of cancer incidence. Moreover, it reinforces the necessity for the elucidation of the mechanisms underlying the biological action of different radiation qualities, and the development of predictive assays for health risk assessment based on the genetic predisposition to radiation-induced early and late effects. Indeed, the individualized response to radiation is increasingly documented, yet the underlying mechanisms are not clearly understood. Consequently, for mass-casualty management in radiation accidents and large-scale radiological emergencies, improved research strategies, adopted for individualized absorbed dose estimates and risk assessments, are critically needed. Specifically, biological dosimetry measurements, based on biomarkers, and the mechanistic insights of the interaction of an exposure with living organisms, can be useful not only for appropriate medical/clinical management, but also for predicting the stochastic effects of exposure to ionizing radiation, such as genomic instability and cancer. Such undesirable effects of radiation depend on radiation quality defined by linear energy transfer (LET), dose, and dose rate. High-LET radiation, such as neutrons and α-particles, produce far more severe biological effects than γ-rays and X-rays, which are low-LET electromagnetic radiation, and epidemiological studies, based on the cancer incidence observed among the A-bomb survivors, have identified radiation-induced cancer risks at doses above 50 mSv.

At present, it is well established that exposure to ionizing radiation results in a variety of biological effects that depend on the nature and quality of radiation, exposure duration, dose, and dose rate. However, although biodosimeters can help in absorbed radiation dose estimation, there is still a big gap in our knowledge regarding prediction of health risks from estimated doses following exposure to different radiation qualities. Therefore, a thorough understanding of the mechanisms underlying the radiation-induced biological effects may help in predicting not only the short- but also the long-term effects of radiation exposure. Among the different biomarkers used for biodosimetry, we considered that chromosomal aberrations in peripheral blood lymphocytes (PBL), and particularly those that can be visualized and analyzed by means of cell-fusion-mediated premature chromosome condensation (PCC) in G_0-lymphocytes, are advantageous as biological dosimeters. This is because the lymphocytes are non-cycling cells, live long and thus have "memory", circulate throughout the body, and are continuously exchanged with lymphocytes in tissue. This means that lymphocytes with chromosome aberrations that have been induced anywhere in the body will eventually be present in the peripheral blood. In addition, radiation-induced chromosomal aberrations can be predictive of processes leading to the development of cancer, and all the evidence concerning their prognostic role in carcinogenesis also applies to the target tissue, on the understanding that the extent of genetic damage observed in blood lymphocytes may reflect as well similar events in cells of the target tissue. This indicates that chromosomal aberrations are not only significant biomarkers of radiation effects, but also are essential for predicting health risk. Indeed, the hypothesis that chromosomal aberrations are associated with cancer and can possibly act as an intermediate step of the causal pathway is supported by many reports. Evidence can be summarized in four major arguments: (1) chromosome rearrangements play an important role in the activation of protooncogenes and inactivation of tumour suppressor genes; (2) subjects with a congenital disease,

such as Fanconi's anemia or Ataxia Telangiectasia (AT), are characterized by abnormally high chromosomal aberration rates and increased incidence of malignancies; (3) alterations of the karyotype have been found in all types of neoplastic cells and are often highly specific for particular diagnostic categories; (4) there is a tendency for carcinogenic chemicals to be clastogenic and that clastogenicity tends to be associated with known human carcinogens.

In the present doctoral thesis, all the above issues, and particularly the processes underlying DNA damage induction and repair, gene mutations, as well as the mechanisms of radiation-induced chromosomal aberrations, chromothripsis and genomic instability, have been thoroughly examined and used for biodosimetry and risk assessment purposes. Emphasis has been given to the potential biomarkers of exposure to different radiation qualities and to the elucidation of the mechanisms underlying the formation of chromosome aberrations and the phenomenon of chromothripsis, which may be the biological basis for the induction of chromosomal instability and carcinogenesis, particularly by high-LET radiation. Using cytogenetic endpoints, we have provided, for the first time, experimental evidence for the mechanistic origin of chromothripsis, and we have clearly demonstrated that high-LET radiation can induce localized chromosome shattering, which is a critical risk for chromothripsis to occur. Rather than by a stepwise accumulation of subsequent genetic alterations that may cause genomic instability, chromothripsis is a mutational process in which large stretches of chromosomes undergo massive but localized shattering and random rearrangements in response to a one-step catastrophic event. Furthermore, we have developed an automatable biodosimetry assay for absorbed dose estimates in large-scale radiological emergencies, predictive biomarkers for early and late health effects, as well as for the evaluation of inherent individualized radiosensitivity using an enhanced G2-assay.

Specifically, this doctoral thesis aims to address the following five key research questions:

1. How can the throughput of the micro-PCC assay we have developed be increased by automating acquisition and analysis of images of lymphocyte prematurely condensed chromosomes (PCC) spreads?

2. What chromosomal rearrangements visualized directly in unstimulated blood lymphocytes by means of the mFISH technique have a potential for risk assessment as predictive biomarkers of exposure for early and late health effects?

3. What are the mechanisms underlying the phenomenon of chromothripsis, whose discovery challenges the long-standing concept of carcinogenesis as the result of progressive genetic events?

4. How can high-LET radiation induce localized chromosome shattering, which is a critical risk for chromothripsis to occur and may underlie their increased effectiveness?

5. How can an enhanced G2-assay be developed for intrinsic individualized radiosensitivity testing and risk assessment in radiation protection, personalized radiotherapy, and space exploration?

Doctoral Thesis Structure

The present doctoral thesis is structured in seven Chapters and two Appendices. Following the General Background, the five core Chapters describe the research conducted in order to provide answers to the key research questions stated above and present the achievements attained. The Epilogue summarizes the key outcomes, provides the overviews of the core Chapters and the future

research directions, while the Appendices provide this same information, and the thesis outline and structure in Greek.

More specifically,

Chapter 1 introduces important concepts in radiation physics, radiation biology and radiation cytogenetics. Also, it describes at the DNA, chromosome, and cell level the main biological endpoints and biomarkers currently available for the detection and quantification of the impact of an exposure to ionizing radiation of different qualities. Emphasis is given to the premature chromosome condensation (PCC) method, as a powerful and unique cytogenetic tool to study conversion of radiation-induced DNA lesions into chromosomal aberrations directly in interphase cells.

Chapter 2 describes the micro-PCC assay that we have developed, as well as the research aiming to investigate how the throughput of this assay can be increased by automating the acquisition of images of lymphocyte prematurely condensed chromosomes (PCC) spreads. In radiation accidents and large-scale radiological emergencies, a fast and reliable triage of individuals, according to their degree of exposure, is important for accident management and identification of those who need medical assistance. The micro-PCC assay is a suitable candidate for high-throughput biodosimetry since we have shown that it requires blood volumes of only 100μl and can be performed in 96-well plates. Towards the automation of the micro-PCC assay, we explored the potential of the Metafer slide scanning platform by MetaSystems to enable the automated acquisition of images, as well as automated analysis based on residual PCC fragments following an accidental exposure.

Chapter 3 describes research aiming to explore potential novel biomarkers for biodosimetry purposes and risk assessment, in the case of radiological or nuclear mass-casualty scenarios. Realizing the advantage of the PCC-assay that can be instantaneously applied to unstimulated lymphocytes, the analysis is based on chromosomal rearrangements visualized directly in PCC spreads, through the application of mFISH and mBAND techniques. Our study clearly demonstrates that these techniques, coupled with the PCC-assay, can efficiently detect both numerical and structural chromosome aberrations at the intra- and inter-chromosomal levels in unstimulated T- and B-lymphocytes. Unstable chromosome aberrations (chromosome fragments and dicentric chromosomes) can be used for early radiation dose estimation, while stable chromosome exchange events (translocations) may help the retrospective monitoring of individualized health risks.

Chapter 4 describes a research study aiming to provide insights into the mechanisms underlying the phenomenon of chromothripsis, whose discovery in cancer genomes challenges the long-standing concept of carcinogenesis as the result of progressive genetic events. Chromothripsis is a mutational process in which large stretches of chromosomes undergo massive but localized shattering and random rearrangements, in response to a one-step catastrophic event. The prevailing conception is that it arises from a massive accumulation of fragmented DNA inside micronuclei (MN), whose defective nuclear envelope ruptures or leads to aberrant DNA replication, before the main nuclei enter mitosis. Using cytogenetic endpoints, we provide, for the first time, experimental evidence supporting an alternative hypothesis. Premature chromosome condensation (PCC) dynamics in asynchronous micronucleated cells underlie the mechanistic origin of chromothripsis. As the main nuclei enter mitosis, premature chromosome condensation provokes the shattering of chromosomes entrapped inside MN in a single catastrophic event, the hallmark of chromothripsis.

Chapter 5 describes a research study aiming to provide insights into the mechanisms underlying the enhanced biological effectiveness of high-LET radiation such as α-particles, accelerated protons and C-ions, as compared to γ-rays. In contrast to the sparse deposition of low-density energy by X- or γ-rays, particle irradiation causes focal DNA damage through high-density energy deposition along the particle tracks. This is characterized by the formation of multiple damage sites, comprising

localized clustered patterns of DNA single- and double-strand breaks as well as base damage, which are considered key determinants of the enhanced relative biological effectiveness (RBE) of energetic nuclei. In this study, we provide for the first time, experimental evidence that such clustered DNA damage can be converted into localized shattering of targeted chromosome domains in a single catastrophic event, which is a critical risk for chromothripsis to occur. Our results highlight the potential use of shattered chromosome domains as a fingerprint of high-LET exposure. Furthermore, they support the new model we propose for the mechanistic origin of chromothripsis-like rearrangements that can be observed following exposure to high-LET radiation.

Chapter 6 describes research towards the development of an enhanced G2-chromosomal radiosensitivity assay for inherent individualized radiosensitivity testing and risk assessment. While the individualized response to radiation is increasingly documented, the underlying mechanisms for the predisposition to radiation-induced early and late effects are not yet clearly understood. The Ataxia Telangiectasia (AT) patients, who have a defective G2/M checkpoint, have been shown to be highly radiosensitive. ATM, ATR, and Chk1 kinases facilitate cell cycle arrest (G2-block) protecting against the conversion of DNA lesions into chromatid breaks during G2/M phase transition. We propose here an enhanced G2-assay for estimating individualized radiosensitivity as a percentage of AT- radiosensitivity (100% radiosensitive). Specifically, we are using the ATR inhibitor VE 821 to abrogate the G2 checkpoint to better approximate the AT response. Moreover, we make use of the CDK1 inhibitor RO-3306 for the enrichment of G2-phase cells before irradiation. This robust cytogenetic assay is very promising for testing inherent individualized radiosensitivity that is of great importance for radiation protection, personalized radiotherapy, and space exploration.

List of Publications

Articles in peer-reviewed journals where part of the research work described in this doctoral thesis has been published.

1. **Pantelias, A.**, Zafiropoulos, D., ..., Georgakilas, A. G., & Terzoudi, G. I. (2020). Interphase cytogenetic analysis of G0 lymphocytes exposed to α-particles, C-ions, and protons reveals their enhanced effectiveness for localized chromosome shattering—a critical risk for chromothripsis. *Cancers*, 12(9), 2336.
2. **Pantelias, A.**, Karachristou, I., Georgakilas, A. G., & Terzoudi, G. I. (2019). Interphase cytogenetic analysis of micronucleated and multinucleated cells supports the premature chromosome condensation hypothesis as the mechanistic origin of chromothripsis. *Cancers*, *11*(8), 1123.
3. Ryan, T. L., **Pantelias, A**., Terzoudi, G. I., …, & Balajee, A. S. (2019). Use of human lymphocyte G0 PCCs to detect intra-and inter-chromosomal aberrations for early radiation biodosimetry and retrospective assessment of radiation-induced effects. *PLoS ONE*, 14(5).
4. **Pantelias, A.**, & Terzoudi, G. I. (2018). Development of an automatable micro-PCC biodosimetry assay for rapid individualized risk assessment in large-scale radiological emergencies. *Mutation Research/Genetic Toxicology and Environmental Mutagenesis*, *836*, 65-71.

Additional publications in peer-reviewed journals contributed to by the author.

5. Terzoudi, G. I., …, **Pantelias, A.**, …, Zafiropoulos, D., & Wojcik, A. (2017). Dose assessment intercomparisons within the RENEB network using G0-lymphocyte prematurely condensed chromosomes. International journal of radiation biology, 93(1), 48-57.
6. Karachristou, I., Karakosta, M., **Pantelias, A.**, ..., & Terzoudi, G. I. (2016). Biodosimetry for high-dose exposures based on dicentric analysis in lymphocytes released from the G2-block by caffeine. *Radiation protection dosimetry*, 172(1-3), 230-237.
7. Karachristou, I., Karakosta, M., **Pantelias, A.**, ..., & Terzoudi, G. I. (2015). Triage biodosimetry using centromeric/telomeric PNA probes and Giemsa staining to score dicentrics or excess fragments in non-stimulated lymphocyte prematurely condensed chromosomes. *Mutation Research/Genetic Toxicology and Environmental Mutagenesis*, 793, 107-114.
8. Terzoudi, G. I., Karakosta, M., **Pantelias, A.**, Hatzi, V. I., et al. (2015). Stress induced by premature chromatin condensation triggers chromosome shattering and chromothripsis at DNA sites still replicating in micronuclei or multinucleate cells when primary nuclei enter mitosis. *Mutation Research/Genetic Toxicology and Environmental Mutagenesis*, 793, 185-198.

Chapter 1: General Background

1.1. The Discovery of X-rays and Radioactivity

On 8 November 1895, as Wilhelm Rontgen was examining the effects of passing an electric current through a partially air evacuated glass tube, a sheet of light-sensitive barium platino-cyanide paper, which happened to be on the bench, was seen to glow every time the current was switched on [1]. The value that the unknown radiation emitted from his "Crookes tube" might have in medicine was clearly understood by Rontgen at the time of his discovery of X-rays. He noticed that the X-rays emitted from the tube caused exposure of photographic plates and that, although radiation passed through cardboard that was opaque to light, it did not pass as readily through metal or various other dense objects. Rontgen also quickly demonstrated that when his hand was placed between the tube and a fluorescent screen, the X-rays passed through the soft tissue of the hand with little diminution, but the bones of the hand were sharply outlined.

In fact, it was early recognized that the X-ray applications in medical diagnosis depended on differences in absorption by different materials, and that the amount of absorption depends on the electron density of the materials through which radiation pass. Light chemical elements, such as the hydrogen, carbon, nitrogen, and oxygen of which the soft tissues of the body are largely composed, have low electron density, and thus radiation is transmitted relatively freely. However, absorption is high in materials composed of heavier chemical elements such as calcium, barium, iodine, and various metals, with absorption varying with the thickness of the material through which the X-rays pass or the concentration of the heavier element in it. X-ray pictures of bone structure or of fractures could therefore be obtained due to greater opacity to X-rays of the calcium-rich bone than of the soft tissues, and the detection of calcium-containing stones in the gallbladder or urinary tract was possible by 1905.

X-rays were soon established to be electromagnetic waves, differing essentially from those of visible light merely by having a much shorter wavelength and a correspondingly higher energy. Absorption of this energy as radiation passes through an object is sufficient to knock electrons from the atoms leaving positively charged ions. X-rays have thus the distinct effect of causing ionization, which radiations in the visible, ultraviolet, or infra-red ranges do not. Following the absorption of energy, the free ions formed and the complex succession of events is instrumental in causing characteristic kinds of chemical damage in important biomolecules that can be reflected as biological damage, particularly in the chromosomes of the cells of body tissues. The production of free radicals, which continue to react with each other and with their environment, may lead to biological effects that can extend over seconds or hours to many years. The harm that could be caused by radiation exposure of the skin was recognized soon after the discovery of X-rays, and already by 1902 a cancer had developed on the hand of a worker in a factory making X-ray tubes.

Other types of radiation, which proved to have a similar ionizing effect, were also identified within a few months of the discovery of X-rays. Henri Becquerel was examining various substances in February 1896, which were known to fluoresce after exposure to sunlight, to see whether X-rays were emitted while they were fluorescing. No such effect was found, but it was discovered that one of the substances tested, a compound of uranium, did cause darkening of the photographic plate, irrespectively whether it had been exposed to sunlight or not. Becquerel's discovery of radioactivity was rapidly followed by the identification by Pierre and Marie Curie of other chemical elements which spontaneously emitted electromagnetic radiation such as γ-rays and particulate such as α-particles. Radium, thorium, and polonium were isolated chemically and found to have these properties in 1898. Particulate radiations such as electrons, protons, neutrons, a-particles, as well as the γ-rays, are also ionizing.

The increasing variety of diagnostic applications, however, and particularly the use of X-rays and radioactive materials in treatment, demonstrated the dangers of over-exposure of patients or staff. The need to secure the fullest medical benefit without causing any undue harm was largely responsible, therefore, for an increasing detailed study during 1920s of the effects of radiation on living organisms. It led also to the development in 1928 of internationally accepted recommendations

on bases for protection against radiation, and methods of measuring amounts of radiation exposure. The present different ways in which people may be exposed to radiation shows the importance of assessing the amounts of each such exposure, and the types and likely frequencies of any resulting harmful effects. Towards this goal, studies are still needed, particularly for the effects of ionizing radiation at low doses, using physical, radiobiological, and medical methods, for dose assessment using adequate biomarkers to make it possible to estimate potential risks with considerable confidence.

1.2. Types of Ionizing Radiation and Absorption of Radiation Energy

It is customary to classify ionizing radiation either as electromagnetic radiation or particulate radiation [2]. Like radio waves, microwaves, visible light and ultraviolet light, X-rays and γ-rays are forms of electromagnetic radiation. The wavelengths of the ionizing electromagnetic radiations are ultra-short, the frequencies very high, and consequently the energy per photon large. Particularly, electromagnetic radiation is considered to be ionizing if it has photon energy in excess of 124eV, which corresponds to a wavelength shorter than 10nm. Thus, X-and γ -rays do not differ in nature or in properties, the designation X- or γ- reflects the way in which they are produced. X-rays are generated extranuclearly. An electrical device accelerates electrons to high energy and stops them abruptly in a target. Part of the kinetic energy of the electrons is converted into X-rays. On the other hand, γ-rays emitted by radioactive isotopes are produced intranuclearly, and represent the excess energy that is given off as the unstable nucleus breaks up and decays in its effort to reach a stable form. Particulate radiations such as electrons, protons and α-particles are also emitted during the decay of radionuclides, whereas neutrons are emitted as a by-product when heavy radioactive atoms split to form smaller atoms, a process called fission.

When any form of radiation is absorbed in biological material, there is a possibility that it will interact directly or indirectly with critical targets in the cells [3]. Specifically, to follow the development of radiation damage is instructive to divide the complex chain of events that follow absorption into four characteristic stages (Figure 1.1). During the first, physical stage (10^{-13} sec) of radiation action, energy is transferred from the radiation to matter. This process leads mainly to molecular excitations and ionizations in a drastically non-uniform spatial distribution. These primary species are usually extremely unstable and promptly undergo secondary reactions, either spontaneously or by collisions with molecules in their vicinity, to yield reactive secondary species. This second or physicochemical stage (duration: 10^{-10} sec) may consist of a single reaction or a complex succession of reactions. The third, or chemical stage (duration: 10^{-6} sec) begins when the system finally reestablishes thermal equilibrium. In this stage the reactive species (usually free atoms or free radicals) continue to react with each other and with their environment.

If the chain of events is initiated by absorption of radiation energy in the system under investigation, for example in a DNA molecule or a particular biological structure, this is referred to as the direct action of radiation or the direct effect. The primary processes of radiation absorption may, however, have occurred in the environment of a biological molecule under investigation, containing other biological molecules in its immediate vicinity. The energy absorbed by these molecules may be transferred to the one under investigation by intermolecular energy transferred mechanisms, or by the liberation of diffusible radicals, such as hydrogen atoms. Alternatively, if the biological molecules are in an aqueous environment, they may be attacked by diffusing reactive species (such as hydroxyl radicals, hydrogen atoms, or hydrated electrons) produced by the radiolysis of water. The term indirect effect of radiation refers to both of these mechanisms. Regardless of their mode of formation, molecular changing occurring in biological organisms may cause alterations in the system which, in passing through the fourth, or biological stage (duration: seconds to many years), finally lead to the development of the observed biological effect. The kind and magnitude of the damage depend very much on whether the defect can be repaired, or whether the cellular processes tend to amplify the damage (Figure 1.1).

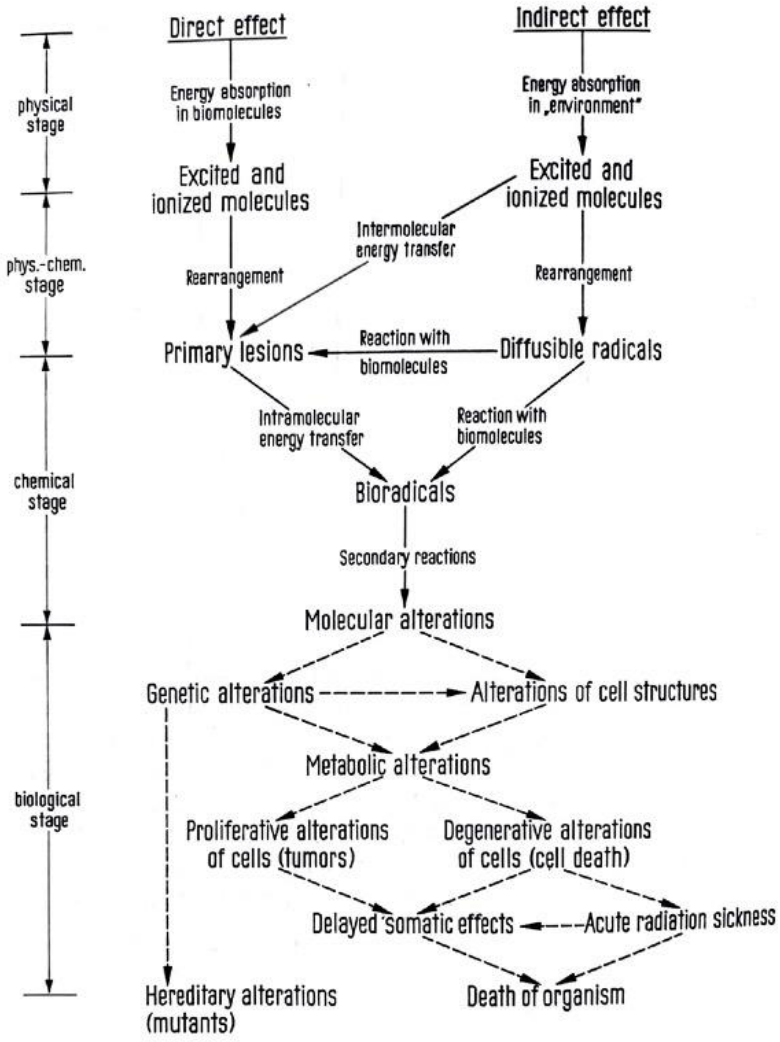

Figure 1.1. The temporal stages of radiation action. The reaction steps represented by broken lines are affected by metabolic processes [3]

1.3. Linear Energy Transfer (LET) and Relative Biological Effectiveness (RBE)

The distribution of primary events, ionizations and excitations along the track of an ionizing particle will vary according to the type of radiation. The average separation of these primary events decreases with increasing charge and mass of the particle. A comparative term to describe the deposition of energy by different types of radiation is the linear energy transfer (LET), which is defined as the average energy deposited per unit length (keV/μm). Various types of radiation can differ considerably in LET values (Table 1.1). The track-average of LET of 250 kV X-rays is about 2keV/μm, whereas heavy charged particles have LET values 100-2000 keV/μm or greater. Exposure to radiation with low LET values, or sparsely ionizing radiation (e.g. X-rays, γ-rays) leads to a random distribution of ionizations between the cells, particularly since there is very large number of tracks. The DNA damage is randomly distributed between cells and the resulting distribution of aberrations between cells might be expected to conform to a Poisson distribution. After high-LET irradiation, or densely ionizing radiation (e.g. protons, carbon ions, α-particles, neutrons), the ionization tracks are non-randomly distributed within the cell nucleus since the energy is deposited in clusters. The result will be a non-random distribution of chromosomal aberrations between cells. There will be more cells with multiple aberrations and less with one aberration (over-dispersion) than expected from a Poisson distribution.

Table 1.1. Typical LET values for various types of radiation [4].

Radiation (Energy)	**Relative LET value** (keV/μm)
^{60}Co γ-rays (1.17, 1.33 MeV)	0.3
X-rays (250 kV_P)	2
Electrons (1 MeV / 10 keV)	0.25 / 2.3
Protons (2 MeV / 10 MeV / 150 MeV)	16 / 4.7 / 0.5
Neutrons (14 MeV)	12
Heavy charged particles	> 100-200
α-particles (2.5 MeV / 5MeV)	166 / 100
Fe ions (2 GeV)	1000

The amount of radiation is expressed as the dose (in Gray, Gy), a physical quantity of the energy absorbed per unit mass of tissue (1Gy = 1 Joule/kg). Equal doses of radiation with different LET values, do not produce equal biological effects. The effectiveness of different types of radiation for inducing a particular biological end-point is usually expressed by the term relative biological effectiveness (RBE). The RBE is defined as the ratio between the dose of the reference radiation (usually 250 kV X-rays) and the dose of the radiation under study that produces the same biological effect. As shown for many end-points (including cell killing and chromosomal aberrations), the RBE values increases with LET up to an optimum value of about 100 keV/μm, and then decreases at higher values of LET. At a density of 100 keV/μm, the average separation between ionizing events just coincides with the diameter of the DNA double helix (2nm). Radiation with this density of ionization is most likely to cause a double–strand break (DSB) by the passage of a single charged particle and these DSBs have the highest biological effect. Radiations with lower LET, might require two tracks to induce a DSB, which is less efficient. On the other hand, radiation with LET above the optimum value deposits more energy in the target than necessary, resulting in a wastage of the energy. Thus, the RBE of radiations with a LET value >100 keV/μm will be lower.

To produce chromosome exchange aberrations (e.g. dicentrics, translocations) a minimum of two ionizations are necessary. Hence, most of the exchanges will be produced by ionization from two independent tracks. At low doses (<0.5 Gy), the probability of two tracks traversing a target is sufficiently low so that exchanges will be produced almost exclusively by just one track and at low frequencies. As the dose increases, the contribution of two track-induced exchanges will increase. Therefore, the dose-response curve for X-rays induced exchanges will be a contribution of one- and two-track events, with the former being more frequent at low doses and the latter being much more frequent at high doses. The resulting dose-response curve is generally well fitted by a linear-quadratic equation: $Y = x + \alpha D + \beta D^2$, where Y is the yield of exchanges, D is the dose, α- is the linear coefficient, β is the dose-squared coefficient, and x is the background frequency.

The radiation-induced DNA lesions can be repaired or mis-repaired, leading to chromosomal aberrations, taking from a few minutes up to several hours depending on the particular lesion. Using conventional cytogenetics, the analysis of chromosomal aberrations is exclusively restricted to mitotic cells arrested at metaphase since only in this phase of the cell cycle the chromosomes can be observed under the light microscope (Figure 1.2). Only by fusion of interphase cells with mitotic cells, premature condensation of interphase chromosomes (PCC) can be induced, allowing visualization also of interphase chromosomes and their analysis at all phases of the cell cycle, as we explain in detail later in this chapter.

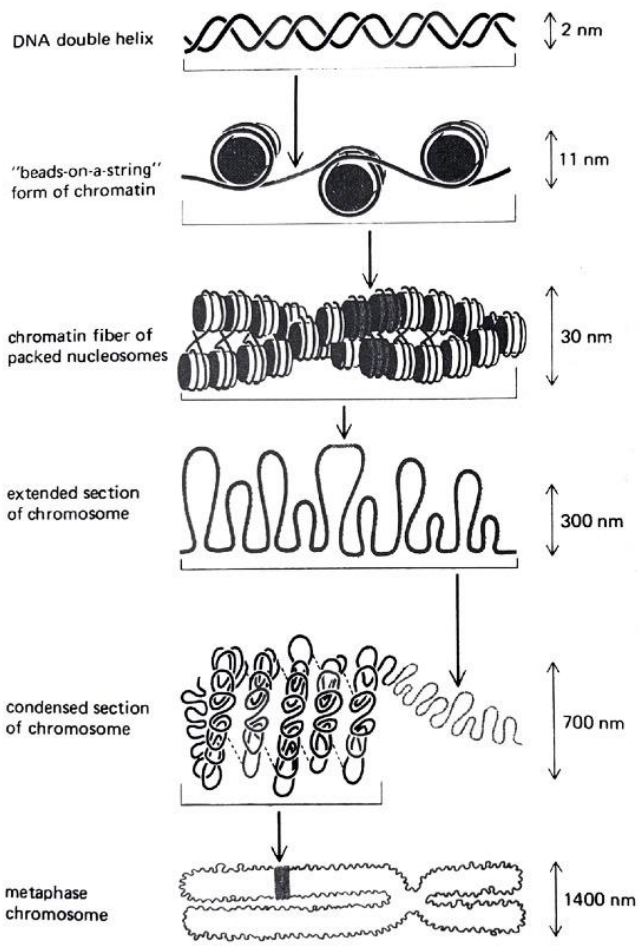

Figure 1.2. Schematic illustration of the many different orders of chromatin packing postulated to give rise to the highly condensed metaphase chromosome [2].

1.4. Repair of DNA Damage Induced by Ionizing Radiation

It has been estimated that a dose of 1Gy of low-LET, and of high-LET radiation results in base damages, DNA single strand breaks (SSBs) and double strand breaks (DSBs) as shown in Table 1.2. The frequency of DNA-protein cross-links is about 3% of the frequency of SSBs. Upon induction of such DNA damages by radiation, cells activate a complex network of sophisticated signaling pathways, known as the DNA damage response (DDR), in order to maintain genomic stability. It includes multiple DNA repair pathways, activation of cell cycle checkpoints that slow down or arrest cell cycle progression to facilitate DNA repair, alterations of gene expression, apoptosis or senescence to ameliorate the threat to the organism [5,6].

Although DSBs are relatively infrequent, they are the major cause of the biological effects induced by ionizing radiation. Also chromosomal aberrations are believed to be the result of mis-or non-repaired DNA DSBs. In fact, DSBs are precursor lesions for translocations and their formation implies error prone DSB processing. Higher eukaryotes have evolved several mechanisms for processing DSBs. The four main pathways for processing of DSBs are the classical or canonical, DNA-PK-dependent non-homologous end joining (C-NHEJ), the homologous recombination (HR) repair, the single strand annealing (SSA) and the alternative end joining (Alt-EJ).

Table 1.2. Average yield of induced damage in a typical mammalian cell after 1 Gy of low- or high-LET radiation [7].

Events / Type of damage	Low-LET	High-LET
Tracks in nucleus	1000	2
Ionizations in DNA	1500	1500
Base damages	10^5	10^5
SSBs	850	450
DSBs	50	70
Chromosome aberrations	1	3
Lethal lesions	0.5	2.6

Non-Homologous End Joining (NHEJ) is the simplest repair mechanism for DSBs. The damaged DNA ends are directly rejoined. This pathway is fast, cell cycle independent but more error-prone as during this process the broken strands are simply rejoined without the need of a homologous template. In the repair process, DNA breaks may fail to rejoin correctly and this could lead to sequence alterations at the damage site and formation of chromosome aberrations, particularly translocations. The homologous recombination (HR) repair is slow but the only error-free repair pathway and it is highly evolutionary conserved through species. In HR the sister chromatid or the homologous chromosome is used as a template and the information is copied. Thus, this pathway is restricted to S and G2 phases of the cell cycle where the sister chromatid is available for the restoration of the damaged sequence. The Single-strand annealing (SSA) is also a slow and cell cycle dependent DNA double-strand break (DSB) repair pathway, which uses homologous repeats to bridge DSB ends. SSA involving repeats that flank a single DSB, causes a deletion rearrangement between the repeats, and hence is relatively mutagenic. The alternative end joining (Alt-EJ) is again slow, error-prone, and cell cycle dependent pathway that becomes active when C-NHEJ fails. This pathway is considered to operate as backup, hence also the term backup non-homologous end joining (B-NHEJ).

In addition, some other DNA damage repair pathways are: Base Excision Repair (BER) - a cellular mechanism which is initiated by the excision of modified base from the DNA. DNA glycosylases recognize, remove and replace specific damaged or mis-incorporated bases, forming abasic (AP) sites. The damaged base is modified and excised forming an SSB that is repaired to regenerate an intact helix; Nucleotide excision repair (NER) - removes bulky damage from the DNA (i.e. bases that have been modified with bulky chemical groups, like the ones that get attached to the DNA when exposed to chemicals in cigarette smoke), and also fixes some types of damage caused by UV radiation; and mismatch repair (MMR), which recognizes and removes errors introduced during DNA replication and recombination, such as mis-inserted nucleotides, small loops, insertions and deletions.

1.5. Need for Effective Biodosimetry Measurements in Large-Scale Radiation Exposure

Currently, awareness is growing regarding the possibility that large-scale radiological accidents or terrorism acts could result in potential radiation exposure of hundreds or thousands of people and that the present guidelines for evaluation after such an event are seriously deficient. There is a great and urgent need, therefore, for after-the-fact biodosimetric methods enabling the assessment of radiation doses, which must be at the individual level, timely, accurate, and plausibly obtained in large-scale disasters [8,9].

By definition, biodosimetry is the quantification of absorbed doses with the help of biological material obtained from exposed individuals. Ideally, the biodosimetric methods for estimating human radiation exposure must have first the ability to determine which individuals did not receive a significant exposure so they can be removed from the acute response system. Second, must have the capacity to classify those initially assessed as needing further evaluation into treatment-level categories, and third, must have the ability to guide both short- and long-term treatments. Towards

this goal, significant attempts have been made for the development of biodosimetric methods using appropriate biomarkers based on biological or physical parameters and considering their features such as speed, accuracy, capacity and ease of getting information for dose assessment. Specifically, there are two main methods of biodosimetry, biologically-based and physically-based, and in practice their use indicates that combining physical and biological techniques may sometimes be most effective.

Biologically-based biodosimetry approaches are essentially based on biological processes or parameters that are affected by IR. Examples include cytogenetic approaches enabling the visualization and evaluation of chromosome integrity following the initial radiation-induced damage at the DNA level. The subsequent activation of repair/misrepair mechanisms may cause production of unusual chromosomal aberrations in case the enzymatic repair processing of DNA damage is not error free. Dose estimation using cytogenetic analysis is based on the relationship between chromosome aberration frequency and the amount of dose absorbed. The preferred choice of sample to analyze aberration frequency is the blood lymphocytes as they are easy to collect, culture and processing for biodosimetric studies. Exposed lymphocytes show different types of chromosome aberrations like dicentric chromosome (DC), centric ring, acentrics and translocation, all of which can be related to dose. For reliable dose estimation, there are several important biological parameters such as low background frequency, specificity to IR, a clear dose- effect relationship for high and low linear energy transfer (LET) radiation with different dose and dose rates, and most importantly reproducibility and comparability of in vitro to in vivo results [10].

Physically-based biodosimetry approaches are mainly based on physical parameters measured in the tissues of exposed individuals. Examples include, levels of long-lived radiation-induced free radicals detected by Electron Paramagnetic Resonance (EPR) [11–13] and Optically Stimulated Luminescence (OSL) [14]. EPR dosimetry is especially well-developed and established as one of the principal methods for estimating doses many years after an exposure. Originally, this technology was based on exfoliated teeth but more recently, EPR has been used for acute dosimetry using measurements of teeth in situ [15,16] and fingernail clippings [17,18].

The use of biodosimetry to measure radiation dose after-the-fact has become a very important and high-priority field due to the need for governments to be prepared for the heightened potential for exposures of large numbers of individuals from radiological accidents or terrorism acts [8]. Estimating radiation doses would greatly help to medically evaluate the injured in four different ways. Biodosimetry would help estimate how many people received doses that did not require acute care, classify those patients who need further evaluation into treatment- level categories, guide actual treatment, and help providers and patients with the long-term consequences of exposures to IR, including planning for treatment and patient compensation.

1.6. Triage patients

The next level of use of biodosimetry, which could follow the initial screening, would be to assist in assigning individuals as rapidly and effectively as possible into major action classes. The number of categories would depend on the volume of people triaged for care and the capabilities of the medical care system for addressing their treatment. Under some circumstances, such as the limited availability of stem-cell transplantation, it would be desirable for the biodosimetry technique to provide reliable estimates for subclasses of risk so that the limited capabilities for high-intensity treatments could be used most effectively. In general, the exposed individuals can be assigned into three categories [9].

Category 1. Identify false positives and those near 2 Gy—These individuals would not need urgent medical care. They might possibly need to be evaluated for risks of long- term effects but would have little need for prompt actions. Individuals assigned to this category could leave the emergency medical care system, at least during the period of time when there is greatest stress and potential for overwhelming the system.

Category 2. Admit patients into the medical care system for observation and, as needed, active medical care—This would be done to reduce the probability of a near-term deleterious clinical course

due to ARS. This group is likely to require active symptomatic medical care and may also receive complex (and potentially risky) more aggressive treatments, such as bone marrow transplantation and/or high doses of radiation- mitigating drugs. The assignment of individuals into this action class would typically occur when the dose is in the range of 3–8 Gy.

Category 3. Provide palliative or expectant care—This level would identify individuals whose radiation exposure is too high for effective active or mitigating therapy. The actual threshold level may vary under the conditions of the event and the ability of the system to provide advanced care; however, a likely threshold would be 8 Gy. If fewer individuals are involved and the treatment capability is not overwhelmed, the threshold for entry into this category would probably be increased. On the other hand, if the healthcare system was potentially overwhelmed, the dose range for active treatment (i.e., placement into Category 2) might be narrowed on both ends. That is, more people could be placed into Category 1 (by raising the minimum dose to qualify for active treatment) and more placed into Category 3 (by lowering the maximum dose to qualify for active treatment).

Many of the useful characteristics of biodosimetry techniques for this more refined sorting into action categories would differ from those required for the initial triage. The information would not need to be available as rapidly. While it would be desirable to avoid the need to transport the samples, it would sometimes be feasible to transport samples, especially to nearby facilities such as an emergency center set up near the event site. The throughput could be less. Techniques for measuring dose could include bringing expert operators to the site. It would be important for the technique to have a low false-assignment rate, i.e., neither assigning too high nor too low a category or subcategory. For this purpose, an estimate of dose within ±0.5 to 1.0 Gy of the actual dose is probably sufficient, because the known variation in response among individuals receiving the same exposure dose is likely to render more precise estimates of dose clinically irrelevant.

1.7. Biomarkers of Radiation Exposure

Exposure to radiation induces certain changes on the proteins, carbohydrates, lipids, nucleic acids and gene expression in the exposed cell, which are collectively known as biomarkers. In particular, traversal of IR in a cellular system can bring about a variety of changes such as base damages, alkylation, intercalation adduct formation, nucleotide modifications, single strand and double strand breaks in the deoxyribonucleic acid (DNA). Those changes can result either due to direct deposition of energy on the nucleic acids (direct action) or can be mediated by the release of electrons and generation of free radicals like $OH^{\cdot}$, released at some point in the interaction with water (indirect action) and membrane (lipid peroxidation) which surrounds the cells. The biomarkers are classified based on the changes being looked into like chromosomal aberrations, alterations in cell number, change in an enzyme level and or activity, proteins, or expression of genes, etc [19,20]. Of late based on the temporal parameters, it has been classified into markers of exposure, marker of susceptibility, markers of late effects and markers of persistent effects [21]. Thus, the manifestations of any of those changes are resulted due to the traversal of ionization track and deposition of energy in exposed cells/tissues. A summary of biomarkers of radiation exposure reported in the literature is given in Figure 1.3.

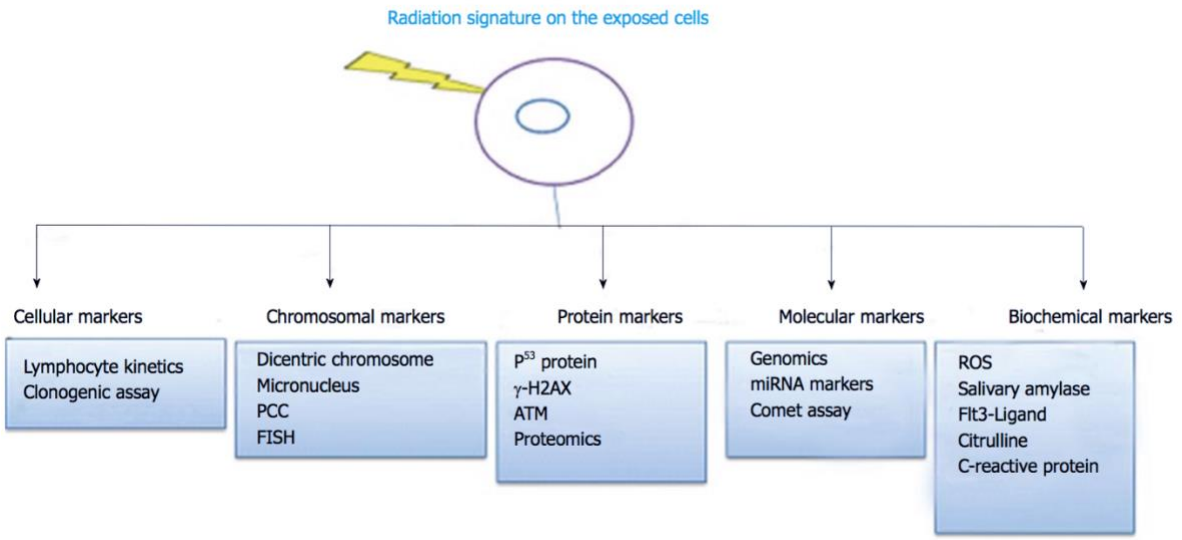

Figure 1.3. Biomarkers of exposure to ionizing radiation. FISH: Fluorescence in situ hybridization; PCC: Premature chromosome condensation; ROS: Reactive oxygen species; ATM: Ataxia telangiectasia mutated [22].

Upon the energy deposition of radiation in the exposed cells, many changes can be induced and in turn the cells respond to those changes explicitly activation player molecules involved in check points activation, DNA repair and apoptosis [23]. The end result and fate of the cells depends on the many physical parameters of the incident photon as well as the cellular biological machinery. The chromosome aberrations are formed predominantly due to the repair activation that results in a not perfect rejoining or mis-rejoin to form chromosome aberrations. Thus, the aberration produced depends on the number of breaks, chromatids and chromosomes as well as its proximity of induced breaks involved [24]. The type, complexity and frequency of aberrations induced by radiations are diverse, which are traditionally being used to quantify and relate to the absorbed dose (Figure 1.4). Chromosomal changes are named based on the methodology employed, or stain used (Giemsa or fluorescence) to observe those changes or the end product (micronucleus, translocations) [25].

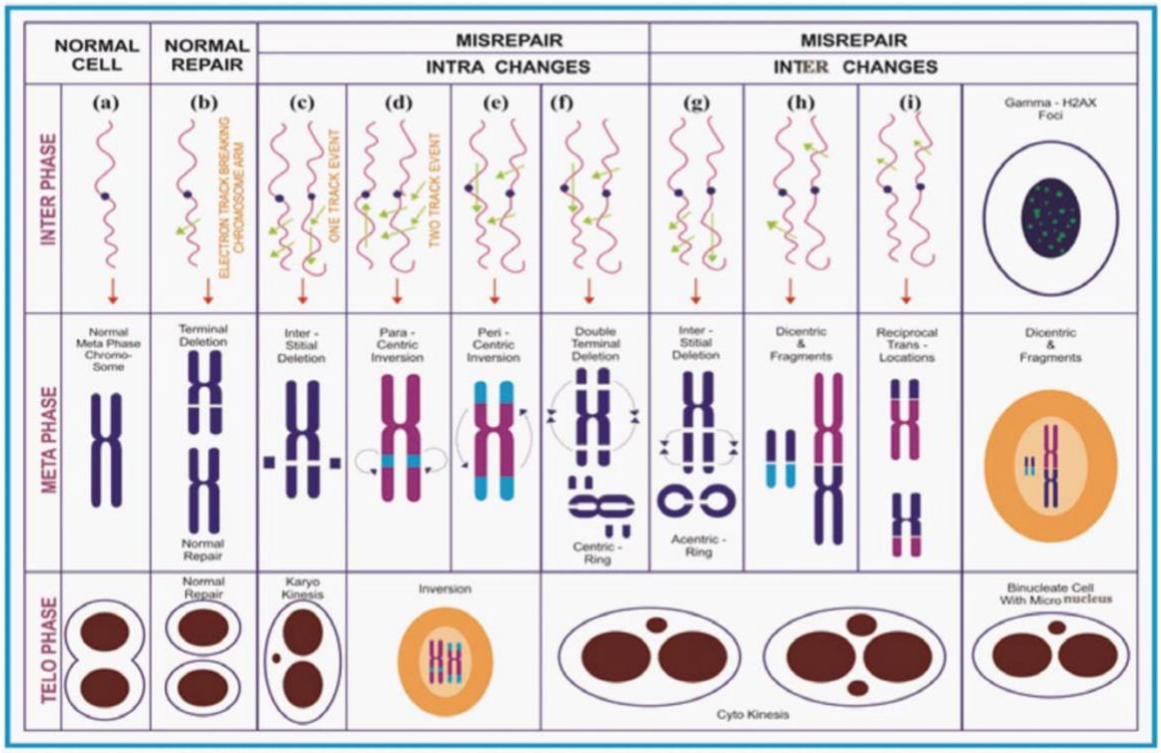

Figure 1.4. Diagrammatic illustration on the formation of ionizing radiation induced chromosome aberrations [22].

1.8. Cytogenetic Biomarkers of Radiation Exposure

Cytogenetics focuses on the study of chromosomes, in particular chromosomal anomalies. Several cytogenetic endpoints are routinely used as biomarkers of exposure as they show a high degree of specificity and sensitivity. Other cytogenetic measurements might be useful as biomarkers of late effects but need to be validated against well-defined outcomes/endpoints. Cytogenetic biomarkers are summarized in Table 1.3.

Table 1.3. Cytogenetic biomarkers [21]

Biomarkers	Assays/methodology	Sensitivity	Specificity to IR and confounders	Time window after exposure during which assays might be performed	Biological material needed to perform the assays[a]
Dicentrics	Dicentric chromosome assay	0.1–5 Gy	Almost exclusively induced by IR	Before renewal of PBL	WB: fresh; PBMC: fresh and frozen[b]
Translocations	Single colour FISH G-banding	0.25–4 Gy	Confounding factors: smoking; strong age effect	Years	WB: fresh; PBMC: fresh and frozen[b]
CCR	Multiple colour FISH	Unknown	High LET and heavy ion exposure	Before renewal of PBL	WB: fresh; PBMC: fresh and frozen
PCC	PCC assay combined or not to FISH chromosome painting or c-banding	PCC fragments: 0.2–20 Gy PCC rings: 1–20 Gy	IR specific to a large extent	PCC fragments: ideally immediately after exposure PCC rings: before renewal of PBL	PBMC: fresh and frozen
Telomere length	Flow cytometry Quantitative-FISH Southern blot qPCR	Not yet established	Not specific: modulated by viral infection Potential confounders: age, oxidative stress	Not yet established	WB, PBMC, cell lines: fresh and frozen
Micronuclei	Cytokinesis block micronucleus assay Micronucleus centromere FISH assay for low doses Flow cytometric detection of DNA in reticulocytes	0.2–4 Gy[c] but limited sensitivity at doses <1 Gy. Selective scoring after centromere FISH: ~100 mGy	Not specific: modulated by genotoxins Confounding factors: age, gender	In lymphocytes: before renewal of PBL In reticulocytes: not yet established	WB, PBMC: fresh and frozen[b]; Reticulocytes: fresh

CCR: complex chromosomal rearrangement; FISH: Fluorescence in situ hybridization; PBMC: Peripheral Blood Mononuclear Cell (lymphocytes, monocytes, etc.); PBL: Peripheral blood lymphocytes (T lymphocytes for assays requiring cycling cells); PCC: premature chromosome condensation; qPCR: quantitative polymerase chain reaction; WB: whole blood.

[a] Sample storage conditions listed when known.

[b] Frozen samples give lower yields of scorable cells.

[c] Dose range for photon equivalent acute whole-body exposure 24 h ago.

1.8.1. Dicentric Chromosomes

The dicentric chromosome, which is a chromosome with two centromeres instead of its normal structure with one centromere (Figure 1.5), is the most widely used cytogenetic biomarker for dose assessment following exposure to IR. Its formation is a complex event because it needs double strand breaks (DSBs) in at least two different chromosomes. The DSBs should be in close proximity to each other so that they will have a high probability for misrepair and formation of abnormal structures [26].

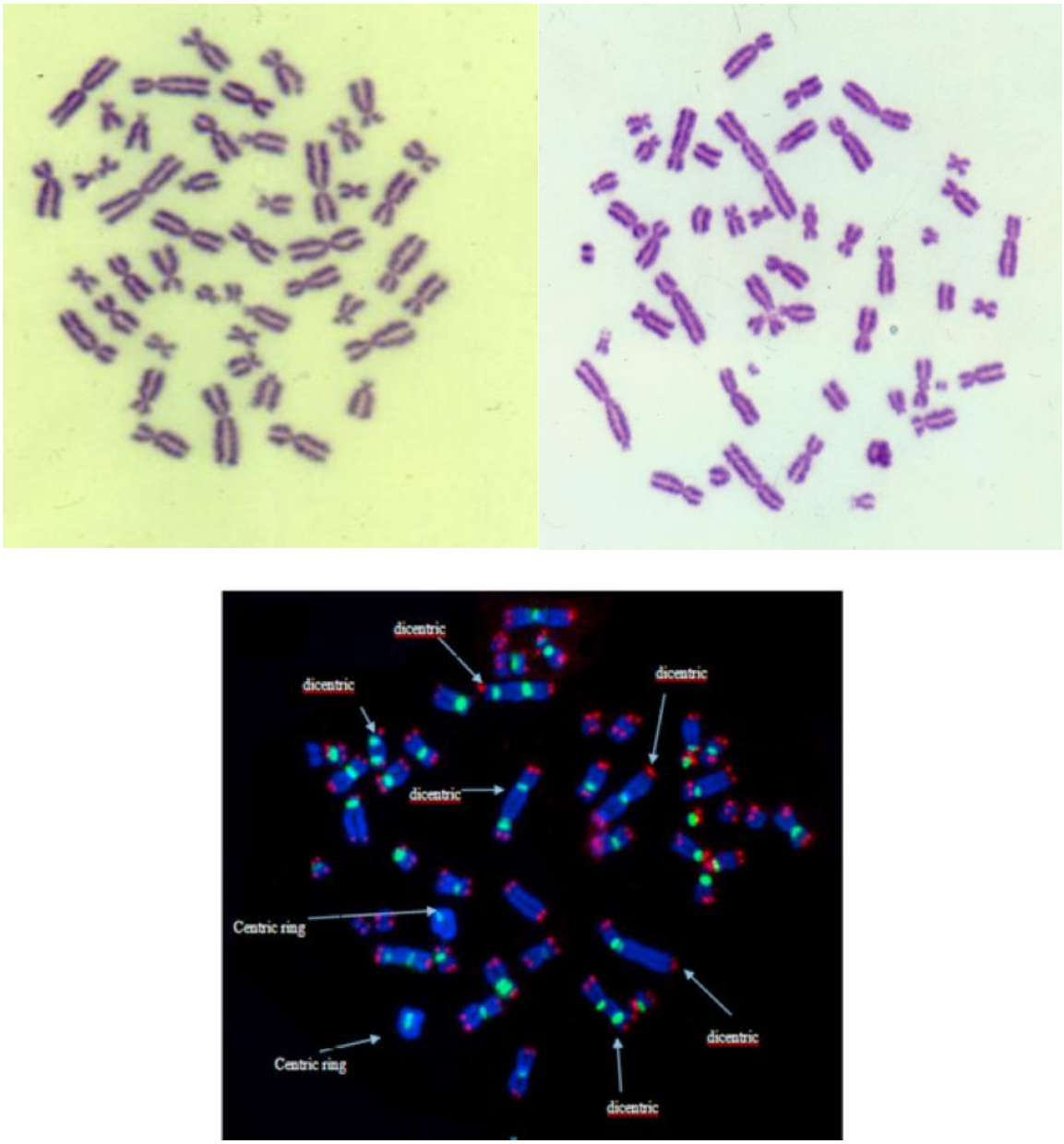

Figure 1.5. Examples of normal chromosomes (top left), dicentric and centric ring chromosomes (top right) as visualized by Giemsa staining; or by combining Centromeric/Telomeric (C/T) Peptide Nucleic Acid (PNA) probes with the FISH technique (bottom).

In order to estimate the dose from accidental exposures, appropriate dose-response curves should be constructed in every biodosimetry laboratory for different radiation qualities by irradiating in vitro heparinized peripheral blood samples using sufficient dose points. The irradiated blood samples are then cultured for 48-50h under aseptic conditions in the presence of phytohaemagglutinin (PHA) and microscope slides are prepared with good quality of metaphase chromosomes and high mitotic index.

Stained slides with Giemsa are used to measure the number of dicentric and centric ring chromosomes at each dose point and their frequency per lymphocyte metaphase is used to construct a reference dose-response curve. Representative images of normal metaphase and a metaphase with DC obtained from human blood lymphocytes exposed to ^{60}Co-γ-irradiation are given in Figure 1.5 top. DC scoring can be supplemented with the application of C/T-FISH, which simultaneously stains centromeres and telomeres (Figure 1.5 bottom). This technique enables the detection of true dicentrics in ambiguous cases with complex configurations, which is technically challenging with classical Giemsa staining only[27,28].

The constructed dose-response curve under in vitro conditions follows the equation $Y=C+\alpha D+\beta D^2$ or $Y=C+\alpha D$, depending upon the quality of radiation, and can be applied for estimating doses of the exposed individuals, where: Y is the yield of dicentrics plus centric rings, D is the dose, C is the background frequency, α is the liner coefficient, and β is the dose squared coefficient (Figure 1.6). The ratio of α/β can be referred to as the cross-over dose. It is equal to the dose at which the linear and the quadratic components contribute equally to the formation of dicentrics. It has been shown that the number of DC obtained with a given amount of dose is the same when irradiated either in vitro or in vivo condition [29].

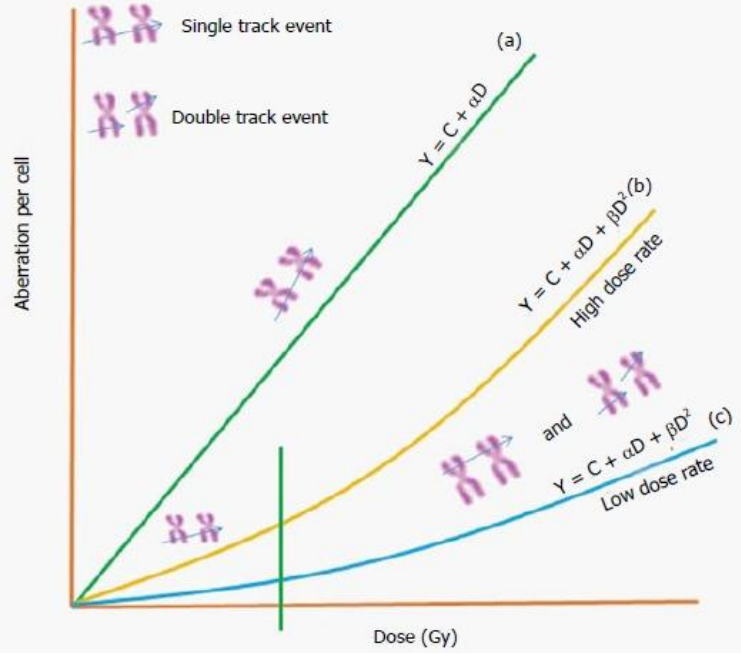

Figure 1.6. Dose response relationship for chromosome aberrations induced by different types of ionizing radiations.[22]

The linear component (αD) often interpreted as the number of aberrations formed due to the traversal of a single particle track and is expected to be independent of dose-rate. The dose squared (βD^2) term is formed due to the interaction between two independent particle tracks and its degree determined by the time interval between the two tracks.

With low LET radiation such as X rays and γ-radiation, the ionization at any particular dose will be randomly distributed between cells, particularly since there will be a very large number of tracks. The DNA damage as well as the chromosomal aberrations will be also randomly distributed between cells. With high LET, or densely-ionizing radiation, the ionization tracks will be non-randomly distributed between cells, with the energy being deposited in more "discrete packets", and consequently the induced aberrations will be non-randomly distributed between cells. Therefore, for low LET radiation, there is greater probability that two lesions within the target will be induced by two ionization events along the same track, resulting in two consequences. In the case of high LET

radiation, there is a greater probability that two lesions within the target to be produced by one track, and the dose-response curve mostly follows the equation $Y = C + \alpha D$ (Figure 1.6).

A useful comparative term to describe the deposition of energy by different types of radiation is the linear energy transfer expressed in keV/μm (LET), and the track average appears to be the better quantity to describe the relative biological effectiveness (RBE) variations for chromosomal damage [27,30]. The track average for LET of 250 kVp (kilovolts peak) X rays is about 2 keV/μm, as compared with heavy charged particles that have track average LET values of 100-2000 keV/μm. The quantity of energy deposited per micrometer of track will determined the biological effectiveness of different types of radiation. By definition, the relative biological effectiveness (RBE) is defined as the ratio of the dose of the reference radiation (200-250 kvp of X rays) to the dose of the particular radiation being studied that produces the same biological effect.

The dicentric chromosomes are stable within non-dividing cells such as G0-lymphocytes but as the half-life of blood lymphocytes is in the order of months/years depending on the sub-population, the dicentric is the biomarker of choice for investigating recent exposure to IR. In general, as there are no major confounders influencing the yield of dicentrics, its natural occurrence is very low (generally in the order of 0.5–1/1000 cells scored) [27]. Individual dose assessment can be achieved for homogeneous whole-body exposures to doses as low as 100 mGy for low-linear energy transfer (LET) IR if up to 1000 cells are analyzed.

The scoring of dicentrics based on chromosomal morphology requires expertise, and time to analyze a large number of cells required particularly for low dose exposures. However, after exposure to low doses, the calculated estimates often carry large uncertainties, mainly due to the insufficient number of cells scored. Since the dicentric assay is very laborious, counting sufficiently large numbers of cells will be a limiting factor and will limit the possibilities for adequate dose estimation in the low dose range on an individual level. Automated systems are under development and provide very reproducible results but their major limitation is the dicentric's detection efficiency that remains around 50–70% [27]. Nevertheless, automated dicentric assays are currently being investigated in the framework of the European Multi- biodose project (http://www.multibiodose.eu) that is aimed at analysing and adapting biodosimetric tools to manage high scale radiological casualties.

In addition to acute whole-body exposures, dose estimation for protracted and partial-body exposure can also be achieved by scoring dicentrics in lymphocytes. It should be noted that in order to estimate dose, calibration curves are necessary. Although the scoring of dicentrics is most suitable as a biomarker for external exposures [31], it can also be informative after internal exposures to radionuclides that disperse fairly uniformly around the body. Isotopes of caesium and tritiated water are two such examples [27]. Dicentric aberrations are unstable because their frequency decreases with the turnover of peripheral blood lymphocytes. Thus, for reliable dose assessment, dicentric aberration assays should be performed within a few weeks of exposure. If performed later, the precision of the assay is diminished as the dose calculation requires the use of half-time estimates for the disappearance of dicentrics.

1.8.2. Translocations

In contrast to dicentrics, reciprocal translocations are chromosomal aberrations that can persist in peripheral blood lymphocytes for years and can thus be used as biomarkers of past exposures [27]. This persistence reflects the presence of translocations in the lymphatic stem cells and is affected by many factors. These include exposure conditions, such as dose rate and whole- body vs. partial-body exposure. As translocations may be parts of complex chromosomal rearrangements (CCRs) [32] that are unstable, it is essential to distinguish their origin within the cell. The cells that are scored also influence measurements and dose calibration for translocations, as it has been shown that the presence of unstable chromosomal aberrations in the same cell reduces the frequency of translocations with time [33]. Therefore, only cells free of any unstable chromosome damage should be scored.

The FISH technique or ''chromosome painting'' is commonly used for the detection of inter-exchanges, such as translocations and dicentrics (Figure 1.7). Currently the assay could be semi-automated, for instance through the use of a metaphase finder system, but there is still a need for a fully automated image analyzer that would reliably differentiate normal cells from cells with chromosomal aberrations [34,35]. Rapid developments in the probe labelling methodology, optics and imaging modalities, the assay has evolved in different directions like m-FISH, SKY-FISH, and m-band where exchanges involved in any chromosomes or regions within chromosomes can be identified easily similar to that, GTG-banding technique have been in use for the identification of aberrations in individual chromosomes as well as in entire genomes. It was an attractive option for many years back; however, RT measurements with latest FISH technology, and G-banding, in dosimetry is limited because of either time factor and/or cost factor. However, it can provide a true estimation of translocation frequency by analyzing the individual chromosomes for chronic dose estimation.

A common feature of translocations among non-exposed subjects is the large inter-individual variation in their number, age being the most important confounding factor [36]. Therefore, natural occurrence and accumulation with lifespan can confound very low dose exposure estimations. Despite the strong age-effect for translocations, subjects of the same age may show large variation in translocation frequencies. The reasons for the age-dependent baseline frequency is not fully established, but some of them may be linked with cellular mechanisms changing with age such as DNA repair. From a number of confounders tested, smoking has been demonstrated to increase translocation frequencies in some studies, but not in others, possibly due to variations in cigarette types or numbers smoked [34]. Other sources of variation may include clastogenic agents in the diet or environment, gender, ethnicity and genetic polymorphisms in genes involved in cellular defense mechanisms. Individual dose assessment using translocations is strongly dependent on the personal baseline frequency of this aberration, and from a practical point of view, the time required for the analysis would severely limit the use of such an approach for triage biodosimetry in large studies.

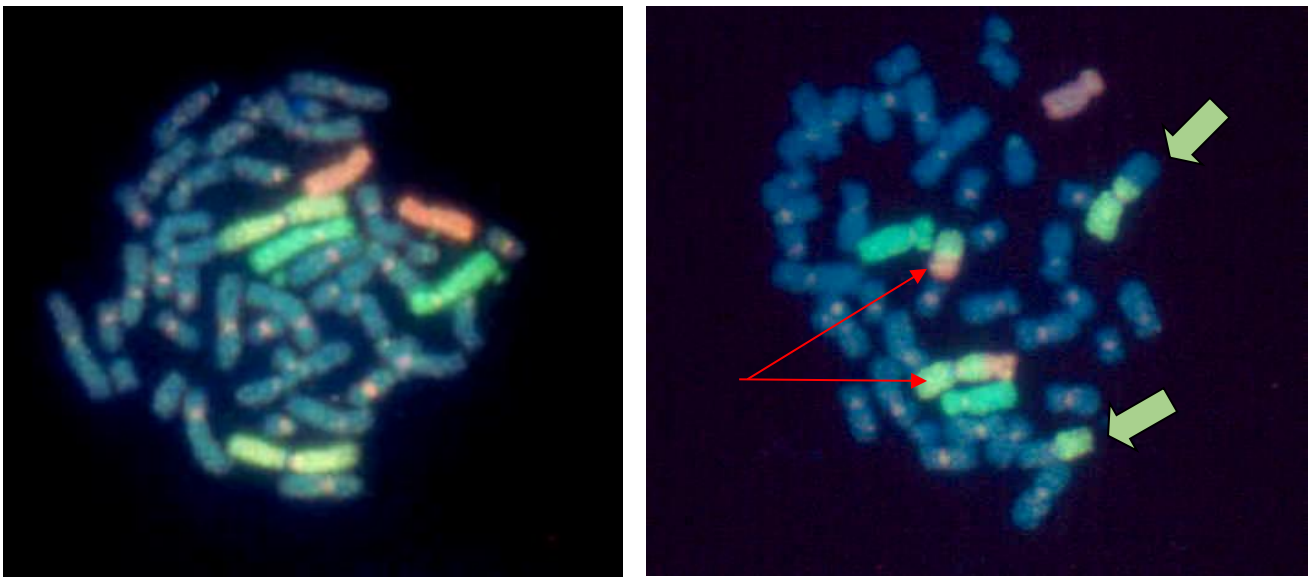

Figure 1.7. Human lymphocyte metaphase illustrating FISH-based chromosome 'painting' to detect chromosomes 1 (yellow/green), 4 (green) and 8 (orange) using whole chromosome and pan-centromeric probes (left). A dicentric chromosome and its associated acentric fragment (red arrows) as well as a reciprocal translocation of chromosome 1 illustrated by the two bicolored chromosomes (green arrows) (right)

1.8.3. Micronuclei

Micronuclei (MN) form when mainly fragments or intact chromosomes are not properly segregated into daughter cell nuclei at anaphase but instead remain in the cytoplasm after cell division. Generally, they are regular in shape with a similar staining intensity to that of daughter nuclei and they can be visualized as small spherical objects using any conventional DNA dye (Figure 1.8). In comparison to most other cytogenetic techniques, MN are far easier to score both manually and using automated microscopy slide scanning and image analysis systems [27,37,38]. As MN form only during cell division and, like dicentrics, are lost when cells continue to divide. Fenech et al [39] developed a simple, most effective and reliable methodology to select cells between first and second mitosis division using cytochalasin-B to inhibit cell division at cytokinesis in a cycling cell and named as cytokinesis blocked micronucleus (CBMN) assay. Indeed, reliable quantitative results are achieved by blocking the cell cycle progression of PHA- stimulated lymphocytes at the stage of cytokinesis after the first mitosis, and by performing microscopic scoring of MN only in binucleated cells. An important caution is that many factors like age, genetic makeup and storage of blood samples could influence the dose estimation using the MN assay [40]. Similar to DC many laboratories have established dose response curves to estimate the dose; it follows linear-quadratic pattern despite the fact that there are differences in the obtained coefficients among the established laboratories.

MN reflects chromosomal damage and thus it is a useful index for monitoring environmental effects on genetic material in human cells [41]. Due to the simplicity and the rapidity of scoring, this assay has shown promising potential in the triage medical management. However, due to background frequency of spontaneous MN frequency (0.002 to 0.036/cells) the sensitivity is 0.25 Gy [27]. The CBMN assay in addition to measuring the MN, it can also be used to measure nuclear-plasmic bridges, nuclear buds, necrotic cells, apoptotic cell and nuclear division rate collectively known as cytome assay [42]. Several studies have been carried out using the MN analysis in vitro and in vivo, for the purposes of biological dosimetry. A good correlation between the doses estimated from the MN frequency was observed in radiation workers [43] and in thyroid cancer patients undergoing radioiodine treatment [44]. A large volume of published reports for in vitro dose response curves is available. MN measured by cytokinesis-blocked micronucleus (CBMN) assay show promise as a biomarker for individual radiosensitivity and susceptibility to environmental carcinogens [45]. Consistent with this notion, a recent twin study provided evidence for the high heritability of baseline and induced MN frequencies [46].

Due to variable base levels in different individuals, the standard CBMN assay cannot detect acute whole-body doses below 200 mGy for low-LET IR. In addition, a wide range of clastogenic and aneugenic agents (i.e. agents causing chromosome breakages and abnormal number of chromosomes, respectively) can induce MN, and confounding factors include age and gender. Most of this background 'noise' of MN in non-exposed individuals can be attributed to the loss of one intact copy of the X-chromosome.

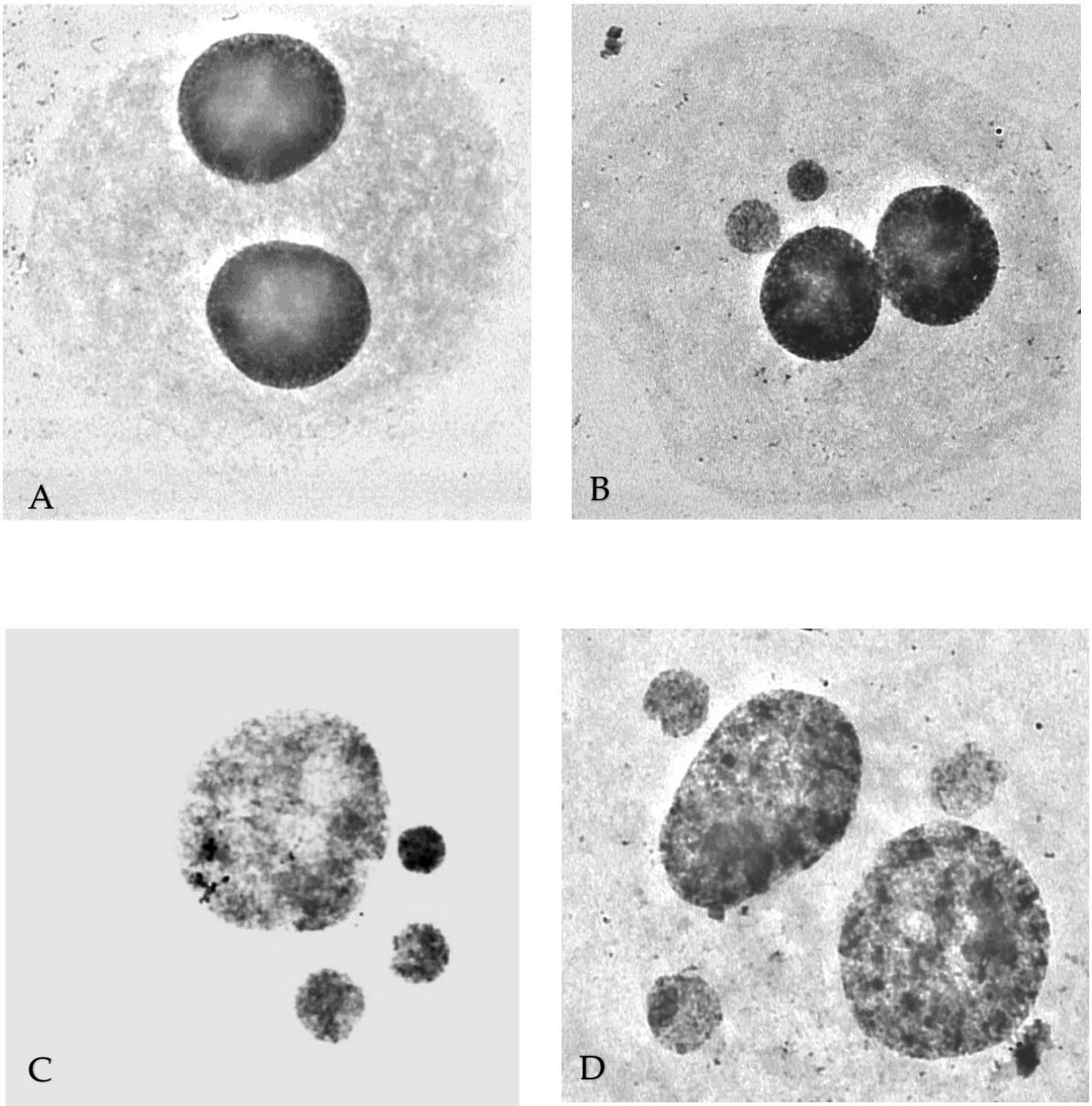

Figure 1.8. Normal cell division (A), aberrant divisions with 2 (B), 3 (C), and 4 (D) micronuclei.

Selective scoring of MN that are negative for centromere-specific FISH signals (Figure 1.9) can significantly improve the sensitivity to a minimum detectable acute whole-body gamma-ray dose of 100mGy for individuals [47]. First steps have been made towards the development of an automated analysis system for the micronucleus centromere assay [48] which would enable large-scale studies of cohorts exposed to low-to-moderate radiation doses. Other limitations of the CBMN assay include the minimum delay of 3 days between sampling and first results becoming available, loss of the signal with lymphocyte turnover (as discussed above for dicentrics) and its inability to detect non- uniform exposures [47].

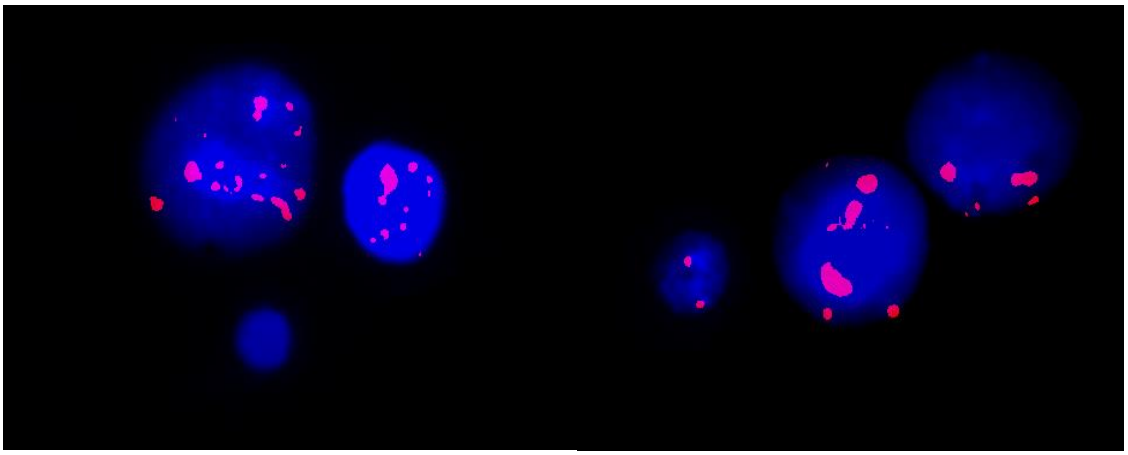

Figure 1.9. Binucleated cells showing a centromere negative MN (left) and a centromere positive MN (right). Centromeres are stained with a pan-centromeric probe (spectrum orange) and nuclei and MN are counterstained with DAPI.

1.8.4. Premature Chromosome Condensation (PCC)

When cycling cells enter mitosis, their nuclear membrane is dissolved and chromatin condenses into the familiar shaped of metaphase chromosomes by the histone phosphorylation processes of phosphokinases, which are generated during G2 to M-phase transition. Therefore, measurement of chromosomal aberrations by means of the conventional metaphase method requires that the cells of interest are in mitotic phase where chromosomes are highly condensed and visible.

Alternatively, techniques have been developed to cause chromatin that is not at mitosis to condense prematurely in cycling, quiescent or even in non-cycling cells. This phenomenon is termed premature chromosome condensation (PCC), and it can be induced by fusing interphase cells to mitotic Chinese hamster ovary (CHO) or HeLa cells using Sendai virus or, particularly for lymphocytes, using the fusing agent polyethylene glycol (PEG). PEG is used for lymphocytes since cell fusion by means of Sendai virus requires cells with membranes especially receptive to the virus particles and it has been reported that G_0 lymphocytes cannot be satisfactorily fused using the Sendai virus. This difficulty was overcome for the purpose of biological dosimetry with the use of PEG for PCC induction in peripheral blood G_0 lymphocytes, as shown in Figure 1.10 [27,49].

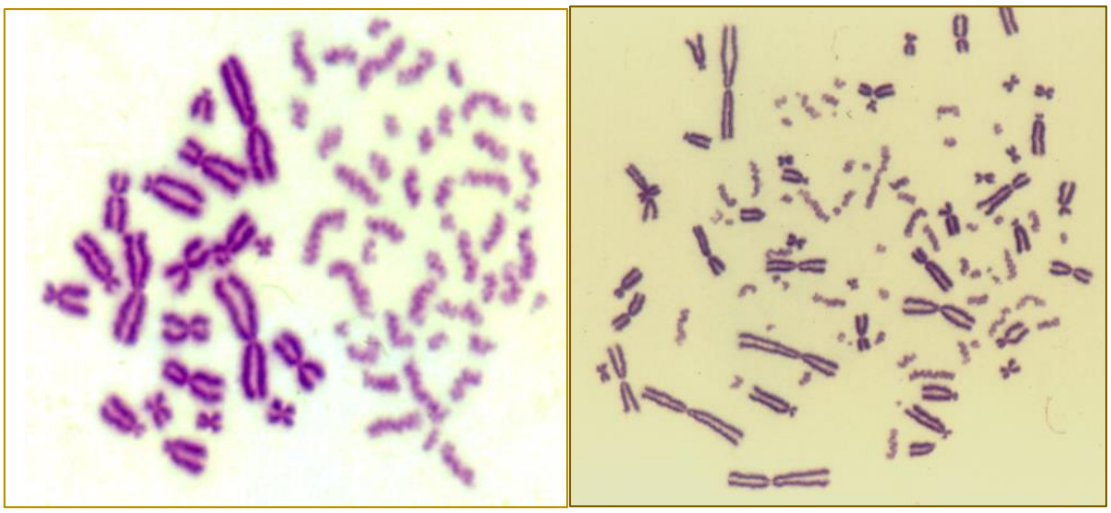

Figure 1.10. Premature chromosome condensation induced by PEG-mediated fusion in an unirradiated human lymphocyte fused with a mitotic CHO cell. Forty-six distinct single chromatid PCCs can be seen (left). In irradiated quiescent cells a number of excess PCC fragments (>46 chromosomes for human) can be scored (right).

The major advantage of the PCC method is that radiation-induced chromosomal damage can be observed shortly after blood sampling (Figure 1.11), and it is also possible to score centric ring chromosomes, dicentrics and translocations if the PCC method is combined with FISH chromosome painting or C-banding [27,50,51]. The PCC technique is a very useful research tool to probe the immediate post-irradiation processes and kinetics of chromosomal break restitution and/or misrepair to form aberrations (i.e. dicentrics and translocations). These studies demonstrate that the dicentrics, complete and incomplete translocations and acentric fragments, that one sees eventually at metaphase, are formed essentially in G_0-lymphocytes and, therefore, their formation does not require lymphocyte stimulation, culture and DNA replication (Figure 1.12).

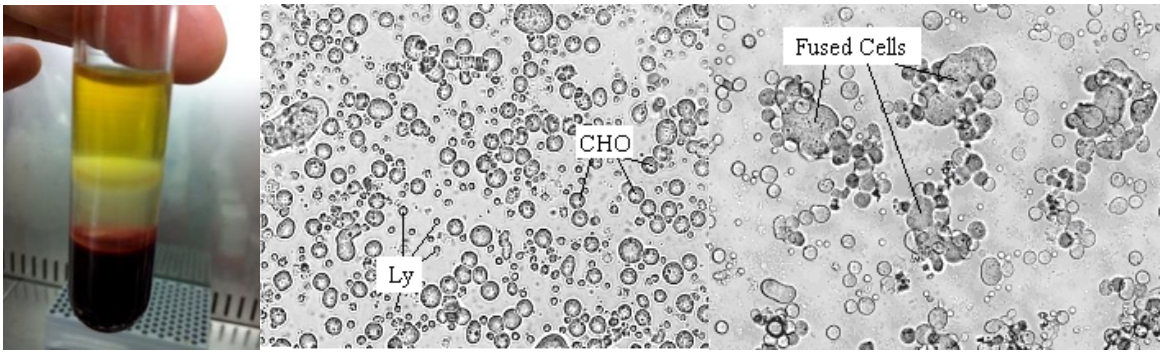

Figure 1.11. Human lymphocytes (Ly) are isolated using Biocoll separating solution (left), mixed with mitotic CHO cells (center) and fused by means of PEG (right).

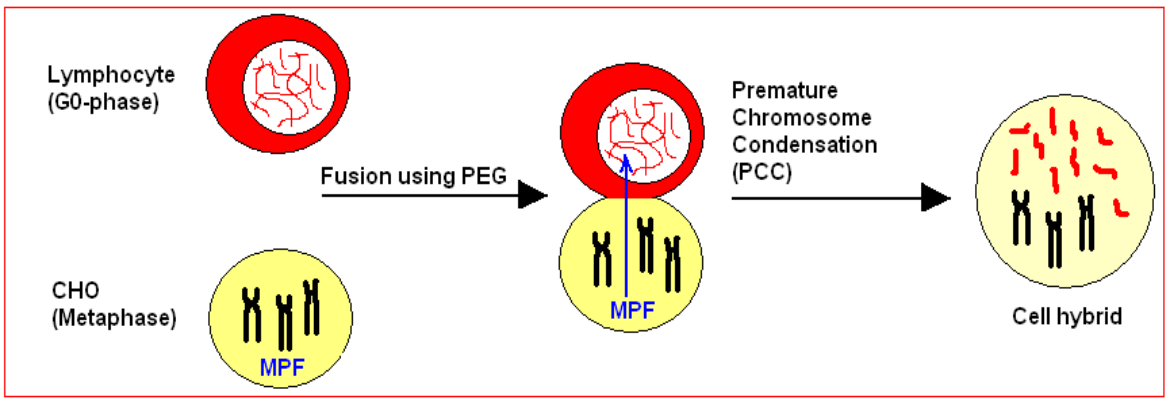

Figure 1.12. The presence of Mitosis-Promoting Factors (MPF) in the hybrid cells dissolves the nuclear membrane of interphase lymphocytes and condenses their diffuse chromatin into distinct chromosomes, enabling thus their visualization.

Chapter 2: Automated Analysis of PCC Spreads and Acquisition of Images Can Increase the Throughput of the micro-PCC Assay for Prompt Individualized Absorbed Dose and Risk Assessment in the Event of Accidental Overexposure

2.1. Introduction

Following a large-scale radiological event, hundreds or thousands of people could have been potentially exposed to unknown and variable doses of radiation. It is a high priority, therefore, to use biomedical tools, sensitive biomarkers and automatable methods in order to reflect promptly the biological importance of the radiation exposure [27,49,52]. At present, it is estimated that the throughput of a cytogenetic laboratory is a few tens of samples per day and even large cytogenetic laboratory networks can only analyse a few hundred of samples per day [53–55]. For large-scale incidents, rapidity and ease of screening are essential in order to obtain quick radiological dose and risk assessments [8]. This will enable categorization of individuals according to the degree of their exposure and, subsequently, identification of those who need medical assistance, which is essential for optimal post-exposure management [56–58]. Towards this goal, two main approaches of biodosimetry, biologically-based and physically-based, have been developed and essentially three criteria are minimally necessary for an effective biodosimetric technique: the dose can be assessed promptly after-the-fact; the technique can assay at the level of an individual; and the technique can provide information sufficient to determine what actions should be taken for that individual [9].

Biologically-based biodosimetry approaches are based on biological processes or biomarkers that can be affected by ionizing radiation allowing thus a dose of radiation to be estimated. The status and suitability of current biomarkers for radiation exposure have been reviewed recently [59–62]. Particularly, cytogenetic biomarkers are the most widely used and, at present, several well-established biological dosimeters exist. They can offer accurate dose estimates but, are both time-and labour-consuming and therefore not ideal for use in radiological mass-casualty scenarios where short turnaround times and high throughput are of prime importance [57]. When an ideal biomarker is used for early triage biodosimetry in radiological events, the collection of the required biological samples from the potentially exposed individuals should be easy and non-invasive, while the procedures involved for dose and risk assessments should be rapid and automatable. The latter will pave the way to the subsequent automation of the assay's workflow so that it could be used in the event of a large-scale radiological emergency. The state-of-the-art advances in radiation biodosimetry for mass casualty events involving radiation exposure have been also reviewed recently [22,63].

Among the different cytogenetic assays used for triage biodosimetry and the estimation of absorbed doses in exposed individuals, the dicentric chromosome (DC) assay remains the most widely used. The DC assay is essentially based on the analysis of dicentrics and centric ring chromosomes present in the peripheral blood metaphase lymphocytes of the exposed individuals. Nevertheless, this assay has a significant drawback with respect to the time needed to obtain dose estimates for rapid decision on the right line of medical treatment. It requires culturing of peripheral blood T-lymphocytes for two days before allowing the analysis of chromosomes at metaphase. Hence, it fails the requirement of rapid dose estimation, which is a high priority in radiation emergency medicine.

On the other hand, it is noteworthy that following radiation-induced DNA damage and the enzymatic repair processing of the lesions, which depend on the quality of radiation and the complexity of DNA damage [64], chromosomal rearrangements in the nuclei of blood lymphocytes are well known to be formed within 8h post-irradiation, without requiring blood culture, T-lymphocyte stimulation and DNA replication for their formation. Following accidental exposure, the biomarkers of exposure i.e. dicentric and centric ring chromosomes as well as residual chromosomal fragments, will be present, therefore, as single chromatid chromosomes in the blood lymphocytes by

the time the blood samples reach a reference Biodosimetry Laboratory for dose estimation. Consequently, rapid dose and risk estimates can be achieved by taking advantage of the unique features of cell fusion mediated premature chromosome condensation (PCC) in blood lymphocytes for biological dosimetry [50,65,66]. This phenomenon enables visualization, analysis and quantification of chromosomal aberrations directly in unstimulated G_0-peripheral blood T- as well as B-lymphocyte prematurely condensed chromosomes (PCCs), without requiring a two-day blood culture [67–69].

In the present study, the main objective is to explore the applicability of the PCC phenomenon in order to devise an automatable micro-PCC assay using very small blood sample volumes of 100μl and 96-well plates to obtain rapid dose estimates and risk assessments for the categorization of a large number of individuals according to the degree of their exposure. For high-throughput triage biodosimetry there are previous interesting attempts using other cytogenetic assays [70–74] including chemically-induced PCCs in G_2-phase cultured lymphocytes [75]. Here cell fusion-mediated induction of PCCs in non-stimulated G_0-phase lymphocytes is used, and for the standardization of the proposed micro-PCC assay the morphology of the lymphocyte PCCs obtained for non-irradiated and irradiated blood samples was first compared to those obtained using the conventional PCC assay. Subsequently, appropriate calibration curves for dose assessments were constructed, while the applicability and reliability of the micro-PCC assay was compared to the conventional DC assay, through the evaluation of speed of analysis and minimum number of cells required to be analyzed for each method. The development and standardization of such a micro-PCC assay for high-throughput analysis could pave the way to its subsequent automation, which is critically needed for timely triage biodosimetry in mass-casualty radiological emergencies.

2.2. Materials and Methods

2.2.1. Blood Samples, Irradiation Conditions and the Conventional DC Assay

Peripheral blood samples in heparinized tubes were obtained from healthy donors and used after their informed consent, according to our institutional ethics procedures. Irradiation of whole blood samples was carried out in vitro using a Co-60 Gamma Cell 220 irradiator (Atomic Energy of Canada Ltd., Ottawa, Canada) at room temperature and at a dose rate of 20 cGy/min. Different irradiation times were applied in order to administer to the whole blood samples doses ranging from 0.5 to 6 Gy. Subsequently, irradiated blood samples were processed according to the experimental design and, for comparison purposes, radiation-induced chromosomal aberrations were visualized and quantified by applying the conventional DC assay, the conventional PCC assay, as well as the micro-PCC assay.

For the conventional DC assay, whole blood cultures were set up by adding 0.5 ml of whole blood to 5ml of RPMI-1640 medium (Gibco) supplemented with 10% fetal bovine serum (FBS), 1% phytohemagglutinin (PHA), 1% glutamine and 1% antibiotics (penicillin, streptomycin). Cultures were then incubated at 37°C in a humidified atmosphere with 5% CO2. After 48-50h at 37°C, cell cultures were harvested, treated with hypotonic solution KCl (0.075 M) and fixed with methanol:glacial acetic acid (3:1, v/v), following standard cytogenetic procedures with centrifugation at 250g. Chromosome spreads were prepared, slides were air-dried and stained with 3% Giemsa solution. Only metaphases with 46 centromeres were analyzed and for the irradiated samples, the yield of dicentric plus centric ring chromosomes was obtained for each experimental point using light microscopy and appropriate image analysis system (Ikaros MetaSystems).

2.2.2. Preparation of the PCC-inducer Mitotic CHO Cells

Chinese hamster Ovary (CHO) cells were grown in McCoy's 5A (Biochrom), culture medium supplemented with 10% FBS, 1% l-glutamine and 1% antibiotics (Penicillin, Streptomycin), incubated at 37 °C in a humidified atmosphere with 5% CO2. CHO cultures were maintained as exponentially growing monolayer cultures in 75 cm^2 plastic flasks at an initial density of 4 x 10^5 cells/flask. For optimizing harvest of mitotic cells via cell synchronization, routinely the cells in a flask were allowed

to grow until confluence and subcultured equally into three new 75 cm^2 plastic flasks. Following a 24-30h incubation at 37 °C, Colcemid (Gibco) at a final concentration of 0.1 μg/ml was added to CHO cultures for 4 hours and the accumulated mitotic cells were harvested by selective detachment. Once a sufficient number of mitotic cells had been obtained, they were used as supplier of mitosis promoting factors (MPF) to induce PCC in human lymphocytes by both the conventional and the micro-PCC assay.

2.2.3. Conventional Cell Fusion-Mediated Induction of Premature Chromosome Condensation

Human lymphocytes were separated from heparinized irradiated whole blood samples using Biocoll separating solution (Biochrom). The blood sample was diluted 1:2 in RPMI-1640 without FBS, and was carefully layered on top of an equal amount of Biocoll in a test tube before centrifugation at 400g for 20 min. Collected lymphocytes were washed with 10 ml culture medium, centrifuged at 300g for 10 min and kept in culture medium (RPMI-1640 supplemented with 10% FBS, 1% glutamine and antibiotics) to be mixed and fused with mitotic CHO cells. When the conventional PCC assay is applied, the mitotic CHO cells harvested from a 75 cm^2 flask were used for 2-3 fusions using lymphocytes isolated from 1-2ml of blood for each experimental point. The conventional procedure for cell fusion mediated PCC-induction in non-stimulated G_o lymphocytes was carried out as described earlier [67,69,76].

2.2.4. The Micro-PCC Assay Using Very Small Blood Volumes and 96-Well Plates

The various steps of the conventional PEG-mediated cell fusion and PCC induction mentioned above were adapted for the development of a micro-PCC assay that could be applied to the very small blood volumes of 100μl using 96-well plates of 2ml per well. Briefly, whole blood samples of 100μl for each experimental point were transferred to each well in 96-well plates and 1.5ml of cold red blood cell (RBC) lysing solution of ammonium chloride was added for 10 min. For the preparation of lysing solution, 8.02g ammonium chloride, 0.84g sodium bicarbonate and 0.37g disodium EDTA were dissolved in 1lt of distilled water. The RBC lysing solution is used as an alternative to the Biocoll gradient required by the conventional PCC assay for the separation of lymphocytes from whole blood before their fusion to the mitotic CHO cells.

Following centrifugation of the 96-well plates at 200g for 6min, the supernatants were discarded all at once and 1.5ml of mitotic CHO cells ($2x10^5$ cells) in serum-free RPMI-1640 medium with Hepes (25mM) and colcemid (0.1μgr/ml) was added to the lymphocyte pellet in each well. Subsequently, the plates were centrifuged for 6min at 200g and supernatants were discarded without disturbing the cell pellets, keeping the plate inverted on a paper towel to drain well the pellets from excess liquid. Immediately after the plates were turned in up-right position and 100μl of 45% (w/v) PEG (mol wt 1,450, Sigma-Aldrich/serum-free RPMI 1640 with Hepes) was injected into each well and held for about 1 min. Subsequently, 1ml of phosphate buffered saline (PBS) was slowly added to each well of the plate, shaken gently and centrifuged at 200g for 6 min. The supernatants were discarded and 0.3 ml RPMI-1640 complete growth medium containing 2% phytohemagglutinin (PHA) and 10% FBS, was added to each well.

After culturing for 75 min at 37°C, 1.5 ml of hypotonic KCL (0.075 M) was added to each well, and cells were fixed twice (1.5 ml/well) with methanol:glacial acetic acid (3:1 v/v), following standard procedures for chromosome preparation. Fixed cells were resuspended in 50μl of fixative and three microscope slides with chromosome spreads were prepared by dropping 15μl aliquots at the centre of each pre-cleaned slide. Finally, air-dried slides were stained with 3% Giemsa solution in Sorensen's buffer (pH 6.8) and covered with cover slips using Entellan mounting medium. The analysis of PCC spreads on the microscope slides and the quantification of radiation-induced excess chromosomal fragments in lymphocyte PCCs was greatly facilitated by combining light microscopy with image analysis systems (Ikaros, MetaSystems). The various steps required by the micro-PCC assay are summarized in the scheme below presented as Figure 2.1.

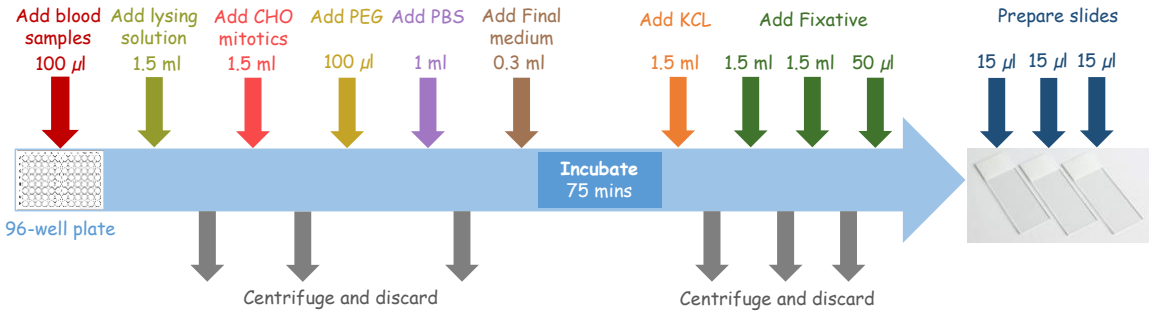

Figure 2.1. Scheme of the automatable micro-PCC assay for simultaneous analysis of 96 individuals. Added volumes refer to each well of the 96-well plate.

2.2.5. Analysis and Scoring Criteria

Lymphocyte PCC spreads were located manually and their analysis was facilitated by the use of a semi-automated image analysis system (Ikaros, MetaSystems). Specifically, the analysis of excess PCC fragments in lymphocyte PCC spreads stained with Giemsa was greatly facilitated by the appearance of the PCCs, which are single chromatid chromosomes and lighter stained than the double chromatid chromosomes of metaphase CHO cells. The lymphocyte PCCs are, therefore, easily distinguished from the darkly stained chromosomes of the PCC-inducer mitotic CHO cells. In unirradiated lymphocytes, 46 single chromatid elements can be scored in the PCC spreads and, in order to calculate the frequency of excess PCC fragments following exposure to ionizing radiation, the number 46 was subtracted from the mean value of lymphocyte PCCs per cell obtained in the irradiated blood samples. Generally, a number of 20-30 PCC-spreads was considered adequate for dose estimation following a single exposure, as we have already shown previously via inter-laboratory accident simulation exercises [76].

2.2.6. Construction of Dose-Response Curves for Dose Assessment Using the Micro-PCC Assay

For dose assessment purposes by means of the micro-PCC assay, three different dose-response calibrations curves were constructed to be used depending on whether the blood samples from potentially exposed individuals are received within 6, 12 or 24 hours post-exposure. Specifically, whole blood samples were exposed *in vitro* to doses of 0, 1, 2, 3, 4, 5, and 6Gy as described earlier, and allowed to repair radiation-induced chromosomal damage for 6, 12 or 24 hours at 37 °C. Subsequently, the blood samples were processed for cell fusion, PCC induction and preparation of slides with lymphocyte PCC spreads as described earlier in this section and summarized in Figure 2.1. The frequencies of excess PCCs per cell for the different doses used were obtained by the analysis of 30 PCC spreads for each experimental point, and mean values ± SD were calculated from two to three independent experiments.

2.3. Results

2.3.1. Development of an Automatable Micro-PCC Assay for Early Triage Biodosimetry

The original protocol for the conventional PCC assay uses 1-2ml blood sample volumes per experimental point, lymphocyte isolation by means of Ficoll-Paque or Biocoll gradients, as well as 15ml round-bottom culture tubes for cell fusion, PCC induction, and chromosome preparation. The various steps of the procedure were adapted successfully towards the development of an automatable micro-PCC assay using blood volumes of only 100µl, and multi-tube racks or 96-well plates of 2ml. In order to comply with the requirements of a high-throughput blood sample collection based on small volumes of around 100µl, we experimented with two methods for lymphocyte isolation, namely the Biocoll separating solution and the ammonium chloride red blood cells lysing

solution. Even though the isolation of lymphocytes by means of Biocoll was feasible, it was time-consuming and less efficient than the ammonium chloride solution, which we adopted.

In this way, the entire procedure including blood sample collection, red blood cell lysis, lymphocyte fusion to mitotic CHO cells, culturing of fused cells for PCC induction, and cell fixation were carried out in a single 2ml well. This improvement reduces the number of sample transfers, minimizes cell loss, and simplifies tracking operations. Our results demonstrate for the first time that lymphocytes isolated from 100μl blood sample via ammonium chloride lysing solution in 96-well plates can be fused with CHO mitotic cells.

2.3.2. Morphology of the Lymphocyte PCCs Obtained Using the Micro-PCC Assay

The morphology of the lymphocyte PCCs obtained with the above micro-PCC procedure is practically identical to that obtained using the conventional PCC assay. It allows, therefore, the analysis of radiation induced excess PCC fragments stained with Giemsa, which is simple, rapid and cost-effective. Interestingly, the use of only 1.5ml of hypotonic solution and the fixation of cells twice with 1.5ml of Carnoy's fixative in 96-well plates of 2ml/well offers high quality PCC images as shown in Figure 2.2. Figure 2.2A presents a typical image of a non-irradiated lymphocyte (46 PCCs), whereas Figures 2.2B and 2.2C enable visualization and quantification of radiation-induced PCC fragments following 0.5Gy (3 excess PCCs) and 2Gy (10 excess PCCs) of Co-60 γ-irradiation, respectively.

(**A**) (**B**) (**C**)

Figure 2.2. Giemsa stained PCCs, obtained by means of the micro-PCC assay, demonstrating 46 single chromatid chromosomes in a non-irradiated lymphocyte (A). Three excess (over 46) PCC fragments can be visualized in an irradiated lymphocyte with 0.5 Gy of Co-60 γ-irradiation (B). Ten excess PCC fragments can be scored following irradiation with 2 Gy (C).

2.3.3. Construction of Appropriate Dose Response Calibration Curves

Following the protocol of the micro-PCC assay described in the previous section, three dose-response calibration curves were constructed using doses of 0 to 6Gy of γ-irradiation, for dose assessment according to the time elapsed from irradiation to sample processing for biodosimetry purposes. Figures 2.3A, 2.3B, 2.3C present these calibration curves for 6, 12 or 24 hours post-exposure repair times, respectively. A comparison of the dose-response curves obtained under the different post-exposure repair times is depicted in Figure 2.3D.

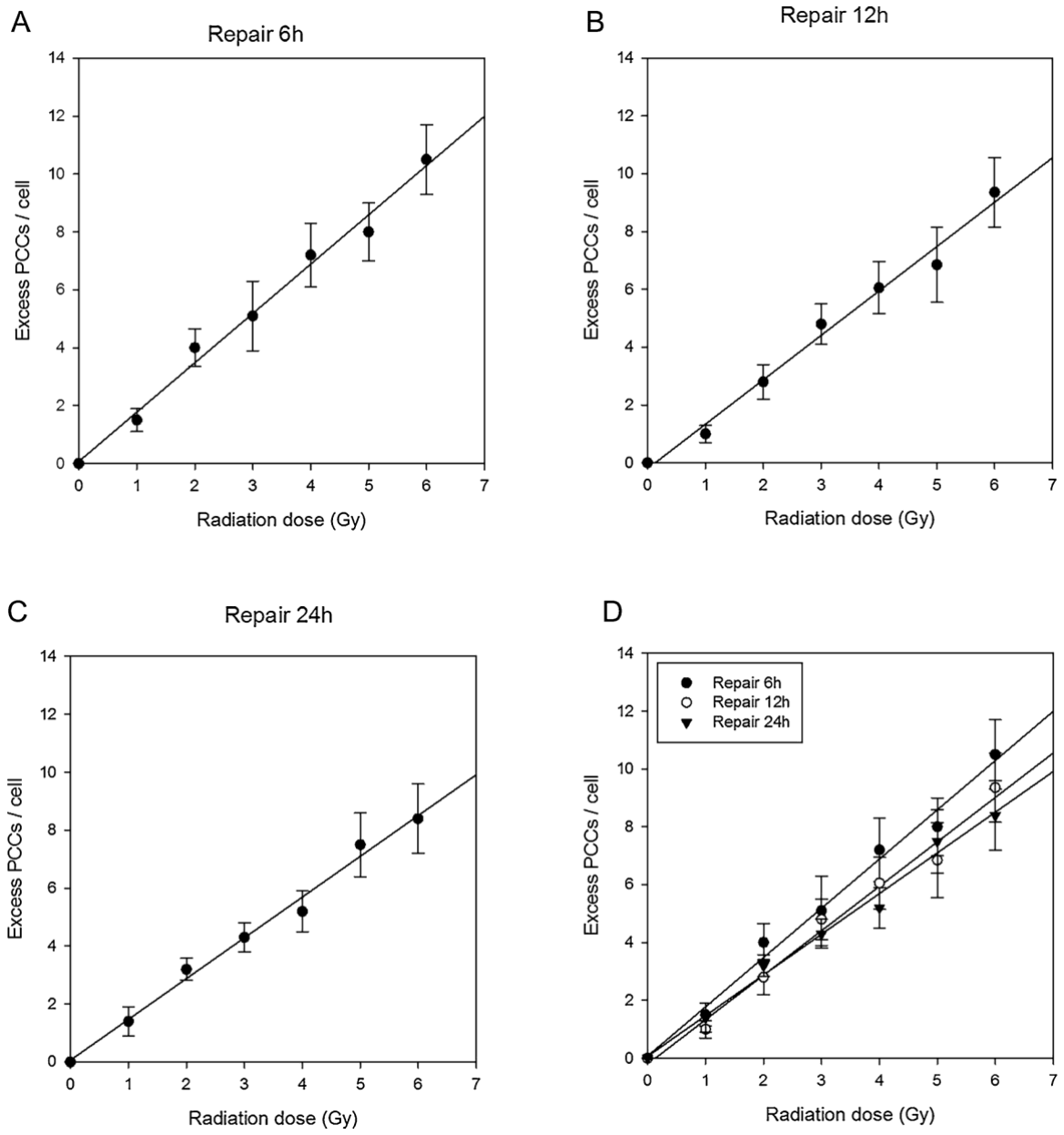

Figure 2.3. Dose-response curves are presented for Giemsa-stained excess lymphocyte PCC fragments per cell for post-exposure repair time of 6 h (Linear, a1 = 1.70 ± 0.08, y01 = 0.075) (A), 12 h (Linear, a2 = 1.54 ± 0.08, y02 = −0.20) (B) and 24 h (Linear, a3 = 1.41 ± 0.06, y03 = 0.06) (C). (D) depicts a comparison of the dose-response curves obtained under the different post-exposure repair times. Mean values ± SD are calculated from three independent experiments.

2.3.4. Dose Estimates by Means of the Micro-PCC and DC Assay

To evaluate the applicability and reliability of the micro-PCC as compared to the conventional DC assay, we examined the speed of analysis and the minimum number of cells required to be analyzed for each method. For this purpose, a simulation of an accident was performed by irradiating blood samples from healthy individuals with doses of 0.5Gy, 1Gy and 2Gy of γ-rays, coded blindly and, subsequently, used for dose estimation by means of the two assays.

Table 2.1 presents the yields of excess fragments in G_0-Lymphocyte PCCs obtained by scoring 10, 20 or 30 cells, while the yields of dicentrics plus centric rings analysed at metaphase were obtained (with a delay of two days due to lymphocyte culturing) by scoring 50, 100, 200 or 300 cells, and are presented in Table 2.2. The results obtained suggest that the analysis of only 20-30 cells by the micro-

PCC assay offers dose estimates with an accuracy that would require the analysis of 200-300 cells by the DC assay.

Table 2.1. Simulated whole body exposure to 0.5, 1 and 2 Gy and dose estimation using the micro-PCC assay for the analysis of Giemsa-stained excess PCC fragments by scoring 10, 20 or 30 PCC spreads in non-stimulated lymphocytes. Mean doses are shown with low- (LCL) and upper- (UCL) confidence limits.

	Analysis of 10Cells					Analysis of 20Cells					Analysis of 30Cells				
			Estimated Dose (Gy)					Estimated Dose (Gy)					Estimated Dose (Gy)		
True PhysicalDose (Gy)	Excess fragms	Excess fragms /cell	Dose	LCL	UCL	Excess fragms	Excess fragms /cell	Dose	LCL	UCL	Excess fragms	Excess fragms /cell	Dose	LCL	UCL
0.5	5	0.5	0.31	0.15	0.49	13	0.65	0.42	0.25	0.60	19	0.63	0.41	0.24	0.58
1.0	11	1.1	0.74	0.56	0.93	23	1.15	0.77	0.59	0.97	42	1.40	0.95	076	1.16
2.0	24	2,4	1.66	1.44	1.90	57	2.85	1.98	1.75	2.23	91	3,03	2.11	1.87	2.36

Table 2.2. Simulated whole body exposure to 0.5, 1 and 2 Gy and dose estimation using the Dicentric plus centric ring (Dic + CR) analysis at metaphase lymphocytes. Mean doses are represented with low- (LCL) and upper- (UCL) confidence limits.

	Analysis of 50Cells				Analysis of 100Cells				Analysis of 200Cells				Analysis of 300Cells			
		Estimated Dose (Gy)				Estimated Dose (Gy)				Estimated Dose (Gy)				Estimated Dose (Gy)		
True Physical Dose (Gy)	Dic + CR	Dose	LCL	UCL	Dic + CR	Dose	LCL	UCL	Dic + CR	Dose	LCL	UCL	Dic + CR	Dose	LCL	UCL
0.5	0	0	0	0.95	1	0.26	0	0.81	3	0.36	0.10	0.70	7	0.47	0.26	0.74
1.0	2	0.66	0.15	1.38	7	0.92	0.54	1.38	18	1.06	0.79	1.37	24	0.99	0.76	1.24
2.0	10	1.65	1.10	2.30	16	1.46	1.07	1.91	44	1.74	1.46	2.04	82	1.96	1.73	2.20

2.4. Discussion

The main goal of biodosimetry is to utilize biological changes caused by ionizing radiation in an individual and use them as biomarkers of exposure in order to estimate the dose received and to predict its clinically relevant consequences. The development of rapid, accurate, and reliable biodosimetry tools has been primarily motivated by the potential need to confront large-scale radiological events. In such cases, it is crucial to be able to identify the exposed individuals who would benefit from receiving urgent medical care.

To this end, it is imperative to set a reasonable cut-off dose of absorbed radiation as a threshold that will allow the categorization of the exposed population. Specifically, for doses below such a cut-off value, countermeasures are not immediately needed and medical treatment would not be expected to impact mortality. On the other hand, for individuals with absorbed doses above the cut-off value, medical treatment would be necessary to improve survival rates. This cut-off is generally set at 2 Gy, yet this threshold could be set higher if the number of affected individuals is beyond the capacity of the available medical facilities [8,53,77–79]. Such biodosimetry screening enables the categorization of the exposed individuals into three categories: those who have suffered radiation injury, for whom immediate medical intervention is vital; those with intermediate exposure close to the threshold cut-off dose, for whom medical intervention is necessary to mitigate the short, medium and long term effects of exposure, and the "worried well" with probable low doses, for whom no deterministic effects are expected but long term monitoring may be required [80].

For timely biodosimetry dose assessments, the 48hour peripheral blood lymphocyte culture required for the standard DC analysis at metaphase remains the major obstacle for rapid dose estimation and the use of the dicentric assay for triage of a population after a mass exposure event. Alternatively, the conventional PCC fusion technique, which is based on the induction of premature chromosome condensation in unstimulated G_0-peripheral blood lymphocytes, allows a rapid

visualization of radiation-induced chromosomal aberrations enabling their analysis. However, the use of this technique for triage biodosimetry has been restricted so far, since it requires 1-2ml blood samples per exposed individual, so that fingerstick blood sampling, which is crucial for large population screening, cannot be utilized.

To overcome this obstacle, we developed in the present work, an automatable micro-PCC assay that is appropriately designed to be suitable for triage biodosimetry to obtain rapid individualized dose estimates in cases of large-scale radiological emergencies or accidental overexposures. Indeed, this new method has the potential to screen fingerstick derived blood samples, in order either to estimate past radiation exposure, or to sort a large number of individuals exposed above or below a pre-set cut-off dose. Compared to the dicentric chromosome assay, which at present is the standard technique for biological dosimetry, our results demonstrate that the micro-PCC assay is quicker as well as reliable and cost effective for early triage biodosimetry. Indeed, Giemsa-stained excess PCC fragments can be visualized for scoring within 2 hours from the moment blood samples are available and dose estimations can be obtained subsequently using the appropriate calibration curves that we have constructed for standardization purposes of this assay.

Specifically, we have introduced for the first time the use of blood samples of 100μl for PCC induction in 96-well plates. Interestingly, the morphology of the lymphocyte PCCs so obtained is practically identical to that obtained using the conventional PCC assay. This innovation in the PCC protocol has two main advantages for its use in early triage of radiation emergencies involving large populations, as such very small amounts of blood need to be sampled together with the use of the 96-well plates, allowing thus a fast and reliable triage of many individuals simultaneously. Indeed, the analysis of only 20-30 lymphocyte PCC spreads are sufficient to obtain reliable dose estimates, as presented in Table 2.1. This is because the analysis is based on radiation-induced chromosomal fragments in excess of 46 PCCs. This number of 46 PCCs constitute the human genome, which is remarkably stable in healthy individuals. This allows to link every single excess fragment above 46 to radiation exposure. In contrast, using the conventional DC analysis at metaphase, radiation-induced dicentric chromosomes are rare, especially at low doses, and therefore many more cells must be analysed for reliable dose assessment. Therefore, the micro-PCC technique has the potential to deliver data for dose assessment in a significantly shorter period of time than any other biological assay being used currently, as only few lymphocyte PCC spreads need to be analysed in order to detect exposed individuals, in agreement with previously reported results [76]. Indeed, the results presented in Table 2.1 and Table 2.2 suggest that the analysis of only 20-30 cells by the micro-PCC assay offers dose estimates with an accuracy that would require the analysis of 200-300 cells by the DC assay.

While overexposed individuals are identified and categorised using the micro-PCC assay through the analysis of Giemsa stained excess lymphocyte PCCs, centromeric and telomeric staining could be applied to lymphocyte PCCs using PNA probes and the FISH technique (C/T-PCC-FISH) for the accurate scoring of dicentric and centric ring chromosomes. This additional analysis would permit the reliable detection of all unstable chromosomal aberrations in lymphocyte PCCs with high level of precision and sensitivity, as we have previously reported [66,67]. Therefore, it can be carried out in order to confirm doses in the overexposed individuals only, given that it is quite an expensive procedure. Additionally, in the event of an accident, the micro-PCC assay combined with C/T FISH staining for the accurate scoring of dicentric and centric ring chromosomes in Go-lymphocyte PCCs, would enable further evaluation of exposed individuals into treatment-level categories.

To conclude, the micro-PCC assay developed in this work has the potential to deliver data for dose assessment in a significantly shorter period of time than any other cytogenetic assay currently being used, as it does not require lymphocyte culture and only a few cells need to be analysed in order to detect exposed individuals. In addition, this automatable assay has the potential to discriminate between whole- and partial-body exposure, based on the frequency between damaged and not damaged lymphocytes encountered in the PCC spreads, as we have previously demonstrated for the conventional PCC assay [76]. Indeed, when all the analysed lymphocyte PCCs exhibit chromosomal damage, whole body exposure is confirmed, which is valuable for designing the

treatment of individuals exposed to life threatening doses of radiation. Finally, the analysis of Giemsa-stained excess PCC-fragments using the micro-PCC assay is a simple and cost-effective biodosimetry tool that enables the rapid estimation of absorbed doses within 2-3hours. The automation of the micro-PCC assay remains a challenge for the near future as it would increase its throughput and scoring objectivity.

Chapter 3: Chromosomal Rearrangements Analyzed in G_0-Lymphocyte PCC Spreads Using mFISH Technique as Potential Biomarkers for Early Biodosimetry and Retrospective Assessment of Radiation-Induced Effects

3.1. Introduction

Exposure to ionizing radiation (IR) can adversely affect human health including mortality from acute radiation syndrome with a LD50/30 value of 3.5 Gy-4.5 Gy without treatment and 6.5 Gy- 7.5 Gy with appropriate therapy. Therefore, it is imperative to determine the absorbed radiation dose to initiate appropriate medical countermeasures. Bender and Gooch (1962) reported for the first time that the detection of dicentric chromosomes (DCs) in peripheral blood lymphocytes can be reflective of the absorbed radiation dose in exposed humans. Since then, Dicentric Chromosome Assay (DCA) has been routinely used for radiation dose assessment of either occupationally or accidentally exposed humans. DCA was effectively utilized in the past for radiation dose assessment in the victims of many well-known accidents such as Chernobyl [81–83], Goiania [84–86] and Fukushima-Daiichi [87–89]. The conventional DCA requires the stimulation of T-lymphocytes *in vitro* by Phytohaemagglutinin-M (PHA-M) for at least 48 hrs with an additional time of 24-48 hrs for cell fixation, DC analysis and radiation dose estimation. Although DCA is considered as the gold standard for radiation dose assessment, its labor-intensive and time-consuming nature make DCA largely unsuitable for mass casualty incidents. Rapid individualized dose assessment is an absolute requirement for segregating people with moderate or high radiation exposure from non-exposed but "worried well" population so that individuals who need urgent care can be prioritized for treatment.

Several efforts have been continually made to reduce the turnaround time for DCA: (I) optimization of chromosome preparation [90], (II) automated dicentric chromosome scoring [91–98], (III) sample tracking [99], (IV) establishment of network for cytogenetic biodosimetry laboratories [53,54,100], (V) data generation through electronic scoring of digital images [101–104] and a triage mode of scoring either 50 cells or 30 dicentrics [105–107]. Although these efforts significantly reduce the turnaround time for dose estimation, *in vitro* culturing of lymphocytes for 48 hrs is still inevitable for performing the conventional DCA. Further, sensitivity of lymphocytes to high doses of IR is yet another confounding factor that restricts the use of DCA in certain situations where radiation exposure exceeds 5 Gy. To overcome the technical limitations of DCA, Prematurely Condensed Chromosome (PCC) technique [fusion of non-stimulated G_0 lymphocytes with Chinese Hamster Ovary (CHO) mitotic cells; hereafter referred as G_0 PCC] was used for analyzing IR induced chromosomal aberrations [50,108,109]. The main advantage of using the PCC technique is that it enables chromosome aberration analysis instantaneously by alleviating the need for lymphocyte stimulation *in vitro* for 48 hrs. The PCC technique was effectively used in an earlier study for estimating the radiation dose from the frequency of excess chromosome fragments and rings [109]. The PCC technique was also utilized for detecting partial and whole body exposure of non-human primates [110]. One drawback of the PCC technique is that the centromeric regions are not readily detectable by conventional Giemsa staining technique. Initially, Pantelias et al. [65] used the centromeric heterochromatin banding technique (C-banding) for analyzing the frequency of IR induced dicentric chromosomes. Subsequently, the fluorescence *in situ* hybridization (FISH) technique was employed using DNA probes specific for human centromeres and telomeres for DC detection in PCCs obtained from non-stimulated lymphocytes [67,111,112]. Karachristou et al. [67] demonstrated the utility of PCC-FISH technique for triage biodosimetry by constructing a dose response curve up to 10Gy of γ-rays. An inter-laboratory comparison study on PCCs was recently undertaken within the RENEB (Realizing the European NEtwork of Biodosimetry) network of laboratories in Europe to improve the harmonization, standardization and optimization of the PCC assay for biological dosimetry [76].

The PCC technique is distinctly advantageous over the conventional DCA because it can be performed instantaneously after blood collection without the need for lymphocyte stimulation. In contrast to conventional DCA which is routinely applied to the analysis of T-lymphocytes, PCC technique offers the flexibility of assessing radiation induced chromosomal aberrations in both T- and B-lymphocytes simultaneously. When lymphocytes are exposed to high radiation doses (> 5Gy), many heavily damaged lymphocytes may either die or may not even reach mitosis resulting in an erroneous dose estimation when assayed by the conventional DCA. As the PCC assay does not involve *in vitro* lymphocyte proliferation, high radiation exposure exceeding 5 Gy is not a constraint for chromosome aberration analysis. Despite these advantages, the PCC technique is not quite widely used for biodosimetry. In the current study, we have evaluated and expanded the applicability of G_0 PCCs for detecting different types of IR induced interchromosmal and intrachromosomal aberrations by multicolor FISH (mFISH) and multicolor band (mBAND) techniques. Our study indicates the potential of using the PCC-FISH technique in detecting a wide variety of stable and unstable chromosomal aberrations for **early radiation biodosimetry and retrospective assessment of radiation-induced effects**.

3.2. Materials and Methods

3.2.1. Collection and Irradiation of Human Blood Samples

Peripheral blood samples in heparinized tubes were obtained from healthy male and female donors and used after their informed consent, according to our institutional ethics procedures. Irradiation of whole blood samples was carried out *in vitro* using a Co-60 Gamma Cell 220 irradiator (Atomic Energy of Canada Ltd., Ottawa, Canada) at room temperature and at a dose rate of 0.2 Gy/min. Blood samples were exposed for different times to deliver doses ranging from 1 to 6 Gy. Blood samples, after irradiation, were allowed to repair at 37°C either for 2 hrs or 6 hrs and subsequently processed for cell fusion and PCC induction. Sometimes, male and female lymphocytes isolated after irradiation were mixed for cell fusion and PCC generation. X-rays irradiation (RS 2000; RAD Source, 0.3mm copper filter that allows 160kV operation at 25mA; dose rate 2 Gy/min) of whole blood samples was performed using the X-ray irradiator at the University of Tennessee Knoxville, TN, USA. G_0 PCCs after X-rays exposure were prepared at 2 hrs of post-recovery time at the Cytogenetic Biodosimetry Laboratory (CBL), Oak Ridge, TN.

3.2.2. Preparation of the PCC-inducer Mitotic CHO Cells

Chinese hamster Ovary (CHO) cells were grown in McCoy's 5A (Biochrom) medium supplemented with 10% FBS, 1% L-glutamine and 1% antibiotics (Penicillin, Streptomycin) at 37 °C in a humidified atmosphere with 5% CO2. CHO cells were maintained as exponentially growing monolayer cultures in 75 cm^2 plastic flasks at an initial density of 4×10^5 cells/flask. For optimizing the harvest of mitotic cells via cell synchronization, cells were allowed to grow until confluence and sub-cultured equally into three new 75 cm^2 plastic flasks. Following 24–30 h of incubation at 37 °C, Colcemid (GIBCO, Life Technologies Corporation, Grand Island, NY) at a final concentration of 0.1 μg/ml was added to CHO cultures for 4 h and the mitotic cells were harvested by selective detachment. Once a sufficient number of mitotic cells had been obtained, they were used as supplier of mitosis promoting factors (MPF) to induce PCC in human G_0 lymphocytes. Alternatively, the harvested mitotic CHO cells can always be stored as frozen stocks to be used for PCC induction in G_0 lymphocytes whenever needed.

3.2.3. Cell Fusion-mediated Induction of Premature Chromosome Condensation in Lymphocytes

Lymphocytes from control and irradiated cells were isolated from whole blood using Biocoll separating solution (Biochrom, Berlin, Germany). The blood samples diluted 1:2 in RPMI-1640 without FBS were carefully layered on top of equal amounts of Biocoll in 12 ml test tubes and centrifuged at 400x g for 20 min. Collected lymphocytes from each tube were washed with 10 ml of culture medium (RPMI-1640 supplemented with 10% FBS, 1% glutamine and antibiotics), centrifuged

at 300x g for 10 min and kept in culture medium before fusing them with mitotic CHO cells. The mitotic CHO cells harvested from a 75 cm^2 flask were used for 2–3 fusions using the lymphocytes isolated from 1ml of whole blood sample for each experimental point.

Cell fusion and PCC induction were performed using 45% polyethylene glycol (PEG, p5402 Sigma–Aldrich, St. Louis, MO) in serum-free RPMI-1640 medium with HEPES. Lymphocytes and mitotic CHO cells were mixed in serum-free RPMI-1640 medium in a 12 ml round-bottom culture tube in the presence of colcemid. After centrifugation at 1000 rpm for 8 min, the supernatant was discarded without disturbing the cell pellet, keeping the tubes always inverted in a test tube rack on a paper towel to drain the pellet from excess liquid. While holding the tubes in an inverted position, 0.15 ml of PEG was injected forcefully against the cell pellet using a micropipette, and immediately after the tube was turned in an upright position and held for about 1 min. Subsequently, 1.5 ml of PBS was slowly added to the tube with gentle shaking and the cell suspension was centrifuged at 1000 rpm for 8 min. The supernatant was discarded and the cell pellet was suspended gently in 0.7 ml RPMI-1640 complete growth medium with HEPES containing PHA and colcemid. The tubes were incubated for 75 min at 37°C for the completion of cell fusion/PCC induction. Cells were then treated with hypotonic KCl (0.075 M) and fixed with two changes of methanol: glacial acetic acid (v/v 3:1). The chromosome spreads were prepared by the standard air-drying technique and slides were stained using 3% Giemsa in Sorensen buffer solution for PCC analysis. G_0 lymphocyte PCCs appear as single chromatid chromosomes and can be easily distinguished from CHO metaphase chromosomes, which have two chromatids per chromosome. Alternately, the slides were subjected to fluorescence *in situ* hybridization (FISH) for detecting both unstable (dicentric chromosomes) and stable (translocations and inversions) chromosomal aberrations induced by IR. Cell fusion after X-rays exposure was performed at the CBL, Oak Ridge using both PEG and Sendai virus (HVJ) Envelope Cell Fusion Kit (Cosmo Bio, Carlsbad, CA) following the manufacturer's instructions.

3.2.4. Fluorescence In Situ Hybridization (FISH), Multicolor FISH (mFISH) and multicolor BAND (mBAND)

Procedure for the fluorescence *in situ* hybridization (FISH) technique using peptide nucleic acid (PNA) based human telomeric and centromeric DNA probes was essentially the same as described in our previous studies [113,114]. A cocktail of probe specific for human chromosomes 1, 2 and 4 was obtained from MetaSystems and the FISH procedure using this probe was performed essentially as described by the manufacturers. The mFISH technique was performed essentially as described before [113]. Briefly, slides were treated for 1 min with 0.001% acidic pepsin solution (0.01N HCl) at 37°C for 1-2 min followed by two washes of 5 min each in phosphate-buffered saline. The slides were post-fixed for 10 min in a solution of formaldehyde/$MgCl_2$ (1% formaldehyde/50mM $MgCl_2$ in PBS). The slides after denaturation (2X SSC at 70°C for 20 min and after cooling to ambient temperature 1 min in 0.07N NaOH) were dehydrated in graded series of ethanol (30%, 70%, 90% and 100%) and air dried. The mBAND probe was denatured separately by incubation at 75°C for 5 min followed by incubation at 37°C for 30 min to allow the annealing of repetitive DNA sequences. An aliquot of 10µl probe was placed on the slide and covered with a coverslip. The slides were kept in a humidified hybridization chamber at 37°C for at least 72hr. The unbound probe was removed by washing the slides in pre-warmed (75°C) 1X SSC (pH 7.0-7.5) for 5 min followed by incubation in 4XSSCT (4X SSC with 0.1% Tween 20) for 5 min. Indirectly labeled probe (Cy5), if needed, was amplified by incubation with antibodies (biotinylated anti-streptavidin and Cy5 conjugated streptavidin; Invitrogen, Carlsbad, CA, USA) sequentially for 30 min followed by two washes of 3 min each in 4XSSCT and in PBS. The nuclei were counterstained with DAPI (Vectashield Laboratories, Burlingame, CA, USA). Images were captured using the Zeiss epifluorescence microscope. Image analysis was performed using the ISIS software (MetaSystems, Boston, MA, USA) essentially according to the published procedure. Normal and aberrant chromosomes were identified by unique chromosome specific processed color generated by the ISIS software based on pixel intensities of combinatorial labeling of the five fluorochromes (FITC, Spectrum Orange, Texas Red, DEAC and Cy5). Human chromosome 5 specific multicolor BAND was obtained from MetaSystems. Procedures for hybridization, post-

hybridization washes and detection were essentially the same as described for mFISH. Intrachromosomal aberrations were scored using the ISIS software. Fluorescently labeled gene specific probes sets were purchased from CytoCell, Lincolnshire, IL, USA. The frequencies of chromosomal aberrations are expressed as mean with lower and upper confidence limits at 95% interval.

3.3. Results

The G_0 PCC-FISH technique is distinctly advantageous because the turnaround time for radiation dose assessment is reduced 12-fold (6-8 hrs after the receipt of blood samples) relative to 72-96 hrs by the conventional DCA. Previous studies on G_0 PCC have focused mainly on dicentric chromosomes for radiation dose assessment [65–67]. The current study was undertaken to determine the applicability of PCC-FISH technique for detecting both inter- and intrachromosomal aberrations using a wide variety of multicolor DNA probes.

3.3.1. Detection of Dicentric Chromosomes by Centromere/Telomere FISH after γ-rays Exposure

As stated before, centromeric regions are not clearly detectable in G_0 PCCs when conventional Giemsa staining technique is used. Therefore, the frequency of dicentric chromosomes was analyzed in the present study by centromere and telomere FISH in G_0 PCCs obtained at 6 hrs after exposure to varying doses of γ-rays (0 Gy, 1 Gy, 2 Gy, 4 Gy and 6 Gy). The frequency as well as the distribution of dicentric chromosomes observed in 50 fused cells for each radiation dose is summarized in Table 3.1. In corroboration with earlier studies, a dose dependent increase in dicentric chromosomes was observed (Mean ± SEM; 0.06 ± 0.03/cell for 1 Gy, 0.14 ± 0.05/cell for 2 Gy, 1.32 ± 0.24 /cell for 4 Gy and 2.48 ± 0.41/cell for 6 Gy) in the PCC spreads. Consistent with the increase in dicentric chromosome number, the total number of chromosome objects (fragments) also increased as a function of radiation dose presumably owing to excess fragments resulting from chromosome breakage. At the highest dose of 6 Gy, the number of excess fragments ranged from 2-12 with mean value of 6.60. Earlier studies [67,68] have demonstrated that the initial yield of fragments was high at 2 hrs after radiation exposure but reached a plateau at 6-8 hrs post-exposure. We compared γ-rays induced dicentric frequencies between G_0 PCC and conventional DCA by the triage mode of scoring (50 cells or 30 dicentrics) and found that the frequencies detected by the two assays were grossly similar for different radiation doses: G_0 PCC (0.06/cell for 1 Gy, 0.14/cell for 2 Gy, 1.32/cell for 4 Gy and 2.48/cell for 6 Gy) and conventional DCA (0.06/ cell for 1 Gy, 0.38/cell for 2 Gy, 1.42/cell for 4 Gy and 2/cell for 6 Gy). It is interesting to note that the dicentric frequency detected by the conventional DCA for 6 Gy was less than that detected by G_0 PCC probably owing to either increased death of severely damaged cells or inability of severely damaged cells to progress to mitosis due to a prolonged cell cycle arrest at G2.

Table 3.1. Detection of dicentric chromosomes in γ-rays irradiated human G_0 PCCs by centromere and telomere FISH.

Dose (Gy)	Cells scored	Distribution of dicentrics							Mean	95% CI
		0	1	2	3	4	5	>5		
0	50	50	0	0	0	0	0	0	0.00	0.00
1	50	47	3	0	0	0	0	0	0.06	0.01–0.11
2	50	45	3	2	0	0	0	0	0.14	0.05–0.23
4	50	12	20	10	6	2	0	0	1.32	0.85–1.79
6	50	6	8	10	14	8	3	1	2.48	1.68–3.28

3.3.2. Detection of Interchromosomal Exchange Events by multicolor FISH after γ-rays Exposure

Although dicentric chromosome detection has been well established in G_0 PCCs, no attempt has been made to determine the feasibility of using G_0 PCCs for detecting stable/symmetrical chromosomal aberrations. We evaluated this feasibility by using a cocktail of fluorescently labeled DNA probes specific for human chromosomes 1 (Texas Red), 2 (fluorescein) and 4 (Both Texas Red

and fluorescein yielding a yellow color). For painting, PCCs prepared at 6 hrs of post-recovery from lymphocytes irradiated with different doses of γ-rays (0 Gy, 1 Gy, 2 Gy, 4 Gy and 6 Gy) were utilized. Color junctions, which are reflective of interchromosomal exchange events involving painted and non-painted chromosomes, were scored in 60-100 cells for each radiation dose (Table 3.2). Representative images with reciprocal translocation and insertion detected by whole chromosome specific cocktail probe are shown in Figure 3.1A. The frequencies of color junctions observed for various doses of γ-rays are shown in Figure 3.1B. The frequency of interchromosomal exchange events showed a dose dependent increase in PCCs prepared after 6 hrs of recovery time (0.01 for 0 Gy, 0.11 for 1 Gy, 0.21 for 2 Gy, 1.35 for 4 Gy and 3.61 for 6 Gy).

Table 3.2. Detection of γ-rays induced inter-chromosome exchange events in prematurely condensed G_0 human chromosomes using whole chromosome specific DNA cocktail probe (Chr. 1, 2 and 4).

Dose (Gy)	Cells scored	Distribution of exchanges							Mean	95% CI
		0	1	2	3	4	5	>5		
0	100	99	1	0	0	0	0	0	0.01	-0.01–0.03
1	100	93	3	4	0	0	0	0	0.11	0.06–0.16
2	67	58	5	3	1	0	0	0	0.21	0.09–0.33
4	100	36	26	20	8	7	2	1	1.35	1.02–1.68
6	85	12	10	13	9	9	8	24	3.61	2.75–4.47

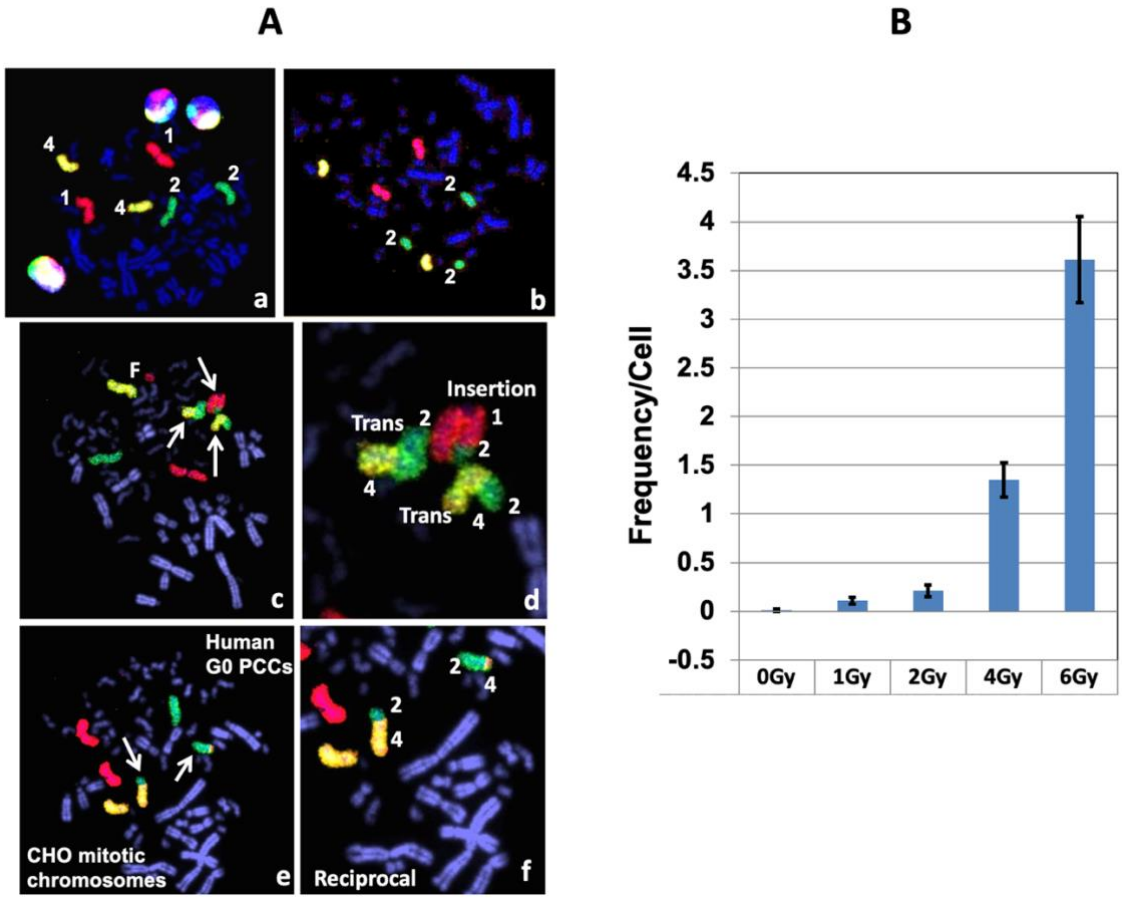

Figure 3.1. (A) Detection of inter-chromosomal exchange events in human G_0 PCCs prepared 6 hrs after exposure to different doses of γ-rays. (a) A cocktail probe specific for chromosomes 1 (red color), 2 (green color) and 4 (yellow color) was used for detection. (b) Detection of chromosome 2 fragment. (c) Detection of reciprocal translocation between painted chromosomes 2 and 4 and an insertion of chromosome 2 on chromosome 1 (arrows). (d) Magnification of the same cell showing reciprocal translocation and insertion. (e) Reciprocal translocation detected between chromosomes 2 and 4 (arrows). (f) Magnification of the same cell shown in e. (B) Frequency of inter- chromosomal exchange events observed at different radiation doses of γ-rays. Mean ± SEM.

Using the mFISH technique, genome wide analysis was performed for the first time in G_0 PCCs to detect IR induced simple and complex chromosome exchange events (translocations). As each of the homologous chromosome pair is color coded, simple and complex translocations can be easily detected. Color junctions, which are reflective of interchromosomal exchange events, were scored in G_0 PCCs prepared at 2hrs (Table 3.3) and 6 hrs (Table 3.4) after exposure to various doses of γ-rays (0 Gy, 1 Gy, 2 Gy, 4 Gy and 6 Gy). Representative images of mFISH karyotypes prepared from mock and 1 Gy γ-rays treated G_0 PCCs are shown in Figure 3.2. The frequencies of chromosome exchanges observed in G_0 PCCs at 2 hrs and 6 hrs post-radiation exposure times are given in Figure 3.3 and Table 3.2. The frequency of color junctions detected in G_0 PCCs did not differ significantly between 2 hrs and 6 hrs for 1 Gy and 2 Gy of γ-rays exposure. However, number of color junctions dramatically increased at 6 hrs relative to 2 hrs for both 4 Gy and 6 Gy doses. The frequency of color junctions observed in G_0 PCCs prepared after 2 hrs of γ-rays exposure was 0.53/cell for 1 Gy, 0.80/cell for 2 Gy, 1.83/cell for 4 Gy and 5.60/cell for 6 Gy while the frequency of color junctions detected in G_0 PCCs after 6 hrs of exposure was 0.60/cell for 1 Gy, 1.27/cell for 2 Gy, 4.10/cell for 4 Gy and 9.20/cell for 6 Gy.

Table 3.3. Multicolor FISH detection of γ-rays induced inter-chromosome exchange events in prematurely condensed G_0 human chromosomes prepared 2 hrs after exposure.

Dose (Gy)	Cells scored	Distribution of exchanges							Mean	95% CI
		0	1	2	3	4	5	>5		
0	30	30	0	0	0	0	0	0	0.00	0.00
1	30	20	5	4	1	0	0	0	0.53	0.22–0.84
2	30	18	5	4	1	2	0	0	0.80	0.39–1.21
4	30	9	5	7	4	2	2	1	1.83	1.03–2.63
6	25	0	0	0	1	4	11	9	5.60	3.23–7.97

Table 3.4. Multicolor FISH detection of γ-rays induced inter-chromosome exchange events in prematurely condensed G_0 human chromosomes prepared 6 hrs after exposure.

Dose (Gy)	Cells scored	Distribution of exchanges							Mean	95% CI
		0	1	2	3	4	5	>5		
0	30	30	0	0	0	0	0	0	0.00	0.00
1	30	19	5	5	1	0	0	0	0.60	0.25–0.95
2	30	16	1	8	1	3	0	1	1.27	0.67–1.87
4	30	2	8	3	2	1	2	12	4.10	2.48–5.72
6	25	0	0	0	1	1	1	22	9.20	5.42–12.98

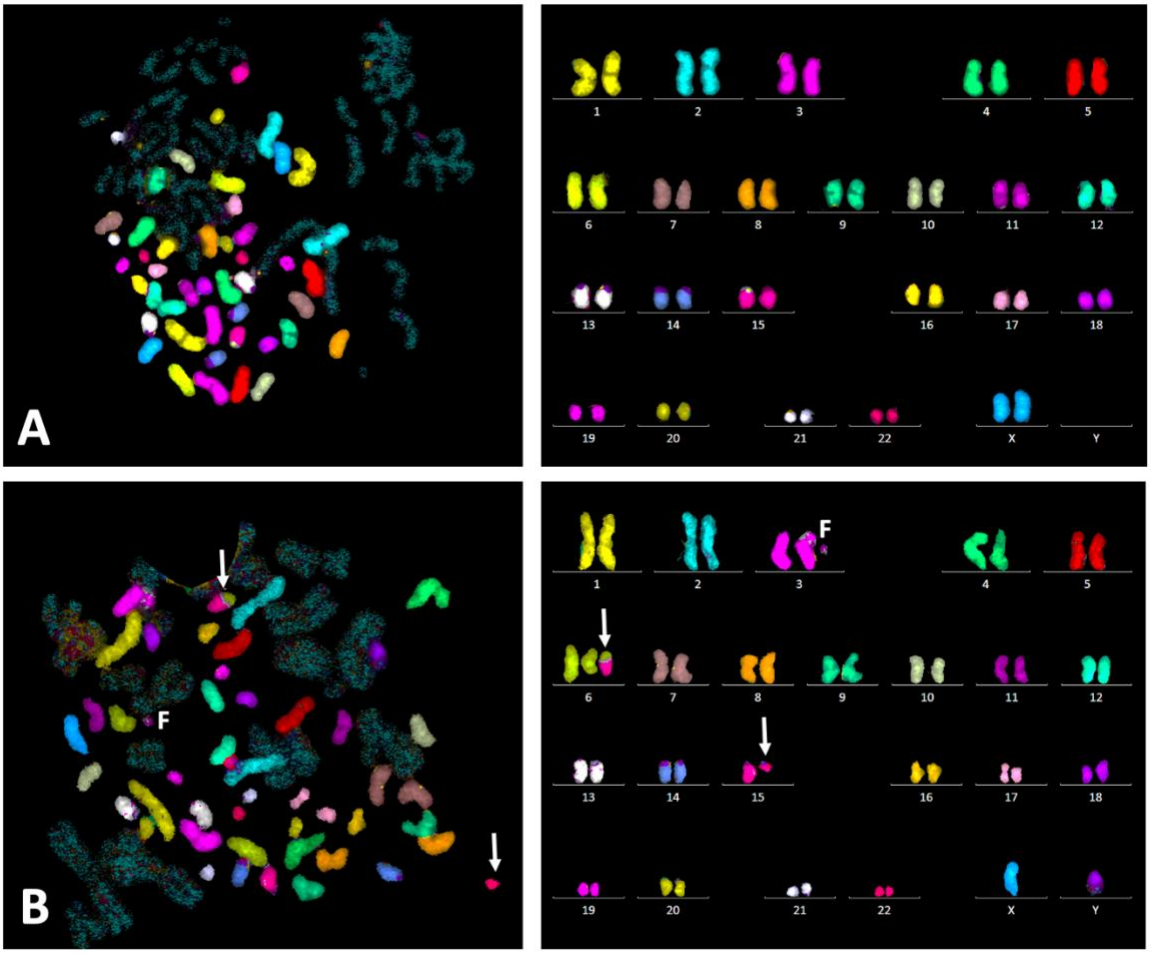

Figure 3.2. Multicolor FISH (mFISH) hybridization of human G_0 PCCs. (A) Normal lymphocyte PCC spread and mFISH karyotype. (B) Abnormal lymphocyte PCC spread (G_0 PCCs prepared 6 hrs after 1 Gy of γ-rays exposure) and mFISH karyotype showing a translocation t(6:15) and a fragment of chromosome 3. Arrows-chromosomes involved in translocation.

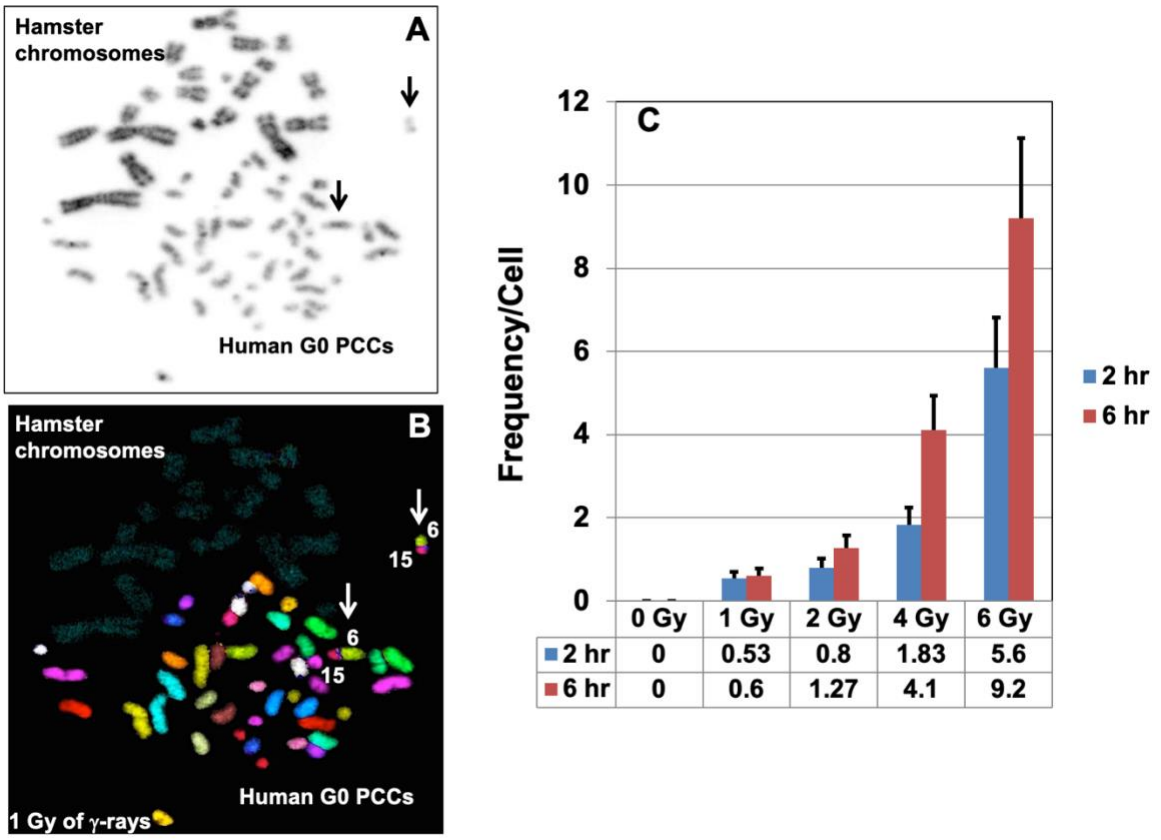

Figure 3.3. Detection of translocations in human G_0 PCCs by mFISH. Note the reciprocal translocation involving chromosomes 6 and 15 (arrows) in G_0 PCCs prepared from 1 Gy γ-rays treated cells at 6 hrs of post-recovery. (A) DAPI counter stained cell shown in grey scale (B) mFISH hybridization pattern of the same cell with a reciprocal translocation involving chromosomes 6 and 15. (C) Frequencies of inter-chromosomal exchanges observed for different doses of γ-rays at different post-recovery times. Mean ± SEM. Arrows-translocated chromosomes.

It is of interest to note that the average number of chromosome fragments in G_0 PCCs showed a decline at 6 hrs for all the radiation doses (46.70/cell for 1 Gy, 47.80/cell for 2 Gy, 49.20/cell for 4 Gy and 54.40/cell for 6 Gy) relative to PCCs prepared at 2 hrs post exposure (47.90/cell for 1Gy, 50.40/cell for 2 Gy, 61/cell for 4 Gy and 68.60/cell for 6 Gy). The decline in the number of painted objects observed in the PCCs at 6 hrs after exposure is probably due to rejoining/mis-rejoining of some of the excess fragments. Similar to the induction of dicentric chromosomes, a dose dependent increase in the number of color junctions was observed by the mFISH technique.

We next determined whether or not IR induced exchange events detected by mFISH occurred randomly or in a chromosome specific manner. The chromosome wide distribution of color junctions observed in the PCCs prepared at 2 hrs and 6 hrs post-recovery are shown in Figure 3.4. In general, the number of color junctions observed for all the chromosomes was more for 6 hr PCCs than 2 hr PCCs without any preferential involvement of specific chromosomes. Interestingly, no color junctions were recorded for chromosomes 5, 12, 19, 20, X and Y for either of the post- recovery times after 1 Gy of γ-rays exposure. Likewise, chromosomes 21 and Y did not involve in any exchange events following 2 Gy exposure at both recovery times. Color junctions involving chromosomes 3, 5 and 6 showed a substantial increase at 6 hrs post recovery relative to 2 hrs after exposure to 6 Gy of γ-rays. The number of cells analyzed (typically 25-30) for each radiation dose and recovery time) was too low for any meaningful statistical analysis.

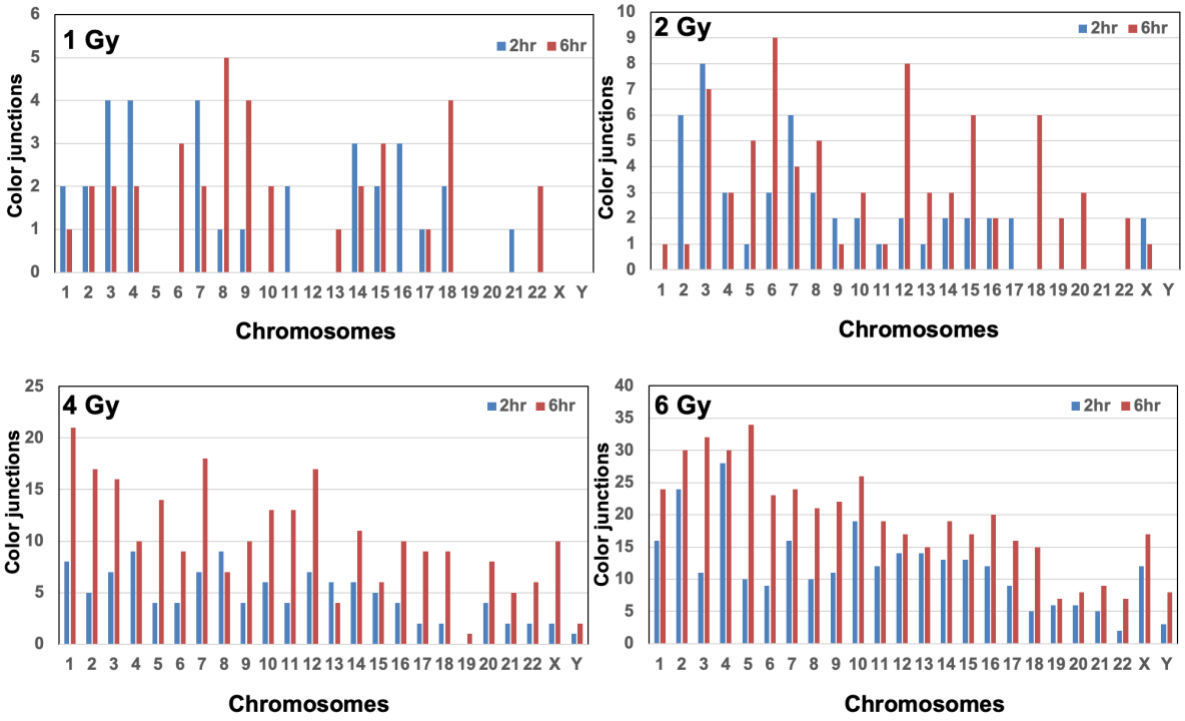

Figure 3.4. Chromosome specific distribution of color junctions detected by mFISH technique in human G_0 PCCs after exposure to varying doses of γ-rays exposure at different post-recovery times (2 hrs and 6 hrs).

3.3.3. Detection of Interchromosomal Exchange Events by Multicolor FISH after X-rays Exposure

Analysis of X-rays induced interchromosomal events was performed on G_0 PCCs using both whole chromosome specific cocktail and mFISH probes. Results obtained on the frequencies of exchanges are shown in Table 3.5. G_0 PCCs were prepared from human lymphocytes 2 hrs after irradiation with different doses of X-rays (0 Gy, 2 Gy and 4 Gy). The frequency of exchanges detected using a cocktail probe specific for chromosomes 1, 2 and 4 was 0/cell for 0 Gy, 0.40/cell for 2 Gy and 0.85/cell for 4 Gy. As expected, genome wide distribution of interchromosomal exchanges detected by mFISH were higher for all the radiation doses (mean ± SE; 0.02 ± 0.02 for 0 Gy, 0.75 ± 0.21 for 2 Gy and 2.10 ± 0.48 for 4 Gy). The results of multicolor FISH for X-rays induced exchange events are shown in Table 3.6. Collectively, we demonstrate that G_0 PCCs can be successfully utilized for detecting interchromosomal exchange events for rapid biodosimetry.

Table 3.5. Detection of X-rays induced inter-chromosome exchange events in prematurely condensed human G_0 chromosomes using whole chromosome specific DNA cocktail probe (Chr. 1, 2 and 4).

Dose (Gy)	Cells scored	Distribution of exchanges				Mean	95% CI
		0	1	2	3		
0	100	100	0	0	0	0.00	0.00
2	65	46	13	5	1	0.40	0.23–0.57
4	60	31	11	12	6	0.85	0.54–1.16

Table 3.6. Detection of X-rays induced inter-chromosome exchange events in prematurely condensed G_0 human chromosomes using multicolor FISH probe.

Dose (Gy)	Cells scored	Distribution of exchanges						Mean	95% CI
		0	1	2	3	4	5		
0	50	49	1	0	0	0	0	0.02	-0.01–0.05
2	28	21	1	2	1	2	1	0.75	0.34–1.16
4	28	8	2	3	10	4	1	2.10	1.16–3.04

3.3.4. Detection of Intrachromosomal Aberrations in G_0 PCCs by mBAND after γ-rays Exposure

Suitability of G_0 PCCs for detecting IR induced intrachromosomal aberrations (inversions, insertions, interstitial and terminal fragments) was next evaluated using chromosome 5 specific mBAND probe. For the detection of intrachromosomal changes, G_0 PCCs prepared at 6 hrs of post-recovery were used. Despite the prematurely condensed nature of G_0 chromosomes, mBAND probe resulted in a reasonably good resolution of bands to enable the detection of intrachromosomal changes (Figure 3.5A-C). The frequencies of total intrachromosomal aberrations on chromosome 5 (chromosome fragments, translocations and inversions) resulting from breaks induced in the p- and q- arms by different doses of γ-rays were scored in a total of 25-50 cells (50 cells for 0 Gy, 2 Gy and 4 Gy and 25 cells for 6 Gy) and the results are summarized in Figure 3.5D. We detected 3 translocations in 4 Gy irradiated G_0 PCCs and 1 inversion in 6 Gy irradiated G_0 PCCs. Although not useful for biodosimetry, mBAND enables the mapping of IR induced chromosome breakage sites and this feature will be particularly useful to determine whether or not certain chromosomal sites are prone to IR induced breaks. A representative lymphocyte PCC spread with a terminal fragment of chromosome 5 is shown in Figure 3.5C. At 2 Gy of exposure, breaks in the p-arm were slightly more than the q-arm but at higher doses (4 Gy and 6 Gy) breaks in the q-arm were substantially higher than the p-arm (Figure 3.5E). Our study indicates the feasibility of using the mBAND technique for detecting IR induced intrachromosomal aberrations in G_0 PCCs.

3.3.5. Detection of Specific Genes on G_0 PCCs

We next evaluated the utility of G_0 PCCs for detecting individual genes. G_0 PCCs obtained from control and X-rays irradiated lymphocytes were probed with gene specific probe sets (c-Myc and IgH and BCR and ABL; Figure 3.6). Recently, we detected γ-rays induced translocation, amplification and gene fusions involving Myc and IgH genes in metaphase chromosomes (unpublished observation). Our demonstration of using gene locus specific FISH on G_0 PCCs holds great promise for evaluating IR induced alterations involving either copy number changes or fusion/fission events at the gene specific level in the future.

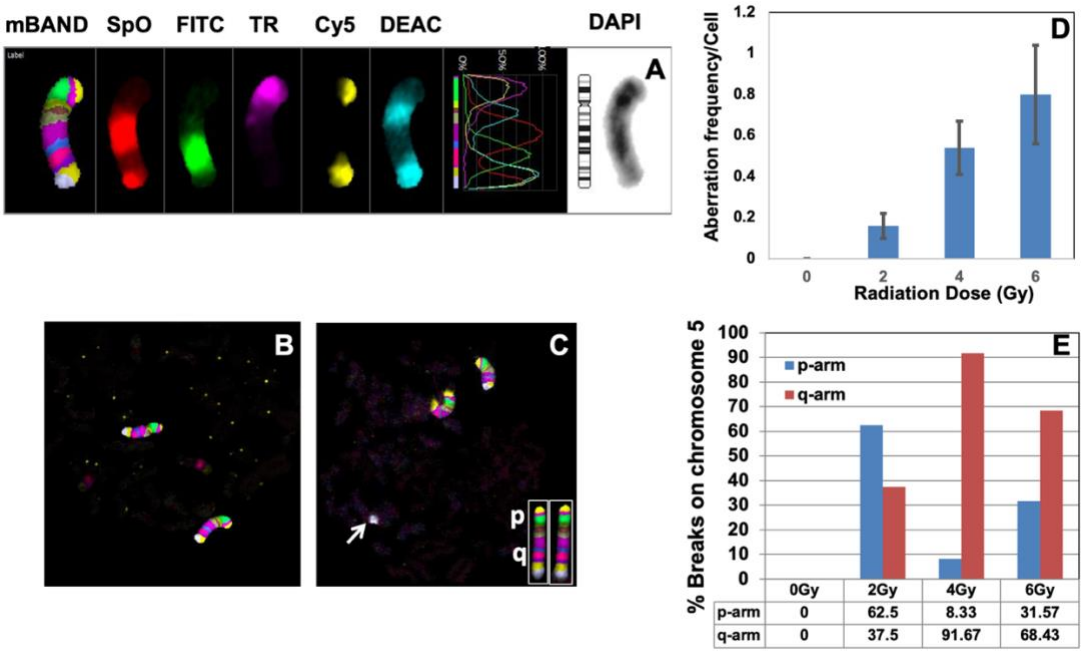

Figure 3.5. Detection of intrachromosomal aberrations in G_0 PCCs using chromosome specific mBAND probe. (A) The hybridization pattern of five different fluorochromes [SpO- Spectrum Orange, FITC-Fluorescein isothiocyanate, TR-Texas Red, Cy5- Cyanine 5 and DEAC-7-diethylaminocoumarin; DAPI (4′, 6-diamidino-2-phenylindole-chromosome counterstain]. Representative G_0 PCCs of control (A) and irradiated (B; 4 Gy of γ-rays) lymphocytes probed with chromosome 5 specific mBAND probe are shown. Note the terminal fragment of one of the chromosomes 5 (arrow) in the irradiated G_0 PCC spread. The hybridization patterns observed in the p- and q-arms of metaphase chromosome 5 are shown in the insert. (D) Frequency of total intrachromosomal aberrations (fragments of p and q arms, translocations and inversions) detected for different γ-rays doses in G_0 PCCs. (E) Frequency of breaks observed in the p- and q-arms of the chromosome 5 detected by mBAND technique. The percentage of breaks observed in the short and long arms of chromosome 5 for different γ-rays doses is shown in the form of histogram. Bars represent SEM.

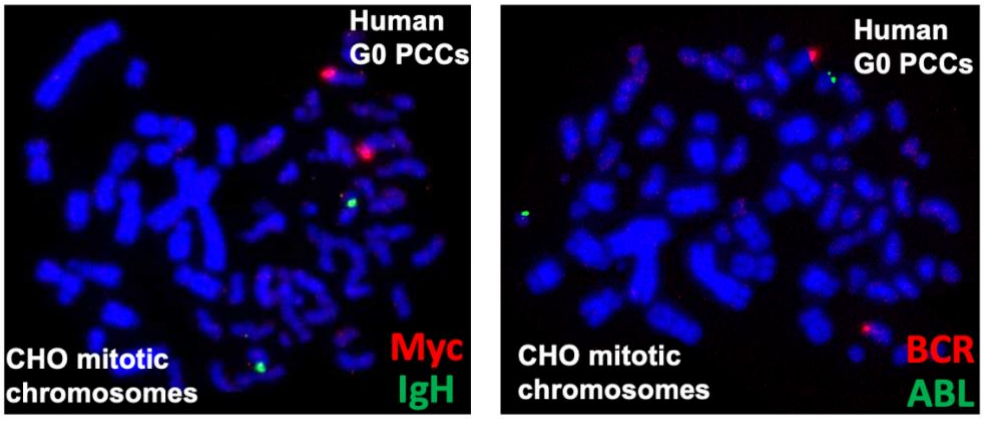

Figure 3.6. Detection of gene loci in G_0 PCCs by FISH using gene specific probe sets. Fluorescently labeled gene probe sets (c-Myc-Texas Red and IgH- Fluorescein; BCR-Fluorescein and ABL-Texas Red) were used for detection. PCCs prepared from 3 Gy X-rays treated lymphocytes were used for detection.

3.4. Discussion

DCA is considered to be the gold standard for radiation dose assessment but it requires proliferation of lymphocytes *in vitro* for 48 hrs to obtain metaphase chromosomes for analysis. Therefore, a turnaround time of 3-4 days is required at minimum for DCA to estimate an individual's absorbed radiation dose. Further, it is somewhat difficult to perform conventional DCA for radiation doses higher than 5 Gy because lymphocytes, owing to their radiation sensitivity, may fail to proliferate or undergo apoptotic death at high radiation doses. Realizing the time-consuming and laborious nature of DCA, an alternative method was developed by preparing prematurely condensed chromosomes in unstimulated human G_0 lymphocytes to detect IR induced chromosomal aberrations. As the PCC assay bypasses the need for lymphocyte proliferation, chromosomal aberrations induced by a wide range of radiation exposures up to 20 Gy can be easily measured within 6-8 hrs of blood collection. PCC assay has been successfully utilized in earlier studies for analyzing IR induced dicentric chromosomes, rings and excess chromosome fragments [50,65,109,115–117]. Recent studies have assessed the utility of G_0 PCCs for triage biodosimetry by using the FISH technique with telomere and centromere specific PNA probes [66,67,112]. Based on the *ex vivo* data obtained, Lamadrid Boada et al., [68] suggested the use of PCC-rings for dose estimation in severely exposed humans. Interestingly, the frequency of rings remained essentially the same in *ex vivo* irradiated lymphocytes irrespective of the post-recovery times used for PCC preparation (8 hrs and 24 hrs). Recently, Pantelias and Terzoudi [118] developed an automatable micro-PCC assay for rapid individualized dose estimation during large-scale radiological emergencies. This technique will enhance the practical applicability of G_0 PCC as an effective triage tool.

In some of the earlier studies, Calyculin A induced G2 PCC technique was used to detect IR induced chromosome translocations [119,120] but this technique, unlike G_0 PCCs, also involves *ex vivo* stimulation of human lymphocytes for 48 hrs. A major advantage of using the G2 PCC technique is that it yields sufficient number of G2 cells even at higher radiation doses (5-20 Gy) as most heavily damaged cells at these doses may not even progress to mitosis for conventional metaphase chromosome analysis. To date, cell fusion mediated G_0 PCCs have been extensively used only for the analysis of asymmetrical or unstable chromosomal aberrations (dicentric chromosomes, rings and fragments). Our study is perhaps the first one to demonstrate the applicability of G_0 PCCs for analyzing both inter- and intrachromosomal aberrations using multicolor FISH and chromosome specific mBAND probes. Efficient detection of chromosomal translocations (simple and complex) by mFISH enables the use of G_0 PCCs for retrospective biodosimetry and for monitoring long-term effects of IR exposure on hematopoietic system. The hybridization signal for either whole chromosome specific probe or mFISH probe was not affected by the prematurely condensed nature of interphase chromosomes. As demonstrated in the current study, G_0 PCCs can be easily karyotyped for numerical and structural analyses of aberrations induced by IR. The mFISH has an additional advantage over conventional Giemsa staining in identifying chromosome specific origin of excess fragments. In the current study, the frequency of interchromosmal exchange events was compared by mFISH in G_0 PCCs after 2 hrs and 6 hrs of exposure with different doses of γ-rays. Using a combination of centromere and telomere staining, an earlier study demonstrated that the rejoining of chromosome fragments reached a plateau at 8 hrs after radiation exposure (Karachristou et al., 2015). Previous studies [110,121] suggested that exchange type aberrations predominantly arising from two lesions from a single ionizing track are formed instantly after low doses of X-rays (< 2Gy), while those exchange events resulting from two ionizing tracks at higher doses (> 2 Gy) increase as a function of post-recovery time. In corroboration, an increased yield of interchromosomal exchange events was detected by mFISH in G_0 PCCs after 6 hrs of radiation exposure relative to 2 hrs, most notably for 4 Gy and 6 Gy doses of γ-rays.

In the current study, color junctions were scored for interchromosomal exchange events, which besides translocations (non-reciprocal and reciprocal exchanges) also included dicentric chromosomes. Using centromere and telomere FISH staining, the frequency of dicentric chromosomes observed per cell was found to be 0.06 for 1 Gy, 0.14 for 2 Gy, 1.32 for 4 Gy and 2.48

for 6 Gy in G_0 PCCs prepared after 6 hrs of post recovery. However, the frequencies of color junctions detected by mFISH were much higher (0.6/cell for 1 Gy, 1.27/cell for 2 Gy, 4.1 for 4 Gy and 9.2 Gy for 6 Gy) than the dicentric frequencies observed by centromere and telomere staining. These observations indicate that the translocation frequency detected in G_0 PCCs was higher than dicentric chromosome frequency, although a direct comparison was not performed in our study to estimate the yields of dicentrics and translocations in the same cells. Using a pan centromeric and whole chromosome specific probes, Bauchinger et al. [122] detected more translocations than dicentrics. Although DNA double strand break is considered to be the critical lesion for the formation of exchange type aberrations (dicentrics and translocations), reports of dicentric to translocation ratios greater than 1 [122–125] suggest that the DSB rejoining processes may be different for their formation. In support, post-treatment of X-rays irradiated human lymphocytes with DNA repair inhibitors [Cytosine arabinoside (araC) – an inhibitor of DNA polymerase α; 3-aminobenzamide (3AB) - an inhibitor of Poly (ADP) Ribose Polymerase] potentiated only the formation of dicentric chromosomes but not translocations [124–128]. Strikingly, treatment of cells with araA (Adenine arabinofuranoside) specifically enhanced the frequencies of translocations but not dicentric chromosomes [125]. Although, we did not perform a direct comparison on the yield of radiation induced interchromosomal exchange events between interphase and metaphase chromosomes, chromatin structure and cell cycle stage may be important determinants for formation of specific types of chromosome aberrations. In corroboration, differential yield of dicentrics and translocation was reported in Calyculin A induced G2 PCCs and colcemid arrested metaphase chromosomes in lymphocytes exposed to protons and carbon ions [129]. In the present study, distribution of color junctions detected by mFISH in G_0 PCCs appeared to be largely random without involving any specific chromosomes. In general, the number of color junctions induced by 6 Gy of γ-rays in the G_0 PCCs prepared 6 hrs after radiation exposure seemed to correlate with chromosome size. Muhlman-Diaz and Bedford [130] analyzed the breaks on chromosomes 4, 19 and Y in non-cycling human skin fibroblasts immediately after X-rays exposure and found no correlation between breakage per unit length and the ratio of AT/GC sequences for these chromosomes. The only exception was the euchromatic portion of the Y chromosome, which showed almost twice the number of chromosome breaks than expected.

In addition to interchromosomal exchanges, intrachromosomal exchanges were also detected in G_0 PCCs using chromosome 5 specific mBAND probe. The banding pattern observed in G_0 PCCs was identical to colcemid arrested metaphase chromosomes despite the difference in chromosome size and chromatin condensation. In addition to chromosome breaks in the p and q-arms, translocation and inversion events were also detectable using the mBAND technique in G_0 PCCs. Although not quite adequate for radiation biodosimetry purposes, it is worth noting that the frequency of breaks detected in the q-arm was much higher than the p-arm at both radiation doses (4 Gy and 6 Gy) in G_0 PCCs. Johannes et al. [131] reported similar observations in the metaphase chromosomes of human lymphocytes irradiated with 4 Gy of X-rays and the increased number of breaks observed in the q-arm correlated well with the DNA content (27% for the p-arm and 73% for the q-arm). Interestingly, we observed almost a 10-fold increase in breaks in the q-arm relative to p-arm after 4 Gy of X-rays. The number of cells analyzed was too small to allow any meaningful statistical analysis for the distribution of breaks in the short and long arms of chromosome 5. Our study indicates that G_0 PCCs can be successfully utilized for detecting intrachromosomal exchange events such as inversions and translocations for retrospective dosimetry.

Although no evidence was provided in this study for gene fusion/fission events, successful demonstration of gene loci indicates the feasibility of detecting some of the radiation induced gene fusion/fission events in unstimulated lymphocytes. As gene fusion and fission events are important for cancer development processes, systematic analysis of these changes using G_0 PCCs may yield valuable information for radiation induced carcinogenesis. Collectively, our study demonstrates that G_0 PCCs can be used effectively for detecting a whole spectrum of inter- and intrachromosomal aberrations. As the cell fusion technique coupled with FISH can dramatically reduce the turnaround time for dose estimation by alleviating the need of *ex vivo* lymphocyte stimulation for 48 hours, we

believe that the G_0 PCC technique has the potential for future development as a biodosimetry tool: unstable chromosome aberrations (chromosome fragments and dicentric chromosomes) for early dose estimation and chromosome exchange events in stable cells for retrospective effects of radiation exposure in unstimulated lymphocytes without any bias or selection for only metaphase cells obtained after *ex vivo* stimulation.

Chapter 4: Premature Chromosome Condensation in Micronucleated Cells in a Single Catastrophic Event May Underlie the Mechanistic Origin of Chromothripsis

4.1. Introduction

First insights into the central role of chromosomes in cancer development emerged in Boveri's hypothesis, formulated more than 100 years ago, which posited that somatic genetic changes leading to uncontrolled cell proliferation caused cancers. By examining cancer cells under the microscope, Boveri observed the presence of peculiar chromosomes and, essentially, proposed that cancers are abnormal clones of cells characterized and caused by abnormalities of hereditary material [132]. At present, one consistent hallmark of human cancer genomes is chromosomal instability [133] and the formation of numerical and structural alterations in chromosomes, including deletions, duplications, inversions, and translocations [134–140]. Potential causes leading to chromosome instability include spindle assembly defects, chromosome segregation defects, erroneous repair of DNA damage, telomere dysfunction, and DNA replication stress. For example, it has been shown that deficiencies in key DNA repair factors for homologous recombination (HR) or canonical non-homologous end joining (cNHEJ) in a p53 deficient environment can result in frequent chromosomal catastrophic events. These complex genome rearrangements can stimulate tumor development by the amplification of oncogenes, for instance [141,142]. These and other pivotal regulatory cellular function defects are also currently considered as the driving mechanisms for the initiation of the striking phenomenon termed chromothripsis, on the basis of its chromosomal hallmarks that point to an underlying process involving chromosome (chromo) shattering (thripsis) [143]. Chromothripsis is characterized by extensive genomic rearrangements with a large number of breakpoints but a limited number of oscillating copy number states [143–146]. The study of the molecular mechanism that leads to chromothripsis remains a challenging research topic [147].

Chromothripsis has been extensively studied in primary tumors of diverse histological origin, and recent studies suggest that it may be far more common that initially inferred from low resolution DNA copy number data, with a frequency of more than 50% in several cancer types [148]. In 2013, Korbel and Campbell [145] suggested criteria to discriminate between rearrangements resulting from chromothripsis and from stepwise DNA alterations. However, chromothripsis is not specific to cancer, as similar random joining of chromosomal fragments has been observed as well in the germline [149]. Despite the progress achieved in elucidating this phenomenon, a detailed picture of the complete process of its mechanistic origin remains elusive, while much remains to be discovered regarding its prevalence and consequences [146,150,151]. Several non-mutually exclusive hypotheses have been proposed and discussed in recent reviews [152–155]: Fragmentation and subsequent reassembly of a single lagging chromosome encapsulated in aberrant extranuclear chromatin bodies surrounded by a nuclear envelope called micronuclei (MN) [146,156–158]; fragmentation of dicentric chromosomes and induction of chromothripsis through the breakage-fusion-bridge cycle following telomere crisis [159,160]; chromosomal shattering and reassembly through excessive shattering of telomeric DNA by ionizing radiation (IR) during cell mitosis [161], when chromosomes are condensed and individualized; induction of chromosomal rearrangements through fragmentation of chromatin by abortive apoptosis; and chromosome shattering and reassembly through premature chromosome condensation (PCC) within micronucleated cells and asynchronous cell-cycle progression between main nucleus and MN [146,156,162,163].

A hallmark of chromothripsis is chromosome shattering, and the precise timing of this event is crucial for determining the underlying mechanisms. Does the massive accumulation of fragmented DNA that could drive chromothripsis originate, through MN disruption and aberrant DNA replication inside MN, before main nuclei enter mitosis? Or does it arise as a consequence of the PCC dynamics in asynchronous micronucleated cells when main nuclei enter mitosis? Consistent with the

latter case, we have previously proposed that chromatin condensation, triggered by the PCC process when main nuclei enter mitosis, causes the collapse of replication forks and the massive accumulation of fragmented DNA in MN [162]. Nevertheless, it is important to note that both potential origins of shattering might play a significant role. Additionally, the molecular events underlying the fragility of replication forks in mitosis and their subsequent collapse remain incompletely understood [150,164]. Following exposure to various genotoxic agents such as IR, MN can encapsulate acentric fragments of chromosomes, as well as whole anaphase lagging chromosomes. Interestingly, even though MN maintain several characteristics of main nuclei, studies differ regarding their ability to undergo normal DNA replication and transcription, exhibit normal DNA damage response, and assemble normal nuclear envelopes [165,166].

In the present study, we conducted interphase cytogenetic analysis of asynchronous micronucleated human lymphocytes and Chinese hamster ovary (CHO) multinucleated cells, to investigate whether the dynamics of the PCC process are an important determinant of the mechanism that leads to chromothripsis. Our hypothesis, based on earlier work [162,167–169], is that the chromatin condensation activated by the PCC process exerts mechanical stress on chromosome sites in MN that are still undergoing normal DNA replication when main nuclei enter mitosis. As a result, the DNA replication forks in MN may collapse and eventually convert into double strand breaks (DSBs), thus causing chromosome shattering in a single catastrophic event. Hence, the extent of chromosome shattering should be proportional to the number of MN replication forks at the entry of main nuclei into mitosis.

In order to test the above hypothesis, we applied IR to generate asynchronous micronucleated cells and employed cell fusion procedures in exponentially growing cells to obtain asynchronous multinucleated cells. Subsequently, using the agent RO-3306, a selective ATP-competitive inhibitor of CDK1 that promotes cell cycle arrest at the G2/M boundary, we controlled and delayed the entrance of main nuclei into mitosis. The rationale is that this delay defers the initiation of the PCC process and allows time for MN to complete DNA replication and progress towards G2 phase. This strategy enabled to test at the cytogenetic level whether MN disruption or defective DNA replication in MN is necessary for chromosome shattering to occur. In fact, if disruption or aberrant DNA replication takes place in MN before the entry of main nuclei into mitosis, one envisions that the duplication of chromosomal material residing in MN is expected to be markedly impaired and/or shattered even if the agent RO-3306 is applied. However, according to our hypothesis, chromosome shattering is not expected if complete DNA replication takes place in MN before the entry of main nuclei into mitosis. Indeed, we demonstrate here, for the first time, that anaphase lagging chromosomes entrapped in MN can proceed into G2 phase without any shattering or impairment in their duplication. Altogether, our data demonstrate that an important determinant of chromosome shattering is the asynchrony between MN and main nuclei, supporting thus the PCC hypothesis as the mechanistic basis of chromothripsis initiation.

4.2. Results

Through four sets of experiments, we demonstrate that the dynamics of the PCC process in asynchronous micronucleated or multinucleated cells can be the cause of shattering of chromosome segments, which are entrapped in MN or heterophasic nuclei, and are still undergoing DNA replication when main nuclei enter mitosis. Specifically, a critical determinant of the extent of chromosome shattering is the degree of cell cycle asynchrony between MN and main nuclei. Furthermore, we show that chromosomes entrapped in MN, if given sufficient time, can undergo chromatid disjunction and complete normal DNA replication, without any impairment in their duplication. This is revealed by means of a thorough G2-PCC assessment upon the entry of main nuclei into mitosis, and the interphase cytogenetic evidence obtained here supports the PCC hypothesis as the mechanistic origin of chromothripsis.

4.2.1. In Asynchronous Micronucleated Cells Generated by γ-Irradiation of G_0-lymphocytes, the PCC Process Triggers Shattering of Chromosomes in MN Still Undergoing DNA Replication When Main Nuclei Enter Mitosis

In the first set of experiments, asynchronous micronucleated cells were generated by in vitro γ-irradiation (4 Gy) of G_0-human blood lymphocytes to induce chromosomal aberrations and anaphase lagging chromosomes, which will be entrapped by nuclear envelopes and form micronuclei, as described in Materials and Methods. The effect of the mechanical stress exerted by the dynamics of PCC on chromosomes trapped in MN when main nuclei enter mitosis was thoroughly examined. Even though the ultimate fate of chromosomes within MN in asynchronous micronucleated cells remains unclear, these experiments enable the visualization of the chromosomes and their progression through the different stages of the cell cycle. Upon entry of main nuclei into mitosis, the nuclear envelope of MN disassembles and, through the activity of mitotic cyclin B1-CDK1 and histone phosphorylation, chromatin condensation occurs. The cell cycle phase of MN can be inferred through the observation of the chromatin architecture and morphology of the prematurely condensed chromosomes. Therefore, based on the degree of completion of DNA replication, the chromosomes in the interphase MN can be classified as being in G1, early-S, mid-S, late-S, or G2 phase. The typical appearance of chromosome shattering in S phase MN, classified as early-S, mid-S, and late-S phase PCCs in interphase MN, is shown in Figure 4.1.

(**A**) (**B**) (**C**)

Figure 4.1. Early-S, mid-S and late-S MN PCCs. In micronucleated cells generated by exposure of G_0-lymphocytes to ionizing radiation (IR) (4 Gy), chromosome shattering of chromosomal material entrapped in micronuclei (MN) can occur through premature chromosome condensation (PCC), if MN are in S phase when main nuclei enter mitosis. Upon entry of main nuclei into mitosis, the nuclear envelope of MN disassembles and, through the mitotic cyclin B1-CDK1 activity and histone phosphorylation, the shattering and morphology of prematurely condensed chromosomes (PCCs) characterizes the stage in S phase of MN. Based on the degree of completion of DNA replication, the MN PCCs can be classified as: (**A**) early-S, (**B**) mid-S, and (**C**) late-S phase. Darkly stained metaphasic chromosomes belong to main nuclei, while lightly stained shattered chromosomal material indicate anaphase lagging chromosomes entrapped in MN.

Figure 4.2 presents the typical appearance of G1 and G2 phase PCCs in interphase MN. The cytogenetic assessment of the chromosome preparations show that PCC-induced chromosome shattering is only observed in MN that are still undergoing DNA replication when main nuclei enter mitosis. Indeed, chromosome shattering was never detected when the chromosomes in MN were in G1 phase or in G2 phase.

(**A**) (**B**)

Figure 4.2. G1 and G2 MN PCCs. When main nuclei in heterophasic micronucleated cells generated by exposure of G_0-lymphocytes to IR (4 Gy) enter mitosis, chromosome shattering is not observed in the MN PCCs if the morphology of chromosomes entrapped in MN is classified as G1 (**A**) or G2 phase (**B**). Anaphase lagging chromosomes entrapped in MN can undergo chromatid disjunction (**A**), and complete DNA replication without impairment in their duplication (**B**). The different level of chromatin condensation between MN chromosomes and those of the main nuclei leads to dissimilar shades of staining, making them easily distinguishable. Darkly stained metaphasic chromosomes belong to main nuclei, while lightly stained chromosomes were entrapped in MN.

Moreover, more than a thousand micronucleated cells per experimental point were assessed for chromosome shattering in asynchronous micronucleated cells. Chromosome shattering was visualized in MN only when main nuclei were in M phase, as shown in Figure 4.3. The percentages of cells in the five different categories of MN PCCs obtained under these experimental conditions are presented in Figure 4.4 (grey). In order to delay the entrance of main nuclei into mitosis, the agent RO-3306, a selective ATP-competitive inhibitor of CDK1, was applied to asynchronous heterophasic micronucleated cells for 20 h. Subsequently, the RO-3306 agent was washed out and the main nuclei were allowed to proceed to mitosis and then blocked in metaphase, using Colcemid for 4 h. The corresponding percentages of cells obtained for the five different categories of induced PCCs in MN are also presented in Figure 4.4 (black). The results of this set of experiments show that, in the absence of RO-3306, most of the MN PCCs are in G1 and early-S phase, whereas in the presence of this agent, most of MN PCCs are in mid-S, late-S, and G2 phase.

In order to test whether chromosome shattering, which is a hallmark of chromothripsis, arises in MN through the PCC process and not as a result of a massive accumulation of fragmented DNA inside MN occurring before main nuclei enter mitosis, we exploited the unique features of RO-3306. Indeed, the presence of the RO-3306 agent delayed the entry of main nuclei into mitosis, thus allowing the progression of DNA replication in the chromosomes entrapped in MN. As a result, an increased number of MN completed DNA replication and chromosome duplication, and thus entered G2 phase without any chromosome shattering. Following aberrant mitosis, if given sufficient time, anaphase lagging chromosomes entrapped in MN can undergo chromatid disjunction and complete normal DNA replication, without any impairment in their duplication or chromosome shattering, as revealed through G2-PCC assessment upon the entry of main nuclei into mitosis. Figure 4.5A shows complete replication and normal duplication of chromosomes 1, 4 and a fragment entrapped in MN, whereas in Figure 4.5B, the duplication of chromosomes 2 and 10 without any shattering is presented.

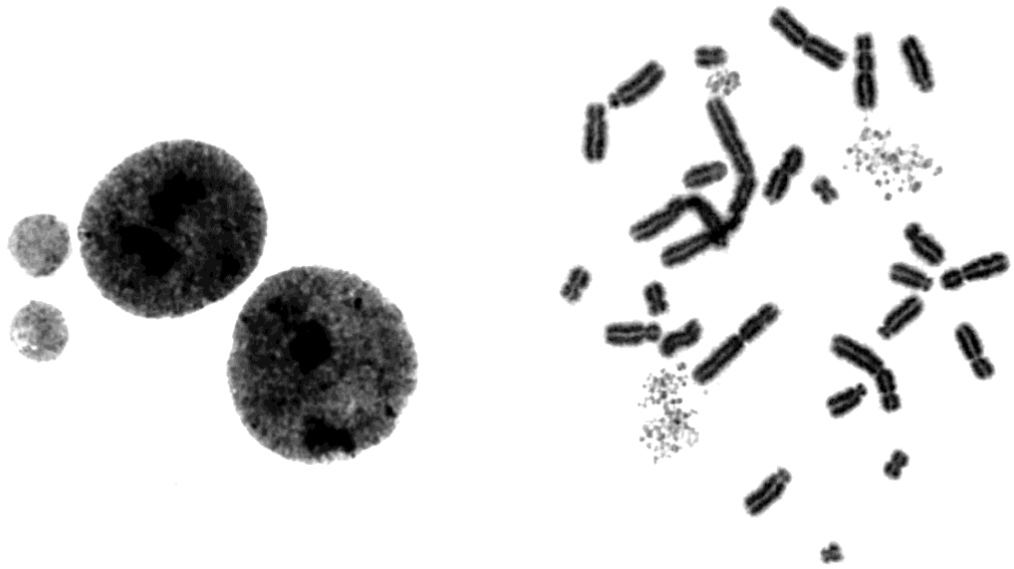

(**A**) (**B**)

Figure 4.3. MN PCCs are visualized only when main nuclei enter mitosis. Through rigorous cytogenetic assessment, more than a thousand heterophasic micronucleated cells per experimental point were analyzed for nuclear envelope rupture and shattering of chromosomal material entrapped in MN. (**A**) Chromosome shattering in MN was never observed if main nuclei were not in mitosis. (**B**) Shattering of chromosomal material entrapped in MN was solely detected if, and only if, the main nuclei were in M phase and the MN were in S phase.

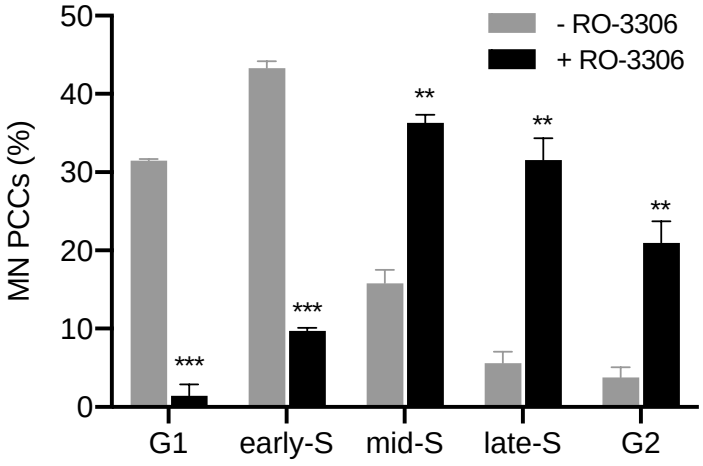

Figure 4.4. Cell cycle distribution of MN PCCs generated by irradiated G_0-lymphocytes. Frequencies of five different cell cycle phase categories of MN PCCs scored in heterophasic micronucleated cells, generated by irradiation of G_0-lymphocytes, upon entry of main nuclei into mitosis. Based on the progress of completion of DNA replication, the chromosomes in the interphase MN can be classified as being in G1, early-S, mid-S, late-S, or G2 phase. The agent RO-3306, a selective ATP-competitive inhibitor of CDK1, was used for 20 h to delay the entrance of main nuclei into mitosis, thus allowing time for completion of DNA replication in MN. In the absence of RO-3306, 75% of MN PCCs are in G1 and early-S phase, while only 25% are in mid-S, late-S, and G2 phase. In the presence of RO-3306, only 11% of MN PCCs are in G1 and early-S phase, while 36% are in mid-S, 32% in late-S, and 21% in G2. As the DNA replication progresses and MN proceed towards G2 phase, the observed chromosome shattering decreases. (Mean ± SEM based on two independent experiments; a total of 457 MN PCC spreads were analyzed; ** $p \leq 0.01$, *** $p \leq 0.001$)

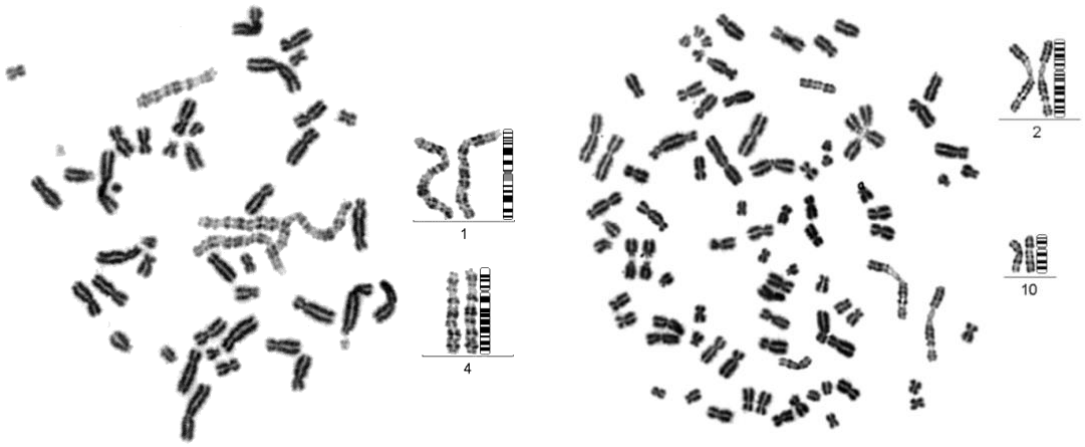

(**A**) (**B**)

Figure 4.5. Normal DNA replication can take place in MN. Following radiation exposure of human lymphocytes to generate micronucleated cells, anaphase lagging chromosomes entrapped in MN can undergo chromatid disjunction and complete DNA replication, without any shattering or impairment in their duplication, if entrance of main nuclei into mitosis is sufficiently delayed by RO-3306. (**A**) Duplication of chromosomes 1, 4 and a fragment entrapped in MN. (**B**) Duplication of chromosomes 2 and 10 entrapped in MN. Based on G-banding ideograms for chromosomes 1, 4, 2, and 10, there is no impairment in the duplication of these chromosomes entrapped in MN.

Figure 4.6 shows replication and duplication of aberrant chromosomal material entrapped in MN following radiation exposure, again without any apparent chromosome shattering.

If massive accumulation of fragmented DNA inside MN had occurred before main nuclei entered mitosis, the duplication of the chromosomes in Figures 4.5 and 4.6 residing in MN would be markedly impaired and result into their shattering, which is not observed in the above experiments. Therefore, these results suggest that chromothripsis may not arise from a massive accumulation of fragmented DNA and unrepaired DSBs inside MN before main nuclei enter mitosis.

(**A**) (**B**)

Figure 4.6. Aberrant chromosomes entrapped in MN can be duplicated. If entrance of main nuclei into mitosis is sufficiently delayed by RO-3306, radiation-induced aberrant anaphase lagging chromosomes entrapped in MN can also undergo chromatid disjunction and complete DNA replication, without any apparent chromosome shattering. (**A**) Duplication of aberrant chromosome 1 (lightly stained) entrapped in MN following radiation exposure (4 Gy) of human G_0-lymphocytes. (**B**) Duplication of aberrant anaphase lagging chromosomes (lightly stained) entrapped in MN following 4 Gy exposure of G_0-lymphocytes.

4.2.2. The PCC Process Underlies the Mechanistic Origin of Chromosome Shattering by a One-Step Cellular Catastrophic Event in Asynchronous Micronucleated Cells Generated by γ-Irradiation of Lymphocytes in the G1/S Phase Border

In the second set of experiments, asynchronous micronucleated cells were generated by in vitro γ-irradiation with 4 Gy delivered to blood cultures at 17 h following their stimulation with PHA, i.e., at the G1/S phase border, as described in the section of Materials and Methods. Since the G1/S phase border is a highly radiosensitive stage, the rationale of this set of experiments was to induce an increased yield of chromosomal aberrations, resulting into an increased yield of MN, to further test our hypothesis. The percentages of cells in the five different categories of MN PCCs obtained under these experimental conditions, in the absence of RO-3306, are presented in Figure 4.7 (grey). The corresponding percentages obtained when micronucleated cells were treated with the RO-3306 agent for 20 h are also presented in Figure 4.7 (black). The results of this set of experiments confirm that, even under different experimental conditions for the generation of micronucleated cells, delaying the entry of main nuclei into mitosis by means of RO-3306 allows progression of DNA replication and progression of MN towards G2 phase.

4.2.3. The PCC Process Induces Shattering of Chromosomes in MN Still Replicating DNA When Main Nuclei Enter Mitosis in Asynchronous Micronucleated Cells Generated by γ-Irradiation of Mitotic CHO Cells

In the third set of experiments, asynchronous micronucleated cells were generated by in vitro γ-irradiation (3 Gy) of M phase CHO cells harvested via cell synchronization and selective detachment, as described in the section of Materials and Methods. The M phase is known to be extremely radiosensitive and the rationale of the experimental design was, again, to induce an increased yield of chromosomal aberrations, in order to obtain an increased yield of asynchronous micronucleated cells. The percentages of cells in the five different categories of MN PCCs under these experimental conditions in the absence of the RO-3306 agent are presented in Figure 4.8 (grey), while the black columns in Figure 4.8 present the corresponding results in the presence of the agent. The results confirm again that the presence of RO-3306 allowed time for the progression of DNA replication in the chromosomes entrapped in MN, alleviating the shattering effect.

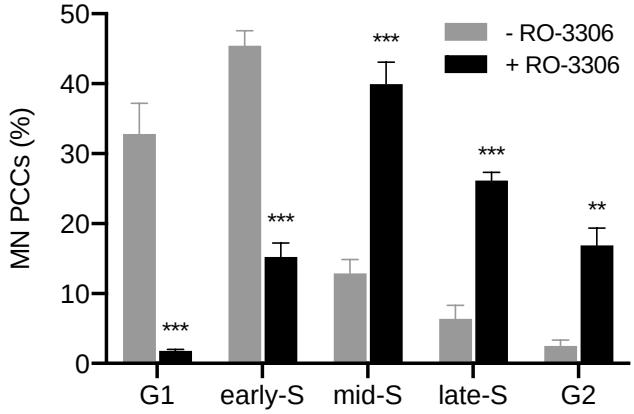

Figure 4.7. Cell cycle distribution of MN PCCs generated by irradiated G1/S lymphocytes. Frequencies of five different cell cycle phase categories of MN PCCs scored in heterophasic micronucleated cells, generated by irradiation of PHA-stimulated lymphocytes at the highly radiosensitive G1/S border to induce an increased yield of MN. In the absence of RO-3306, 78% of MN PCCs are in G1 and early-S phase, while only 22% are in mid-S, late-S, and G2 phase. In the presence of RO-3306 for 20 h, only 17% of MN PCCs are in G1 and early-S phase, while 40% are in mid-S, 26% in late-S, and 17% in G2. Following complete DNA replication, the anaphase lagging chromosomes entrapped in MN can proceed to G2 phase, without any apparent chromosome shattering. (Mean ± SEM based on four independent experiments; a total of 499 MN PCC spreads were analyzed; ** $p \leq 0.01$, *** $p \leq 0.001$).

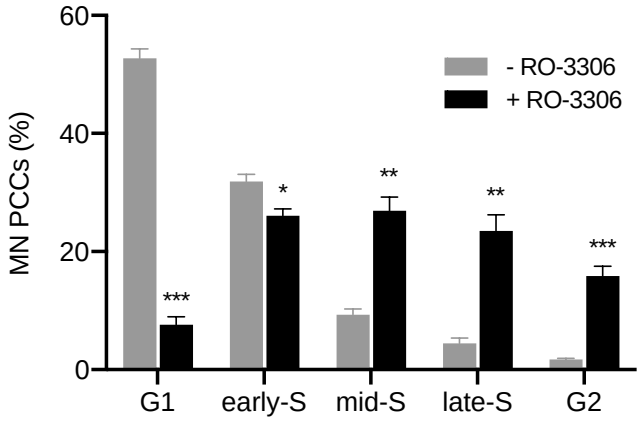

Figure 4.8. Cell cycle distribution of MN PCCs generated by irradiated mitotic Chinese hamster ovary (CHO) cells. Frequencies in five different cell cycle phase categories of MN PCCs scored in heterophasic micronucleated cells, generated by irradiation of CHO mitotic cells with 3 Gy γ-rays. In the absence of RO-3306, 85% of MN PCCs are in G1 and early-S phase, and only 15% are in mid-S, late-S, and G2 phase. In the presence of RO-3306 for 12 h, 33% are in G1 and early-S phase, while 27% of MN PCCs are in mid-S, 24% in late-S, and 16% in G2 phase. The presence of RO-3306 in micronucleated cells effectively delayed the main nuclei to proceed to mitosis, allowing time for the progression of DNA replication in chromosomes entrapped in MN. (Mean ± SEM based on four independent experiments; a total of 958 MN PCC spreads were analyzed; * $p \leq 0.05$, ** $p \leq 0.01$, *** $p \leq 0.001$).

4.2.4. The Presence of Asynchronous Mitosis in Multinucleated Cells Generated by Fusion of Exponentially Growing Cells is an Important Determinant of the Shattering of Genetic Material in a Single Catastrophic Event

To further test the proposed hypothesis, in the fourth set of experiments, asynchronous multinucleated cells were generated by the cell fusion procedure using exponentially growing CHO cells and the fusogen polyethylene glycol, as described in the section of Materials and Methods. The rationale of this set of experiments is based on the fact that, when a nucleus in asynchronous multinucleated cells is in S phase, while a neighboring nucleus proceeds to mitosis, the chromosomes in the S phase nucleus will be forced to condense prematurely and will shatter when the neighboring nucleus enters mitosis. According to the degree of completion of DNA replication, the chromosomes visualized in interphase nuclei can be classified as being in early-S or late-S, shown in Figure 4.9, and early-G2 or late-G2, shown in Figure 4.10.

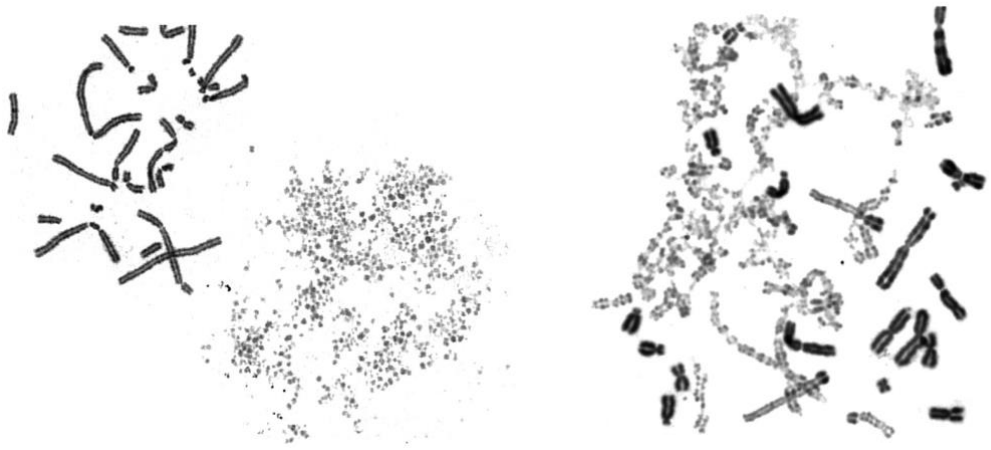

(**A**) (**B**)

Figure 4.9. Early-S and late-S induced PCCs in multinucleated CHO cells. When main nuclei in heterophasic multinucleated cells generated by cell fusion procedures using exponentially growing CHO cells enter mitosis, the shattering and morphology of prematurely condensed chromosomes (PCCs) characterizes the stage in S phase of interphase nuclei. Based on the degree of completion of DNA replication, the induced PCCs in interphase nuclei can be classified as early-S (**A**) and late-S phase (**B**).

The percentages of PCCs obtained in the absence of RO-3306 (grey), or in the presence of 5 μM (black diagonal) or 10 μM (black) of the agent, are shown in Figure 4.11. The synchronization of heterophasic nuclei is more effective when 10 μM of the agent RO-3306 is applied.

These results demonstrate that chromosome shattering is induced in interphase nuclei by the dynamics of premature chromosome condensation in asynchronous multinucleated cells and depends on the stage of the nucleus in S phase. Indeed, the use of RO-3306 to synchronize the cell cycle phase of the nuclei of multinucleated cells shows that the extent of chromosome shattering is inversely related to the degree of synchronization achieved, which is more effective when 10 μM of the agent is used. In fact, as the nuclei complete DNA replication and proceed to G2 phase, there is no chromosome shattering when the main nucleus enters mitosis.

(**A**) (**B**)

Figure 4.10. Early-G2 and late-G2 induced PCCs in multinucleated CHO cells. Based on the degree of completion of DNA replication in interphase nuclei in CHO multinucleated cells, the induced PCCs in interphase nuclei, upon entry of main nuclei into mitosis, can be classified as early-G2 with long lightly stained double chromatid chromosomes (**A**) or late-G2 with short lightly stained double chromatid chromosomes (**B**). The darkly stained condensed metaphase chromosomes belong to the main nuclei. Chromosome shattering in G2 phase PCCs was never observed.

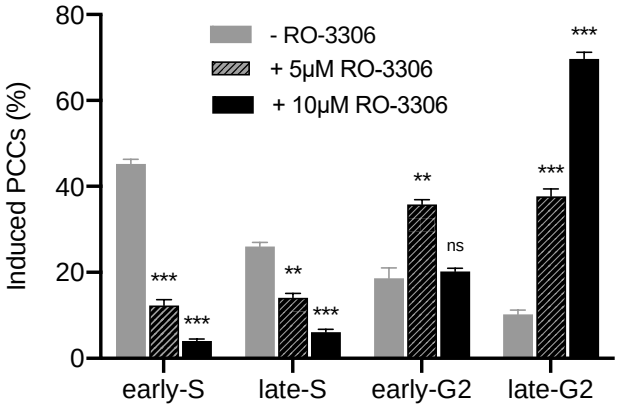

Figure 4.11. Cell cycle distribution of induced PCCs in multinucleated cells generated by fusion of asynchronous CHO cells. Frequencies in four different cell cycle phase categories of PCCs in asynchronous heterophasic multinucleated cells generated by cell fusion procedures using exponentially growing CHO cells. In the absence of RO-3306, 45% of PCCs observed are in early-S, 26% in late-S phase, 19% in early-G2, and 10% in late-G2; whereas in the presence of 5 μM RO-3306 for 12 h, only 12% were in early-S, 14% in late-S, 36% in early-G2, and 38% in late-G2. When 10 μM RO-3306 was used to inhibit CDK1 and delay more effectively the entrance of main nuclei into mitosis, 90% of heterophasic nuclei proceeded into early-G2 and late-G2, without any chromosome shattering, whereas only 10% of PCCs were left in early-S and late-S cell cycle phase, exhibiting chromosome shattering. The use of RO-3306 to synchronize heterophasic nuclei in multinucleated cells demonstrates that the extent of chromosome shattering is inversely related to the degree of synchronization achieved. (Mean ± SEM based on three independent experiments; a total of 1083 induced PCC spreads were analyzed; ns $p > 0.05$, ** $p \leq 0.01$, *** $p \leq 0.001$)

4.3. Discussion

Chromothripsis is a phenomenon characterized by chaotic localized rearrangements, all curiously restricted to one or a few chromosomes. Specifically, at the cytogenetic level, a simple model that fits the observed rearranged chromosomes, most likely entrapped in MN, involves a shattering of chromosomes into pieces with narrowly spaced breakpoints. This is initiated by a one-step cellular catastrophic event, followed by reassembly of the chromosomal segments in random order and orientation. As a result, some fragments are lost and others preserved into functioning highly derivative chromosomes, so that an alternating pattern of heterozygosity emerges [170]. Consequently, chromothripsis provides a mechanism for the rapid accumulation of hundreds of rearrangements in few cell divisions, in contrast to the traditional view of carcinogenesis as a gradual Darwinian process of progressive mutation accumulation. Yet, considering that chromosome shattering usually reflects induction of DSBs and DNA fragmentation [171,172], a number of questions have been raised: How is shattering of the genetic material initiated by a one-step cellular catastrophic event? Why is shattering confined to only one or a few chromosomes? How is the shattered DNA not lost but integrated into the genome? Which DNA repair mechanisms are involved? In addition, at which stage are DSBs generated in MN? Does the massive accumulation of DNA damage that leads to chromosome shattering and chromothripsis originate from MN disruption or aberrant DNA replication in MN before main nuclei enter mitosis?

It has been previously proposed that the physical isolation of chromosomes in aberrant nuclear structures called MN, which are considered to be built with dysfunctional nuclear envelopes [173,174], might explain the localization of DNA lesions in chromothripsis [156]. However, the interesting question that still remains is why does DNA in MN get fragmented as the cell progresses to the next cycle? It has been shown that many processes taking place in the main nucleus are dysfunctional in the MN [173], including transcription and DNA replication [156,175]. Therefore, DNA damage can result as a direct consequence of aberrant DNA replication, potentially due to a reduced density of replication origins. DSBs could then be generated by stalled or slowed replication

forks [176], but why forks are so fragile in mitosis is unclear. Furthermore, it has been reported that the ensuing loss of nucleocytoplasmic compartmentalization throughout interphase triggers micronucleus-specific DSBs, which were hypothesized to persist unrepaired into mitosis. These DSBs are expected to subsequently resolve into highly fragmented chromatin during mitotic entry [156,163], which reintegrates into daughter cell genomes after mitotic exit [146,156]. In addition, defects in repair inside MN have been reported to be associated with defects in the assembly of nuclear pore complexes on the MN envelope. This may prevent recruitment of DNA replication or repair enzymes inside MN, producing DNA breakage [177].

Further work has shown that MN in cancer cells may undergo rupture of the MN envelope, which is associated with loss of compartmentalization and extensive DNA damage, and that this rupture represents an essential step for chromosome shattering to occur [173]. These findings led to the hypothesis that envelope disruption could expose DNA in the MN to cytoplasmic components, including endo and exonucleases that recognize collapsed replication forks or unrepaired DNA extruded from the MN, thereby generating pulverized chromosomal regions at mitotic entry [173]. Finally, DNA replication in MN was found to be asynchronous relative to the main nucleus [156,162]. Therefore, if the replicating DNA within the MN is exposed to "mitotic signals" when the main nucleus is in mitosis, the micronuclear envelope disassembles, while the residing chromosomes could potentially undergo PCC and pulverization, a phenomenon that was observed long ago [178–180]. Using different cytogenetic approaches, we previously provided experimental evidence supporting the above PCC model for chromosome shattering in MN as the mechanism underlying chromothripsis initiation [162]. Specifically, we reported that PCC induction in micronucleated cells exerts mechanical stress and shattering of chromosome segments still undergoing DNA replication in MN, when main nuclei enter mitosis. These results suggest that replication forks, which are sensitive to mechanical stress, may be directly damaged and collapse through premature chromatin condensation at the DNA replicating sites, causing chromosome shattering.

In the present study, we further assessed whether the dynamics of the PCC process studied earlier [162,167,169] represent an important determinant of the mechanistic origin of chromothripsis. The experimental design we used allowed for the examination of whether massive accumulation of DSBs, which underlie chromosome shattering and chromothripsis, originate necessarily through MN disruption or aberrant DNA replication in MN, before main nuclei enter mitosis. Through four different experimental setups and using asynchronous micronucleated or multinucleated cells, we demonstrated that a decisive parameter for the extent of chromosome shattering is the degree of cell cycle asynchrony between MN and main nuclei. Indeed, using asynchronous micronucleated cells generated by in vitro γ-irradiation of G0 human blood lymphocytes combined with the agent RO-3306, a thorough cytogenetic assessment was carried out at the time main nuclei proceeded to mitosis.

The induced MN PCCs were classified as G1, early-S, mid-S, late-S, or G2 phase, as shown in Figures 4.1 and 4.2. Analysis of MN PCCs in asynchronous micronucleated cells was possible only if main nuclei were in M phase, as explained in Figure 4.3. The results presented in Figure 4.4 show that in the absence of RO-3306, 75% of MN PCCs are in G1 and early-S phase, and only 25% are of mid-S, late-S, and G2 phase. Whereas in the presence of RO-3306, 36% of MN PCCs are in mid-S, 32% in late-S, 21% in G2, and only 11% are now in G1 and early-S phase. As the DNA replication is progressing and MN proceed towards G2, the observed chromosome shattering decreases. In fact, the extent of chromosome shattering increases as the number of MN replication forks becomes larger at the entry of main nuclei into mitosis. Furthermore, we show that, if given sufficient time, chromosomes entrapped in MN can undergo chromatid disjunction (Figure 4.2A) and complete DNA replication (Figure 4.2B), without any impairment in their duplication or shattering, as it is demonstrated for chromosomes 1, 4 and a fragment (Figure 4.5A), and for chromosomes 2 and 10 (Figure 4.5B). If given sufficient time, radiation-induced aberrant chromosomes entrapped in MN can also replicate their DNA, without any apparent chromosome shattering, as shown in Figure 4.6.

If disruption, aberrant DNA replication, or accumulation of MN-specific DSBs that can persist unrepaired into G2/M phase had taken place in MN before the entry of main nuclei into mitosis, then the duplication of chromosomal material residing in MN would have been markedly impaired and

chromosome shattering would be expected to be present in (at least) some of the sites of MN G2-PCCs. However, following a thorough interphase PCC assessment upon the entry of main nuclei into mitosis, no such shattering was observed in any of the MN G2-PCCs analyzed. Therefore, under the experimental conditions used in this work, the presence of unrepaired DSBs in MN could not be confirmed. Yet, the results obtained demonstrate that the PCC dynamics during asynchronous mitosis in micronucleated or multinucleated cells are an important determinant of chromosome shattering in a single catastrophic event, suggesting that they may underlie the mechanistic origin of chromothripsis.

Similar results were obtained from the second set of experiments using micronucleated cells generated by γ-irradiation of PHA-stimulated lymphocytes at the highly radiosensitive G1/S border to induce an increased yield of chromosomal aberrations and, thus, an increased yield of MN. Figure 4.7 shows that in the absence of RO-3306, 78% of MN PCCs are in G1 and early-S phase, and only 22% are in mid-S, late-S, and G2 phase. Whereas in the presence of RO-3306, 40% of MN PCCs are in mid-S, 26% in late-S, 17% in G2, and only 17% are now in G1 and early-S phase. In the third set of experiments, an increased yield of asynchronous micronucleated cells was generated by in vitro γ-irradiation of M phase CHO cells. Figure 4.8 shows that in the absence of RO-3306, 85% of MN PCCs are in G1 and early-S phase, and only 15% are in mid-S, late-S, and G2 phase. Whereas in the presence of RO-3306, 27% of MN PCCs are in mid-S, 24% in late-S, 16% in G2, and 33% are now in G1 and early-S phase. The presence of the RO-3306 agent in micronucleated cells effectively delayed the main nuclei to proceed to mitosis, thus allowing time for the progression of DNA replication in the chromosomes entrapped in MN. These results confirm that, when the RO-3306 agent is used in micronucleated cells generated under different experimental conditions in order to delay entry of main nuclei into mitosis, the DNA replication in MN continues, showing less chromosome shattering as they proceed in the cell cycle and no shattering upon their entry in G2 phase.

In the fourth set of experiments, the proposed hypothesis was tested in asynchronous heterophasic multinucleated cells generated by cell fusion procedures using exponentially growing CHO cells. The interphase nuclei in these multinucleated cells show different PCC morphologies and shattering upon the entry of main nuclei into mitosis, which are characteristic of their stage in the cell cycle (Figures 4.9 and 4.10). As shown in Figure 4.11, in the absence of RO-3306, 45% of PCCs observed are in early-S, 26% in late-S, 19% in early-G2, and 10% in late-G2. Whereas in the presence of 5 μM RO-3306, only 12% are in early-S, 14% in late-S, 36% in early-G2, and 38% in late-G2. The use of 10 μM RO-3306 to inhibit CDK1 and delay more effectively the entrance of main nuclei into mitosis, gave the best cell cycle synchronization between heterophasic nuclei. After releasing cells from RO-3306, thus allowing the main nuclei to enter mitosis, 90% of heterophasic nuclei proceeded into early-G2 and late-G2, without any chromosome shattering, whereas only 10% of PCCs were still in early-S and late-S, as shown also in Figure 4.11. These results demonstrate that chromosome shattering is induced by the dynamics of premature chromosome condensation in asynchronous multinucleated cells and depends on the stage of the nucleus in S phase when main nuclei enter mitosis. Indeed, the use of RO-3306 to synchronize heterophasic nuclei in multinucleated cells shows that the extent of chromosome shattering is inversely related to the degree of synchronization achieved.

Altogether, the results obtained demonstrate that the PCC dynamics are an important determinant of the mechanistic origin of the chromosome shattering that is a hallmark of chromothripsis. They also suggest that the massive accumulation of DSBs that underlie chromothripsis may not necessarily originate through MN disruption or aberrant DNA replication in MN, before main nuclei enter mitosis. Alternatively, when main nuclei enter mitosis, the PCC dynamics, provoked by chromatin condensation, can exert a mechanical stress on the DNA replication sites of chromosomes entrapped in MN, or interphase nuclei in multinucleated cells, still undergoing DNA replication. As a result, the DNA replication forks in MN may collapse and eventually convert into DSBs, causing thus the observed chromosome shattering in a single catastrophic event. The extent of chromosome shattering decreases as the MN proceed towards G2 and the number of replication forks becomes smaller at the entry of main nuclei into mitosis.

Can the mechanical stress exerted by premature chromatin condensation on DNA replicating sites cause collapse of replication forks? In agreement with our findings, Falk et al. very recently provided experimental evidence supporting that chromatin architecture changes can induce replication fork collapse. Specifically, the authors, using DNA replicating cells, demonstrated that chromatin condensation, provoked by the freeze-thaw process, causes replication fork collapse, potentially leading to DSBs, which represent an important source of genome instability [181]. Yet, experimental evidence for a similar impact of interphase chromatin architecture changes on radiation-induced DNA damage repairing sites was already recognized and reported in our earlier work [167–169].

The mechanism proposed in the present work may help to deepen our understanding of most of the criteria for chromothripsis, including the important one related to why chromothriptic genome profiles exhibit clustering of DNA breaks. Such clustering is defined by specific chromosomal regions having multiple breaks in close proximity, surrounded by large sections of intact chromosomal sequence. Considering the pattern of DNA replication and distribution of replication sites in a chromosome segment progressing towards G2, the chromothriptic genome profiles obtained can be justified. Indeed, only the segments of the genome still undergoing replication when main nuclei enter mitosis are affected by the dynamics of the induced PCC process. One envisions that the affected genome can be surrounded by large sections that have completed DNA replication, thus demonstrating intact chromosomal sequences.

4.4. Materials and Methods

4.4.1. Lymphocyte Whole Blood Cultures, Production of Micronucleated Cells, and Irradiation Conditions

Peripheral blood samples in heparinized tubes were obtained from healthy donors and used after their informed consent, according to our institutional ethics procedures. The ethical approval was granted on the 26 February 2016, taking into consideration the Hellenic Law (N. 2472/97 and 886/B' 20/12/84) and the European Community Directives (Directive 95/46/EC). Irradiation of whole blood samples was carried out in vitro using a Co-60 Gamma Cell 220 irradiator (Atomic Energy of Canada Ltd., Ottawa, OT, Canada) at room temperature and at a dose rate of 20 cGy/min. Different irradiation times were applied in order to administer to the whole blood samples doses.

For the first set of experiments, micronucleated cells were generated using irradiation of blood with 4 Gy to induce chromosomal aberrations and formation of micronuclei (MN). Following radiation exposure, cultures were set up for 72 h at 37 °C, by adding for each 0.5 mL of whole blood, 5 mL of RPMI-1640 medium (Gibco) supplemented with 10% fetal bovine serum (FBS), 1% Phytohaemagglutinin (PHA), and 1% glutamine and antibiotics (penicillin: 10,000 U/mL; streptomycin: 10,000 μg/mL (Biochrom GmbH, Berlin, Germany)). For the PCC analysis of interphase MN in the absence of the CDK1 inhibitor RO-3306 (Tocris, Abingdon, United Kingdom), Colcemid at a final concentration of 0.1 μg/mL (Gibco) was added to the blood cultures for 5 h before their harvest at 72 h for chromosome preparation. For the categorization of interphase MN PCCs after delaying the entrance of main nuclei into mitosis by means of RO-3306, blood cultures were centrifuged at 72 h culture time, resuspended in fresh culture medium with 10 μM final concentration of RO-3306 (in DMSO), and the cells were further incubated at 37 °C for 20 h. At that time, cultures were centrifuged and washed twice to remove RO-3306, and cells resuspended in fresh culture medium plus Colcemid and cultured for additional 5 h, before they were harvested for chromosome preparation. Chromosome spreads were prepared by standard cytogenetic procedures and air-dried slides were stained in 3% Giemsa solution for interphase analysis of MN PCCs induced at the entry of main nuclei into mitosis. The corresponding data presented in Figure 4.4 are mean values ± SEM based on two independent experiments. A total of 457 MN PCC spreads were analyzed. Statistical significance was determined by means of five unpaired *t*-tests, corrected for multiple comparisons using the Holm-Sidak method with alpha = 0.05. Each row was analyzed individually, without assuming a consistent SD. Asterisks indicate statistical significance of the difference between untreated and treated samples; * $p \leq 0.05$, ** $p \leq 0.01$, *** $p \leq 0.001$.

For the second set of experiments, the same procedures were followed, except that the dose of 4 Gy was delivered to blood cultures at 17 h following their stimulation with PHA, i.e., as they were approaching the highly radiosensitive G1/S border. The corresponding data presented in Figure 4.7 are mean values ± SEM based on four independent experiments. A total of 499 MN PCC spreads were analyzed. The statistical analysis was performed following the same method as in the first set of experiments.

4.4.2. Micronucleated Cells Generated by Irradiation of Mitotic CHO Cells

Chinese hamster ovary cells (CHO-K1) were grown in McCoy's 5A (Biochrom) culture medium supplemented with 5% FBS, 1% l-glutamine, and 1% antibiotics (Penicillin, Streptomycin), incubated at 37 °C in a humidified atmosphere with 5% CO_2. CHO cultures were maintained as exponentially growing monolayer cultures in 75 cm^2 plastic flasks at an initial density of 4×10^5 cells/flask. For the third set of experiments, mitotic CHO cells were harvested via cell synchronization and selective detachment. The cells in a flask were routinely allowed to grow until confluence and, subsequently, subcultured into three new 75 cm^2 plastic flasks. Following a 24–30 h incubation at 37 °C, Colcemid (Gibco) at a final concentration of 0.1 μg/mL was added to CHO cultures for 4 h and the accumulated mitotic cells were harvested by selective detachment. To generate CHO micronucleated cells, CHO mitotics were irradiated to 3 Gy and cultured at 37 °C for 24 h after their release from the colcemid block.

For the PCC analysis of interphase MN in CHO micronucleated cells in the absence of RO-3306 CDK1 inhibitor, Colcemid at a final concentration of 0.1 μg/mL (Gibco) was added to the cultures 5 h before their harvest at 24 h for chromosome preparation. For the categorization of interphase MN PCCs after delaying the entrance of the CHO main nuclei into mitosis by means of the RO-3306 inhibitor, cultures were centrifuged at 24 h culture time, resuspended in fresh culture medium with 10 μM RO-3306 final concentration, and the cells were further incubated at 37 °C for 12 h. At that time, cultures were centrifuged and washed twice to remove RO-3306, and cells resuspended in fresh culture medium plus Colcemid and cultured for additional 5 h, before they were harvested for chromosome preparation. Four independent experiments were carried out and the corresponding data presented in Figure 4.8 are mean values ± SEM. A total of 958 MN PCC spreads were analyzed. The statistical analysis was performed following the same method as in the first set of experiments.

4.4.3. Heterophasic Multinucleated Cells Produced by Cell Fusion of Exponentially Growing CHO Cells

For the fourth set of experiments, cell fusion of exponentially growing CHO cells to generate heterophasic multinucleated cells, using 45% polyethylene glycol (PEG, p5402 Sigma–Aldrich, St. Louis, MO, USA) in serum-free RPMI-1640 medium with HEPES, was performed essentially as described previously [169]. Briefly, exponentially growing CHO cells harvested by trypsinization in 15 mL round-bottom culture tubes were used. After centrifugation at 1200 rpm for 8 min, the supernatant was discarded without disturbing the cell pellet, and cells were resuspended in 10 mL serum-free RPMI-1640 medium with HEPES. Following centrifugation at 1000 rpm for 8 min, the tubes were kept inverted in a test tube rack on a paper towel to drain the pellet from excess liquid. While holding each tube in an inverted position, 0.15 mL of PEG was injected forcefully against the cell pellet using a micropipette and, immediately after, the tube was turned in an upright position and held for about 1 min. Subsequently, 1.5 mL of PBS was slowly added to each tube with gentle shaking and the cell suspension was centrifuged at 1000 rpm for 8 min. The supernatant was discarded, and the cell pellet was suspended gently in 1 mL RPMI-1640 complete growth medium with HEPES containing 1% PHA and 0.1 μg/mL Colcemid. The tubes were then incubated for 15 min at 37 °C for the cell fusion to take place. Immediately after, fused cells were plated in petri dishes with 10 mL of McCoy's 5A complete culture medium and cultured for 20 h at 37 °C so that the asynchronous heterophasic multinucleated cells could be attached and proceed to the cell cycle. Upon the entry of main nuclei into mitosis, PCCs are induced and have the characteristic appearance of pulverized chromosomes for S phase cells, but without any chromosome shattering for G1 or G2-PCCs.

For the PCC analysis of interphase CHO heterophasic nuclei in the absence of RO-3306 CDK1 inhibitor, Colcemid at a final concentration of 0.1 μg/mL (Gibco) and fresh culture medium were added to the fused cells for 5 h before their harvest for chromosome preparation. For the categorization of interphase PCCs after delaying the entrance of the main CHO nuclei into mitosis by means of the RO-3306 inhibitor, following the 20 h culture of hybrid cells at 37 °C, they were further incubated at 37 °C for 12 h in fresh culture medium containing 10 μM final concentration of RO-3306. At that time, culture dishes were washed twice to remove RO-3306, and cultured in fresh medium plus Colcemid for 5 h, before they were harvested for chromosome preparation by selective detachment. Cells were then treated with hypotonic KCl (0.075 M) and fixed with two changes of methanol:glacial acetic acid (v/v 3:1). The chromosome spreads were prepared by the standard air-drying technique and slides were stained using 3% Giemsa in Sorensen buffer solution for PCC analysis. Three independent experiments were carried out and the corresponding data presented in Figure 4.11 are mean values ± SEM, obtained by cytogenetic assessment of interphase nuclei in hybrid cells when the main CHO nuclei entered mitosis. A total of 1083 induced PCC spreads were analyzed. Statistical significance was determined by means of four unpaired *t*-tests for each condition, corrected for multiple comparisons using the Holm-Sidak method with alpha = 0.05. Each row was analyzed individually, without assuming a consistent SD. Asterisks indicate statistical significance of the difference between untreated and treated samples; ns $p > 0.05$, * $p \leq 0.05$, ** $p \leq 0.01$, *** $p \leq 0.001$.

4.5. Conclusions

The results obtained provide direct experimental evidence indicating that the occurrence of asynchronous mitosis in heterophasic micronucleated or multinucleated cells is an important determinant of the shattering of genetic material in a single catastrophic event, which is a hallmark of chromothripsis. Chromosome shattering and genomic rearrangements appear to depend on the number of replication forks and the degree of completion of DNA replication, in MN or in heterophasic nuclei in multinucleated cells, when main nuclei enter mitosis. Consistent with our recent work [162], the results here support a simple model to explain how shattering of the genetic material can be initiated by a one-step cellular catastrophic event, and why it can be confined to one or a few chromosomes, or a chromosome arm. This model is an alternative to the one that considers nuclear envelope rupture or aberrant DNA replication in MN resulting in DSBs that must persist unrepaired into the next mitosis.

The mechanical stress exerted by chromatin condensation on sites still undergoing normal DNA replication in MN when main nuclei enter mitosis has, in itself, the potential to induce the collapse of replication forks that may develop into DSBs and cause chromosome shattering. Moreover, the extent of chromosome shattering depends on the magnitude of chromosome segments with late DNA replicating sites when main nuclei enter mitosis. Although shattering can possibly affect multiple chromosomes as well, leading to random fusion of their fragments, one envisions that only cells with one or a few rearranged chromosomal regions could survive and be detected in real cancers, probably determined by a selective advantage. When cells are affected by severe DNA damage, they undergo apoptosis, and this may happen in most cases when chromothripsis affects multiple chromosomes. Exceptionally, however, chromothripsis can cause disruption of tumor suppressor genes and activation of oncogenes, leading to cell survival.

Altogether, our results demonstrate that the dynamics of the PCC process arising during asynchronous mitosis in micronucleated or multinucleated cells, known to take place also in vivo [182], are an important determinant of chromosome shattering in a single catastrophic event, suggesting that they may underlie the mechanistic origin of chromothripsis. Among the several non-mutually exclusive cellular mechanisms that have been proposed, the present work supports the PCC hypothesis in MN. Nevertheless, additional studies are needed to provide definitive insights into this striking phenomenon and, subsequently, into its role in cancer initiation and progression. Deciphering chromothripsis may also be crucial for the development of strategies to interfere with the underlying processes in a therapeutic setup.

Chapter 5: Interphase Cytogenetic Analysis of G0 Lymphocytes Exposed to α-Particles, C-Ions, and Protons Reveals their Enhanced Effectiveness for Localized Chromosome Shattering—a Critical Risk for Chromothripsis

5.1. Introduction

For precision cancer radiotherapy purposes, the biological effects of energetic nuclei with high linear energy transfer (LET) have received growing attention lately, particularly regarding the mechanisms underlying their increased relative biological effectiveness (RBE) and potential risk for induction of secondary malignancies. Interestingly, despite their significant therapeutic benefits, particle irradiation has recently been reported to induce chromothripsis-like complex chromosomal alterations, similar to those generated by the phenomenon of chromothripsis in tumors [183,184]. Rather than by a stepwise accumulation of subsequent alterations, chromothripsis is a mutational process in which large stretches of chromosomes undergo massive but localized shattering and random rearrangements in response to a one-step catastrophic event [143–146]. By provoking inaccurate rejoining of chromosome fragments, this phenomenon leads to a new genome configuration and the formation of complex chromosomal alterations that may cause carcinogenesis [7–12], by amplification of oncogenes, for instance [142]. Therefore, full understanding of the processes underlying chromosome shattering and the formation of chromothripsis-like complex chromosomal alterations is an important step towards the clarification of the increased biological effectiveness and long-term health risk of high-LET particle irradiation. In this respect, we have recently provided experimental evidence supporting that localized chromosome shattering in micronuclei (MN) is triggered in a single catastrophic event by the dynamics of premature chromosome condensation (PCC) in asynchronous micronucleated cells [189]. Consequently, we consider it of interest to examine whether the dynamics of chromatin condensation during the cell cycle can transform persistent DNA and chromatin alterations into breaks, thereby explaining the increased efficacy of particle irradiation for killing cancerous cells and the formation of chromothripsis-like chromosomal alterations.

Towards this aim, we analyze chromosomal damage directly in interphase cells following the traversal of particle radiation through the nucleus, since chromosome alterations are correlated to both early (e.g., cell killing) and late effects (e.g., carcinogenesis) [190]. Low- and high-LET studies carried out in vitro and in vivo demonstrate that the types of chromosome aberrations observed, and the biological impact of an exposure depends on the radiation quality and energy deposited [191]. As a result of their low-density energy deposition, X- and γ-rays induce sparsely distributed damage, causing mostly indirect DNA lesions via increased oxidative stress to the interphase chromosomes that occupy localized domains of the nucleus [192–194]. Among the DNA lesions, double-strand breaks (DSBs) in the G0/G1 phase are the most dangerous, since there is no complementary strand available (like in the G2 phase) that could serve as a repair template [195–198]. In contrast to low-LET radiation, particle irradiation deposits high-density energy that is expected to induce direct focal DNA damage in chromosome domains along the particle tracks, leading to effective cell killing and increased tumorigenicity. In fact, accumulated evidence suggests that the increased RBE of high-LET radiation compared with photons is driven by the formation of complex DNA lesions [171,199–201], defined as DNA damage containing both DSBs and single-strand breaks (SSBs), as well as base damage within 1–2 helical turns. This is also referred to as clustered DNA damage and, together with clustered DSBs, defined as multiple DSBs, are generally accepted as the key lesions that determine the effectiveness of high-LET radiation [64,172,198–205]. However, their consequences at the chromosomal level and, particularly their role in the formation of chromothripsis-like chromosomal alterations are not clearly understood. This is mainly because the spectrum of DNA lesions induced by the traversal of high-LET particles through nuclei has proven very complex and difficult to study.

Indeed, the experimental validation of the induction of clustered DNA damage and the comprehension of the repair mechanisms involved have not been easy tasks [198,205]. In particular, the yields reported on chromosome aberrations and their complexity are time dependent due to repair effects, cell cycle delays, and the removal of non-surviving and apoptotic cells from the sample. This fact complicates the interpretation of the results obtained by means of the conventional analysis of irradiated cells at metaphase. Irradiation, especially with high-LET particles, retards the entry of damaged cells into mitosis and, therefore, one major problem in the analysis of heavy-ion induced aberrations is the cell cycle delay and G2-block, which depend not only on LET and dose, but also on the cell type [206–209].

In the present work, we investigate the impact of clustered DNA lesions, as indicated by the induction and post-irradiation repair of chromosomal damage, directly in interphase chromosomes. For this purpose, we use a clearly detectable cytogenetic endpoint of exposure in order to obtain reliable RBE values of different radiation qualities, as well as to investigate the mechanisms underlying the induction of chromosome shattering and the formation of chromothripsis-like chromosomal alterations. Towards this goal, the fusion PCC assay is employed to visualize and analyze chromosome fragmentation directly in G_0 human lymphocytes, without the requirement of exposed cells entering into mitosis [76,118]. Specifically, lymphocytes isolated from whole blood were exposed to various doses (up to 6 Gy) of α-particles (4.70 MeV, 92 keV/μm), accelerated C-ions (56.5 MeV, 295 keV/μm), and protons (2.2 MeV, 28.5 keV/μm). The yields of chromosome fragmentation obtained for induction and post-irradiation repair (up to 24 h) were compared with those obtained for γ-rays, in order to derive RBE values. Furthermore, we tested the hypothesis that clustered DNA lesions and persistent chromatin decompaction induced by high-LET irradiation at the damage sites along the particle tracks, can subsequently evolve into localized chromosome shattering if chromatin condensation occurs. The detection and quantification of such localized shattering of chromosome domains induced by each type of radiation quality was enabled by means of the PCC assay and a rigorous interphase cytogenetic assessment. The observed cytogenetic effect has the potential to serve as a fingerprint of high-LET exposure and instructs our proposal of a new model of the mechanistic origin of chromothripsis-like complex chromosomal rearrangements following particle irradiation.

5.2. Results

5.2.1. Interphase Cytogenetic Analysis of G_0 Lymphocytes by Means of the PCC Assay is a Promising Tool to Study the Mechanisms Underlying the Biological Effectiveness of Particle Irradiation

Cells irradiated with α-particles, accelerated C-ions, and protons, face a drastic alteration of their cell cycle kinetics and increased difficulties to reach mitosis. To overcome this problem, the PCC assay offers a unique tool to study induction and repair of radiation-induced chromosome aberrations directly in G_0 lymphocytes, without the requirement of exposed cells entering into mitosis. A representative image of non-irradiated peripheral blood G_0 lymphocytes exhibiting 46 prematurely condensed chromosomes (PCCs) is shown in Figure 5.1. The stable number of 46 PCCs in non-irradiated blood samples can be considered as a clearly detectable interphase cytogenetic endpoint. Indeed, it allows the detection and quantification of radiation-induced DNA lesions, as reflected at the level of interphase chromosomes by means of excess (over 46) PCC fragments. In the present study, the yields obtained for the different radiation qualities were used to derive RBE values and to investigate the mechanisms underlying their distinct effectiveness. As a result of low-density energy deposition, γ-rays induce chromosome fragmentation in interphase lymphocytes with a mostly random distribution among the chromosome domains in the nucleus, as shown in Figure 5.2A.

Figure 5.1. Representative image of a non-irradiated peripheral blood G_0 lymphocyte exhibiting 46 lightly stained single chromatid prematurely condensed chromosomes (PCCs) obtained by fusion with a mitotic Chinese Hamster Ovary (CHO) cell. The stable number of 46 PCCs in non-irradiated peripheral blood lymphocytes from healthy donors represents a clearly detectable interphase cytogenetic endpoint. In fact, it allows quantification of radiation-induced DNA lesions, as reflected at the level of interphase chromosomes by means of excess (over 46) PCC fragments.

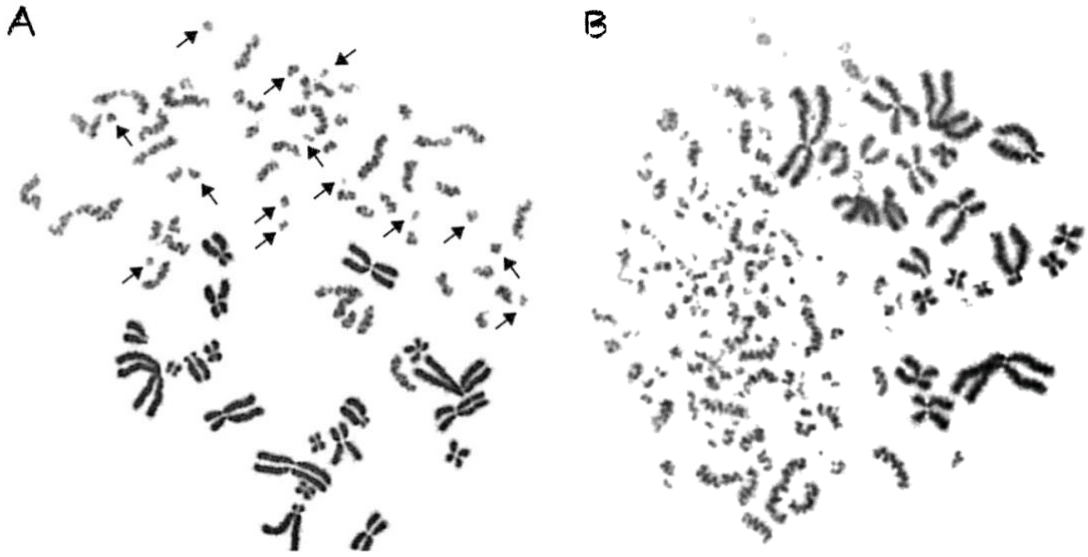

Figure 5.2. Irradiated peripheral blood G_0 lymphocytes with 4 Gy of γ-rays or 6 Gy of α-particles. (**A**) The impact of low-density energy deposition by 4 Gy of γ-rays translates into chromosome fragmentation in interphase lymphocyte PCCs with a sparse distribution among the chromosome domains of the nucleus, as shown by arrows. Fourteen excess (over 46) PCC fragments can be scored. (**B**) In contrast to γ-rays, even high-density energy deposited by 6 Gy of high-LET α-particle radiation induces direct focal clustered DNA lesions. These DNA lesions can be transformed into localized chromosome shattering in the domains along the particle track, leaving thus intact the non-targeted chromosomes, as shown in the lower part of the PCCs in this panel. One hundred excess (over 46) PCC fragments can be scored.

In contrast to γ-rays, the traversal of particle radiations through the nucleus deposits high-density energy that mainly induces—even at high doses—direct intense localized DNA lesions. These DNA lesions can be transformed into chromosome fragments only in the domains along the particle tracks, leaving thus intact the non-targeted chromosomes, as shown in the lower part of Figure 5.2B, for α-particles, as well as in Figure 5.3 for C-ions and protons. To analyze and quantify the impact of particle radiation-induced clustered DNA lesions at the chromosome level, we define a "localized shattered chromosome domain" as the fragmentation of an interphase chromosome into five or more clearly detectable fragments in close proximity. Such localized shattered chromosome domains, as shown by arrows in Figure 5.3A and 5.3B for C-ions and protons, respectively, may be used as a fingerprint of exposure to particle radiations. Furthermore, this observed cytogenetic endpoint may be easily quantified and may as well play a potential role in the elucidation of the mechanisms underlying differences in effectiveness among different radiation qualities, as explained in the paragraphs below and in the Discussion section.

The PCC analysis enables the follow-up examination of the observed chromosome shattering at progressing times after irradiation. In the case of low-LET radiation, such as γ-rays, a significant reduction in the number of excess PCC breaks takes place. This reduction of chromosome fragmentation reflects the processing of the underpinning subsets of DNA damage in interphase G_0 lymphocytes during the time between exposure and analysis. Regarding particle irradiation, a reduction in the number of excess PCC breaks may also be observed, as shown in Figure 5.4A for 24 h post-irradiation repair at 37 °C following a 6 Gy exposure to α-particles. However, a high percentage of the irradiated lymphocytes under the same conditions exhibit increased yields of excess PCC fragments and shattered chromosome domains even at 24 h repair time, as shown by arrows in Figure 5.4B. This observation suggests the presence of persistent particle radiation-induced clustered DNA lesions and chromatin alterations, even at 24 h post-irradiation repair time.

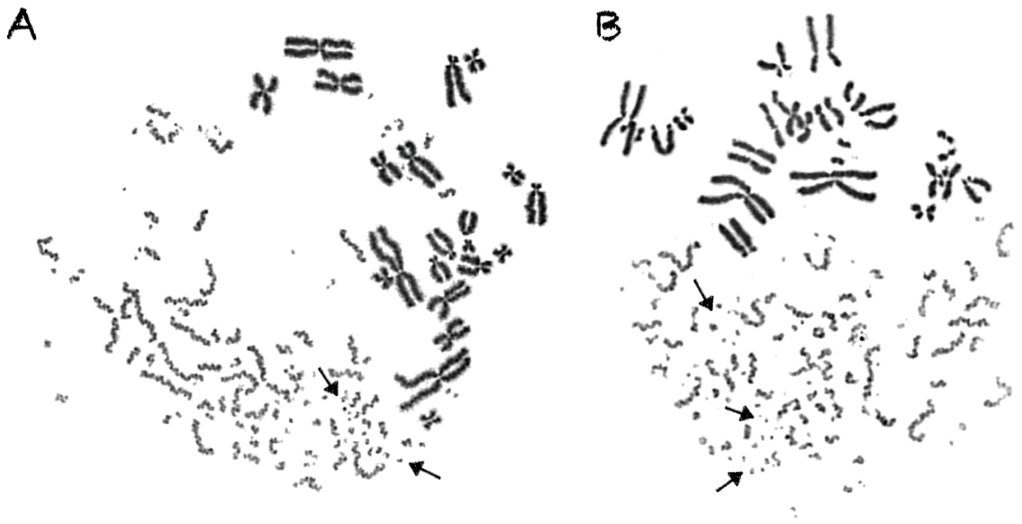

Figure 5.3. High-LET particle irradiation induces localized chromosome shattering, as revealed in G_0 lymphocyte PCC spreads. For analysis and quantification purposes regarding the impact of particle radiation-induced clustered DNA lesions at the level of interphase chromosomes, we define localized shattered chromosome domains as the fragmentation of an interphase chromosome into five or more clearly detectable fragments in close proximity to each other. Examples are shown by arrows for a G_0 lymphocyte spread obtained following exposure to 6 Gy of accelerated C-ions (**A**) and 4 Gy of protons (**B**). It is apparent that the non-targeted chromosome domains remain intact.

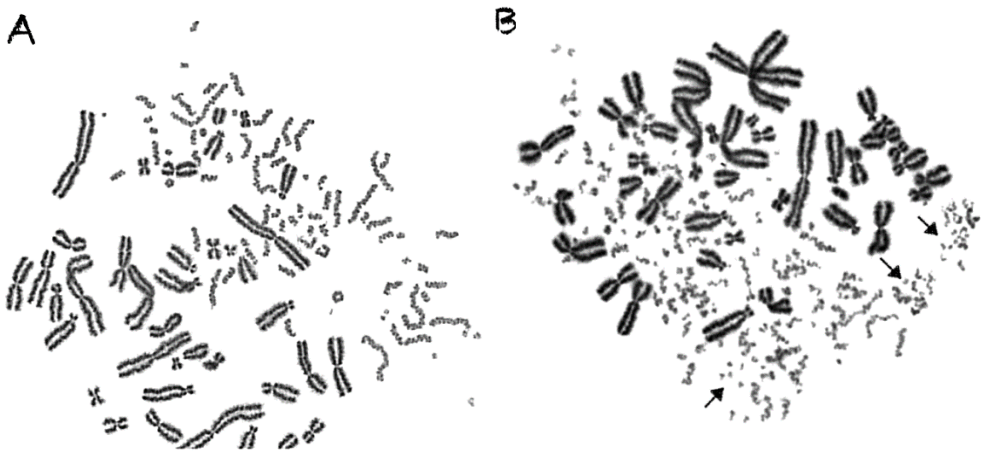

Figure 5.4. Following exposure to different radiation qualities, persistent shattered chromosome domains can be visualized and quantified in G_0 lymphocyte PCC spreads. (**A**) Ring formation and a reduction in the number of excess PCC breaks may be observed at 24 h post-irradiation repair time at 37°C, following exposure to 6 Gy of α-particles. (**B**) Under the same conditions, however, most of the irradiated lymphocytes still exhibit a high number of excess PCC fragments and shattered chromosome domains after 24 h of repair, as shown by arrows.

5.2.2. RBE Values for Different Radiation Qualities Can Be Obtained Using Chromosome Fragmentation Analysis Directly in Interphase G_0 Lymphocyte PCCs

RBE values were obtained using the PCC assay for the assessment and quantification of radiation-induced chromosomal aberrations directly in human peripheral blood G_0 lymphocytes, following exposure to different radiation qualities. Compared with γ-rays, a significant increase in damage induction and subsequent yields of excess PCCs per nucleus was obtained for doses up to 6 Gy of α-particles, C-ions, and protons, as depicted in Figure 5.5. Based on our analysis, the RBE values obtained for induction of chromosomal damage were calculated to be 4.1 for α-particles, 2.6 for C-ions, and 2.1 for protons.

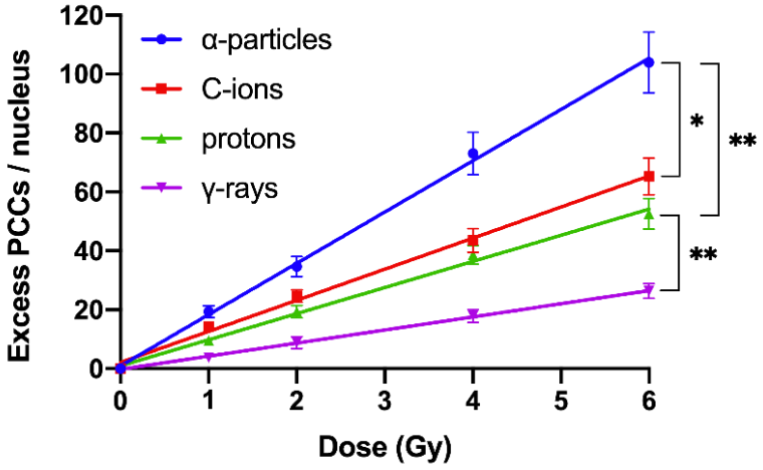

Figure 5.5. Dose–response curves for the initial DNA lesions induced by different radiation qualities as reflected in G_0 lymphocyte PCCs and constructed by means of excess PCC fragments per nucleus at various doses up to 6 Gy of α-particles, C-ions, protons, and γ-rays. Based on this cytogenetic endpoint of initial induction of radiation damage, the relative biological effectiveness (RBE) values obtained were 4.1 for α-particles, 2.6 for C-ions, and 2.1 for protons. (Mean ± SD based on three independent experiments; $n \geq 50$ cells analyzed per experimental point; * $p \leq 0.05$, ** $p \leq 0.01$).

Our studies also revealed differences in the repair kinetics of radiation-induced chromosomal aberrations in G_0 lymphocytes for the different radiation qualities used. The yields of excess PCCs

following repair were quantified by the residual un-rejoined fragments at various post-irradiation repair times up to 24 h at 37 °C, as presented in Figure 5.6. Increased post-repair RBE values were obtained, when compared with those obtained for the initial induction of chromosomal damage. Specifically, post-repair RBE values at 24 h were found to be 10.7 for α-particles, 5.4 for C-ions, and 3.9 for protons.

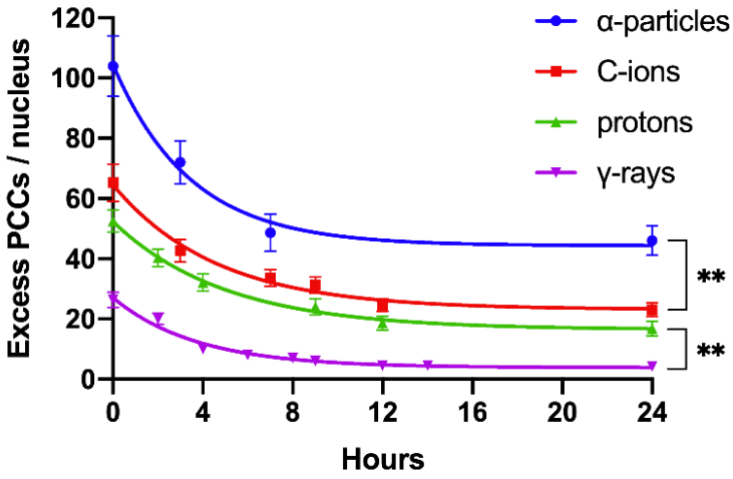

Figure 5.6. Repair kinetics of the initial DNA lesions induced by 6 Gy of different radiation qualities as reflected in G_0 lymphocyte PCCs and constructed by means of excess PCC fragments per nucleus at various repair times up to 24 h. Based on this cytogenetic endpoint of residual lesions at 24 h repair time, the derived RBE values were 10.7 for α-particles, 5.4 for C-ions and 3.9 for protons. (Mean ± SD based on three independent experiments; $n \geq 50$ cells analyzed per experimental point; ** $p \leq 0.01$).

5.2.3. Shattered Chromosome Domains are a Fingerprint of Exposure to High-LET Particle Radiation and their Yield Depends on Dose and Radiation Quality

An additional aim of our experimental design was to search for a specific fingerprint of exposure to high-LET particle radiation, since this important issue remains open and the data are controversial [15]. Towards this goal, we exploited our observation that focal deposition of high-density energy by particle irradiation can shatter a targeted chromosome domain along the particle tracks into several (five or more) clearly detectable fragments in close proximity (Figure 5.3). Indeed, such shattered chromosome domains are very frequent in G_0 lymphocyte PCCs following exposure to high-LET particle radiations, compared with γ-rays. For instance, when G_0 lymphocytes are exposed even to only 1 Gy of α-particles, three shattered chromosome domains can be scored in the PCC spread shown in Figure 5.7A, but none in the case of exposure to 1 Gy of γ-rays, as shown in Figure 5.7B. Therefore, such localized shattering of a targeted chromosome domain visualized in G_0 lymphocyte PCCs may be considered as a fingerprint of exposure to high-LET particle radiation. The yields of shattered chromosome domains per nucleus, following exposure to various doses up to 6 Gy for the different radiation qualities used, are shown in Figure 5.8. Linear dose–response relationships were obtained, with RBE values of 14.3 for α-particles, 7.5 for C-ions, and 4.9 for protons.

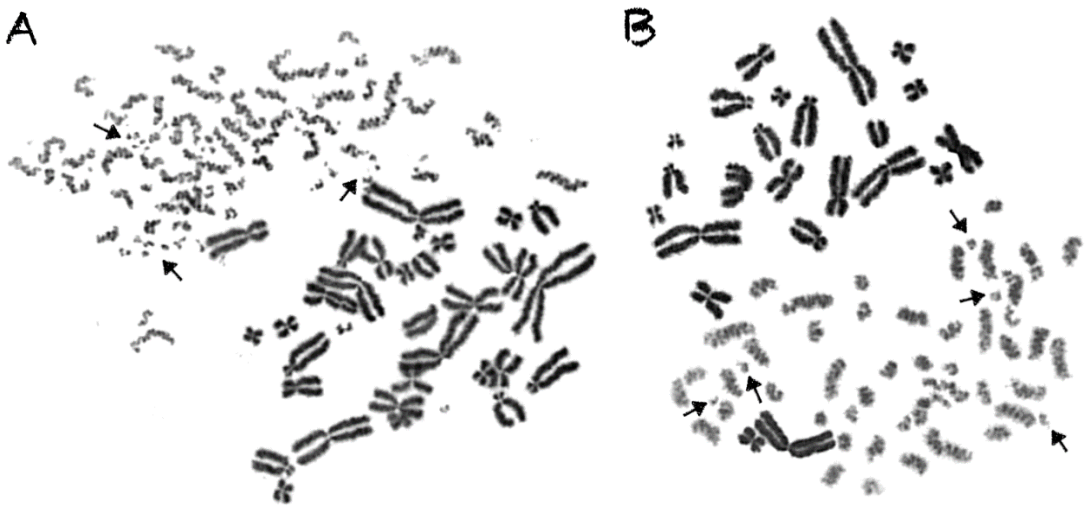

Figure 5.7. Shattered chromosome domains are very frequent in G_0 lymphocyte PCCs following exposure to high-LET particle radiations, compared with γ-rays. (**A**) Exposure to even 1 Gy of α-particles can result in three localized shattered chromosome domains, as shown by arrows. (**B**) In contrast, following 1 Gy of γ-rays, only single randomly distributed chromosome fragments could be visualized. Therefore, such localized shattering of targeted chromosome domains may be considered as a fingerprint of exposure to high-LET particle radiation.

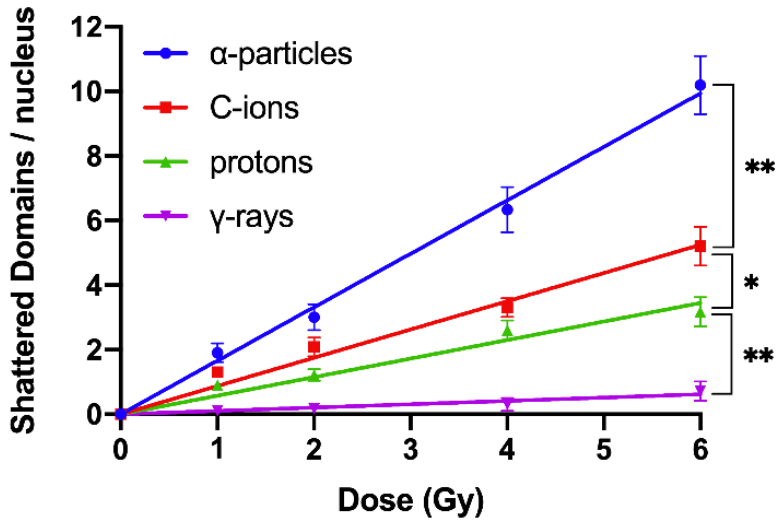

Figure 5.8. Dose–response curves for the yields of shattered chromosome domains per nucleus, following exposure to various doses up to 6 Gy of the different radiation qualities. Linear dose–response relationships were obtained with most effective being the α-particles, followed by C-ions, protons, and γ-rays. Based on this cytogenetic endpoint of the initial induction of clustered DNA lesions and formation of shattered chromosome domains, the RBE values obtained were 14.3 for α-particles, 7.5 for C-ions, and 4.9 for protons. (Mean ± SD based on three independent experiments; $n \geq 50$ cells analyzed per experimental point; * $p \leq 0.05$, ** $p \leq 0.01$).

5.2.4. Persistent Shattered Chromosome Domains may Explain Differences in Biological Effectiveness among Different Radiation Qualities and the Induction of Chromothripsis-like Rearrangements

The transformation of particle irradiation-induced clustered DNA lesions into the observed localized shattering of chromosome domains is revealed in our experiments by means of the premature chromosome condensation dynamics. Yet, this transformation can also take place by means of the cell cycle dependent chromatin condensation dynamics when cells proceed to G2/M phase transition, assuming that the lesions induced by particle radiation in the targeted chromosome

domains are persistent. In order to investigate this assumption, G_0 lymphocytes were irradiated with 6 Gy of α-particles, C-ions, protons, and γ-rays. The yields of shattered chromosome domains were obtained, either immediately after exposure or at 24 h post-irradiation repair time, as shown in Figure 5.9. Particle radiation-induced persistent lesions in the chromosome domains of a nucleus remain higher for α-particles with an RBE value of 28.6, followed by C-ions with 10.5, and protons with 4. All the RBE values calculated in the present work are summarized in Table 5.1. Persistent lesions are thus of importance, since chromatin dynamics during G2/M phase may transform them into localized chromosome shattering, a hallmark of chromothripsis. Moreover, random rejoining of shattered chromosomes may evolve into chromothripsis-like rearrangements, as we describe in the Discussion section.

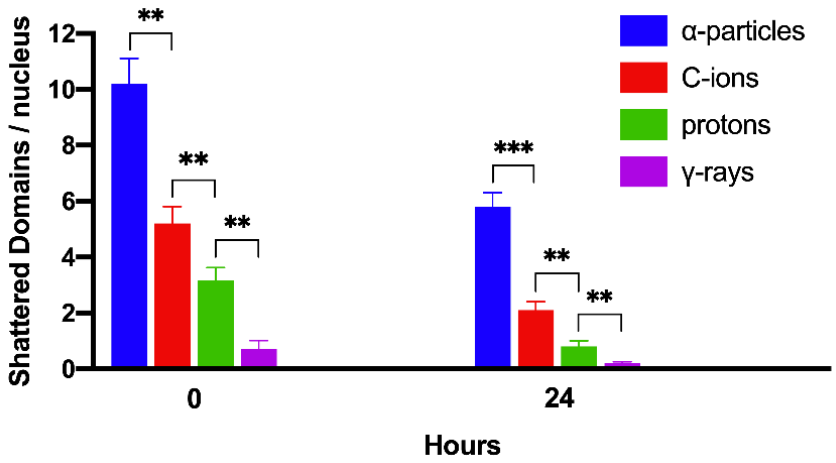

Figure 5.9. Persistent shattered chromosome domains at 24 h repair time, following exposure to different radiation qualities. G_0 lymphocytes were irradiated with 6 Gy of α-particles, C-ions, protons or γ-rays and the yields of shattered chromosome domains were obtained, either immediately after exposure (0 h) or at 24 h post-irradiation repair time. Particle radiation-induced persistent shattered chromosome domains of the nucleus remain higher for α-particles, followed by C-ions and protons, being the least for γ-rays. Based on this cytogenetic endpoint of persistent shattered chromosome domains after 24 h, the RBE values obtained were 28.6 for α-particles, 10.5 for C-ions, and 4 for protons. (Mean ± SD based on three independent experiments; $n \geq 50$ cells analyzed per experimental point; ** $p \leq 0.01$, *** $p \leq 0.001$).

Table 5.1. Summary of all the RBE Values Compared with γ-rays.

Radiation quality	RBE Excess PCCs / nucleus		RBE Shattered Domains / nucleus	
	0 h	24 h	0 h	24 h
α-particles	4.1	10.7	14.3	28.6
C-ions	2.6	5.4	7.5	10.5
protons	2.1	3.9	4.9	4

5.3. Discussion

5.3.1. Can Clustered DNA Lesions Alone Account for the Formation of Complex Chromosomal Aberrations and the Increased Relative Biological Effectiveness of Particle Irradiation?

While it is commonly accepted that clustered DNA damage is characteristic of high-LET radiation, the mechanisms through which it causes complex and, particularly, chromothripsis-like alterations [183,184] similar to those generated by the phenomenon of chromothripsis in tumors, have not yet been clarified. This is mainly because the scale of clustered DNA damage is in the order of

10–30 bp, i.e., < 3–4 nm, whereas the scale of chromosomal rearrangements is in the order of > 1000 bp, i.e., > 50–100 nm distance. To explain this discrepancy between clustered DNA lesions and chromosomal rearrangements in terms of scale, the possibility of mis-rejoining two DSBs belonging to distinct loci must be considered [210]. Indeed, this difference may be resolved by the existence of clustered DSBs in close proximity along the tracks of high-LET particle radiation. Specifically, 3D-structured illumination microscopy revealed the formation of clustered DSBs within γH2AX foci signals in C-ion-irradiated G2 phase cells [211]. While clustered DNA damage is typically defined by the presence of additional lesions in the immediate vicinity of the DSBs, clustered DSBs or multiple DSBs represent a further level of overall damage complexity. As a result, clustered DSBs likely add a substantially higher accident risk to any repair process attempt [196,198]. Therefore, this form of damage may underpin the increased efficacy of high-LET radiation, since clustered DSBs are more challenging to repair and have a larger probability of lethality [171,199–201]. The spectrum of clustered DNA lesions induced by the traversal of high-LET particles through nuclei has proven very challenging and difficult to study, when considering interactions only at the DNA level and not at the chromosome level, where the dynamics of chromatin conformation changes during the cell cycle come into play. However, elucidating the link between clustered DNA lesions and formation of complex chromosome rearrangements is crucial for both particle radiotherapy and space radiation protection.

5.3.2. Chromosome Aberration Analysis of G_0 Lymphocyte PCCs Enables the Assessment of DNA Damage without the Requirement of Irradiated Cells Entering into Metaphase

In the present study, our experimental strategy focused on the impact of clustered DNA lesions on chromosome fragmentation under the dynamics of chromatin organization changes in interphase cells. As shown in Figure 5.1, the fusion PCC assay offers a clearly detectable cytogenetic endpoint of exposure based on chromosome fragmentation analysis in G_0 lymphocyte PCCs. The presence of 46 prematurely condensed chromosomes in non-irradiated lymphocytes represents the normal human genome and is, thus, a clearly stable number without variability among healthy blood donors. As a result of energy deposition by ionizing radiation, the induced clustered DNA lesions can be transformed into interphase chromosomal fragmentation with a random and homogeneous distribution following low-LET exposure (Figure 5.2A) [162,168]. However, following high-LET particle irradiation, the focal deposition of high-density energy induces clustered DSBs and affects chromatin at their sites only in the chromosome domains along the particle tracks [198,212]. As a result, localized chromosome shattering occurs under the dynamics of chromatin condensation—even at high doses—as shown in Figure 5.2B for α-particles, in Figure 5.3A for C-ions, and in Figure 5.3B for protons. Analysis of PCCs at progressing times after irradiation up to 24 h can show a reduction in the number of excess PCC breaks. This reduction of chromosome fragmentation reflects the processing of the underpinning subsets of DNA damage and formation of rings and translocations during the time between exposure and analysis in interphase G_0 lymphocytes (Figure 5.4A) [213]. However, a high percentage of the irradiated lymphocytes under the same conditions exhibit the presence of localized chromosome shattering even at 24 h post-irradiation repair time (Figures 5.4B and 5.9), plausibly due to persistent clustered DNA lesions and chromatin alterations.

5.3.3. Reliable RBE Values for Particle Radiations Can Be Established Using Fragmentation of Interphase Chromosomes as a Biological Endpoint

To obtain dose–response relationships for different radiation qualities, the yield of radiation-induced chromosome fragments in interphase G_0 lymphocytes can be expressed as excess (over 46) PCCs (shown in Figure 5.2). The results obtained demonstrate that excess PCCs increase linearly with radiation dose and that high-LET radiation generates a higher level of excess PCCs than low-LET γ-rays (Figure 5.5). An examination of the reduction in excess PCCs up to 24 h post-irradiation reveals that the fragments decrease with time but are at a significantly higher level following high-LET radiation (Figure 5.6). Furthermore, a quantification of shattered chromosome domains shows as well that their frequency increases linearly with radiation dose (Figure 5.8), whereas at 24 h post-

irradiation repair time persistent shattered chromosome domains remain higher for α-particles, followed by C-ions and protons, being the least for γ-rays (Figure 5.9). When compared with γ-rays, the RBE values obtained using the above biological endpoints, range from 4.1 to 28.6 for α-particles, 2.6 to 10.5 for C-ions, and 2.1 to 4.9 for protons, as presented in Table 5.1.

Top of FormBottom of FormEarlier studies using fusion-induced PCC in G1 cells from mammalian cell lines reported RBE values ranging only from 1 to 2 for high-LET α-particles [214,215] or swift heavy-ions [216–220]. However, recent experiments at the Heavy Ion Medical Accelerator (HIMAC) in Japan using G0/G1 phase of normal human fibroblasts report values as high as 30 at low doses [221,222]. For protons, an RBE of 1.1 is used clinically, although this depends on various physical and biological factors and there is an ongoing debate about its accuracy (reviewed in [223]). Based on the endpoints examined in the present work, we calculated higher RBE values (2.1–4.9) for protons, which could be the result of the high LET values obtained (28.5 keV/μm) when using low energy protons (2.2 MeV incident energy). Overall, the increased RBE values obtained in our repair experiments (Table 5.1) can be of interest, since the intrinsic radiosensitivity of normal or tumor human cells often correlates with the level of residual breaks [217,224,225].

5.3.4. Localized Chromosome Shattering Induced by Energetic Nuclei May be Used as a Fingerprint of Exposure

When using conventional cytogenetics for chromosome aberration analysis at metaphase, high RBE values are obtained if analyzed in the first post-irradiation metaphases, but they are only close to 1 if the analysis takes place in the progeny of irradiated cells. Such data may suggest that most of heavy ion induced chromosome aberrations are non-transmissible to the progeny cells. Consequently, this observation could translate into diminishing late effects and, therefore, could be considered a significant advantage of particle radiotherapy. However, such possibility should be validated, particularly in the light of recent reports that show formation of chromothripsis-like alterations related to potential late effects of particle irradiation [183,184]. Indeed, these reports provide evidence that particle radiation can induce chromothripsis-like complex chromosomal alterations similar to those generated by the phenomenon of chromothripsis in tumors. These new data could have a profound impact on RBE for potential late effects of energetic nuclei and, especially for initiation of carcinogenesis by specific chromosome rearrangements. In this respect, it is crucial to understand how chromothripsis-like complex chromosomal alterations can be formed following high-LET exposure and, to what extent, the localized chromosome shattering within the nucleus can be initiated by particle irradiation. Therefore, the identification of a fingerprint of particle radiation exposure, particularly regarding the late effects and carcinogenesis, is important.

When G_0 lymphocytes are exposed even to only 1 Gy of α-particles, three shattered chromosome domains can be scored in the PCC spread shown in Figure 5.7A, but none can be scored in the case of exposure to 1 Gy of γ-rays, as shown in Figure 5.7B. These results suggest that high-LET particle radiations are more efficient biologically because they generate more shattered chromosome domains along their tracks in the nucleus. Indeed, the observed localized shattering of interphase chromosomes, with high risk for random rejoining, is probably the precursor of complex intra-chromosomal rearrangements that are recognized as characteristic events of particle irradiation [131,226]. Furthermore, our observation that α-particles, accelerated C-ions, and protons have a dose-dependent enhanced effectiveness to induce localized chromosome shattering (Figure 5.8), a hallmark of chromothripsis, and may contribute towards the identification of a fingerprint of exposure that could be related to an increased risk of secondary malignancies. Specifically, clustered DNA damage and clusters of DSBs, which are induced by the focal deposition of high-density energy in chromosome domains along the particle tracks, can be reflected and visualized in G_0 lymphocyte PCCs as localized shattered chromosome domains. Such localized chromosome shattering is characterized by the presence of multiple closely spaced fragments within individual chromosomes and could be considered as a fingerprint of exposure (Figures 5.3, 5.4B, and 5.7A). The RBE values established using such a fingerprint as biological endpoint are significantly higher than those obtained for excess PCCs/nucleus (Table 5.1). Altogether, our results suggest that localized

chromosome shattering can be used to elucidate the mechanistic origin of the differences in biological effectiveness obtained experimentally for the various radiation modalities used (Figures 5.8 and 5.9).

5.3.5. *Our Model: Clustered DNA Lesions are Transformed through Chromatin Condensation into Localized Chromosome Shattering and, via Random Rejoining, Evolve into Chromothripsis-like Rearrangements*

At the DNA level, particle irradiation is expected to induce a variety of complex DNA lesions, challenging the DNA repair enzymatic machinery (reviewed in [227]). A shifting of the DNA damage response (DDR) system towards less-accurate non-homologous end joining (NHEJ) repair pathways for DSBs and all other neighboring DNA lesions has been suggested [228]. It is a general current consensus that the fidelity of repair depends on the complexity of the lesion, with clustered DSBs being more difficult to repair than isolated breaks [229]. Complex DSBs, either formed directly by irradiation or by the processing of non-DSB clustered lesions, are expected to be processed by slow kinetics or left unrepaired and cause cell death or pass mitosis. In these surviving cells, large deletions, translocations, and chromosomal aberrations have been detected (reviewed in [230]). Nevertheless, the exact mechanism underlying the transformation of clustered DNA lesions into such chromosomal alterations is not yet clearly understood. Based on our previously published evidence on the dynamics of chromatin condensation changes in transforming DNA lesions with chromatin decompaction at their sites into visual breaks [117,162,168], we propose here that high-LET radiation induces not only clustered DNA lesions, but also physical perturbation of the chromatin organization and persistent chromatin decompaction at the sites of clustered DNA lesions. This dual action of energetic nuclei on DNA and chromatin is a key characteristic of high-LET radiation and can translate into localized chromosome shattering in a one-off event, by the dynamics of chromatin condensation during the cell cycle. The fact that shattering of chromosome domains can be observed immediately after irradiation by means of premature chromosome condensation (Figure 5.8), together with their relative persistence (Figure 5.9), suggest that the dynamics of chromatin condensation can initiate the single destructive event needed for the phenomenon of chromothripsis to occur. Indeed, localized chromosome shattering in neighboring chromosome domains along the particle tracks followed by random rejoining may evolve into chromothripsis-like complex chromosomal rearrangements.

According to our hypothesis, when clustered DNA lesions and their associated chromatin decompaction are induced by particle irradiation, e.g., in the S phase, their conversion into localized chromosome shattering may also take place by means of cell cycle dependent chromatin condensation dynamics as cells proceed to the G2/M-phase transition. Therefore, the critical parameter for radiation-induced chromothripsis is not the dose itself but the radiation quality and the potential of high-LET particle irradiation to induce persistent clustered DNA lesions and chromatin decompaction at their sites. Direct experimental evidence reinforcing this view was provided recently by Timm et al. [212]. These authors demonstrated experimentally that clustered DNA damage concentrated in particle trajectories causes persistent rearrangements in chromatin architecture, which may affect the structural and functional organization of cell nuclei. In fact, they demonstrated that chromatin decompaction and remodeling during repair of clustered DNA damage fails to restore the original nucleosomal organization at damage sites. On the contrary, after low-LET irradiation, the induced single DSBs throughout the nucleus in euchromatin and heterochromatin were efficiently repaired without damage-associated large-scale remodeling of chromatin. Their results suggest, therefore, that the impact of low-LET radiations on chromatin is not persistent. This difference in response at the chromatin level, together with the induction of clustered DNA lesions, constitute the high-LET dual action that we consider in our model to explain why particle radiations are more prone to induce chromothripsis-like rearrangements.

Chromothripsis-like chromosomal rearrangement could be as well generated following particle radiation-induced localized chromosome shattering through the formation of MN in the progeny of irradiated cells [146,156,189]. Since particle radiation-induced clustered DNA lesions and chromatin decompaction at their sites are more persistent than those induced by low-LET radiation [212], they have an increased capacity to proceed to G2/M transition and undergo chromatin condensation. As a result, chromosome fragmentation will take place leading to aberrant cell mitosis and formation of

micronucleated cells via asymmetrical cell division. When main nuclei in micronucleated cells enter mitosis, premature chromosome condensation in MN provokes shattering of the chromosomes entrapped inside micronuclei, if they are still undergoing DNA replication and thus have maximum chromatin decompaction at their replication sites. Under these conditions, chromatin condensation dynamics exert mechanical stress causing DNA replication forks to collapse into DSBs, leading to localized chromosome shattering in a single catastrophic event that may be followed by random rejoining and subsequently evolve into chromothripsis-like chromosomal rearrangements in the progeny cells, as we have recently proposed [189].

5.4. Materials and Methods

5.4.1. Cell Cultures and Preparation of PCC-Inducer Mitotic CHO Cells

Chinese Hamster Ovary (CHO) cells were grown in McCoy's 5A (Biochrom, Berlin, Germany) culture medium supplemented with 10% FBS, 1% l-glutamine, and 1% antibiotics (Penicillin, Streptomycin), and incubated at 37 °C in a humidified atmosphere with 5% CO_2. CHO cultures were maintained as exponentially growing monolayer cultures in 75 cm^2 plastic flasks at an initial density of 4×10^5 cells/flask. Colcemid (Gibco) at a final concentration of 0.1 μg/mL was added to CHO cultures for 4 h and the accumulated mitotic cells were harvested by selective detachment. Once a sufficient number of mitotic cells had been obtained, they were used as supplier of mitotic promoting factors (MPF) to induce PCC in human lymphocytes. The mitotic CHO cells harvested from one 75 cm^2 flask were used for 2–3 fusions.

5.4.2. Lymphocyte Isolation from Human Peripheral Blood

Peripheral blood samples in heparinized tubes were obtained from healthy male and female donors. Lymphocytes were isolated from whole blood using Biocoll separating solution (Biochrom). The blood samples diluted 1:2 in RPMI-1640 without FBS were carefully layered on top of equal amounts of Biocoll in 14mL test tubes and centrifuged at 400× *g* for 20 min. Collected lymphocytes from each tube were washed with 10 mL culture medium (RPMI-1640 supplemented with 10% FBS, 1% glutamine, and antibiotics), centrifuged at 250× *g* for 10 min, and kept in culture medium before irradiation with different radiation qualities. Lymphocytes isolated from 1 mL of blood were used for each experimental point.

5.4.3. Irradiation and Sample Preparation

In the present work, lymphocytes isolated from whole peripheral blood were exposed to a gamma irradiator, a source of α-particles, accelerated C-ions, and to a proton beam. For γ-rays exposure, irradiation of lymphocytes was carried out in vitro using a Co-60 Gamma Cell 220 irradiator (Atomic Energy of Canada Ltd., Ottawa, Canada) at room temperature with 1.3 MeV photons and LET at 0.2 keV/μm with a dose rate of 20 cGy/min. Lymphocyte suspensions in culture medium were exposed for different times in order to deliver doses ranging from 0 to 6 Gy. Following irradiation, lymphocytes were either processed immediately for their fusion and PCC induction (a procedure that permits approximately a repair time of 1 h) or allowed to repair at 37 °C for different times up to 24 h. Subsequently, the samples were processed for cell fusion, PCC induction, and preparation of microscope slides in order to analyze the PCC spreads.

For exposure to α-particles, a Curium-244 alpha source (Isotope Producers Laboratories, CA, USA) was used with particle energy 4.70 MeV at the cell surface entrance and LET at 92 keV/μm. For C-ions exposure, accelerated Carbon-12 ions at 56.5 MeV with LET at 295 keV/μm was applied. For exposure to protons, a proton beam with an incident energy of 2.2 MeV and LET of 28.5 keV/μm was used. For the particle irradiation, lymphocytes were exposed as a monolayer in a special cube. The density of lymphocyte suspension was adjusted using an inverted microscope so that lymphocytes were exposed as a monolayer in contact to each other without gaps.

For α-particles (perpendicular beam), 20 μL of dense lymphocyte suspension were diluted in 0.5 mL of medium, it was loaded into the cube and allowed to sediment onto a mylar surface of 6 μm

thickness and 13 mm diameter before sample irradiation. For protons and accelerated C-ions (horizontal beam), 20 μL of dense lymphocyte suspension was sandwiched between two mylar surfaces, enabling thus their exposure to the horizontal beams. The irradiation of samples was carried out at the Legnaro Lab accelerators and the homogeneous exposure of the targeted cells in the entire mylar surface by the radiation beam was ensured by means of appropriate testing. The dose-rate for α-particles was 0.22 Gy/min, whereas for proton irradiation was 1 Gy/min and for 295 keV/um carbon-ion irradiation was 2 Gy/min. The energies of particle and ion irradiations, as well as the experimental set-up, were chosen in a way to always guarantee the so-called "track segment conditions" (or to be very close to these) in order to obtain the correct evaluation of the deposited energy in the cell and then of the dose [231,232]. All particle energy values, and corresponding LET refer to incident energy at the cell entrance. Considering that in our experiments the targeted cells were lymphocyte monolayers, the particles traversed the cells retaining considerable energy, so the Bragg peak was not totally contained in the exposed sample, even though the biological endpoints proposed in this work were found to be sensitive enough to distinguish the effectiveness of the different radiation qualities used.

5.4.4. Cell fusion-Mediated Induction of Premature Chromosome Condensation in Lymphocytes

Cell fusion and PCC induction were performed using 45% polyethylene glycol (PEG, P5402, Sigma-Aldrich, Darmstadt, Germany) in serum-free RPMI-1640 medium. Lymphocytes and mitotic CHO cells were mixed in serum-free RPMI-1640 medium in a 14 mL round-bottom culture tube in the presence of colcemid as originally described [108] with some modifications. After centrifugation at 1000 rpm (100× *g*) for 8 min, the supernatant was discarded without disturbing the cell pellet, keeping the tubes always inverted in a test tube rack on a paper towel to drain the pellet from excess liquid. While holding the tubes in an inverted position, 0.15 mL of PEG was injected forcefully against the cell pellet using a micropipette and, immediately after, the tube was turned in an upright position and held for about 1 min. Subsequently, 1.5 mL of PBS was slowly added to the tube with gentle shaking and the cell suspension was centrifuged at 1000 rpm for 8 min. The supernatant was discarded, and the cell pellet was suspended gently in 0.7 mL RPMI-1640 complete growth medium containing PHA and colcemid. After 75 min at 37 °C, cell fusion/PCC induction was completed. Cells were then treated with hypotonic KCl (0.075 M) and fixed with three changes of methanol: glacial acetic acid (v/v 3:1).

5.4.5. Cytogenetic Analysis, Scoring Criteria, Statistical Analysis

The chromosome spreads were prepared by the standard air-drying technique and slides were stained using 3% Giemsa in buffered solution for PCC analysis. The PCC fragments per cell characterized as "Excess PCCs/Cell" (i.e., in excess of 46 PCCs) were scored for damage induction or post-irradiation repair points using light microscopy. The analysis of PCC spreads was greatly facilitated by an image analysis system (Ikaros, MetaSystems, Germany). Detection and quantification of the impact of radiation-induced clustered DNA lesions (i.e., clustered DNA damage and clustered DSBs) on interphase chromosomes, in terms of localized chromosome shattering, was made through the visualization and subsequent analysis of the 46 chromosome domains in G_0 lymphocyte PCC spreads. For this purpose, we defined "shattered chromosome domains/nucleus" as the yields per nucleus of shattered interphase chromosomes containing five or more clearly detectable fragments in close proximity to each other (e.g., Figures 5.3, 5.4B, and 5.7A). For each experimental point, at least 50 cells (G_0 lymphocyte PCC spreads) were analyzed and the experimental results shown in Figures 5.5, 5.6, 5.8, and 5.9, represent mean values ± SD based on three independent experiments for α-particles, C-ions, and γ-rays; and two independent experiments for protons. Statistical significance was determined by means of unpaired t-tests, corrected for multiple comparisons using the Holm–Sidak method with alpha = 0.05. Each dose was analyzed individually, without assuming a consistent SD. Asterisks indicate statistical significance; * $p \leq 0.05$, ** $p \leq 0.01$, *** $p \leq 0.001$.

5.5. Conclusions

By means of a clearly detectable biological endpoint, we obtained reliable RBE values for α-particles, C-ions, and protons, and studied the mechanisms underlying the efficacy of particle irradiation to induce localized chromosome shattering, a hallmark of chromothripsis. Specifically, based on chromosome fragmentation analysis of G_0 lymphocyte PCCs, our test system reflects the impact of radiation-induced clustered DNA lesions on induction and post-irradiation repair in interphase chromosomes. The results provide the first direct experimental evidence that high-LET particle radiations have an increased effectiveness for localized chromosome shattering in domains along the particle track. This specific effect is shown to be a fingerprint of exposure, which can improve our understanding and unravel the differences in biological effectiveness exhibited by various radiation qualities. It points as well to our proposal of a new model for the mechanisms underlying the formation of critical complex chromosome alterations.

Indeed, the potential of particle irradiation to induce persistent lesions at the level of DNA as well as of chromatin, in neighboring chromosome domains along the particle tracks, may be a key determinant of the formation of chromothripsis-like chromosomal rearrangements. Such dual action of particle radiation may lead to localized chromosome shattering under the dynamics of chromatin condensation, which may be followed either by random rejoining of chromosome fragments, or aberrant mitosis and MN formation. In both cases, chromothripsis-like rearrangements similar to those caused by chromothripsis in tumors may be generated with a potential impact on long-term health risks. High-LET particle radiation is more likely, therefore, to cause complex focal genomic changes leading to a higher level of genomic instability. To examine this possibility, additional insights into the fate of the localized shattered chromosomes could be obtained for different radiation qualities by combining the PCC assay with the Fluorescence in Situ Hybridization (FISH) technique, as we have already demonstrated for low-LET radiation [67,213]. Overall, our results are of importance to radiation oncology and space radiation protection, since the induction of complex and chromothripsis-like alterations by particle radiation may generate adverse effects and increased risk of secondary malignancies.

Chapter 6: An Enhanced G2-Assay for Individualized Radiosensitivity (IRS) Assessment

6.1. Introduction

Genes coding for cytoplasmic proteins that act as phosphorylation substrates of the key mediators in DNA damage response activation are perhaps the most crucial factors determining radiosensitivity. In particular, ATM, ATR, and Chk1 kinases facilitate cell cycle arrest protecting against the conversion of DNA lesions into chromatid breaks during G2/M phase transition. Based on this hypothesis, a standardized G2-assay has been developed: a predictive cytogenetic assay for estimating the level of individualized radiosensitivity (IRS), as a percentage of the highly radiosensitive Ataxia Telangiectasia (AT) patients, who have a compromised G2/M checkpoint [233].

The assay involves *in vitro* irradiation of exponentially growing peripheral blood lymphocytes, split of irradiated culture into two identical samples, and G2-checkpoint abrogation by caffeine in one of the two samples. As a result, the sample treated with caffeine will approximate the response of AT patients [234], and serve as an internal control for obtaining the IRS value of the testing sample [235]. The analysis is based on the yield of chromatid breaks (Figure 6.1) as a function of G2-checkpoint capability to facilitate DNA damage recognition and cell cycle arrest, as well as of the effectiveness of Cdk1/Cyclin B activity in the conversion of unrepaired DNA damage into chromatid breaks during G2/M phase transition and chromatin condensation. IRS is then estimated as a percentage of the yield of chromatid breaks obtained in the sample with abrogated G2-checkpoint, which approximate the response of AT patients. The IRS cut-off value, below which an individual is classified as radioresistant, was set at 30%; 30—50% as normal; 50—70% as radiosensitive, and above 70% as highly radiosensitive [233].

Yet, this approach has two crucial limitations. Firstly, it requires a 72 h culture of stimulated blood lymphocytes to obtain an adequate number of G2 phase cells, before their exposure to 1 Gy irradiation with gamma or X-rays. Secondly, despite their 72 h culture, only a very small percentage of the irradiated G2-lymphocytes are able to proceed to mitosis, due to the strong G2-checkpoint block. This second problem is particularly apparent when the assay is applied for radiosensitivity testing of tumor or normal cell lines. To overcome these limitations, in the present study we employed the selective CDK1 inhibitor, RO-3306 for 19 hours, to achieve G2/M cell cycle arrest, and thus enrich with an increased percentage of lymphocytes in the G2-phase. As a result, following G2-phase irradiation, a higher percentage of the irradiated G2-cells is expected to proceed to metaphase enabling thus the analysis of chromatid breaks. In addition, we used the ATR inhibitor, VE-821, instead of caffeine to induce a stronger abrogation of the G2 checkpoint, and thus increase the conversion of radiation-induced DNA damage into chromatid breaks since the released cells from the G2-block will proceed fast to mitosis with unrepaired DNA lesions [236]. This increased yield of chromatid breaks approximates better the yield obtained when lymphocytes from AT patients are used.

Specifically, our enhanced G2-assay was applied to primary human blood lymphocytes using VE-821 or caffeine and the yields of chromatid breaks obtained were compared to those obtained for AT patients. Furthermore, the proposed G2-chromosomal radiosensitivity assay was applied to three cell lines: epidermoid carcinoma (A431), lung cancer (A549) and HeLa cells. The radiosensitivity estimates obtained for these cell lines were evaluated on the basis of the D_0 values obtained using conventional survival curves.

6.2. Materials and Methods

6.2.1. Blood Samples and Culture Conditions

Heparinized blood samples were taken from healthy individuals and AT-patients for analysis of chromosomal radiosensitivity in the G2-phasee, using the standardized G2-assay and the proposed G2-assay using the ATR inhibitor VE-821 instead of caffeine, as well as the selective CDK1 inhibitor

RO-3306 for 19 hours to achieve G2/M cell cycle arrest. Blood lymphocytes were cultured adding 0.5 ml of whole blood to 4.5 ml of RPMI 1640 (Biochrom AG, Germany) medium supplemented with 10% FBS, 1% PHA (phytohaemagglutinin), 1% glutamine and antibiotics (penicillin: 100 U/ml; streptomycin: 100 μg/ml). Cultures were incubated before their irradiation for 72 h, at 37 °C in a humidified incubator in an atmosphere of 5% CO2 and 95% air. PHA was dissolved in water at a concentration of 0.24 mg/ml. Caffeine was prepared as a 100 mM stock solution in PBS and used at a final concentration of 4mM. VE-821 was dissolved in DMSO at 10 mM used at final concentration of 2.5 μM. The immortalized cell lines A549 and A431 were grown in Dulbecco's Modified Eagle Medium (DMEM), and the HeLa in McCoy's *5A* medium with 10% fetal bovine serum and antibiotics, at 37°C in 5% CO_2 and 95% air in a humidified incubator.

6.2.2. Irradiation Conditions

Irradiation was carried out in a GammaCell 220 irradiator (Atomic Energy of Canada Ltd., Ottawa, Canada) at room temperature and at a dose rate of 20 cGy/min. Detailed protocol for the standardized G2-assay Proliferating cells were irradiated in vitro in G2-phase with 1Gy, 72 h after culture initiation. Each culture was divided immediately after irradiation, so that one half was treated with caffeine (4 mM) or VE-821 and incubated for 20 min at 37 °C to allow division of cells irradiated at mitosis, while the other half was cultured for the same time period without the presence of caffeine or VE-821. Colcemid was subsequently added to cell cultures for 60 min. At approximately 90 min post irradiation, cells were harvested and collected by centrifugation, treated in 75 mM KCl, fixed in methanol:glacial acetic acid (3:1 v/v), and processed for chromosomal aberration analysis. Standard procedures were used for chromosome preparation and staining and chromosomal damage was visualized and quantified as chromatid breaks in cells at metaphase.

6.2.3. Analysis

For each experimental point, approximately 50 cells were scored for chromatid breaks, based on standard criteria. Chromatid breaks and gaps were scored, the latter only when longer than a chromatid width. Light microscopy was coupled with an image analysis system (MetaSystems, Germany) to facilitate scoring. The spontaneous aberration yield was subtracted to obtain the radiation-induced G2 yield of chromatid breaks. Standard deviations of the mean values were calculated from three independent experiments.

6.3. Results and Discussion

6.3.1. IRS Estimates Based on G2-Chromosomal Radiosensitivity of Blood Lymphocytes

The overall objective of this study is to validate the proposed enhanced G2-assay using the CDK1 inhibitor RO-3306 and ATR inhibitor VE-821, for individualized radiosensitivity assessment. Following G2-phase irradiation with 1 Gy and analysis of chromatid breaks at the subsequent metaphase, three distinct yields of chromatid breaks were obtained for the cultured blood samples. The first (G2-yield), represents the G2-chromosomal fragility of the testing blood sample. The second represents the yield of chromatid breaks obtained when G2-checkpoint is abrogated by means of caffeine (G2-Caf yield), and the third represents the yield of chromatid breaks obtained using VE-821 (G2-VE yield) instead of caffeine. Based on the yields of chromatid breaks obtained, the individualized radiosensitivity (IRS) can be evaluated as a percentage of the high radiosensitivity level of AT patients using the formula IRS_{Caf} = (G2/G2-Caf)x100% or IRS_{VE} = (G2/G2-VE)x100%.

Representative examples of chromatid breaks in blood lymphocytes at metaphase following 1 Gy of γ-radiation in G2 phase, in the absence or presence of VE-821, are shown in Figure 6.1. The chromatid breaks shown by arrows, indicate that they become significantly more numerous in the presence of the ATR inhibitor VE-821. Comparative experiments were carried out to test whether the enrichment of cells in G2-phase by means of RO 3306 could modify the IRS value. The IRS value obtained without using RO-3306 was 47,1 ± 3,2%, whereas using treatment with RO-3306 for 19 hours,

and subsequently removed after irradiation, was 44,4 ± 2,55 %. The results are presented in Figure 6.2 and demonstrate that the enrichment in G2 cells by RO-3306 did not alter significantly the IRS estimate. Blood samples from three Ataxia Telangiectasia (AT) patients, who have a defective G2/M checkpoint, were also tested with the G2-assay following 1 Gy of γ-irradiation, yielding a mean number of 8,9 ± 0,66 chromatid breaks per cell, as shown in Table 6.1. This yield was compared with the yields obtained without using any inhibitor as well as with those obtained using VE-821 or caffeine, as presented in Figure 6.3. The number of chromatid breaks/cell observed using VE-821 is closer to the number exhibited in Ataxia Telangiectasia (AT) patients. The results obtained for the mitotic index (MI) in the absence of RO-3306 or in the presence before and after irradiation are presented in Figure 6.4. The highest MI was achieved when RO-3306 was applied for 19h and removed immediately after irradiation. Hence, approximately a 5-fold enrichment of G2 cells was achieved using the CDK1 inhibitor RO-3306.

Figure 6.1. Examples of cultured blood lymphocytes, exposed to 1 Gy of γ-radiation in G2 phase, without (A) or with VE-821 (B), as visualized in the subsequent metaphase. Grey arrows indicate chromatid breaks, which become significantly more numerous in the presence of the ATR inhibitor VE-821.

Table 6.1. Blood samples from three Ataxia Telangiectasia (AT) patients, who have a defective G2/M checkpoint, were also tested with the G2-assay yielding a mean number of 8,9 ± 0,66 breaks per cell, following 1 Gy of γ-irradiation.

Ataxia Telangiectasia Patients	Chromatid breaks per cell
Patient A	8,7
Patient B	9,5
Patient C	8,2
Mean value	8,9 ± 0,66

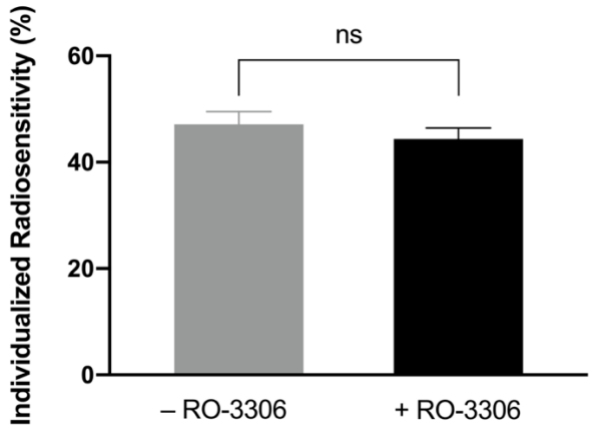

Figure 6.2. Individualized Radiosensitivity (IRS) with or without RO-3306. In the conventional G2-assay (w/o) the IRS was 47,1 ± 3,2%. The IRS after treatment with RO-3306 for 19 hours and its removal after irradiation was 44,4 ± 2,55 %. (Mean ± SD based on three independent experiments; ns $p > 0.05$).

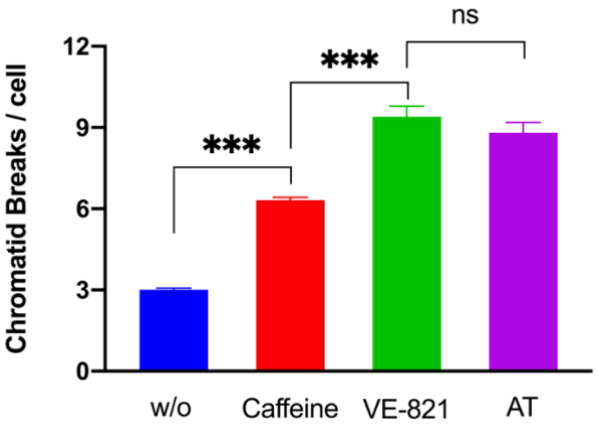

Figure 6.3. The number of chromatid breaks/cell observed using VE-821 is closer to the number exhibited in Ataxia Telangiectasia (AT) patients. Blood samples from 3 AT patients were tested for G2-chromosomal radiosensitivity, yielding a mean number of 8,9 ± 0,66 chromatid breaks per cell, following 1 Gy of γ-irradiation. VE-821 is a better G2-checkpoint abrogator than caffeine, and it enables to obtain a more representative internal control, not significantly different than AT patients. (Mean ± SD based on three independent experiments; ns $p > 0.05$; *** $p \leq 0.001$).

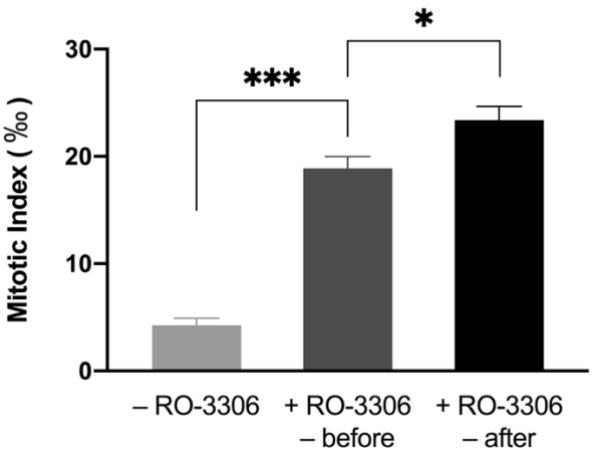

Figure 6.4. Mitotic index (MI) of the enhanced G2-assay in 48 hours, as compared to the conventional version (w/o). Without the use of RO-3306, the MI was 4,27 ± 0,42 ‰. The MI after treatment with RO-3306 for 19 hours and its removal before irradiation was increased to 18,9 ± 1,89 ‰. The MI after treatment with RO-3306 for 19 hours and its removal after irradiation was increased to 23,4 ± 3,71 ‰. Hence, the highest MI was achieved when RO-3306 was applied and removed after irradiation, resulting in a 5-fold increase of G2 cells. (Mean ± SD based on three independent experiments; * $p \leq 0.05$; *** $p \leq 0.001$).

6.3.2. IRS Estimates for Normal and Tumor Cell Lines

The proposed G2-chromosomal radiosensitivity assay was applied also to three tumor cell lines: epidermoid carcinoma (A431), lung cancer (A549) and HeLa cells. Examples chromatid breaks in a metaphase A431 epidermoid carcinoma cell following exposure to 1 Gy of γ-radiation in G2-phase in the absence (A) or presence (B) of the ATR inhibitor VE-821 are sown in Figure 6.5. Arrows indicate chromatid breaks, which become significantly more numerous in the presence of the ATR inhibitor VE-821. The IRS values for these cell lines were obtained and evaluated on the basis of the D_0 values obtained using conventional survival curves. The results are presented in Table 6.2 and demonstrate that the use of ATR inhibitor VE-821 provides radiosensitivity estimates that better match the radiosensitivity based on the D_0 values obtained by means of the conventional clonogenic assay.

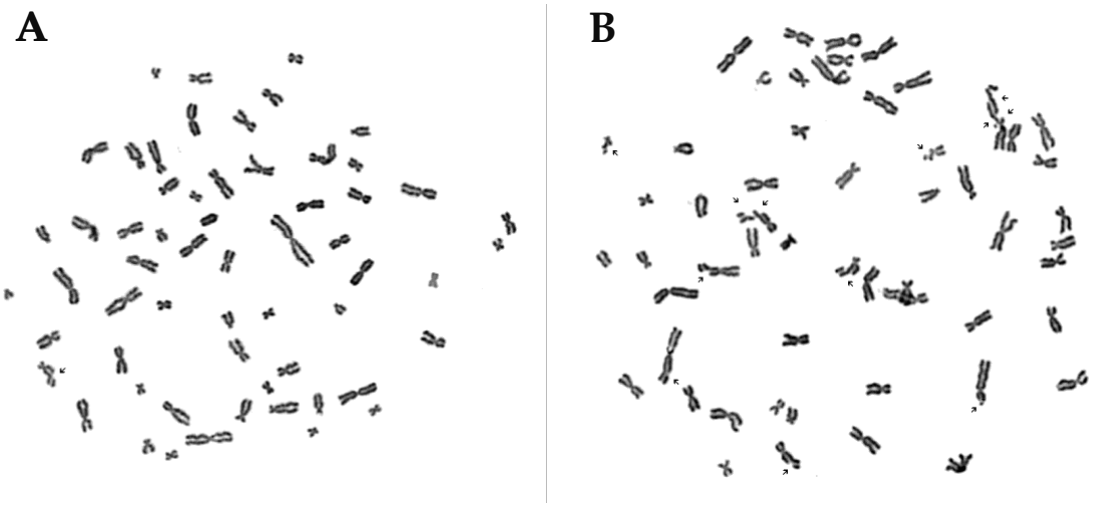

Figure 6.5. Examples of A431 epidermoid carcinoma cells, exposed to 1 Gy of γ-radiation in G2 phase, without (A) or with VE-821 (B), as visualized in the subsequent metaphase. Grey arrows indicate chromatid breaks, which become significantly more numerous in the presence of the ATR inhibitor VE-821.

Table 6.2. Individualized Radiosensitivity (IRS) for the A431, A549 and HeLa cells estimated using the G2-assay with either Caffeine or VE-821, following 1 Gy of γ-irradiation. The ATR inhibitor VE-821 provides radiosensitivity estimates that better match the radiosensitivity obtained with the conventional clonogenic assay based on the D_0 values for these cell lines.

Cell line	A431		A549		HeLa	
Clonogenic assay (D_0, Gy)	1.5		1.4		1.81	
Radiosensitivity	Resistant		Resistant		Resistant	
Inhibitor	Caffeine	VE-821	Caffeine	VE-821	Caffeine	VE-821
G2-assay (IRS %)	37	26	34	27	40	29
Radiosensitivity	Normal	Resistant	Normal	Resistant	Normal	Resistant

The results clearly show that the G2-VE yield simulates better the high radiosensitivity level of chromatid breaks obtained for AT patients. This robust cytogenetic method has the potential to be of great importance for personalized radiation oncology and space exploration radiation protection. Furthermore, it can be used for radiosensitivity testing of tumor and normal cell lines. In this case, the IRS values using VE-821 are comparable to those obtained on the basis of the D_0 values using conventional survival curves.

6.4. Conclusions

To overcome the limitations of the conventional G2-assay, we employed the selective CDK1 inhibitor, RO-3306, to achieve G2/M cell cycle arrest, and thus to increase the percentage of lymphocytes in G2 phase. Also, we used the ATR inhibitor, VE-821, instead of caffeine to induce a stronger abrogation of the G2 checkpoint, thus increasing the conversion of radiation-induced DNA damage into chromatid breaks to the level obtained for AT-patients. Therefore, using VE-821 the yield of chromatid breaks can be served as a more representative internal control to assess individual radiosensitivity (IRS) as a percentage of the highly radiosensitive AT patients.

Overall, the main characteristics and advantages of the proposed enhanced G2-assay:

- ✓ The use of RO-3306 does not modify the individualized radiosensitivity (IRS), permitting its use without altering the outcome of the radiosensitivity assessment.
- ✓ The enrichment of lymphocytes in G2 phase by means of the RO-3306 allows the completion of the IRS assessment in 50 h instead of 72 h.
- ✓ The use of VE-821 instead of caffeine as a G2-checkpoint abrogator provides a more representative internal control, matching the yield of chromatid breaks observed in AT patients.
- ✓ The increased mitotic index of the enhanced G2-assay enables its application to tumor and normal cell lines.
- ✓ The use of VE-821 enabled a more accurate radiosensitivity estimation of epidermoid carcinoma (A431), lung cancer (A549) and HeLa cell lines, as compared to the radiosensitivity obtained with the conventional clonogenic assay based on the D_0 values for these cell lines.
- ✓ The assay may prove to be of great importance for radiosensitivity estimation since it requires only 1–3 days instead of the 15 days needed for the conventional clonogenic assay.

Chapter 7: Epilogue

Summary of Key Outcomes

In the present doctoral thesis, the mechanisms underlying the conversion of DNA damage into chromosomal aberrations, chromothripsis and genome instability by different radiation qualities, have been thoroughly examined and used for biodosimetry and risk assessment purposes. Using cell fusion mediated interphase chromosome analysis in peripheral blood lymphocytes, we developed an automatable micro-PCC assay for biodosimetry purposes. The micro-PCC assay may pave the way for the automation and increased throughput for individualized absorbed dose estimates and risk assessment in the event of large-scale radiological emergencies. In addition, we have proposed potential predictive biomarkers for early and late health effects using the analysis of chromosomal rearrangements in G_0-peripheral blood lymphocyte PCC spreads. Particular emphasis has been given to the phenomenon of chromothripsis, which may underlie the biological basis for induction of chromosomal instability and carcinogenesis, particularly following exposure to high-LET radiation. We have provided, for the first time, experimental evidence for the mechanistic origin of chromothripsis, and we have clearly demonstrated that high-LET radiation can induce localized chromosome shattering, which is a critical risk for chromothripsis to occur. Furthermore, we have developed an enhanced G2-chromosomal radiosensitivity assay for the evaluation of individualized radiosensitivity in blood lymphocytes and normal or tumour cell lines.

To conclude, the overviews of the five research chapters, that constitute the core of this doctoral thesis, as well as the future research directions are presented below.

Chapter 2 Overview

In radiation accidents and large-scale radiological emergencies, a fast and reliable triage of individuals according to their degree of exposure is important for accident management and identification of those who need medical assistance. In this work, the applicability of cell-fusion-mediated premature chromosome condensation (PCC) in G_0-lymphocytes is examined for the development of a rapid, minimally invasive and automatable micro-PCC assay, which requires blood volumes of only 100μl and can be performed in 96-well plates, towards risk assessments and categorization of individuals based on dose estimates. Chromosomal aberrations are visualized for dose-estimation analysis within two hours, without the need of blood culturing for two days, as required by conventional cytogenetics. The various steps of the standard-PCC procedure were adapted and, for the first time, lymphocytes in blood volumes of 100μl were successfully fused with CHO-mitotics in 96-well plates of 2ml/well. The plates are advantageous for high-throughput analysis since the various steps required are applied to all 96-wells simultaneously. Interestingly, the use of only 1.5ml hypotonic and Carnoy's fixative per well offers high quality PCC-images, and the morphology of lymphocyte PCCs is identical to that obtained using the conventional PCC-assay, which requires much larger blood volumes and 15ml tubes. For dose assessments, appropriate calibration curves were constructed and for PCC analysis specialized software (MetaSystems) was used. The micro-PCC assay can be combined with fluorescence in situ hybridization (FISH), using simultaneously centromeric/telomeric (C/T) peptide nucleic acid (PNA) probes. This allows dose assessments on the basis of accurate scoring of dicentric and centric ring chromosomes in G_0-lymphocyte PCCs, which is particularly helpful when further evaluation into treatment-level categories of exposed individuals is needed. The micro-PCC assay has significant advantages for early triage biodosimetry when compared to other cytogenetic biodosimetry assays. It is rapid, cost-effective, and could pave the way to its subsequent automation.

Chapter 3 Overview

A sensitive biodosimetry tool is required for rapid individualized dose estimation and risk assessment in the case of radiological or nuclear mass casualty scenarios to prioritize exposed humans for immediate medical countermeasures to reduce radiation related injuries or morbidity risks. Unlike the conventional Dicentric Chromosome Assay (DCA), which takes about 3–4 days for radiation dose estimation, cell fusion mediated Premature Chromosome Condensation (PCC) technique in G_0 lymphocytes can be rapidly performed for radiation dose assessment within 6–8 hrs of sample receipt by alleviating the need for *ex vivo* lymphocyte proliferation for 48 hrs. Despite this advantage, the PCC technique has not yet been fully exploited for radiation biodosimetry. Realizing the advantage of the G_0 PCC technique that can be instantaneously applied to unstimulated lymphocytes, we evaluated the utility of G_0 PCC technique in detecting ionizing radiation (IR) induced stable and unstable chromosomal aberrations for biodosimetry purposes. Our study demonstrates that PCC coupled with mFISH and mBAND techniques can efficiently detect both numerical and structural chromosome aberrations at the intra- and inter-chromosomal levels in unstimulated T- and B-lymphocytes. Collectively, we demonstrate that the G_0 PCC technique has the potential for development as a biodosimetry tool for detecting unstable chromosome aberrations (chromosome fragments and dicentric chromosomes) for early radiation dose estimation and stable chromosome exchange events (translocations) for retrospective monitoring of individualized health risks in unstimulated lymphocytes.

Chapter 4 Overview

The discovery of chromothripsis in cancer genomes challenges the long-standing concept of carcinogenesis as the result of progressive genetic events. Despite recent advances in describing chromothripsis, its mechanistic origin remains elusive. The prevailing conception is that it arises from a massive accumulation of fragmented DNA inside micronuclei (MN), whose defective nuclear envelope ruptures or leads to aberrant DNA replication, before main nuclei enter mitosis. An alternative hypothesis is that the premature chromosome condensation (PCC) dynamics in asynchronous micronucleated cells underlie chromosome shattering in a single catastrophic event, a hallmark of chromothripsis. Specifically, when main nuclei enter mitosis, premature chromatin condensation provokes the shattering of chromosomes entrapped inside MN, if they are still undergoing DNA replication. To test this hypothesis, the agent RO-3306, a selective ATP-competitive inhibitor of CDK1 that promotes cell cycle arrest at the G2/M boundary, was used in this study to control the degree of cell cycle asynchrony between main nuclei and MN. By delaying the entrance of main nuclei into mitosis, additional time was allowed for the completion of DNA replication and duplication of chromosomes inside MN. We performed interphase cytogenetic analysis using asynchronous micronucleated cells generated by exposure of human lymphocytes to γ-rays, and heterophasic multinucleated Chinese hamster ovary (CHO) cells generated by cell fusion procedures. Our results demonstrate that the PCC dynamics during asynchronous mitosis in micronucleated or multinucleated cells are an important determinant of chromosome shattering and may underlie the mechanistic origin of chromothripsis.

Chapter 5 Overview

For precision cancer radiotherapy, high linear energy transfer (LET) particle irradiation offers a substantial advantage over photon-based irradiation. In contrast to the sparse deposition of low-density energy by X- or γ-rays, particle irradiation causes focal DNA damage through high-density energy deposition along the particle tracks. This is characterized by the formation of multiple damage sites, comprising localized clustered patterns of DNA single- and double-strand breaks as well as

base damage. These clustered DNA lesions are key determinants of the enhanced relative biological effectiveness (RBE) of energetic nuclei. However, the search for a fingerprint of particle exposure remains open, while the mechanisms underlying the induction of chromothripsis-like chromosomal rearrangements by high-LET radiation (resembling chromothripsis in tumors) await to be elucidated. In this work, we investigate the transformation of clustered DNA lesions into chromosome fragmentation, as indicated by the induction and post-irradiation repair of chromosomal damage under the dynamics of premature chromosome condensation in G_0 human lymphocytes. Specifically, this study provides, for the first time, experimental evidence that particle irradiation induces localized shattering of targeted chromosome domains. Yields of chromosome fragments and shattered domains are compared with those generated by γ-rays; and the RBE values obtained are up to 28.6 for α-particles (92 keV/μm), 10.5 for C-ions (295 keV/μm), and 4.9 for protons (28.5 keV/μm). Furthermore, we test the hypothesis that particle radiation-induced persistent clustered DNA lesions and chromatin decompaction at damage sites evolve into localized chromosome shattering by subsequent chromatin condensation in a single catastrophic event—posing a critical risk for random rejoining, chromothripsis, and carcinogenesis. Consistent with this hypothesis, our results highlight the potential use of shattered chromosome domains as a fingerprint of high-LET exposure, while conforming to the new model we propose for the mechanistic origin of chromothripsis-like rearrangements.

Chapter 6 Overview

The kinases ATM and ATR facilitate cell cycle arrest protecting against the conversion of unrepaired DNA lesions into chromatid breaks during G2/M phase transition. Based on this notion, a standardized predictive cytogenetic assay, the G2-assay, has been developed that enables evaluation individualized radiosensitivity (IRS) as a percentage of the highly radiosensitive Ataxia Telangiectasia (AT) patients, who have a compromised G2/M checkpoint. The IRS cut-off value, below which an individual is classified as radioresistant, was set at 30%; 30—50% as normal; 50—70% as radiosensitive, and above 70% as highly radiosensitive [Ref standardized G2-assay 2011]. Yet, this approach requires a 72 h culture of stimulated blood lymphocytes to obtain an adequate number of G2 phase cells, before their exposure to 1 Gy. Also, only a very small percentage of the irradiated G2-lymphocytes are able to proceed to mitosis due to radiation-induced G2-block, which is particularly apparent when the assay is applied for radiosensitivity testing of tumor or normal cell lines. To overcome these limitations, we employed in the present work the selective CDK1 inhibitor RO-3306 to achieve G2/M cell cycle arrest to increase the percentage of lymphocytes in G2 phase. Also, we used the selective ATR inhibitor VE-821 instead of caffeine to induce a stronger abrogation of the G2 checkpoint, increasing thus the conversion of radiation-induced DNA damage into chromatid breaks to the level obtained for AT patients. Therefore, using RO-3306 and VE-821 in cultured lymphocytes or cell lines, the increased yield of chromatid breaks following irradiation can be now served as a more representative internal control for reliable assessments of individualized radiosensitivity (IRS) as a percentage of the highly radiosensitive AT patients.

Conclusions and Future Research Directions

The main achievements of this doctoral thesis may contribute substantially to the experimental design for conducting further research in new important directions:

- ✓ Development of a rapid and minimally invasive biodosimetry method using 96-well plates and only 100μl of blood to assess doses in large-scale radiological emergencies.

  The development of the micro-PCC method using plates of 96 wells and quantities of blood of only 100 μl is important because it does indeed pave the way for large-scale accident management and the automation of individualized risk assessment of exposure to ionizing radiation. Based on the conventional methodology, to obtain post-irradiation dose estimates through the analysis of excess PCC fragments using appropriate dose-response calibration curves, 1-2 hours per sample are required. To accelerate the analysis of multiple samples, in collaboration with MetaSystems (Germany), which specializes in automated microscopic imaging and analysis of chromosomal preparations, we propose to adapt the Metafer slide scanning platform and its related software for the micro-PCC method. Our preliminary results confirm the automatic capture and analysis of PCC images in less than 5 minutes per sample and the possibility of constructing a corresponding calibration curve. Due to the automated feeding system, the Metafer platform could automatically analyze up to 800 chromosomal preparations. Further investigation in this direction will be an important step towards the automated rapid dose estimation, primarily for the management of large-scale radiological events.

- ✓ Investigation of new chromosomal predictive biomarkers for the evaluation of doses and stochastic effects of an exposure by combining the PCC method with the FISH technique.

  The reciprocal translocations detected by the combination of PCC and FISH techniques in lymphocytes after radiation exposure are also important and potentially predictive of stochastic health effects because they are related to cancer biology. Therefore, further investigation in this direction, combining the PCC method with the FISH technique for the identification of predictive chromosomal biomarkers for the stochastic effects of an exposure, will contribute substantially to the optimal assessment of cases of overexposure to ionizing radiation.

- ✓ Demonstration, for the first time using cytogenetic endpoints, of the premature chromosome condensation (PCC) in micronuclei as the mechanistic basis of chromothripsis and the localized chromosome shattering in micronuclei in a single catastrophic event.

  The cytogenetic results demonstrate, for the first time, that the dynamics of premature chromosome condensation (PCC) in asynchronous cells with micronuclei form the basis of the mechanistic origin of chromothripsis and the localized chromosome shattering, are important and this phenomenon needs further investigation. The experimental design in this direction will contribute to the confirmation and deeper understanding of the mechanistic biological basis of chromothripsis. In addition, it will substantially contribute to investigating whether exposure to ionizing radiation has the potential to activate the mechanism of chromothripsis. Based on its discovery in the genome of cancer cells, chromothripsis has been proposed as an alternative mechanism to the progressive induction of carcinogenesis through successive stepwise mutations.

- ✓ Presentation of results documenting the localized chromosome shattering, a hallmark of chromothripsis, as a fingerprint of high-LET radiation.

  For particle radiation, our experimental results demonstrate, for the first time, that high LET radiation can cause localized chromosome shattering. This localized chromosome shattering, which we first proposed as a high-LET radiation fingerprint, is important because it could potentially activate mechanisms of carcinogenesis. Therefore, further research in this direction by combining the PCC and mFISH methods could confirm, with greater reliability, the localized shattering of chromosomes by high LET radiation as well as the RBE values we have obtained for radiation of different qualities. In addition, by employing next-generation DNA sequencing and mFISH, the evolution of localized chromosome shattering to the phenomenon of chromothripsis could be confirmed.

- ✓ Optimization of a cytogenetic method for the detection of endogenous radiosensitivity for radiation protection and radiotherapy purposes in the context of the individualization of the risk of radiation exposure.

  Regarding the development of a method for detecting the genetic predisposition to increased sensitivity to radiation to enable the individualized risk assessment of an exposure, the enhanced cytogenetic method we have proposed needs clinical validation for purposes of Radiation Protection and Personalized Radiotherapy. The experimental design in this direction will include both patients scheduled to undertake radiotherapy and patients who, during or after their treatment, presented a hypersensitivity to radiation. Additionally, further investigation of endogenous radiosensitivity may include normal and cancerous cell lines of different radiosensitivities. Ultimately, the goal of investigating in this direction would be to evaluate the reliability and predictive reproducibility of our method.

Appendix 1: Περιγραφή Ερευνητικού Αντικειμένου και Δομή της Διδακτορικής Διατριβής

Είναι καλά τεκμηριωμένο σήμερα ότι η έκθεση σε ιοντίζουσα ακτινοβολία οδηγεί σε μια πληθώρα βιολογικών επιδράσεων που εξαρτώνται από τη φύση της ακτινοβολίας, τη διάρκεια έκθεσης, τη δόση και το ρυθμό δόσης. Είναι επίσης γνωστό ότι η έκθεση του ανθρώπου στην ακτινοβολία συμβαίνει λόγω της ποικίλης χρήσης της σε ιατρικές και βιομηχανικές εφαρμογές και παρά τις πιθανές επιπτώσεις της στην υγεία, η ακτινοβολία είναι πράγματι ένα ισχυρό διαγνωστικό εργαλείο στην ιατρική και η προτιμώμενη μέθοδος θεραπείας για τους περισσότερους ανθρώπινους καρκίνους. Επιπλέον, η έκθεση μετά από ραδιολογικά ή πυρηνικά ατυχήματα μπορεί να προκαλέσει σοβαρές επιπτώσεις στην υγεία και ενδέχεται εκατοντάδες ή και χιλιάδες άνθρωποι να εκτεθούν σε ακτινοβολία σε περίπτωση σοβαρού ατυχήματος ή πυρηνικής τρομοκρατικής ενέργειας. Αυτό καταδεικνύει σαφώς την αναγκαιότητα για την ανάπτυξη κατάλληλων βιοδεικτών έκθεσης και αυτοματοποιημένων μεθόδων με αυξημένη απόδοση για εξατομικευμένες εκτιμήσεις δόσεων σε μεγάλης κλίμακας ατυχήματα.

Οι δόσεις αυτές των εκτιθέμενων είναι αναγκαίες για την εκτίμηση του κινδύνου εμφάνισης των άμεσων αποτελεσμάτων της έκθεσης ή και των απώτερων με βάση τις επιδημιολογικές μελέτες εμφάνισης καρκίνου μετά από έκθεση σε ιοντίζουσες ακτινοβολίες. Στην εκτίμηση του κινδύνου αναμφίβολα θα συμβάλλει και η διαλεύκανση των μηχανισμών που διέπουν τη βιολογική δράση ακτινοβολιών διαφορετικών ποιοτήτων καθώς και η ανάπτυξη προγνωστικών μεθόδων για την εκτίμηση του κινδύνου για δυσμενείς άμεσες ή απώτερες επιπτώσεις στην υγεία βάσει της γενετικής προδιάθεσης των εκτιθέμενων. Πράγματι, παρότι τα φυσικά και βιολογικά δοσίμετρα μπορούν να βοηθήσουν στην εκτίμηση των απορροφούμενων δόσεων ακτινοβολίας, εξακολουθεί να υπάρχει έλλειψη στις γνώσεις μας σχετικά με την πρόβλεψη σε ατομικό επίπεδο των κινδύνων για την υγεία με βάση τις εκτιμώμενες εξατομικευμένες δόσεις. Ως εκ τούτου, η πλήρης κατανόηση των μηχανισμών δράσης των ιοντιζουσών ακτινοβολιών διαφορετικών ποιοτήτων σε επίπεδο DNA, χρωμοσωμικό και κυτταρικό θα μπορέσει να βοηθήσει στην πρόβλεψη τόσο των βραχυπρόθεσμων όσο και των μακροπρόθεσμων επιπτώσεων στην υγεία.

Στην παρούσα διδακτορική διατριβή, εξετάζονται διεξοδικά οι μηχανισμοί που διέπουν τη μετατροπή βλαβών του DNA σε χρωμοσωμικές αλλοιώσεις και αναδιατάξεις, το φαινόμενο της χρωμοθρύψης και τη γονιδιωματική αστάθεια για σκοπούς βιοδοσιμετρίας και εκτίμησης κινδύνου μετά από έκθεση σε ακτινοβολίες διαφορετικών ποιοτήτων. Μεταξύ των διαφορετικών βιοδεικτών που χρησιμοποιούνται για τη βιοδοσιμετρία, δίνεται έμφαση στις χρωμοσωμικές αλλοιώσεις στα λεμφοκύτταρα του περιφερικού αίματος και ιδιαίτερα σε εκείνες που μπορούν να απεικονιστούν και να αναλυθούν μετά από πρόωρη συμπύκνωση χρωμοσωμάτων (PCC) μέσω κυτταρικής σύντηξης. Ο κύριος λόγος είναι επειδή τα λεμφοκύτταρα δεν πολλαπλασιάζονται στο περιφερικό αίμα, κυκλοφορούν σε όλο το σώμα και ανταλλάσσονται συνεχώς με λεμφοκύτταρα στους ιστούς, έχουν μεγάλη διάρκεια ζωής και έτσι έχουν «μνήμη» και διατηρούν την πληροφορία της έκθεσης για μεγάλα χρονικά διαστήματα. Αυτό σημαίνει ότι λεμφοκύτταρα με χρωμοσωμικές αλλοιώσεις που έχουν προκληθεί από ακτινοβολία οπουδήποτε στο σώμα θα είναι τελικά παρόντα και στο περιφερικό αίμα.

Συγκεκριμένα, χρησιμοποιώντας ανάλυση χρωμοσωμάτων λεμφοκυττάρων στη μεσόφαση μέσω της σύντηξής τους με μιτωτικά κύτταρα Χάμστερ, αναπτύχθηκε μια αυτοματοποιήσιμη μέθοδος micro-PCC για σκοπούς βιοδοσιμετρίας. Η μέθοδος αυτή μπορεί να ανοίξει το δρόμο για την αυτοματοποίηση της εξατομικευμένης εκτίμησης απορροφούμενης δόσης και κινδύνου σε περιπτώσεις ραδιολογικών καταστάσεων έκτακτης ανάγκης μεγάλης κλίμακας. Επίσης, χρησιμοποιώντας χρώση Giemsa και βαφή χρωμοσωμάτων με μοριακούς ανιχνευτές DNA σε συνδυασμό με τεχνικές FISH και mFISH, οι επαγόμενες από την ακτινοβολία χρωμοσωμικές αναδιατάξεις στα λεμφοκύτταρα προτείνονται ως προγνωστικοί βιοδείκτες για άμεσες και

απώτερες επιπτώσεις στην υγεία. Επιπλέον, με βάση τη συμβατική κυτταρογενετική, αναπτύχθηκε και μια ενισχυμένη G2-χρωμοσωμική μέθοδος (enhanced G2-assay) για την εξατομικευμένη αξιολόγηση της εγγενούς ακτινοευαισθησίας.

Η ανάλυση των χρωμοσωμικών αλλοιώσεων μετά από έκθεση σε ακτινοβολίες διαφορετικών ποιοτήτων μπορεί επίσης να είναι προγνωστική για τυχόν διαδικασίες καρκινογένεσης και η έκταση των χρωμοσωμικών αναδιατάξεων που παρατηρούνται στα λεμφοκύτταρα του αίματος μπορεί να αντικατοπτρίζει παρόμοια συμβάντα και στα κύτταρα του ιστού-στόχου. Αυτό δείχνει ότι οι χρωμοσωμικές αλλοιώσεις δεν είναι μόνο σημαντικοί βιοδείκτες για την εκτίμηση δόσεων και επιπτώσεων της ακτινοβολίας, αλλά είναι επίσης χρήσιμοι για την πρόβλεψη του κινδύνου των απώτερων αποτελεσμάτων στην υγεία. Πράγματι, η υπόθεση ότι οι χρωμοσωμικές ανωμαλίες σχετίζονται με τον καρκίνο και μπορούν ενδεχομένως να λειτουργήσουν ως ενδιάμεσο βήμα της αιτιώδους οδού υποστηρίζεται από πολλές αναφορές. Τα στοιχεία μπορούν να συνοψιστούν σε πέντε κύρια επιχειρήματα: (1) οι αναδιατάξεις των χρωμοσωμάτων παίζουν σημαντικό ρόλο στην ενεργοποίηση των πρωτοογκογονιδίων και στην αδρανοποίηση των γονιδίων καταστολής όγκων· (2) τα άτομα με συγγενή νόσο, όπως η αναιμία Fanconi ή η Ataxia Telangiectasia (AT), χαρακτηρίζονται από ασυνήθιστα υψηλά ποσοστά χρωμοσωμικών ανωμαλιών και αυξημένη συχνότητα εμφάνισης κακοηθειών· (3) αλλοιώσεις καρυότυπου έχουν βρεθεί σε όλους τους τύπους νεοπλασματικών κυττάρων και συχνά είναι ιδιαίτερα ειδικές για συγκεκριμένες διαγνωστικές κατηγορίες· (4) υπάρχει τάση οι καρκινογόνες χημικές ουσίες να προκαλούν χρωμοσωμικές αλλοιώσεις και επίσης ότι η επαγωγή χρωμοσωμικών αλλοιώσεων τείνει να συνδέεται με γνωστούς καρκινογόνους παράγοντες για τον άνθρωπο· (5) το φαινόμενο της χρωμοθρύψης (chromothripsis) που ονομάστηκε με βάση τα χρωμοσωμικά χαρακτηριστικά του (chromo) και την υποκείμενη διαδικασία που περιλαμβάνει θραύση χρωμοσωμάτων (thripsis) σε ένα και μόνο καταστροφικό συμβάν. Βάσει της ανακάλυψής της στο γονιδίωμα καρκινικών κυττάρων, η χρωμοθρύψη έχει προταθεί ως εναλλακτικός μηχανισμός καρκινογένεσης, σε αντίθεση με τον κλασικό μηχανισμό καρκινογένεσης ως αποτέλεσμα προοδευτικών γενετικών μεταλλάξεων.

Λαμβάνοντας υπόψη τον σημαντικό ρόλο των χρωμοσωμικών αναδιατάξεων στην καρκινογένεση, δόθηκε έμφαση στο φαινόμενο της χρωμοθρύψης που μπορεί να αποτελέσει τη βιολογική βάση για την επαγωγή χρωμοσωμικής αστάθειας και καρκινογένεσης, ιδιαίτερα από ακτινοβολίες υψηλού LET. Χρησιμοποιώντας κυτταρογενετικές μεθόδους, τα αποτελέσματα παρέχουν για πρώτη φορά πειραματικά δεδομένα για τη μηχανιστική και βιολογική βάση του φαινομένου της χρωμοθρύψης και αποδεικνύουν επίσης για πρώτη φορά ότι η ακτινοβολία υψηλού LET μπορεί να προκαλέσει τοπική θραύση χρωμοσωμάτων, η οποία είναι προϋπόθεση για να συμβεί η χρωμοθρύψη και αποτελεί χαρακτηριστικό του φαινομένου. Σε αντίθεση με τη σταδιακή συσσώρευση επακόλουθων γενετικών αλλοιώσεων και μεταλλάξεων, που μπορεί να προκαλέσουν γονιδιωματική αστάθεια, η χρωμοθρύψη είναι μια διαδικασία μετάλλαξης που συμβαίνει σε ένα και μόνο καταστροφικό συμβάν κατά το οποίο τμήματα χρωμοσωμάτων υφίστανται μαζική αλλά εντοπισμένη θραύση και τυχαίες αναδιατάξεις.

Συγκεκριμένα, η παρούσα διδακτορική διατριβή πραγματεύεται τα ακόλουθα πέντε ερωτήματα βασικής και εφαρμοσμένης έρευνας:

1. Πώς μπορεί να αναπτυχθεί μια αυτοματοποιήσιμη micro-PCC μέθοδος για εξατομικευμένες εκτιμήσεις απορροφούμενης δόσης και κινδύνου σε περιπτώσεις ραδιολογικών καταστάσεων έκτακτης ανάγκης μεγάλης κλίμακας;

2. Ποιες χρωμοσωμικές αναδιατάξεις, που απεικονίζονται άμεσα σε μη διεγερμένα λεμφοκύτταρα αίματος με μοριακούς ανιχνευτές DNA σε συνδυασμό με τεχνικές FISH και mFISH, μπορούν να δράσουν ως προγνωστικοί βιοδείκτες έκθεσης προσφέροντας τη δυνατότητα εκτίμησης κινδύνου για άμεσες και απώτερες επιπτώσεις στην υγεία;

3. Ποιοι μηχανισμοί διέπουν το φαινόμενο της χρωμοθρύψης, που βάσει της ανακάλυψής της στο γονιδίωμα καρκινικών κυττάρων έχει προταθεί ως εναλλακτικός μηχανισμός καρκινογένεσης;

4. Μπορεί η ακτινοβολία υψηλού LET να προκαλέσει τοπική θραύση χρωμοσωμάτων που χαρακτηρίζει το φαινόμενο της χρωμοθρύψης ώστε να οδηγήσει σε χρωμοσωμική και γονιδιωματική αστάθεια που είναι χαρακτηριστικά της καρκινογένεσης;

5. Πώς μπορεί να αναπτυχθεί μια ενισχυμένη κυτταρογενετική μέθοδος G2-assay για την εξατομικευμένη ανίχνευση γενετικής προδιάθεσης σε αυξημένη ευαισθησία στην ακτινοβολία, ώστε να συμβάλλει ουσιαστικά στην ακτινοπροστασία, την εξατομικευμένη ακτινοθεραπεία, καθώς και στην προστασία του προσωπικού που σχετίζεται με την εξερεύνηση του διαστήματος;

Δομή της Διδακτορικής Διατριβής

Η παρούσα διδακτορική διατριβή διαρθρώνεται σε επτά Κεφάλαια και δυο Παραρτήματα. Το πρώτο Κεφάλαιο παρουσιάζει το γενικό υπόβαθρο που σχετίζεται με το ερευνητικό θέμα και τα επόμενα πέντε Κεφάλαια περιγράφουν τις ερευνητικές μελέτες και επιτεύγματα σχετικά με τα ερευνητικά ερωτήματα που αναφέρονται παραπάνω. Το έβδομο Κεφάλαιο, ο Επίλογος, συνοψίζει τα κύρια αποτελέσματα και συμπεράσματα της διατριβής, καθώς και τις μελλοντικές ερευνητικές κατευθύνσεις. Το περιεχόμενο του έβδομου κεφαλαίου παρατίθεται επίσης στα Ελληνικά στο Παράρτημα 2.

Πιο συγκεκριμένα,

Το Κεφάλαιο 1 εισάγει σημαντικές έννοιες της ακτινοφυσικής, της ραδιοβιολογίας και της ακτινοκυτταρογενετικής. Επίσης, περιγράφει σε επίπεδο DNA, χρωμοσώματος και κυττάρων τις κύριες μεθόδους και τους βιοδείκτες που είναι επί του παρόντος διαθέσιμοι για την ανίχνευση και ποσοτικοποίηση των επιπτώσεων μιας έκθεσης σε ιοντίζουσες ακτινοβολίες διαφορετικών ποιοτήτων. Έμφαση δίνεται στη μέθοδο της πρόωρης συμπύκνωσης χρωμοσωμάτων (PCC), ως ένα ισχυρό και μοναδικό κυτταρογενετικό εργαλείο για τη μελέτη, απευθείας σε μεσοφασικά κύτταρα, της μετατροπής των βλαβών του DNA που προκαλούνται από την ακτινοβολία σε χρωμοσωμικές αλλοιώσεις.

Το Κεφάλαιο 2 περιγράφει τη μέθοδο micro-PCC που αναπτύχθηκε και την έρευνα που στοχεύει στην αύξηση της απόδοσης αυτής της μεθόδου μέσω της αυτοματοποίησης της λήψης εικόνων των πρόωρα συμπυκνωμένων χρωμοσωμάτων (PCC) των λεμφοκυττάρων. Σε ατυχήματα ακτινοβολίας και μεγάλης κλίμακας ραδιολογικές καταστάσεις έκτακτης ανάγκης, μια γρήγορη και αξιόπιστη διαλογή των ατόμων ανάλογα με τον βαθμό έκθεσής τους είναι σημαντική για τη διαχείριση ατυχημάτων και τον εντοπισμό εκείνων που χρειάζονται ιατρική βοήθεια. Η μέθοδος micro-PCC ενδείκνυται για βιοδοσιμετρία υψηλής απόδοσης, καθώς απαιτεί όγκους αίματος μόνο 100μl και μπορεί να πραγματοποιηθεί σε τρυβλία 96 κοιλοτήτων. Προς την κατεύθυνση της αυτοματοποίησης της ανάλυσης micro-PCC, διερευνάται η χρήση της πλατφόρμας σάρωσης διαφανειών Metafer από την MetaSystems για να καταστεί δυνατή η αυτοματοποιημένη λήψη εικόνων καθώς και η αυτοματοποιημένη ανάλυση με βάση τα απομένοντα θραύσματα PCC μετά από έκθεση.

Το Κεφάλαιο 3 περιγράφει την έρευνα που στοχεύει στη διερεύνηση πιθανών νέων βιοδεικτών για σκοπούς βιοδοσιμετρίας και στην εκτίμηση κινδύνου σε περίπτωση ραδιολογικών ή πυρηνικών ατυχημάτων μεγάλης κλίμακας. Αξιοποιώντας το πλεονέκτημα της μεθόδου PCC που μπορεί να εφαρμοστεί άμεσα σε μη διεγερμένα λεμφοκύτταρα, η ανάλυση

μπορεί να βασιστεί και στις χρωμοσωμικές αναδιατάξεις που απεικονίζονται εφαρμόζοντας τεχνικές mFISH και mBAND. Τα αποτελέσματα δείχνουν σαφώς ότι οι τεχνικές αυτές μπορούν να ανιχνεύσουν αποτελεσματικά τόσο αριθμητικές όσο και δομικές χρωμοσωμικές αλλοιώσεις σε ενδο- και διαχρωμοσωμικά επίπεδα σε μη διεγερμένα Τ- και Β-λεμφοκύτταρα. Οι ασταθείς χρωμοσωμικές αλλοιώσεις (θραύσματα χρωμοσωμάτων και δικεντρικά χρωμοσώματα) μπορούν να αξιοποιηθούν για την έγκαιρη εκτίμηση της δόσης ακτινοβολίας και των άμεσων επιπτώσεων. Οι σταθερές αμοιβαίες χρωμοσωμικές αναδιατάξεις (αντιμεταθέσεις) αξιοποιούνται για αναδρομική εκτίμηση της δόσης και ως προγνωστικοί βιοδείκτες εκτίμησης κινδύνου για απώτερες επιπτώσεις στην υγεία.

Το Κεφάλαιο 4 περιγράφει τη μελέτη διερεύνησης του μηχανισμού και της βιολογικής βάσης του φαινομένου της χρωμοθρύψης, που βάσει της ανακάλυψής της στο γονιδίωμα καρκινικών κυττάρων έχει προταθεί ως εναλλακτικός μηχανισμός καρκινογένεσης, σε αντίθεση με τον κλασικό μηχανισμό καρκινογένεσης που προϋποθέτει συσσώρευση προοδευτικών γενετικών μεταλλάξεων. Η χρωμοθρύψη είναι μια διαδικασία μετάλλαξης κατά την οποία μεγάλα τμήματα χρωμοσωμάτων υφίστανται μαζική αλλά εντοπισμένη θραύση και τυχαίες ανακατατάξεις ως αποτέλεσμα ενός και μόνο καταστροφικού συμβάντος. Η επικρατούσα αντίληψη είναι ότι προκύπτει από μια μαζική συσσώρευση κατακερματισμένου DNA μέσα σε μικροπυρήνες (MN), των οποίων η ελαττωματική πυρηνική μεμβράνη διασπάται ή οδηγεί σε ανώμαλη αντιγραφή του DNA, πριν οι κύριοι πυρήνες εισέλθουν στη μίτωση. Χρησιμοποιώντας κυτταρογενετικές μεθόδους, τα αποτελέσματα που λαμβάνονται παρέχουν για πρώτη φορά πειραματικά δεδομένα που υποστηρίζουν μια εναλλακτική υπόθεση. Η δυναμική της πρόωρης συμπύκνωσης χρωμοσωμάτων (PCC) σε ασύγχρονα μικροπυρηνικά κύτταρα αποτελεί τη βάση της μηχανιστικής προέλευσης της χρωμοθρύψης. Καθώς οι κύριοι πυρήνες εισέρχονται στη μίτωση, η πρόωρη συμπύκνωση χρωματίνης κατά τη διάρκεια του αναδιπλασιασμού του DNA προκαλεί τη θραύση των χρωμοσωμάτων που είναι παγιδευμένα μέσα στον μικροπυρήνα σε ένα και μόνο καταστροφικό γεγονός, το οποίο αποτελεί το βασικό χαρακτηριστικό της χρωμοθρύψης.

Το Κεφάλαιο 5 περιγράφει μια ερευνητική μελέτη που στοχεύει να παράσχει πληροφορίες σχετικά με τους μηχανισμούς που διέπουν τις ακτινοβολίες υψηλού LET, όπως σωματίδια α, επιταχυνόμενα πρωτόνια και ιόντα C, και την αυξημένη βιολογική αποτελεσματικότητά τους σε σύγκριση με τις ακτίνες-Χ και -γ. Σε αντίθεση με τη χαμηλή γραμμική εναπόθεση ενέργειας από ακτίνες-Χ ή –γ, οι σωματιδιακές ακτινοβολίες προκαλούν εστιακές βλάβες στο DNA μέσω εναπόθεσης ενέργειας υψηλής πυκνότητας κατά μήκος των τροχιών των σωματιδίων που διαπερνούν τους πυρήνες των κυττάρων. Αυτό χαρακτηρίζει τις σωματιδιακές ακτινοβολίες ως υψηλής γραμμικής μεταφοράς ενέργειας (LET) με αποτέλεσμα τον σχηματισμό πολλαπλών σύνθετων βλαβών, που περιλαμβάνουν εντοπισμένες ομαδοποιημένες βλάβες με μονόκλωνες (SSBs) και δίκλωνες (DSBs) θραύσεις DNA καθώς και βλάβες βάσεων. Οι σύνθετες αυτές βλάβες DNA θεωρούνται βασικοί καθοριστικοί παράγοντες της αυξημένης σχετικής βιολογικής αποτελεσματικότητας (RBE) των σωματιδιακών ακτινοβολιών. Τα αποτελέσματα παρέχουν για πρώτη φορά, πειραματικές αποδείξεις ότι τέτοιες ομαδοποιημένες βλάβες στο DNA μπορεί να μετατραπούν σε τοπική θραύση περιοχών χρωμοσωμάτων σε ένα και μόνο καταστροφικό συμβάν, κάτι που χαρακτηρίζει το φαινόμενο της χρωμοθρύψης. Επιπλέον, τα δεδομένα υπογραμμίζουν την χρήση θρυμματισμένων περιοχών χρωμοσωμάτων ως δακτυλικό αποτύπωμα έκθεσης σε ακτινοβολία υψηλού LET και υποστηρίζουν ένα νέο μοντέλο που προτείνεται για τη μηχανιστική προέλευση γονιδιωματικών αναδιατάξεων τύπου χρωμοθρύψης που έχουν παρατηρηθεί μετά από έκθεση σε σωματιδιακή ακτινοβολία.

Το Κεφάλαιο 6 περιγράφει την έρευνα για την ανάπτυξη μιας ενισχυμένης μεθόδου G2-assay χρωμοσωμικής ακτινοευαισθησίας για την εξατομικευμένη ανίχνευση γενετικής προδιάθεσης σε αυξημένη ευαισθησία στην ακτινοβολία ατόμων του πληθυσμού. Ενώ η

εξατομικευμένη απόκριση στην ακτινοβολία τεκμηριώνεται όλο και περισσότερο, οι υποκείμενοι μηχανισμοί για την προδιάθεση σε δυσμενείς άμεσες και απώτερες επιπτώσεις που προκαλούνται από ακτινοβολία δεν είναι ακόμη σαφώς κατανοητοί. Οι ασθενείς AT, οι οποίοι έχουν ελαττωματικό σημείο ελέγχου G2/M, έχει αποδειχθεί ότι είναι εξαιρετικά ακτινοευαίσθητοι. Οι κινάσες ATM, ATR και Chk1 διευκολύνουν τη διακοπή του κυτταρικού κύκλου στη G2 φάση (G2-block) προστατεύοντας από τη μετατροπή των βλαβών του DNA σε χρωματιδιακά θραύσματα κατά τη διάρκεια της μετάβασης από τη φάση G2 στη μίτωση (M). Με βάση τα αποτελέσματα, προτείνεται μια ενισχυμένη μέθοδος G2 για την εκτίμηση της ακτινοευαισθησίας ατόμων του πληθυσμού ως ποσοστό της υψηλής ακτινοευαισθησίας ασθενών AT (100% ακτινοευαίσθητοι). Συγκεκριμένα, ο αναστολέας ATR, VE 821, χρησιμοποιείται για την κατάργηση του σημείου ελέγχου G2, επιτυγχάνοντας απόκριση παρόμοια με εκείνη των ασθενών AT, που είναι απαραίτητη για τη σύγκριση. Επίσης, ο αναστολέας CDK1, RO-3306, εφαρμόζεται για τον εμπλουτισμό των κυττάρων φάσης G2 πριν από την ακτινοβόληση. Η κυτταρογενετική αυτή μέθοδος δίνει τη δυνατότητα ελέγχου γενετικής προδιάθεσης αυξημένης ακτινοευαισθησίας ατόμων του πληθυσμού και αναμένεται να συμβάλλει ουσιαστικά στην ακτινοπροστασία, την εξατομικευμένη ακτινοθεραπεία, καθώς και στην προστασία του προσωπικού που σχετίζεται με την εξερεύνηση του διαστήματος.

Appendix 2: Εκτενής Περίληψη Επιτευγμάτων και Συμπερασμάτων

Στην παρούσα διδακτορική διατριβή, εξετάστηκαν διεξοδικά οι μηχανισμοί που διέπουν τη μετατροπή βλαβών του DNA σε χρωμοσωμικές αλλοιώσεις και αναδιατάξεις, το φαινόμενο της χρωμοθρύψης και τη γονιδιωματική αστάθεια για σκοπούς βιοδοσιμετρίας και εκτίμησης κινδύνου μετά από έκθεση σε ακτινοβολίες διαφορετικών ποιοτήτων. Αξιοποιώντας την ανάλυση χρωμοσωμάτων μετά από πρόωρη συμπύκνωση μέσω της σύντηξης κυττάρων στη μίτωση με λεμφοκύτταρα περιφερικού αίματος στη μεσόφαση, αναπτύξαμε μια αυτοματοποιήσιμη μέθοδο micro-PCC για σκοπούς βιοδοσιμετρίας. Η μέθοδος micro-PCC μπορεί να ανοίξει το δρόμο για την αυτοματοποίηση της εξατομικευμένης εκτίμησης απορροφούμενης δόσης και κινδύνου σε περιπτώσεις ραδιολογικών καταστάσεων έκτακτης ανάγκης μεγάλης κλίμακας. Επιπλέον, προτείναμε πιθανούς προγνωστικούς βιοδείκτες για άμεσες και απώτερες επιπτώσεις στην υγεία, χρησιμοποιώντας την ανάλυση χρωμοσωμικών αναδιατάξεων σε παρασκευάσματα PCC λεμφοκυττάρων περιφερειακού αίματος G_0. Ιδιαίτερη έμφαση δόθηκε στο φαινόμενο της χρωμοθρύψης, το οποίο μπορεί να αποτελεί τη βιολογική βάση για την πρόκληση χρωμοσωμικής αστάθειας και καρκινογένεσης, ιδιαίτερα μετά από έκθεση σε ακτινοβολία υψηλού LET. Παρουσιάσαμε, για πρώτη φορά, πειραματικά αποτελέσματα για τη μηχανιστική προέλευση της χρωμοθρύψης και δείξαμε πως η ακτινοβολία υψηλού LET μπορεί να προκαλέσει τοπικό θρυμματισμό χρωμοσωμάτων. Επιπρόσθετα, αναπτύξαμε μια ενισχυμένη χρωμοσωμική μέθοδο G2 (enhanced G2-assay) για την εξατομικευμένη αξιολόγηση της εγγενούς ακτινοευαισθησίας που μπορεί να εφαρμοστεί σε λεμφοκύτταρα του περιφερικού αίματος, καθώς και σε φυσιολογικές και καρκινικές κυτταρικές σειρές.

Εν κατακλείδι, παρατίθενται παρακάτω οι συνόψεις των πέντε ερευνητικών κεφαλαίων που αποτελούν τον πυρήνα της παρούσας διδακτορικής διατριβής, καθώς και οι μελλοντικές ερευνητικές κατευθύνσεις.

Σύνοψη Κεφαλαίου 2

Σε περίπτωση ραδιολογικού ή πυρηνικού ατυχήματος μεγάλης κλίμακας, μια γρήγορη και αξιόπιστη ταξινόμηση των ατόμων ανάλογα με το βαθμό σοβαρότητας της έκθεσής τους είναι σημαντική για τη διαχείριση της έκτακτης ανάγκης και τον εντοπισμό εκείνων που χρειάζονται άμεσα ιατρική βοήθεια. Στην παρούσα εργασία εξετάζουμε συνεπώς τη δυνατότητα ανάπτυξης μιας ταχείας, ελάχιστα επεμβατικής και αυτοματοποιήσιμης κυτταρογενετικής μεθόδου για την εξατομικευμένη εκτίμηση απορροφούμενων δόσεων και κινδύνου από υπερέκθεση σε ιοντίζουσες ακτινοβολίες. Για το σκοπό αυτό, επιλέξαμε τη μεθοδολογία της πρόωρης συμπύκνωσης χρωμοσωμάτων (PCC) σε G_0-λεμφοκύτταρα περιφερικού αίματος, μέσω της σύντηξής τους με μιτωτικά κύτταρα Χάμστερ. Δείξαμε ότι μπορεί να εφαρμοστεί σε όγκους αίματος μόνο 100 μl και σε τρυβλία των 96 κοιλοτήτων και ότι, βάσει του πρωτοκόλλου αυτής της micro-PCC μεθόδου, η διαχείριση καθώς και η επεξεργασία των δειγμάτων είναι αυτοματοποιήσιμη και υψηλής απόδοσης. Πράγματι, οι χρωμοσωματικές αλλοιώσεις που επάγονται από την ακτινοβολία απεικονίζονται για εκτίμηση της δόσης εντός δύο ωρών, χωρίς την ανάγκη καλλιέργειας αίματος για δύο ημέρες, όπως απαιτείται από τη συμβατική κυτταρογενετική μέθοδο ανάλυσης στη μετάφαση. Τα διάφορα στάδια της μεθοδολογίας PCC προσαρμόστηκαν και, για πρώτη φορά, λεμφοκύτταρα συντήχτηκαν επιτυχώς με CHO-μιτωτικά σε όγκους αίματος 100 μl και σε τρυβλία 96 κοιλοτήτων των 2 ml/κοιλότητα. Τα τρυβλία είναι κατάλληλα για αναλύσεις υψηλής απόδοσης, καθώς τα διάφορα βήματα που απαιτούνται εφαρμόζονται ταυτόχρονα και στις 96 κοιλότητες του τρυβλίου. Είναι ενδιαφέρον ότι η χρήση

μόνο 1,5 ml υποτονικού διαλύματος και μονιμοποιητικού Carnoy ανά φρεάτιο προσφέρει υψηλής ποιότητας εικόνες PCC και η μορφολογία των PCC λεμφοκυττάρων είναι ίδια με αυτή που λαμβάνεται χρησιμοποιώντας το συμβατικό πρωτόκολλο της μεθόδου PCC, που απαιτεί όμως πολύ μεγαλύτερους όγκους αίματος και δοκιμαστικούς σωλήνες των 15 ml. Για τις αξιολογήσεις των δόσεων, κατασκευάστηκαν κατάλληλες καμπύλες βαθμονόμησης και για την ανάλυση των χρωμοσωματικών αλλοιώσεων χρησιμοποιήθηκε εξειδικευμένο λογισμικό ανάλυσης εικόνας (MetaSystems). Επιπλέον, η micro-PCC μέθοδος μπορεί να συνδυαστεί με in situ υβριδισμό φθορισμού (FISH), χρησιμοποιώντας ταυτόχρονα πεπτιδικούς ανιχνευτές νουκλεϊκού οξέος (PNA) κεντρομεριδίων/τελομεριδίων (C/T). Η ανάλυση αυτή επιτρέπει εκτιμήσεις δόσεων με βάση την ανάλυση δικεντρικών χρωμοσωμάτων και κεντρικών δακτυλίων άμεσα στα G_0 λεμφοκύτταρα. Αυτό είναι ιδιαίτερα χρήσιμο όταν απαιτείται σε επίπεδο θεραπείας περαιτέρω αξιολόγηση των εκτιθέμενων ατόμων. Η μέθοδος micro-PCC έχει σημαντικά πλεονεκτήματα για τη βιοδοσιμετρία και έγκαιρη ταξινόμηση εκτιθέμενων ατόμων σε σύγκριση με άλλες μεθόδους. Είναι γρήγορη, οικονομικά αποδοτική και θα μπορούσε να ανοίξει το δρόμο για την αυτοματοποίησή της.

Σύνοψη Κεφαλαίου 3

Για την ταχεία εκτίμηση της δόσης και του κινδύνου στην περίπτωση ραδιολογικών ή πυρηνικών ατυχημάτων μεγάλης κλίμακας, απαιτείται μια αξιόπιστη μέθοδος εξατομικευμένης βιοδοσιμετρίας για την αξιολόγηση του συμβάντος και την ταξινόμηση των εκτιθέμενων ώστε να ληφθούν έγκαιρα τα αναγκαία ιατρικά μέτρα. Σε αντίθεση με τη συμβατική μεθοδολογία δικεντρικών χρωμοσωμάτων, η οποία απαιτεί περίπου 3-4 ημέρες για την εκτίμηση της δόσης ακτινοβολίας, η τεχνική της πρόωρης συμπύκνωσης χρωμοσωμάτων (μέθοδος PCC) σε G_0 λεμφοκύτταρα περιφερικού αίματος, μπορεί να δώσει αποτελέσματα εντός 6-8 ωρών από τη λήψη του δείγματος. Αυτό επιτυγχάνεται μέσω κυτταρικής σύντηξης μιτωτικών CHO κυττάρων με λεμφοκύτταρα στη G_0 φάση, χωρίς δηλαδή την ανάγκη για *ex vivo* πολλαπλασιασμού τους για 48 ώρες που απαιτεί η συμβατική ανάλυση δικεντρικών χρωμοσωμάτων. Εντούτοις, παρά το πλεονέκτημα αυτό, η τεχνική PCC δεν έχει ακόμη αξιοποιηθεί πλήρως για σκοπούς βιοδοσιμετρίας. Συνειδητοποιώντας τα πλεονέκτημα της τεχνικής PCC, που κυρίως επιτρέπουν τη χρωμοσωμική ανάλυση σε μη διεγερμένα G_0 λεμφοκύτταρα, διερευνήσαμε και αξιολογήσαμε τη χρησιμότητα της τεχνικής για την ανίχνευση σταθερών και ασταθών χρωμοσωμικών ανωμαλιών που προκαλούνται από έκθεση σε ιοντίζουσα ακτινοβολία. Τα αποτελέσματα υποδεικνύουν ότι η μέθοδος PCC σε συνδυασμό με τις τεχνικές mFISH και mBAND μπορεί να ανιχνεύσει αποτελεσματικά τόσο αριθμητικές όσο και δομικές χρωμοσωμικές ανωμαλίες σε ενδο- και διαχρωμοσωμικό επίπεδο σε μη διεγερμένα (G_0) T- και B-λεμφοκύτταρα. Παρέχει επομένως τη δυνατότητα ανάπτυξής της σε βασική μέθοδο βιοδοσιμετρίας για την ανίχνευση τόσο των ασταθών χρωμοσωμικών ανωμαλιών (θραύσματα χρωμοσωμάτων και δικεντρικά χρωμοσώματα), όσο και των σταθερών αμοιβαίων χρωμοσωμικών αντιμεταθέσεων. Οι ασταθείς χρωμοσωμικές αλλοιώσεις (θραύσματα χρωμοσωμάτων και δικεντρικά χρωμοσώματα) μπορούν να αξιοποιηθούν για την έγκαιρη εκτίμηση της δόσης ακτινοβολίας και των άμεσων επιπτώσεων μιας υπερέκθεσης. Οι σταθερές αμοιβαίες αντιμεταθέσεις αξιοποιούνται για αναδρομική εκτίμηση της δόσης, καθώς και ως προγνωστικοί βιοδείκτες εκτίμησης κινδύνου για τυχόν απώτερες επιπτώσεις στην υγεία.

Σύνοψη Κεφαλαίου 4

Η ανακάλυψη του φαινομένου της χρωμοθρύψης στο γονιδίωμα του καρκίνου θέτει υπό αμφισβήτηση τη μακροχρόνια θεώρηση του μηχανισμού καρκινογένεσης ως αποτέλεσμα προοδευτικών γενετικών μεταλλάξεων. Εντούτοις, παρά τις πρόσφατες προόδους στην περιγραφή της χρωμοθρύψης, η μηχανιστική προέλευσή της παραμένει ασαφής. Η επικρατούσα αντίληψη είναι ότι προκύπτει από μια μαζική συσσώρευση κατακερματισμένου DNA μέσα σε μικροπυρήνες (MN), των οποίων η ελαττωματική πυρηνική μεμβράνη διασπάται ή οδηγεί σε ανώμαλη αντιγραφή του DNA, πριν οι κύριοι πυρήνες εισέλθουν στη μίτωση. Μια εναλλακτική υπόθεση που προτείνουμε είναι ότι η δυναμική πρόωρης συμπύκνωσης χρωμοσωμάτων (PCC) σε ασύγχρονα μικροπυρηνικά κύτταρα αποτελεί τη βάση του τοπικού θρυμματισμού χρωμοσωμικών περιοχών σε ένα και μόνο καταστροφικό συμβάν, που είναι το χαρακτηριστικό γνώρισμα της χρωμοθρύψης. Συγκεκριμένα, όταν οι κύριοι πυρήνες εισέρχονται στη μίτωση, η πρόωρη συμπύκνωση χρωματίνης που επάγεται στους MN προκαλεί το θρυμματισμό των περιοχών των χρωμοσωμάτων που είναι παγιδευμένα μέσα στους MN, εάν την στιγμή εκείνη εξακολουθούν να υφίστανται αντιγραφή DNA. Για να ελεγχθεί αυτή η υπόθεση, ο παράγοντας RO-3306, ένας εκλεκτικός ATP-ανταγωνιστικός αναστολέας του CDK1 που προάγει τη διακοπή του κυτταρικού κύκλου στο όριο G2/M, χρησιμοποιήθηκε σε αυτή τη μελέτη για τον έλεγχο του βαθμού συγχρονισμού του κυτταρικού κύκλου μεταξύ των κύριων πυρήνων και των μικροπυρήνων. Καθυστερώντας την είσοδο των κύριων πυρήνων στη μίτωση, δόθηκε επιπλέον χρόνος για την ολοκλήρωση της αντιγραφής του DNA και του διπλασιασμού των χρωμοσωμάτων μέσα στους μικροπυρήνες. Για τον έλεγχο της ανωτέρω υπόθεσης, πραγματοποιήσαμε εμπεριστατωμένες κυτταρογενετικές αναλύσεις σε ασύγχρονα μικροπύρηνα κύτταρα που παρήχθησαν από την έκθεση ανθρώπινων λεμφοκυττάρων σε ακτινοβολία-γ, καθώς και σε ετεροφασικά πολυπύρηνα κύτταρα ωοθήκης κινέζικου Hamster (CHO) που παρήχθησαν με τη μεθοδολογία κυτταρικών συντήξεων. Τα αποτελέσματα αποδεικνύουν ότι η δυναμική της πρόωρης συμπύκνωσης χρωμοσωμάτων κατά τη διάρκεια της ασύγχρονης μίτωσης σε μικροπυρηνικά ή πολυπύρηνα κύτταρα είναι ένας σημαντικός καθοριστικός παράγοντας τοπικού θρυμματισμού περιοχών των χρωμοσωμάτων και μπορεί να αποτελεί τη βιολογική βάση της μηχανιστικής προέλευσης του φαινομένου της χρωμοθρύψης.

Σύνοψη Κεφαλαίου 5

Για την εξατομικευμένη ακτινοθεραπεία καρκίνου, η ακτινοβολία σωματιδίων υψηλής γραμμικής μεταφοράς ενέργειας (LET) προσφέρει ένα σημαντικό πλεονέκτημα έναντι της ακτινοβολίας με βάση τα φωτόνια. Σε αντίθεση με τη διάχυτη εναπόθεση ενέργειας χαμηλής πυκνότητας από ακτίνες-Χ ή -γ, η ακτινοβολία σωματιδίων προκαλεί εστιακές βλάβες στο DNA μέσω εναπόθεσης ενέργειας υψηλής πυκνότητας κατά μήκος των τροχιών των σωματιδίων στους πυρήνες των κυττάρων. Αυτό χαρακτηρίζεται από το σχηματισμό πολλαπλών σύνθετων βλαβών, που περιλαμβάνουν εντοπισμένες ομαδοποιημένες βλάβες με μονόκλωνες (SSBs) και δίκλωνες (DSBs) θραύσεις DNA καθώς και βλάβες βάσεων. Αυτές οι σύνθετες βλάβες DNA είναι βασικοί καθοριστικοί παράγοντες της ενισχυμένης σχετικής βιολογικής αποτελεσματικότητας (RBE) των ενεργειακών πυρήνων. Ωστόσο, η αναζήτηση δακτυλικού αποτυπώματος έκθεσης σε σωματιδιακή ακτινοβολία παραμένει ανοιχτή, ενώ οι μηχανισμοί που διέπουν την επαγωγή από ακτινοβολία υψηλού LET χρωμοσωμικών αναδιατάξεων τύπου χρωμοθρύψης (όμοιας της χρωμοθρύψης που παρατηρείται σε όγκους) δεν έχουν διευκρινιστεί επαρκώς. Σε αυτή την εργασία, διερευνούμε σε επίπεδο χρωμοσωμάτων στη μεσόφαση την μετατροπή των σύνθετων βλαβών του DNA σε τοπικό θρυμματισμό χρωμοσωμικών περιοχών, όπως υποδεικνύεται από πειράματα επαγωγής και επιδιόρθωσης βλαβών DNA μετά από ακτινοβόληση. Η απεικόνιση και ανάλυση των χρωμοσωμικών αλλοιώσεων στη μεσόφαση επιτυγχάνεται μέσω της μεθόδου

της πρόωρης συμπύκνωσης χρωμοσωμάτων σε ανθρώπινα λεμφοκύτταρα (G_0) περιφερικού αίματος. Συγκεκριμένα, αυτή η μελέτη παρέχει, για πρώτη φορά, πειραματικές αποδείξεις ότι η σωματιδιακή ακτινοβολία προκαλεί τοπικό θρυμματισμό των στοχευμένων χρωμοσωμάτων. Για τον υπολογισμό σχετικών τιμών RBE, η ποσοτικοποίηση των χρωμοσωμικών θραυσμάτων και των θρυμματισμένων χρωμοσωμικών περιοχών συγκρίνονται με εκείνες που παράγονται αντιστοίχως από ακτίνες-γ. Οι τιμές RBE που προκύπτουν είναι έως 28,6 για σωματίδια α (92 keV/μm), 10,5 για ιόντα C (295 keV/μm) και 4,9 για πρωτόνια (28,5 keV/μm). Επιπλέον, διερευνούμε την υπόθεση ότι οι απομένουσες βλάβες DNA που προκαλούνται από τις σωματιδιακές ακτινοβολίες και η αναδιάταξη της χρωματίνης στα σημεία βλάβης εξελίσσονται σε τοπικό θρυμματισμό χρωμοσωμικών περιοχών, σε ένα και μόνο καταστροφικό συμβάν, κατά τη συμπύκνωση των χρωμοσωμάτων. Αυτό είναι χαρακτηριστικό του φαινομένου της χρωμοθρύψης και ενέχει υψηλό κίνδυνο καρκινογένεσης μέσω τυχαίας επανένωσης και γονιδιακής αναδιάταξης των θρυμματισμένων χρωμοσωμικών περιοχών. Τα αποτελέσματά υπογραμμίζουν τη χρήση των θρυμματισμένων χρωμοσωμάτων σε λεμφοκύτταρα περιφερικού αίματος ως δακτυλικό αποτύπωμα έκθεσης σε ακτινοβολία υψηλού LET. Επίσης, αποτελούν τη βιολογική βάση του νέου μοντέλου που προτείνουμε για τη μηχανιστική προέλευση των αναδιατάξεων τύπου χρωμοθρύψης που έχουν παρατηρηθεί μετά από έκθεση σε σωματιδιακή ακτινοβολία.

Σύνοψη Κεφαλαίου 6

Μετά από έκθεση κυττάρων σε ακτινοβολία, οι κινάσες ATM και ATR διευκολύνουν τη διακοπή του κυτταρικού κύκλου στη φάση G2 (G2 block) προστατεύοντας έτσι τα χρωμοσώματα από τον κίνδυνο μετατροπής των μη επιδιορθωμένων βλαβών DNA σε χρωματιδικές θραύσεις καθώς συμπυκνώνονται κατά τη μετάβασή τους από τη G2 στη μίτωση (M). Βάσει της αποτελεσματικότητας ελέγχου του G2 block και της επεξεργασίας βλαβών DNA σε μοριακό επίπεδο, καθώς και της δυναμικής της χρωματίνης στη μετατροπή μη επιδιορθωμένων αλλοιώσεων σε χρωματιδικές θραύσεις όπως τα κύτταρα προχωρούν στη μίτωση, αναπτύχθηκε μια ενισχυμένη μέθοδος G2 χρωμοσωμικής ακτινοευαισθησίας (enhanced G2-assay). Η μέθοδος αυτή επιτρέπει την αξιολόγηση εξατομικευμένης ακτινοευαισθησίας (IRS) ατόμων του πληθυσμού ή κυτταρικών σειρών συγκριτικά με την ακτινοευαισθησία ασθενών Ataxia Telangiectasia (AT). Τα κύτταρα ασθενών AT έχουν ελαττωματικό σημείο ελέγχου στη G2 / M φάση και δεν παρουσιάζουν G2 block μετά από έκθεση σε ιοντίζουσα ακτινοβολία. Συνεπώς, έχουν εξαιρετικά υψηλή ακτινοευαισθησία (100% ακτινοευαίσθητοι) έτσι ώστε η αξιολόγηση IRS δύναται να εκφραστεί ως ποσοστό της ακτινοευαισθησίας κυττάρων ασθενών AT. Η μέθοδος απαιτεί καλλιέργεια 72 ωρών διεγερμένων λεμφοκυττάρων αίματος ή εκθετικής καλλιέργειας κυτταρικής σειράς ώστε να υπάρχει επαρκής αριθμός κυττάρων στη G2 φάση του κυτταρικού κύκλου πριν την έκθεσή τους σε 1 Gy και την ανάλυση των χρωματοσωμάτων στη μετάφαση. Εντούτοις, μόνο ένα πολύ μικρό ποσοστό των ακτινοβολημένων G2 κυττάρων είναι σε θέση να προχωρήσει στη μίτωση λόγω του G2 block που ενεργοποιείται για την επισκευή των βλαβών DNA που προκαλεί η ακτινοβολία. Το πρόβλημα αυτό είναι ιδιαίτερα εμφανές όταν η δοκιμασία εφαρμόζεται για έλεγχο ακτινοευαισθησίας καρκινικών ή φυσιολογικών κυτταρικών σειρών. Για να ξεπεράσουμε τους περιορισμούς αυτούς, χρησιμοποιούμε στην παρούσα εργασία τον εκλεκτικό αναστολέα του CDK1, RO-3306, ώστε να επιτύχουμε τη διακοπή του κυτταρικού κύκλου στη G2/M φάση και να αυξήσουμε το ποσοστό των κυττάρων στη φάση G2. Επίσης, χρησιμοποιούμε τον εκλεκτικό αναστολέα του ATR, VE-821, για να προκαλέσουμε κατάργηση του σημείου ελέγχου G2/M και G2 block μετά την ακτινοβόληση, αυξάνοντας έτσι τη μετατροπή ακτινοεπαγώμενων βλαβών DNA σε χρωματιδικά θραύσματα σε όμοιο επίπεδο με αυτό που παρατηρούμε σε κύτταρα ασθενών AT. Η προσέγγιση αυτή επιτρέπει να έχουμε τιμή αναφοράς για 100% ακτινοευαισθησία στο δείγμα που αξιολογείται χωρίς τη χρήση κυττάρων ασθενών

AT. Η τιμή αποκοπής IRS, κάτω από την οποία τα κύτταρα αξιολογούνται ως ακτινοάντοχα, ορίζεται στο 30% της τιμής αναφοράς. Στο ποσοστό 30—50% ορίζεται η αναμενόμενη φυσιολογική ακτινοαυαισθησία, 50—70% ως η περιοχή των ακτινοευαίσθητων κυττάρων και πάνω από 70% των εξαιρετικά ακτινοευαίσθητων.

Συμπεράσματα και Μελλοντικές Ερευνητικές Κατευθύνσεις

Τα κύρια επιτεύγματα αυτής της διδακτορικής διατριβής μπορούν να συμβάλουν ουσιαστικά στον πειραματικό σχεδιασμό για τη διεξαγωγή περαιτέρω έρευνας σε νέες σημαντικές κατευθύνσεις.

- ✓ Ανάπτυξη μιας ταχείας και ελάχιστα επεμβατικής μεθόδου βιοδοσιμετρίας, χρησιμοποιώντας τρυβλία 96 κοιλοτήτων και μόνο 100μl αίματος για την εκτίμηση δόσεων σε ραδιολογικά συμβάντα μεγάλης κλίμακας.

  Η ανάπτυξη της micro-PCC μεθόδου χρησιμοποιώντας τρυβλία 96 κοιλοτήτων και ποσότητες αίματος μόνο 100 μl είναι σημαντική διότι ανοίγει πράγματι το δρόμο στη διαχείριση ατυχημάτων μεγάλης κλίμακας και την αυτοματοποίηση εξατομικευμένης εκτίμησης κινδύνου έκθεσης σε ιοντίζουσα ακτινοβολία. Βάσει της συμβατικής μεθοδολογίας, για να ληφθούν εκτιμήσεις δόσης μετά την έκθεση σε ακτινοβολία, μέσω της ανάλυσης των επιπλέον θραυσμάτων PCC (excess PCCs) χρησιμοποιώντας κατάλληλες καμπύλες βαθμονόμησης δόσης-απόκρισης, απαιτούνται 1-2 ώρες ανά δείγμα. Για να επιταχυνθεί η ανάλυση πολλαπλών δειγμάτων, σε συνεργασία με την MetaSystems (Γερμανία), που εξειδικεύεται στην αυτοματοποιημένη μικροσκοπική απεικόνιση και ανάλυση χρωμοσωμικών παρασκευασμάτων, προτείνουμε να προσαρμοστεί η πλατφόρμα σάρωσης Metafer και το σχετικό λογισμικό για τη μέθοδο micro-PCC. Τα πρώτα αποτελέσματα επιβεβαιώνουν την αυτόματη λήψη και ανάλυση εικόνων PCC σε λιγότερο από 5 λεπτά ανά δείγμα και τη δυνατότητα κατασκευής αντίστοιχης καμπύλης βαθμονόμησης. Λόγω του αυτοματοποιημένου συστήματος τροφοδοσίας, η πλατφόρμα Metafer θα μπορούσε να αναλύσει αυτόματα έως και 800 χρωμοσωμικά παρασκευάσματα. Η περαιτέρω διερεύνηση προς την κατεύθυνση αυτή θα αποτελέσει ένα σημαντικό βήμα προς την αυτοματοποιημένη ταχεία εκτίμηση δόσεων, πρωτίστως για τη διαχείριση ραδιολογικών ατυχημάτων μεγάλης κλίμακας.

- ✓ Διερεύνηση νέων χρωμοσωμικών προγνωστικών βιοδεικτών για την αξιολόγιση δόσεων και στοχαστικών επιπτώσεων μιας έκθεσης συνδυάζοντας τη μέθοδο PCC με την τεχνική FISH.

  Οι αμοιβαίες αντιμεταθέσεις που ανιχνεύονται με τον συνδυασμό των τεχνικών PCC και FISH στα λεμφοκύτταρα μετά από έκθεση σε ακτινοβολία είναι επίσης σημαντικές και δυνητικά προγνωστικές για τις απώτερες επιπτώσεις στην υγεία διότι σχετίζονται με τη βιολογία καρκινογένεσης. Η περαιτέρω διερεύνηση στην κατεύθυνση αυτή και η ταυτοποίηση προγνωστικών χρωμοσωμικών βιοδεικτών των στοχαστικών επιπτώσεων μιας έκθεσης, συνδυάζοντας τη μέθοδο PCC με την τεχνική FISH, θα συμβάλλει ουσιαστικά στη βέλτιστη αξιολόγηση περιστατικών υπερέκθεσης σε ιοντίζουσες ακτινοβολίες.

- ✓ Ανάδειξη, για πρώτη φορά, της πρόωρης συμπύκνωσης χρωμοσωμάτων στους μικροπυρήνες ως τη μηχανιστική βάση της χρωμοθρύψης και του τοπικού θρυμματισμού χρωμοσωμάτων σε ένα και μόνο καταστροφικό συμβάν.

  Τα κυτταρογενετικά αποτελέσματα που υποστηρίζουν για πρώτη φορά ότι η δυναμική της πρόωρης χρωμοσωμικής συμπύκνωσης (PCC) σε ασύγχρονα κύτταρα με μικροπυρήνες αποτελεί τη βάση της μηχανιστικής προέλευσης της χρωμοθρύψης και του τοπικού θρυμματισμού χρωμοσωμάτων, είναι σημαντικά και το φαινόμενο χρήζει περαιτέρω διερεύνησης. Ο πειραματικός σχεδιασμός προς την κατεύθυνση αυτή θα συμβάλλει στην επιβεβαίωση και σε βάθος κατανόηση της μηχανιστικής βιολογικής βάσης του φαινομένου της χρωμοθρύψης. Επιπλέον, θα συμβάλλει ουσιαστικά στο να διερευνηθεί κατά πόσο είναι δυνατόν έκθεση σε ιοντίζουσα ακτινοβολία να ενεργοποιήσει τον μηχανισμό της χρωμοθρύψης, που βάσει της ανακάλυψής της στο γονιδίωμα καρκινικών κυττάρων έχει προταθεί ως εναλλακτικός μηχανισμός της σταδιακά επαγόμενης καρκινογένεσης μέσω διαδοχικών μεταλλάξεων.

- ✓ Παρουσίαση αποτελεσμάτων που τεκμηριώνουν, για πρώτη φορά, ως δακτυλικό αποτύπωμα ακτινοβολίας υψηλού LET τον τοπικό θρυμματισμό χρωμοσωμάτων, που είναι χαρακτηριστικό γνώρισμα της χρωμοθρύψης.

  Για τις σωματιδιακές ακτινοβολίες, τα πειραματικά αποτελέσματα τεκμηριώνουν για πρώτη φορά πως η ακτινοβολία υψηλού LET μπορεί να προκαλέσει τοπική θραύση χρωμοσωμάτων, η οποία αποτελεί χαρακτηριστικό γνώρισμα της χρωμοθρύψης. Ο τοπικός αυτός θρυμματισμός χρωμοσωμάτων, που τον προτείναμε για πρώτη φορά ως δακτυλικό αποτύπωμα ακτινοβολίας υψηλού LET, είναι σημαντικός διότι δυνητικά θα μπορούσε να ενεργοποιήσει μηχανισμούς καρκινογένεσης. Επομένως, περαιτέρω έρευνα προς την κατεύθυνση αυτή, με τον συνδυασμό των μεθόδων PCC και mFISH, θα μπορούσε να επιβεβαιώσει με μεγαλύτερη αξιοπιστία τον τοπικό θρυμματισμό των χρωμοσωμάτων από ακτινοβολία υψηλού LET καθώς και τις τιμές RBE για τις διαφορετικές ποιότητες ακτινοβολιών που χρησιμοποιήσαμε. Επιπλέον, αξιοποιώντας την αλληλούχιση DNA επόμενης γενιάς και mFISH, θα μπορούσε να επιβεβαιωθεί η μετεξέλιξη του τοπικού θρυμματισμού χρωμοσωμάτων στο φαινόμενο της χρωμοθρύψης.

- ✓ Βελτιστοποίηση κυτταρογενετικής μεθόδου ανίχνευσης ενδογενούς ακτινοευαισθησίας για σκοπούς Ακτινοπροστασίας και Ακτινοθεραπείας στο πλαίσιο εξατομίκευσης του κινδύνου έκθεσης σε ακτινοβολία.

  Σχετικά με την ανάπτυξη μιας μεθόδου ανίχνευσης γενετικής προδιάθεσης σε αυξημένη ευαισθησία στην ακτινοβολία για την εξατομικευμένη εκτίμηση του κινδύνου μιας έκθεσης, η βελτιστοποιημένη κυτταρογενετική μέθοδος που προτείναμε χρήζει κλινικής επικύρωσης για σκοπούς Ακτινοπροστασίας και εξατομικευμένης Ακτινοθεραπείας. Ο πειραματικός σχεδιασμός προς την κατεύθυνση αυτή θα συμπεριλάβει τόσο ασθενείς ακτινοθεραπείας όσο και ασθενείς που κατά τη διάρκεια ή

μετά τη θεραπεία τους παρουσίασαν υπερευαισθησία στην ακτινοβολία. Επίσης, η περαιτέρω διερεύνηση της ενδογενούς ακτινοευαισθησίας μπορεί να συμπεριλάβει φυσιολογικές και καρκινικές κυτταρικές σειρές διαφορετικής ακτινοευαισθησίας. Απώτερος στόχος της διερεύνησης προς την κατεύθυνση αυτή είναι η αξιολόγηση των χαρακτηριστικών της αξιοπιστίας και προγνωστικής επαναληψιμότητας της μεθόδου.

References

1. Kalet, I.J. Nuclear Radiation: Risks and Benefits Edited by E. Pochin . *Med Phys* **1985**, *12*, doi:10.1118/1.595728.
2. Boei, J.J.W.A. Radiation Induced Chromosomal Aberrations in Mammalian Cells: Analysis by Fluorescence in Situ Hybridization, Rijksuniversiteit, 1998.
3. Dertinger, H.; Jung, H. *Molecular Radiation Biology*; Springer US: New York, NY, 1970; ISBN 978-0-387-90013-1.
4. Hall, E.J.; Giaccia, A.J. *Radiobiology for the Radiologist: Seventh Edition*; 2012;
5. Maréchal, A.; Zou, L. DNA Damage Sensing by the ATM and ATR Kinases. *Cold Spring Harb Perspect Biol* **2013**, *5*, doi:10.1101/cshperspect.a012716.
6. Nogueira, A.; Fernandes, M.; Catarino, R.; Medeiros, R. RAD52 Functions in Homologous Recombination and Its Importance on Genomic Integrity Maintenance and Cancer Therapy. *Cancers (Basel)* 2019, *11*.
7. NIKJOU, H. Radiation Track and DNA Damage. *Iran. J. Radiat. Res.* **2003**, *1*.
8. Grace, M.B.; Moyer, B.R.; Prasher, J.; Cliffer, K.D.; Ramakrishnan, N.; Kaminski, J.; Coleman, C.N.; Manning, R.G.; Maidment, B.W.; Hatchett, R. Rapid Radiation Dose Assessment for Radiological Public Health Emergencies: Roles of NIAID and BARDA. *Health Phys* **2010**, *98*, 172–178, doi:10.1097/01.HP.0000348001.60905.c0.
9. Swartz, H.M.; Flood, A.B.; Gougelet, R.M.; Rea, M.E.; Nicolalde, R.J.; Williams, B.B. A Critical Assessment of Biodosimetry Methods for Large-Scale Incidents. *Health Phys* **2010**, *98*, 95–108, doi:10.1097/HP.0b013e3181b8cffd.
10. Romm, H.; Oestreicher, U.; Kulka, U. Cytogenetic Damage Analysed by the Dicentric Assay. *Ann Ist Super Sanita* **2009**, *45*, 251–259.
11. Brady, J.M.; Aarestad, N.O.; Swartz, H.M. In Vivo Dosimetry by Electron Spin Resonance Spectroscopy. *Health Phys* **1968**, *15*, 43–47.
12. Swartz, H.M.; Molenda, R.P.; Lofberg, R.T. Long-Lived Radiation-Induced Electron Spin Resonances in an Aqueous Biological System. *Biochem Biophys Res Commun* **1965**, *21*, 61–65.
13. Swartz, H.M.; Iwasaki, A.; Walczak, T.; Demidenko, E.; Salikhov, I.; Khan, N.; Lesniewski, P.; Thomas, J.; Romanyukha, A.; Schauer, D.; et al. In Vivo EPR Dosimetry to Quantify Exposures to Clinically Significant Doses of Ionising Radiation. *Radiat Prot Dosimetry* **2006**, *120*, 163–170, doi:10.1093/rpd/nci554.
14. Dewitt, R.; Klein, D.M.; Yukihara, E.G.; Simon, S.L.; McKeever, S.W. Optically Stimulated Luminescence (OSL) of Tooth Enamel and Its Potential Use in Post-Radiation Exposure Triage. *Health Phys* **2010**, *98*, 432–439, doi:10.1097/01.HP.0000347997.57654.17.
15. Swartz, H.M.; Burke, G.; Coey, M.; Demidenko, E.; Dong, R.; Grinberg, O.; Hilton, J.; Iwasaki, A.; Lesniewski, P.; Kmiec, M.; et al. In Vivo EPR For Dosimetry. *Radiat Meas* **2007**, *42*, 1075–1084, doi:10.1016/j.radmeas.2007.05.023.
16. Williams, B.B.; Dong, R.; Kmiec, M.; Burke, G.; Demidenko, E.; Gladstone, D.; Nicolalde, R.J.; Sucheta, A.; Lesniewski, P.; Swartz, H.M. Development of in Vivo

Tooth EPR for Individual Radiation Dose Estimation and Screening. *Health Phys* **2010**, *98*, 327–338, doi:10.1097/HP.0b013e3181a6de5d.

17. Romanyukha, A.; Reyes, R.A.; Trompier, F.; Benevides, L.A. Fingernail Dosimetry: Current Status and Perspectives. *Health Phys* **2010**, *98*, 296–300, doi:10.1097/01.HP.0000347999.01948.74.
18. Wilcox, D.E.; He, X.; Gui, J.; Ruuge, A.E.; Li, H.; Williams, B.B.; Swartz, H.M. Dosimetry Based on EPR Spectral Analysis of Fingernail Clippings. *Health Phys* **2010**, *98*, 309–317, doi:10.1097/HP.0b013e3181b27502.
19. Guipaud, O.; Benderitter, M. Protein Biomarkers for Radiation Exposure: Towards a Proteomic Approach as a New Investigation Tool. *Ann Ist Super Sanita* **2009**, *45*, 278–286.
20. Amundson, S.A.; Fornace Jr., A.J. Gene Expression Profiles for Monitoring Radiation Exposure. *Radiat Prot Dosimetry* **2001**, *97*, 11–16.
21. Pernot, E.; Hall, J.; Baatout, S.; Benotmane, M.A.; Blanchardon, E.; Bouffler, S.; el Saghire, H.; Gomolka, M.; Guertler, A.; Harms-Ringdahl, M.; et al. Ionizing Radiation Biomarkers for Potential Use in Epidemiological Studies. *Mutat Res* **2012**, *751*, 258–286, doi:10.1016/j.mrrev.2012.05.003.
22. Perumal, V.; Gnana Sekaran, T.S.; Raavi, V.; Basheerudeen, S.A.; Kanagaraj, K.; Chowdhury, A.R.; Paul, S.F. Radiation Signature on Exposed Cells: Relevance in Dose Estimation. *World J Radiol* **2015**, *7*, 266–278, doi:10.4329/wjr.v7.i9.266.
23. Sancar, A.; Lindsey-Boltz, L.A.; Unsal-Kacmaz, K.; Linn, S. Molecular Mechanisms of Mammalian DNA Repair and the DNA Damage Checkpoints. *Annu Rev Biochem* **2004**, *73*, 39–85, doi:10.1146/annurev.biochem.73.011303.073723.
24. Sasaki, M.S. Advances in the Biophysical and Molecular Bases of Radiation Cytogenetics. *Int J Radiat Biol* **2009**, *85*, 26–47, doi:10.1080/09553000802641185.
25. Manning, G.; Rothkamm, K. Deoxyribonucleic Acid Damage-Associated Biomarkers of Ionising Radiation: Current Status and Future Relevance for Radiology and Radiotherapy. *Br J Radiol* **2013**, *86*, 20130173, doi:10.1259/bjr.20130173.
26. Durante, M.; Bedford, J.S.; Chen, D.J.; Conrad, S.; Cornforth, M.N.; Natarajan, A.T.; van Gent, D.C.; Obe, G. From DNA Damage to Chromosome Aberrations: Joining the Break. *Mutat Res* **2013**, *756*, 5–13, doi:10.1016/j.mrgentox.2013.05.014.
27. IAEA *Cytogenetic Dosimetry: Applications in Preparedness for and Response to Radiation Emergencies*; EPR Biodosimetry 2011 Vienna, I.A.E.A., Ed.; 2011;
28. Finnon, P.; Lloyd, D.C.; Edwards, A.A. Fluorescence in Situ Hybridization Detection of Chromosomal Aberrations in Human Lymphocytes: Applicability to Biological Dosimetry. *Int J Radiat Biol* **1995**, *68*, 429–435.
29. Bender, M.A.; Awa, A.A.; Brooks, A.L.; Evans, H.J.; Groer, P.G.; Littlefield, L.G.; Pereira, C.; Preston, R.J.; Wachholz, B.W. Current Status of Cytogenetic Procedures to Detect and Quantify Previous Exposures to Radiation. *Mutat Res* **1988**, *196*, 103–159.
30. Lloyd, D.C. Chromosomal Analysis to Assess Radiation Dose. *Stem Cells* **1997**, *15 Suppl 2*, 195–201, doi:10.1002/stem.5530150727.

31. Horn, S.; Barnard, S.; Rothkamm, K. Gamma-H2AX-Based Dose Estimation for Whole and Partial Body Radiation Exposure. *PLoS One* **2011**, *6*, e25113, doi:10.1371/journal.pone.0025113.
32. Cornforth, M.N. Analyzing Radiation-Induced Complex Chromosome Rearrangements by Combinatorial Painting. *Radiat Res* **2001**, *155*, 643–659.
33. Edwards, A.A.; Lindholm, C.; Darroudi, F.; Stephan, G.; Romm, H.; Barquinero, J.; Barrios, L.; Caballin, M.R.; Roy, L.; Whitehouse, C.A.; et al. Review of Translocations Detected by FISH for Retrospective Biological Dosimetry Applications. *Radiat Prot Dosimetry* **2005**, *113*, 396–402, doi:10.1093/rpd/nch452.
34. Tucker, J.D. Low-Dose Ionizing Radiation and Chromosome Translocations: A Review of the Major Considerations for Human Biological Dosimetry. *Mutat Res* **2008**, *659*, 211–220, doi:10.1016/j.mrrev.2008.04.001.
35. Furukawa, A.; Minamihisamatsu, M.; Hayata, I. Low-Cost Metaphase Finder System. *Health Phys* **2010**, *98*, 269–275, doi:10.1097/HP.0b013e3181b357c1.
36. Sigurdson, A.J.; Ha, M.; Hauptmann, M.; Bhatti, P.; Sram, R.J.; Beskid, O.; Tawn, E.J.; Whitehouse, C.A.; Lindholm, C.; Nakano, M.; et al. International Study of Factors Affecting Human Chromosome Translocations. *Mutat Res* **2008**, *652*, 112–121, doi:10.1016/j.mrgentox.2008.01.005.
37. Willems, P.; August, L.; Slabbert, J.; Romm, H.; Oestreicher, U.; Thierens, H.; Vral, A. Automated Micronucleus (MN) Scoring for Population Triage in Case of Large Scale Radiation Events. *Int J Radiat Biol* **2010**, *86*, 2–11, doi:10.3109/09553000903264481.
38. Rossnerova, A.; Spatova, M.; Schunck, C.; Sram, R.J. Automated Scoring of Lymphocyte Micronuclei by the MetaSystems Metafer Image Cytometry System and Its Application in Studies of Human Mutagen Sensitivity and Biodosimetry of Genotoxin Exposure. *Mutagenesis* **2011**, *26*, 169–175, doi:10.1093/mutage/geq057.
39. Fenech, M.; Morley, A. Solutions to the Kinetic Problem in the Micronucleus Assay. *Cytobios* **1985**, *43*, 233–246.
40. Fenech, M. Important Variables That Influence Base-Line Micronucleus Frequency in Cytokinesis-Blocked Lymphocytes-a Biomarker for DNA Damage in Human Populations. *Mutat Res* **1998**, *404*, 155–165.
41. Odagiri, Y.; Uchida, H.; Shibazaki, S. Interindividual Variation in Cytogenetic Response to X-Ray and Colchicine Measured with the Cytokinesis-Block Micronucleus Assay. *Mutat Res* **1997**, *381*, 1–13.
42. Fenech, M. Cytokinesis-Block Micronucleus Assay Evolves into a “Cytome” Assay of Chromosomal Instability, Mitotic Dysfunction and Cell Death. *Mutat Res* **2006**, *600*, 58–66, doi:10.1016/j.mrfmmm.2006.05.028.
43. Lee, T.K.; O’Brien, K.F.; Naves, J.L.; Christie, K.I.; Arastu, H.H.; Eaves, G.S.; Wiley Jr., A.L.; Karlsson, U.L.; Salehpour, M.R. Micronuclei in Lymphocytes of Prostate Cancer Patients Undergoing Radiation Therapy. *Mutat Res* **2000**, *469*, 63–70.

44. Monsieurs, M.A.; Bacher, K.; Brans, B.; Vral, A.; de Ridder, L.; Dierckx, R.A.; Thierens, H.M. Patient Dosimetry for 131I-Lipiodol Therapy. *Eur J Nucl Med Mol Imaging* **2003**, *30*, 554–561, doi:10.1007/s00259-002-1108-7.
45. El-Zein, R.; Vral, A.; Etzel, C.J. Cytokinesis-Blocked Micronucleus Assay and Cancer Risk Assessment. *Mutagenesis* **2011**, *26*, 101–106, doi:10.1093/mutage/geq071.
46. Surowy, H.; Rinckleb, A.; Luedeke, M.; Stuber, M.; Wecker, A.; Varga, D.; Maier, C.; Hoegel, J.; Vogel, W. Heritability of Baseline and Induced Micronucleus Frequencies. *Mutagenesis* **2011**, *26*, 111–117, doi:10.1093/mutage/geq059.
47. Vral, A.; Fenech, M.; Thierens, H. The Micronucleus Assay as a Biological Dosimeter of in Vivo Ionising Radiation Exposure. *Mutagenesis* **2011**, *26*, 11–17, doi:10.1093/mutage/geq078.
48. Baeyens, A.; Swanson, R.; Herd, O.; Ainsbury, E.; Mabhengu, T.; Willem, P.; Thierens, H.; Slabbert, J.P.; Vral, A. A Semi-Automated Micronucleus-Centromere Assay to Assess Low-Dose Radiation Exposure in Human Lymphocytes. *Int J Radiat Biol* **2011**, *87*, 923–931, doi:10.3109/09553002.2011.577508.
49. Wojcik, A.; Lloyd, D.; Romm, H.; Roy, L. Biological Dosimetry for Triage of Casualties in a Large-Scale Radiological Emergency:Capacity of the EU Member States. *Radiat Prot Dosimetry* **2010**, *138*, 397–401, doi:10.1093/rpd/ncp279.
50. Pantelias, G.E.; Maillie, H.D. The Use of Peripheral Blood Mononuclear Cell Prematurely Condensed Chromosomes for Biological Dosimetry. *Radiat Res* **1984**, *99*, 140–150.
51. Lindholm, C.; Stricklin, D.; Jaworska, A.; Koivistoinen, A.; Paile, W.; Arvidsson, E.; Deperas-Standylo, J.; Wojcik, A. Premature Chromosome Condensation (PCC) Assay for Dose Assessment in Mass Casualty Accidents. *Radiat Res* **2010**, *173*, 71–78, doi:10.1667/RR1843.1.
52. Garty, G.; Bigelow, A.W.; Repin, M.; Turner, H.C.; Bian, D.; Balajee, A.S.; Lyulko, O. v; Taveras, M.; Yao, Y.L.; Brenner, D.J. An Automated Imaging System for Radiation Biodosimetry. *Microsc Res Tech* **2015**, *78*, 587–598, doi:10.1002/jemt.22512.
53. Kulka, U.; Ainsbury, L.; Atkinson, M.; Barnard, S.; Smith, R.; Barquinero, J.F.; Barrios, L.; Bassinet, C.; Beinke, C.; Cucu, A.; et al. Realising the European Network of Biodosimetry: RENEB-Status Quo. *Radiat Prot Dosimetry* **2015**, *164*, 42–45, doi:10.1093/rpd/ncu266.
54. Blakely, W.F.; Carr, Z.; Chu, M.C.; Dayal-Drager, R.; Fujimoto, K.; Hopmeir, M.; Kulka, U.; Lillis-Hearne, P.; Livingston, G.K.; Lloyd, D.C.; et al. WHO 1st Consultation on the Development of a Global Biodosimetry Laboratories Network for Radiation Emergencies (BioDoseNet). *Radiat Res* **2009**, *171*, 127–139, doi:10.1667/RR1549.1.
55. Kulka, U.; Abend, M.; Ainsbury, E.; Badie, C.; Barquinero, J.F.; Barrios, L.; Beinke, C.; Bortolin, E.; Cucu, A.; de Amicis, A.; et al. RENEB - Running the European Network of Biological Dosimetry and Physical Retrospective Dosimetry. *Int J Radiat Biol* **2017**, *93*, 2–14, doi:10.1080/09553002.2016.1230239.

56. Sullivan, J.M.; Prasanna, P.G.; Grace, M.B.; Wathen, L.K.; Wallace, R.L.; Koerner, J.F.; Coleman, C.N. Assessment of Biodosimetry Methods for a Mass-Casualty Radiological Incident: Medical Response and Management Considerations. *Health Phys* **2013**, *105*, 540–554, doi:10.1097/HP.0b013e31829cf221.
57. Jaworska, A.; Ainsbury, E.A.; Fattibene, P.; Lindholm, C.; Oestreicher, U.; Rothkamm, K.; Romm, H.; Thierens, H.; Trompier, F.; Voisin, P.; et al. Operational Guidance for Radiation Emergency Response Organisations in Europe for Using Biodosimetric Tools Developed in EU MULTIBIODOSE Project. *Radiat Prot Dosimetry* **2015**, *164*, 165–169, doi:10.1093/rpd/ncu294.
58. Coleman, C.N.; Koerner, J.F. Biodosimetry: Medicine, Science, and Systems to Support the Medical Decision-Maker Following a Large Scale Nuclear or Radiation Incident. *Radiat Prot Dosimetry* **2016**, *172*, 38–46, doi:10.1093/rpd/ncw155.
59. Hall, J.; Jeggo, P.A.; West, C.; Gomolka, M.; Quintens, R.; Badie, C.; Laurent, O.; Aerts, A.; Anastasov, N.; Azimzadeh, O.; et al. Ionizing Radiation Biomarkers in Epidemiological Studies - An Update. *Mutat Res* **2017**, *771*, 59–84, doi:10.1016/j.mrrev.2017.01.001.
60. Zeegers, D.; Venkatesan, S.; Koh, S.W.; Low, G.K.; Srivastava, P.; Sundaram, N.; Sethu, S.; Banerjee, B.; Jayapal, M.; Belyakov, O.; et al. Biomarkers of Ionizing Radiation Exposure: A Multiparametric Approach. *Genome Integr* **2017**, *8*, 6, doi:10.4103/2041-9414.198911.
61. Rothkamm, K.; Beinke, C.; Romm, H.; Badie, C.; Balagurunathan, Y.; Barnard, S.; Bernard, N.; Boulay-Greene, H.; Brengues, M.; de Amicis, A.; et al. Comparison of Established and Emerging Biodosimetry Assays. *Radiat Res* **2013**, *180*, 111–119.
62. Nikitaki, Z.; Hellweg, C.E.; Georgakilas, A.G.; Ravanat, J.L. Stress-Induced DNA Damage Biomarkers: Applications and Limitations. *Front Chem* **2015**, *3*, 35, doi:10.3389/fchem.2015.00035.
63. Sproull, M.; Camphausen, K. State-of-the-Art Advances in Radiation Biodosimetry for Mass Casualty Events Involving Radiation Exposure. *Radiat Res* **2016**, *186*, 423–435, doi:10.1667/RR14452.1.
64. Nikitaki, Z.; Nikolov, V.; Mavragani, I. v; Mladenov, E.; Mangelis, A.; Laskaratou, D.A.; Fragkoulis, G.I.; Hellweg, C.E.; Martin, O.A.; Emfietzoglou, D.; et al. Measurement of Complex DNA Damage Induction and Repair in Human Cellular Systems after Exposure to Ionizing Radiations of Varying Linear Energy Transfer (LET). *Free Radic Res* **2016**, *50*, S64–S78, doi:10.1080/10715762.2016.1232484.
65. Pantelias, G.E.; Iliakis, G.E.; Sambani, C.D.; Politis, G. Biological Dosimetry of Absorbed Radiation by C-Banding of Interphase Chromosomes in Peripheral Blood Lymphocytes. *Int J Radiat Biol* **1993**, *63*, 349–354.
66. M'Kacher, R.; el Maalouf, E.; Terzoudi, G.; Ricoul, M.; Heidingsfelder, L.; Karachristou, I.; Laplagne, E.; Hempel, W.M.; Colicchio, B.; Dieterlen, A.; et al. Detection and Automated Scoring of Dicentric Chromosomes in Nonstimulated Lymphocyte Prematurely Condensed Chromosomes after Telomere and Centromere

Staining. *Int J Radiat Oncol Biol Phys* **2015**, *91*, 640–649, doi:10.1016/j.ijrobp.2014.10.048.

67. Karachristou, I.; Karakosta, M.; Pantelias, A.; Hatzi, V.I.; Karaiskos, P.; Dimitriou, P.; Pantelias, G.; Terzoudi, G.I. Triage Biodosimetry Using Centromeric/Telomeric PNA Probes and Giemsa Staining to Score Dicentrics or Excess Fragments in Non-Stimulated Lymphocyte Prematurely Condensed Chromosomes. *Mutat Res Genet Toxicol Environ Mutagen* **2015**, *793*, 107–114, doi:10.1016/j.mrgentox.2015.06.013.
68. Lamadrid Boada, A.I.; Romero Aguilera, I.; Terzoudi, G.I.; Gonzalez Mesa, J.E.; Pantelias, G.; Garcia, O. Rapid Assessment of High-Dose Radiation Exposures through Scoring of Cell-Fusion-Induced Premature Chromosome Condensation and Ring Chromosomes. *Mutat Res* **2013**, *757*, 45–51.
69. Sebastia, N.; Montoro, A.; Hervas, D.; Pantelias, G.; Hatzi, V.I.; Soriano, J.M.; Villaescusa, J.I.; Terzoudi, G.I. Curcumin and Trans-Resveratrol Exert Cell Cycle-Dependent Radioprotective or Radiosensitizing Effects as Elucidated by the PCC and G2-Assay. *Mutat Res* **2015**, *766–767*, 49–55.
70. Repin, M.; Pampou, S.; Karan, C.; Brenner, D.J.; Garty, G. RABiT-II: Implementation of a High-Throughput Micronucleus Biodosimetry Assay on Commercial Biotech Robotic Systems. *Radiat Res* **2017**, *187*, 492–498, doi:10.1667/RR011CC.1.
71. Repin, M.; Turner, H.C.; Garty, G.; Brenner, D.J. Next Generation Platforms for High-Throughput Biodosimetry. *Radiat Prot Dosimetry* **2014**, *159*, 105–110, doi:10.1093/rpd/ncu161.
72. Garty, G.; Chen, Y.; Turner, H.C.; Zhang, J.; Lyulko, O. v; Bertucci, A.; Xu, Y.; Wang, H.; Simaan, N.; Randers-Pehrson, G.; et al. The RABiT: A Rapid Automated Biodosimetry Tool for Radiological Triage. II. Technological Developments. *Int J Radiat Biol* **2011**, *87*, 776–790, doi:10.3109/09553002.2011.573612.
73. Garty, G.; Chen, Y.; Salerno, A.; Turner, H.; Zhang, J.; Lyulko, O.; Bertucci, A.; Xu, Y.; Wang, H.; Simaan, N.; et al. The RABIT: A Rapid Automated Biodosimetry Tool for Radiological Triage. *Health Phys* **2010**, *98*, 209–217, doi:10.1097/HP.0b013e3181ab3cb6.
74. Wilkins, R.C.; Rodrigues, M.A.; Beaton-Green, L.A. The Application of Imaging Flow Cytometry to High-Throughput Biodosimetry. *Genome Integr* **2017**, *8*, 7, doi:10.4103/2041-9414.198912.
75. Romero, I.; Lamadrid, A.I.; González, J.E.; Mandina, T.; García, O. Culture Time and Reagent Minimization in the Chemical PCC Assay. *Int J Radiat Biol* **2016**, *92*, doi:10.1080/09553002.2016.1206236.
76. Terzoudi, G.I.; Pantelias, G.; Darroudi, F.; Barszczewska, K.; Buraczewska, I.; Depuydt, J.; Georgieva, D.; Hadjidekova, V.; Hatzi, V.I.; Karachristou, I.; et al. Dose Assessment Intercomparisons within the RENEB Network Using G0-Lymphocyte Prematurely Condensed Chromosomes (PCC Assay). *Int J Radiat Biol* **2017**, *93*, 48–57, doi:10.1080/09553002.2016.1234725.

77. Swartz, H.M.; Williams, B.B.; Flood, A.B. Overview of the Principles and Practice of Biodosimetry. *Radiat Environ Biophys* **2014**, *53*, 221–232, doi:10.1007/s00411-014-0522-0.
78. Rea, M.E.; Gougelet, R.M.; Nicolalde, R.J.; Geiling, J.A.; Swartz, H.M. Proposed Triage Categories for Large-Scale Radiation Incidents Using High-Accuracy Biodosimetry Methods. *Health Phys* **2010**, *98*, 136–144, doi:10.1097/HP.0b013e3181b2840b.
79. Flood, A.B.; Nicolalde, R.J.; Demidenko, E.; Williams, B.B.; Shapiro, A.; Wiley Jr., A.L.; Swartz, H.M. A Framework for Comparative Evaluation of Dosimetric Methods to Triage a Large Population Following a Radiological Event. *Radiat Meas* **2011**, *46*, 916–922, doi:10.1016/j.radmeas.2011.02.019.
80. Ainsbury, E.A.; Barquinero, J.F. Biodosimetric Tools for a Fast Triage of People Accidentally Exposed to Ionizing Radiation. Statistical and Computational Aspects. *Ann Ist Super Sanita* **2009**, *45*.
81. Nugis, V.Y.; Filushkin, I. v.; Chistopolskij, A.S. Retrospective Dose Estimation Using the Dicentric Distribution in Human Peripheral Lymphocytes. In Proceedings of the Applied Radiation and Isotopes; 2000; Vol. 52.
82. Sevan'kaev, A. v.; Khvostunov, I.K.; Mikhailova, G.F.; Golub, E. v.; Potetnya, O.I.; Shepel, N.N.; Nugis, V.Y.; Nadejina, N.M. Novel Data Set for Retrospective Biodosimetry Using Both Conventional and FISH Chromosome Analysis after High Accidental Overexposure. In Proceedings of the Applied Radiation and Isotopes; 2000; Vol. 52.
83. Sevan'kaev, A. v.; Lloyd, D.C.; Edwards, A.A.; Khvostunov, I.K.; Mikhailova, G.F.; Golub, E. v.; Shepel, N.N.; Nadejina, N.M.; Galstian, I.A.; Nugis, V.Y.; et al. A Cytogenetic Follow-up of Some Highly Irradiated Victims of the Chernobyl Accident. *Radiat Prot Dosimetry* **2005**, *113*, doi:10.1093/rpd/nch435.
84. Natarajan, A.T.; Ramalho, A.T.; Vyas, R.C.; Bernini, L.F.; Tates, A.D.; Ploem, J.S.; Nascimento, A.C.; Curado, M.P. Goiania Radiation Accident: Results of Initial Dose Estimation and Follow up Studies. *Prog Clin Biol Res* **1991**, *372*, 145–153.
85. Natarajan, A.T.; Vyas, R.C.; Darroudi, F.; Vermeulen, S. Frequencies of X-Ray-Induced Chromosome Translocations in Human Peripheral Lymphocytes as Detected by in Situ Hybridization Using Chromosome-Specific DNA Libraries. *Int J Radiat Biol* **1992**, *61*, 199–203.
86. Ramalho, A.T.; Nascimento, A.C. The Fate of Chromosomal Aberrations in 137cs-Exposed Individuals in the Goiania Radiation Accident. *Health Phys* **1991**, *60*, doi:10.1097/00004032-199101000-00010.
87. Lee, J.K.; Han, E.A.; Lee, S.S.; Ha, W.H.; Barquinero, J.F.; Lee, H.R.; Cho, M.S. Cytogenetic Biodosimetry for Fukushima Travelers after the Nuclear Power Plant Accident: No Evidence of Enhanced Yield of Dicentrics. *J Radiat Res* **2012**, *53*, doi:10.1093/jrr/rrs065.

88. Suto, Y. Review of Cytogenetic Analysis of Restoration Workers for Fukushima Daiichi Nuclear Power Station Accident. *Radiat Prot Dosimetry* **2016**, *171*, doi:10.1093/rpd/ncw187.
89. Suto, Y.; Hirai, M.; Akiyama, M.; Kobashi, G.; Itokawa, M.; Akashi, M.; Sugiura, N. Biodosimetry of Restoration Workers for the Tokyo Electric Power Company (TEPCO) Fukushima Daiichi Nuclear Power Station Accident. *Health Phys* **2013**, *105*, doi:10.1097/HP.0b013e3182995e42.
90. Hill, M.A. Fishing for Radiation Quality: Chromosome Aberrations and the Role of Radiation Track Structure. *Radiat Prot Dosimetry* **2015**, *166*, doi:10.1093/rpd/ncv151.
91. de Amicis, A.; de Sanctis, S.; di Cristofaro, S.; Franchini, V.; Regalbuto, E.; Mammana, G.; Lista, F. Dose Estimation Using Dicentric Chromosome Assay and Cytokinesis Block Micronucleus Assay. *Health Phys* **2014**, *106*, doi:10.1097/hp.0000000000000097.
92. Gruel, G.; Grégoire, E.; Lecas, S.; Martin, C.; Roch-Lefevre, S.; Vaurijoux, A.; Voisin, P.; Voisin, P.; Barquinero, J.F. Biological Dosimetry by Automated Dicentric Scoring in a Simulated Emergency. *Radiat Res* **2013**, *179*, doi:10.1667/RR3196.1.
93. Rogan, P.K.; Liu, J.; Li, Y.; Wilkins, R.; Flegal, F.; Knoll, J.H.M. Accurate Cytogenetic Biodosimetry through Automated Dicentric Chromosome Curation and Metaphase Cell Selection. *F1000Res* **2017**, *6*, doi:10.12688/f1000research.12226.1.
94. Rogan, P.K.; Li, Y.; Wilkins, R.C.; Flegal, F.N.; Knoll, J.H.M. Radiation Dose Estimation by Automated Cytogenetic Biodosimetry. *Radiat Prot Dosimetry* **2016**, *172*, doi:10.1093/rpd/ncw161.
95. Romm, H.; Ainsbury, E.; Barnard, S.; Barrios, L.; Barquinero, J.F.; Beinke, C.; Deperas, M.; Gregoire, E.; Koivistoinen, A.; Lindholm, C.; et al. Automatic Scoring of Dicentric Chromosomes as a Tool in Large Scale Radiation Accidents. *Mutat Res Genet Toxicol Environ Mutagen* **2013**, *756*, doi:10.1016/j.mrgentox.2013.05.013.
96. Schunck, C.; Johannes, T.; Varga, D.; Lörch, T.; Plesch, A. New Developments in Automated Cytogenetic Imaging: Unattended Scoring of Dicentric Chromosomes, Micronuclei, Single Cell Gel Electrophoresis, and Fluorescence Signals. In Proceedings of the Cytogenetic and Genome Research; 2004; Vol. 104.
97. Shirley, B.; Li, Y.; Knoll, J.H.M.; Rogan, P.K. Expedited Radiation Biodosimetry by Automated Dicentric Chromosome Identification (ADCI) and Dose Estimation. *Journal of Visualized Experiments* **2017**, *2017*, doi:10.3791/56245.
98. Balajee, A.S.; Smith, T.; Ryan, T.; Escalona, M.; Dainiak, N. Development of a Miniaturized Version of Dicentric Chromosome Assay Tool for Radiological Triage. *Radiat Prot Dosimetry* **2018**, *182*, doi:10.1093/RPD/NCY127.
99. Martin, P.R.; Berdychevski, R.E.; Subramanian, U.; Blakely, W.F.; Prasanna, P.G.S. Sample Tracking in an Automated Cytogenetic Biodosimetry Laboratory for Radiation Mass Casualties. *Radiat Meas* **2007**, *42*, doi:10.1016/j.radmeas.2007.05.021.
100. Romm, H.; Wilkins, R.C.; Coleman, C.N.; Lillis-Hearne, P.K.; Pellmar, T.C.; Livingston, G.K.; Awa, A.A.; Jenkins, M.S.; Yoshida, M.A.; Oestreicher, U.; et al.

Biological Dosimetry by the Triage Dicentric Chromosome Assay: Potential Implications for Treatment of Acute Radiation Syndrome in Radiological Mass Casualties. *Radiat Res* **2011**, *175*, doi:10.1667/RR2321.1.

101. García, O.; di Giorgio, M.; Vallerga, M.B.; Radl, A.; Taja, M.R.; Seoane, A.; de Luca, J.; Stuck Oliveira, M.; Valdivia, P.; Lamadrid, A.I.; et al. Interlaboratory Comparison of Dicentric Chromosome Assay Using Electronically Transmitted Images. *Radiat Prot Dosimetry* **2013**, *154*, doi:10.1093/rpd/ncs139.
102. Oestreicher, U.; Samaga, D.; Ainsbury, E.; Antunes, A.C.; Baeyens, A.; Barrios, L.; Beinke, C.; Beukes, P.; Blakely, W.F.; Cucu, A.; et al. RENEB Intercomparisons Applying the Conventional Dicentric Chromosome Assay (DCA). *Int J Radiat Biol* **2017**, *93*, doi:10.1080/09553002.2016.1233370.
103. Romm, H.; Ainsbury, E.A.; Barquinero, J.F.; Barrios, L.; Beinke, C.; Cucu, A.; Domene, M.M.; Filippi, S.; Monteiro Gil, O.; Gregoire, E.; et al. Web Based Scoring Is Useful for Validation and Harmonisation of Scoring Criteria within RENEB. *Int J Radiat Biol* **2017**, *93*, doi:10.1080/09553002.2016.1206228.
104. Sugarman, S.L.; Livingston, G.K.; Stricklin, D.L.; Abbott, M.G.; Wilkins, R.C.; Romm, H.; Oestreicher, U.; Yoshida, M.A.; Miura, T.; Moquet, J.E.; et al. The Internet's Role in a Biodosimetric Response to a Radiation Mass Casualty Event. *Health Phys* **2014**, *106*, doi:10.1097/HP.0000000000000080.
105. Ainsbury, E.A.; Livingston, G.K.; Abbott, M.G.; Moquet, J.E.; Hone, P.A.; Jenkins, M.S.; Christensen, D.M.; Lloyd, D.C.; Rothkamm, K. Interlaboratory Variation in Scoring Dicentric Chromosomes in a Case of Partial-Body x-Ray Exposure: Implications for Biodosimetry Networking and Cytogenetic "Triage Mode" Scoring. *Radiat Res* **2009**, *172*, doi:10.1667/RR1934.1.
106. di Giorgio, M.; Barquinero, J.F.; Vallerga, M.B.; Radl, A.; Taja, M.R.; Seoane, A.; de Luca, J.; Oliveira, M.S.; Valdivia, P.; Lima, O.G.A.; et al. Biological Dosimetry Intercomparison Exercise: An Evaluation of Triage and Routine Mode Results by Robust Methods. *Radiat Res* **2011**, *175*, doi:10.1667/RR2425.1.
107. Romm, H.; Ainsbury, E.; Bajinskis, A.; Barnard, S.; Barquinero, J.F.; Barrios, L.; Beinke, C.; Puig-Casanovas, R.; Deperas-Kaminska, M.; Gregoire, E.; et al. Web-Based Scoring of the Dicentric Assay, a Collaborative Biodosimetric Scoring Strategy for Population Triage in Large Scale Radiation Accidents. In Proceedings of the Radiation and Environmental Biophysics; 2014; Vol. 53.
108. Pantelias, G.E.; Maillie, H.D. A Simple Method for Premature Chromosome Condensation Induction in Primary Human and Rodent Cells Using Polyethylene Glycol. *Somatic Cell Genet* **1983**, *9*, 533–547.
109. Pantelias, G.E.; Maillie, H.D. Direct Analysis of Radiation-Induced Chromosome Fragments and Rings in Unstimulated Human Peripheral Blood Lymphocytes by Means of the Premature Chromosome Condensation Technique. *Mutat Res* **1985**, *149*, 67–72.
110. Darroudi, F.; Natarajan, A.T.; Bentvelzen, P.A.; Heidt, P.J.; van Rotterdam, A.; Zoetelief, J.; Broerse, J.J. Detection of Total- and Partial-Body Irradiation in a Monkey

Model: A Comparative Study of Chromosomal Aberration, Micronucleus and Premature Chromosome Condensation Assays. *Int J Radiat Biol* **1998**, *74*, 207–215.

111. M'kacher, R.; Maalouf, E.E.L.; Ricoul, M.; Heidingsfelder, L.; Laplagne, E.; Cuceu, C.; Hempel, W.M.; Colicchio, B.; Dieterlen, A.; Sabatier, L. New Tool for Biological Dosimetry: Reevaluation and Automation of the Gold Standard Method Following Telomere and Centromere Staining. *Mutation Research - Fundamental and Molecular Mechanisms of Mutagenesis* **2014**, *770*, doi:10.1016/j.mrfmmm.2014.09.007.
112. Suto, Y.; Gotoh, T.; Noda, T.; Akiyama, M.; Owaki, M.; Darroudi, F.; Hirai, M. Assessing the Applicability of FISH-Based Prematurely Condensed Dicentric Chromosome Assay in Triage Biodosimetry. *Health Phys* **2015**, *108*, 371–376, doi:10.1097/HP.0000000000000182.
113. Livingston, G.K.; Escalona, M.; Foster, A.; Balajee, A.S. Persistent in Vivo Cytogenetic Effects of Radioiodine Therapy: A 21-Year Follow-up Study Using Multicolor FISH. *J Radiat Res* **2018**, *59*, doi:10.1093/jrr/rrx049.
114. Smith, T.; Escalona, M.; Ryan, T.; Livingston, G.K.; Sanders, J.T.; Balajee, A.S. Extension of Lymphocyte Viability for Radiation Biodosimetry: Potential Implications for Radiological/Nuclear Mass Casualty Incidents. *J Cell Biochem* **2019**, *120*, doi:10.1002/jcb.28150.
115. Okayasu, R.; Pantelias, G.E.; Iliakis, G. Increased Frequency of Formation of Interphase Ring-Chromosomes in Radiosensitive Irs-1 Cells Exposed to X-Rays. *Mutat Res* **1993**, *294*, 199–206.
116. Sipi, P.; Lindholm, C.; Salomaa, S. Kinetics of Formation of Exchanges and Rejoining of Breaks in Human G0 and G2 Lymphocytes after Low-LET Radiation. *Int J Radiat Biol* **2000**, *76*, doi:10.1080/09553000050028986.
117. Terzoudi, G.I.; Pantelias, G.E. Conversion of DNA Damage into Chromosome Damage in Response to Cell Cycle Regulation of Chromatin Condensation after Irradiation. *Mutagenesis* **1997**, *12*, 271–276.
118. Pantelias, A.; Terzoudi, G.I. Development of an Automatable Micro-PCC Biodosimetry Assay for Rapid Individualized Risk Assessment in Large-Scale Radiological Emergencies. *Mutat Res Genet Toxicol Environ Mutagen* **2018**, *836*, 65–71, doi:10.1016/j.mrgentox.2018.05.013.
119. Durante, M.; Kawata, T.; Nakano, T.; Yamada, S.; Tsujii, H. Biodosimetry of Heavy Ions by Interphase Chromosome Painting. *Advances in Space Research* **1998**, *22*, doi:10.1016/S0273-1177(99)00030-7.
120. Foster, H.A.; Estrada-Girona, G.; Themis, M.; Garimberti, E.; Hill, M.A.; Bridger, J.M.; Anderson, R.M. Relative Proximity of Chromosome Territories Influences Chromosome Exchange Partners in Radiation-Induced Chromosome Rearrangements in Primary Human Bronchial Epithelial Cells. *Mutat Res Genet Toxicol Environ Mutagen* **2013**, *756*, doi:10.1016/j.mrgentox.2013.06.003.
121. Greinert, R.; Detzler, E.; Volkmer, B.; Harder, D. Kinetics of the Formation of Chromosome Aberrations in X-Irradiated Human Lymphocytes: Analysis by

Premature Chromosome Condensation with Delayed Fusion. *Radiat Res* **1995**, *144*, 190–197.

122. Bauchinger, M.; Schmid, E.; Zitzelsberger, H.; Braselmann, H.; Nahrstedt, U. Radiation-Induced Chromosome Aberrations Analysed by Two-Colour Fluorescence in Situ Hybridization with Composite Whole Chromosome-Specific DNA Probes and a Pancentromeric DNA Probe. *Int J Radiat Biol* **1993**, *64*, doi:10.1080/09553009314551271.
123. Bauchinger, M.; Schmid, E. LET Dependence of Yield Ratios of Radiation-Induced Intra- and Interchromosomal Aberrations in Human Lymphocytes. *Int J Radiat Biol* **1998**, *74*, doi:10.1080/095530098141681.
124. Natarajan, A.T.; Balajee, A.S.; Boei, J.J.; Chatterjee, S.; Darroudi, F.; Grigorova, M.; Noditi, M.; Oh, H.J.; Slijepcevic, P.; Vermeulen, S. Recent Developments in the Assessment of Chromosomal Damage. *Int J Radiat Biol* **1994**, *66*, 615–623.
125. Natarajan, A.T.; Balajee, A.S.; Boei, J.J.; Darroudi, F.; Dominguez, I.; Hande, M.P.; Meijers, M.; Slijepcevic, P.; Vermeulen, S.; Xiao, Y. Mechanisms of Induction of Chromosomal Aberrations and Their Detection by Fluorescence in Situ Hybridization. *Mutat Res* **1996**, *372*, 247–258.
126. Holmberg, M.; Gumauskas, E. The Role of Short-Lived DNA Lesions in the Production of Chromosome-Exchange Aberrations. *Mutation Research - Fundamental and Molecular Mechanisms of Mutagenesis* **1986**, *160*, doi:10.1016/0027-5107(86)90131-4.
127. Natarajan, A.T.; van Zeeland, A.A.; Zwanenburg, T.S. Influence of Inhibitors of Poly(ADP-Ribose) Polymerase on DNA Repair, Chromosomal Alterations, and Mutations. *Princess Takamatsu Symp* **1983**, *13*, 227–242.
128. Preston, R.J. The Effect of Cytosine Arabinoside on the Frequency of X-Ray-Induced Chromosome Aberrations in Normal Human Leukocytes. *Mutation Research - Fundamental and Molecular Mechanisms of Mutagenesis* **1980**, *69*, doi:10.1016/0027-5107(80)90177-3.
129. Manti, L.; Durante, M.; Grossi, G.; Ortenzia, O.; Pugliese, M.; Scampoli, P.; Gialanella, G. Measurements of Metaphase and Interphase Chromosome Aberrations Transmitted through Early Cell Replication Rounds in Human Lymphocytes Exposed to Low-LET Protons and High-LET 12C Ions. *Mutation Research - Fundamental and Molecular Mechanisms of Mutagenesis* **2006**, *596*, doi:10.1016/j.mrfmmm.2005.12.010.
130. Mühlmann-Díaz, M.C.; Bedford, J.S. Breakage of Human Chromosomes 4, 19 and y in G0 Cells Immediately after Exposure to Γrays. *Int J Radiat Biol* **1994**, *65*, doi:10.1080/09553009414550201.
131. Johannes, C.; Chudoba, I.; Obe, G. Analysis of X-Ray-Induced Aberrations in Human Chromosome 5 Using High-Resolution Multicolour Banding FISH (MBAND). *Chromosome Research* **1999**, *7*, 625–633, doi:10.1023/A:1009284018942.
132. Boveri, T. Zur Frage Der Entstehung Maligner Tumoren. *Gustav Fisher* **1914**, 1–64.

133. Duijf, P.H.G.; Nanayakkara, D.; Nones, K.; Srihari, S.; Kalimutho, M.; Khanna, K.K. Mechanisms of Genomic Instability in Breast Cancer. *Trends Mol Med* **2019**, *25*, 595–611, doi:10.1016/j.molmed.2019.04.004.
134. Venkatesan, S.; Natarajan, A.T.; Hande, M.P. Chromosomal Instability--Mechanisms and Consequences. *Mutat Res Genet Toxicol Environ Mutagen* **2015**, *793*, 176–184, doi:10.1016/j.mrgentox.2015.08.008.
135. Natarajan, A.T. Chromosome Aberrations: Past, Present and Future. *Mutat Res* **2002**, *504*, 3–16.
136. Natarajan, A.; Simpson, D.A.; Sanders, G.M. An Unusual Complication of a Bivona Hyperflex Tracheostomy Tube. *Anaesthesia* **2005**, *60*, 208; discussion 208.
137. Natarajan, A.T.; Palitti, F. DNA Repair and Chromosomal Alterations. *Mutat Res* **2008**, *657*, 3–7, doi:10.1016/j.mrgentox.2008.08.017.
138. Palumbo, E.; Russo, A. Chromosome Imbalances in Cancer: Molecular Cytogenetics Meets Genomics. *Cytogenet Genome Res* **2016**, *150*, 176–184, doi:10.1159/000455804.
139. Campbell, P.J.; Stephens, P.J.; Pleasance, E.D.; O'Meara, S.; Li, H.; Santarius, T.; Stebbings, L.A.; Leroy, C.; Edkins, S.; Hardy, C.; et al. Identification of Somatically Acquired Rearrangements in Cancer Using Genome-Wide Massively Parallel Paired-End Sequencing. *Nat Genet* **2008**, *40*, 722–729, doi:10.1038/ng.128.
140. Stephens, P.J.; McBride, D.J.; Lin, M.L.; Varela, I.; Pleasance, E.D.; Simpson, J.T.; Stebbings, L.A.; Leroy, C.; Edkins, S.; Mudie, L.J.; et al. Complex Landscapes of Somatic Rearrangement in Human Breast Cancer Genomes. *Nature* **2009**, *462*, 1005–1010, doi:10.1038/nature08645.
141. Ratnaparkhe, M.; Wong, J.K.L.; Wei, P.-C.; Hlevnjak, M.; Kolb, T.; Simovic, M.; Haag, D.; Paul, Y.; Devens, F.; Northcott, P.; et al. Defective DNA Damage Repair Leads to Frequent Catastrophic Genomic Events in Murine and Human Tumors. *Nat Commun* **2018**, *9*, 4760, doi:10.1038/s41467-018-06925-4.
142. Hair, J.M.; Terzoudi, G.I.; Hatzi, V.I.; Lehockey, K.A.; Srivastava, D.; Wang, W.; Pantelias, G.E.; Georgakilas, A.G. BRCA1 Role in the Mitigation of Radiotoxicity and Chromosomal Instability through Repair of Clustered DNA Lesions. *Chem Biol Interact* **2010**, *188*, 350–358.
143. Stephens, P.J.; Greenman, C.D.; Fu, B.; Yang, F.; Bignell, G.R.; Mudie, L.J.; Pleasance, E.D.; Lau, K.W.; Beare, D.; Stebbings, L.A.; et al. Massive Genomic Rearrangement Acquired in a Single Catastrophic Event during Cancer Development. *Cell* **2011**, *144*, 27–40.
144. Leibowitz, M.L.; Zhang, C.-Z.; Pellman, D. Chromothripsis: A New Mechanism for Rapid Karyotype Evolution. *Annu Rev Genet* **2015**, *49*, 183–211, doi:10.1146/annurev-genet-120213-092228.
145. Korbel, J.O.; Campbell, P.J. Criteria for Inference of Chromothripsis in Cancer Genomes. *Cell* **2013**, *152*, 1226–1236, doi:10.1016/j.cell.2013.02.023.

146. Zhang, C.-Z.; Spektor, A.; Cornils, H.; Francis, J.M.; Jackson, E.K.; Liu, S.; Meyerson, M.; Pellman, D. Chromothripsis from DNA Damage in Micronuclei. *Nature* **2015**, *522*, 179–184, doi:10.1038/nature14493.
147. Marcozzi, A.; Pellestor, F.; Kloosterman, W.P. The Genomic Characteristics and Origin of Chromothripsis. *Methods in Molecular Biology* **2018**, *1769*, 3–19, doi:10.1007/978-1-4939-7780-2_1.
148. Cortés-Ciriano, I.; Lee, J.-K.; Xi, R.; Jain, D.; Jung, Y.L.; Yang, L.; Gordenin, D.; Klimczak, L.J.; Zhang, C.-Z.; Pellman, D.S.; et al. Comprehensive Analysis of Chromothripsis in 2,658 Human Cancers Using Whole-Genome Sequencing. *bioRxiv* **2018**, 333617, doi:10.1101/333617.
149. Kloosterman, W.P.; Guryev, V.; van Roosmalen, M.; Duran, K.J.; de Bruijn, E.; Bakker, S.C.M.; Letteboer, T.; van Nesselrooij, B.; Hochstenbach, R.; Poot, M.; et al. Chromothripsis as a Mechanism Driving Complex de Novo Structural Rearrangements in the Germline†. *Hum Mol Genet* **2011**, *20*, 1916–1924, doi:10.1093/hmg/ddr073.
150. Deng, L.; Wu, R.A.; Sonneville, R.; Kochenova, O. V.; Labib, K.; Pellman, D.; Walter, J.C. Mitotic CDK Promotes Replisome Disassembly, Fork Breakage, and Complex DNA Rearrangements. *Mol Cell* **2019**, *73*, 915-929.e6, doi:10.1016/j.molcel.2018.12.021.
151. Ly, P.; Brunner, S.F.; Shoshani, O.; Kim, D.H.; Lan, W.; Pyntikova, T.; Flanagan, A.M.; Behjati, S.; Page, D.C.; Campbell, P.J.; et al. Chromosome Segregation Errors Generate a Diverse Spectrum of Simple and Complex Genomic Rearrangements. *Nat Genet* **2019**, *51*, 705–715, doi:10.1038/s41588-019-0360-8.
152. Luijten, M.N.H.; Lee, J.X.T.; Crasta, K.C. Mutational Game Changer: Chromothripsis and Its Emerging Relevance to Cancer. *Mutation Research/Reviews in Mutation Research* **2018**, *777*, 29–51, doi:10.1016/j.mrrev.2018.06.004.
153. Russo, A.; Degrassi, F. Molecular Cytogenetics of the Micronucleus: Still Surprising. *Mutation Research/Genetic Toxicology and Environmental Mutagenesis* **2018**, *836*, 36–40, doi:10.1016/j.mrgentox.2018.05.011.
154. Terradas, M.; Martín, M.; Genescà, A. Impaired Nuclear Functions in Micronuclei Results in Genome Instability and Chromothripsis. *Arch Toxicol* **2016**, *90*, 2657–2667, doi:10.1007/s00204-016-1818-4.
155. Rode, A.; Maass, K.K.; Willmund, K.V.; Lichter, P.; Ernst, A. Chromothripsis in Cancer Cells: An Update. *Int J Cancer* **2016**, *138*, 2322–2333, doi:10.1002/ijc.29888.
156. Crasta, K.; Ganem, N.J.; Dagher, R.; Lantermann, A.B.; Ivanova, E. V; Pan, Y.; Nezi, L.; Protopopov, A.; Chowdhury, D.; Pellman, D. DNA Breaks and Chromosome Pulverization from Errors in Mitosis. *Nature* **2012**, *482*, 53–58.
157. Natarajan, A.; Guo, Y.; Arthanari, H.; Wagner, G.; Halperin, J.A.; Chorev, M. Synthetic Studies toward Aryl-(4-Aryl-4H-[1,2,4]Triazole-3-Yl)-Amine from 1,3-Diarylthiourea as Urea Mimetics. *J Org Chem* **2005**, *70*, 6362–6368.
158. Guo, X.; Ni, J.; Liang, Z.; Xue, J.; Fenech, M.F.; Wang, X. The Molecular Origins and Pathophysiological Consequences of Micronuclei: New Insights into an Age-Old

Problem. *Mutation Research/Reviews in Mutation Research* **2019**, *779*, 1–35, doi:10.1016/j.mrrev.2018.11.001.

159. Maciejowski, J.; Li, Y.; Bosco, N.; Campbell, P.J.; de Lange, T. Chromothripsis and Kataegis Induced by Telomere Crisis. *Cell* **2015**, *163*, 1641–1654, doi:10.1016/j.cell.2015.11.054.
160. Mardin, B.R.; Drainas, A.P.; Waszak, S.M.; Weischenfeldt, J.; Isokane, M.; Stutz, A.M.; Raeder, B.; Efthymiopoulos, T.; Buccitelli, C.; Segura-Wang, M.; et al. A Cell-Based Model System Links Chromothripsis with Hyperploidy. *Mol Syst Biol* **2015**, *11*, 828–828, doi:10.15252/msb.20156505.
161. Shim, G.; Ricoul, M.; Hempel, W.M.; Azzam, E.I.; Sabatier, L. Crosstalk between Telomere Maintenance and Radiation Effects: A Key Player in the Process of Radiation-Induced Carcinogenesis. *Mutation Research/Reviews in Mutation Research* **2014**, *760*, 1–17, doi:10.1016/j.mrrev.2014.01.001.
162. Terzoudi, G.I.; Karakosta, M.; Pantelias, A.; Hatzi, V.I.; Karachristou, I.; Pantelias, G. Stress Induced by Premature Chromatin Condensation Triggers Chromosome Shattering and Chromothripsis at DNA Sites Still Replicating in Micronuclei or Multinucleate Cells When Primary Nuclei Enter Mitosis. *Mutat Res Genet Toxicol Environ Mutagen* **2015**, *793*, 185–198, doi:10.1016/j.mrgentox.2015.07.014.
163. Ly, P.; Teitz, L.S.; Kim, D.H.; Shoshani, O.; Skaletsky, H.; Fachinetti, D.; Page, D.C.; Cleveland, D.W. Selective Y Centromere Inactivation Triggers Chromosome Shattering in Micronuclei and Repair by Non-Homologous End Joining. *Nat Cell Biol* **2017**, *19*, 68–75, doi:10.1038/ncb3450.
164. Toledo, L.; Neelsen, K.J.; Lukas, J. Replication Catastrophe: When a Checkpoint Fails Because of Exhaustion. *Mol Cell* **2017**, *66*, 735–749, doi:10.1016/j.molcel.2017.05.001.
165. Terradas, M.; Martín, M.; Tusell, L.; Genescà, A. Genetic Activities in Micronuclei: Is the DNA Entrapped in Micronuclei Lost for the Cell? *Mutation Research/Reviews in Mutation Research* **2010**, *705*, 60–67, doi:10.1016/j.mrrev.2010.03.004.
166. Martin, M.; Terradas, M.; Iliakis, G.; Tusell, L.; Genesca, A. Breaks Invisible to the DNA Damage Response Machinery Accumulate in ATM-Deficient Cells. *Genes Chromosomes Cancer* **2009**, *48*, 745–759.
167. Pantelias, G.E. Radiation-Induced Cytogenetic Damage in Relation to Changes in Interphase Chromosome Conformation. *Radiat Res* **1986**, *105*, 341–350.
168. Pantelias, G.E.; Terzoudi, G.I. Functional Cell-Cycle Chromatin Conformation Changes in the Presence of DNA Damage Result into Chromatid Breaks: A New Insight in the Formation of Radiation-Induced Chromosomal Aberrations Based on the Direct Observation of Interphase Chromatin. *Mutat Res* **2010**, *701*, 27–37.
169. Terzoudi, G.I.; Hatzi, V.I.; Donta-Bakoyianni, C.; Pantelias, G.E. Chromatin Dynamics during Cell Cycle Mediate Conversion of DNA Damage into Chromatid Breaks and Affect Formation of Chromosomal Aberrations: Biological and Clinical Significance. *Mutat Res* **2011**, *711*, 174–186.

170. Holland, A.J.; Cleveland, D.W. Chromoanagenesis and Cancer: Mechanisms and Consequences of Localized, Complex Chromosomal Rearrangements. *Nat Med* **2012**, *18*, 1630–1638.
171. Schipler, A.; Mladenova, V.; Soni, A.; Nikolov, V.; Saha, J.; Mladenov, E.; Iliakis, G. Chromosome Thripsis by DNA Double Strand Break Clusters Causes Enhanced Cell Lethality, Chromosomal Translocations and 53BP1-Recruitment. *Nucleic Acids Res* **2016**, *44*, 7673–7690, doi:10.1093/nar/gkw487.
172. Mladenov, E.; Saha, J.; Iliakis, G. Processing-Challenges Generated by Clusters of DNA Double-Strand Breaks Underpin Increased Effectiveness of High-LET Radiation and Chromothripsis. In *Advances in Experimental Medicine and Biology*; 2018; pp. 149–168.
173. Hatch, E.M.; Fischer, A.H.; Deerinck, T.J.; Hetzer, M.W. Catastrophic Nuclear Envelope Collapse in Cancer Cell Micronuclei. *Cell* **2013**, *154*, 47–60, doi:10.1016/j.cell.2013.06.007.
174. Liu, S.; Kwon, M.; Mannino, M.; Yang, N.; Renda, F.; Khodjakov, A.; Pellman, D. Nuclear Envelope Assembly Defects Link Mitotic Errors to Chromothripsis. *Nature* **2018**, *561*, 551–555, doi:10.1038/s41586-018-0534-z.
175. Terradas, M.; Martín, M.; Tusell, L.; Genescà, A. DNA Lesions Sequestered in Micronuclei Induce a Local Defective-Damage Response. *DNA Repair (Amst)* **2009**, *8*, 1225–1234, doi:10.1016/j.dnarep.2009.07.004.
176. Forment, J. V; Kaidi, A.; Jackson, S.P. Chromothripsis and Cancer: Causes and Consequences of Chromosome Shattering. *Nat Rev Cancer* **2012**, *12*, 663–670.
177. Terradas, M.; Martín, M.; Hernández, L.; Tusell, L.; Genescà, A. Nuclear Envelope Defects Impede a Proper Response to Micronuclear DNA Lesions. *Mutation Research/Fundamental and Molecular Mechanisms of Mutagenesis* **2012**, *729*, 35–40, doi:10.1016/j.mrfmmm.2011.09.003.
178. Johnson, R.T.; Rao, P.N. Mammalian Cell Fusion: Induction of Premature Chromosome Condensation in Interphase Nuclei. *Nature* **1970**, *226*, 717–722.
179. Kato, H.; Sandberg, A.A. Chromosome Pulverization in Human Cells With Micronuclei. *JNCI: Journal of the National Cancer Institute* **1968**, *40*, 165–179, doi:10.1093/jnci/40.1.165.
180. Obe, G.; Beek, B. The Human Leulocyte Test System. VII. Further Investigations Concerning Micronucleus-Derived Premature Chromosome Condensation. *Humangenetik* **1975**, *30*, 143–154.
181. Falk, M.; Falková, I.; Kopečná, O.; Bačíková, A.; Pagáčová, E.; Šimek, D.; Golan, M.; Kozubek, S.; Pekarová, M.; Follett, S.E.; et al. Chromatin Architecture Changes and DNA Replication Fork Collapse Are Critical Features in Cryopreserved Cells That Are Differentially Controlled by Cryoprotectants. *Sci Rep* **2018**, *8*, 14694, doi:10.1038/s41598-018-32939-5.
182. Williams, D.M.; Scott, C.D.; Beck, T.M. Premature Chromosome Condensation in Human Leukemia. *Blood* **1976**, *47*, 687–693.

183. Rose Li, Y.; Halliwill, K.D.; Adams, C.J.; Iyer, V.; Riva, L.; Mamunur, R.; Jen, K.-Y.; del Rosario, R.; Fredlund, E.; Hirst, G.; et al. Mutational Signatures in Tumours Induced by High and Low Energy Radiation in Trp53 Deficient Mice. *Nat Commun* **2020**, *11*, 394, doi:10.1038/s41467-019-14261-4.
184. Morishita, M.; Muramatsu, T.; Suto, Y.; Hirai, M.; Konishi, T.; Hayashi, S.; Shigemizu, D.; Tsunoda, T.; Moriyama, K.; Inazawa, J. Chromothripsis-like Chromosomal Rearrangements Induced by Ionizing Radiation Using Proton Microbeam Irradiation System. *Oncotarget* **2016**, *7*, 10182–10192, doi:10.18632/oncotarget.7186.
185. Aziz, K.; Nowsheen, S.; Pantelias, G.; Iliakis, G.; Gorgoulis, V.G.; Georgakilas, A.G. Targeting DNA Damage and Repair: Embracing the Pharmacological Era for Successful Cancer Therapy. *Pharmacol Ther* **2012**, *133*, 334–350, doi:10.1016/j.pharmthera.2011.11.010.
186. Kloosterman, W.P.; Tavakoli-Yaraki, M.; Van Roosmalen, M.J.; Van Binsbergen, E.; Renkens, I.; Duran, K.; Ballarati, L.; Vergult, S.; Giardino, D.; Hansson, K.; et al. Constitutional Chromothripsis Rearrangements Involve Clustered Double-Stranded DNA Breaks and Nonhomologous Repair Mechanisms. *Cell Rep* **2012**, *1*, 648–655, doi:10.1016/j.celrep.2012.05.009.
187. Molenaar, J.J.; Koster, J.; Zwijnenburg, D.A.; Van Sluis, P.; Valentijn, L.J.; Van Der Ploeg, I.; Hamdi, M.; Van Nes, J.; Westerman, B.A.; Van Arkel, J.; et al. Sequencing of Neuroblastoma Identifies Chromothripsis and Defects in Neuritogenesis Genes. *Nature* **2012**, *483*, 589–593, doi:10.1038/nature10910.
188. Iliakis, G.; Murmann, T.; Soni, A. Alternative End-Joining Repair Pathways Are the Ultimate Backup for Abrogated Classical Non-Homologous End-Joining and Homologous Recombination Repair: Implications for the Formation of Chromosome Translocations. *Mutat Res Genet Toxicol Environ Mutagen* **2015**, *793*, 166–175, doi:10.1016/j.mrgentox.2015.07.001.
189. Pantelias, A.; Karachristou, I.; Georgakilas, A.G.; Terzoudi, G.I. Interphase Cytogenetic Analysis of Micronucleated and Multinucleated Cells Supports the Premature Chromosome Condensation Hypothesis as the Mechanistic Origin of Chromothripsis. *Cancers (Basel)* **2019**, *11*, doi:10.3390/cancers11081123.
190. Ritter, S.; Durante, M. Heavy-Ion Induced Chromosomal Aberrations: A Review. *Mutation Research/Genetic Toxicology and Environmental Mutagenesis* **2010**, *701*, 38–46, doi:10.1016/j.mrgentox.2010.04.007.
191. Durante, M.; Cucinotta, F.A. Heavy Ion Carcinogenesis and Human Space Exploration. *Nat Rev Cancer* **2008**, *8*, 465–472, doi:10.1038/nrc2391.
192. Cremer, T.; Cremer, M.; Dietzel, S.; Müller, S.; Solovei, I.; Fakan, S. Chromosome Territories – a Functional Nuclear Landscape. *Curr Opin Cell Biol* **2006**, *18*, 307–316, doi:10.1016/j.ceb.2006.04.007.
193. McCord, R.P.; Balajee, A. 3D Genome Organization Influences the Chromosome Translocation Pattern. In *Advances in Experimental Medicine and Biology*; 2018; pp. 113–133.

194. Zheng, H.; Xie, W. The Role of 3D Genome Organization in Development and Cell Differentiation. *Nat Rev Mol Cell Biol* **2019**, *20*, 535–550, doi:10.1038/s41580-019-0132-4.
195. Shibata, A.; Jeggo, P.A. DNA Double-Strand Break Repair in a Cellular Context. *Clin Oncol* **2014**, *26*, 243–249, doi:10.1016/j.clon.2014.02.004.
196. Schipler, A.; Iliakis, G. DNA Double-Strand-Break Complexity Levels and Their Possible Contributions to the Probability for Error-Prone Processing and Repair Pathway Choice. *Nucleic Acids Res* **2013**, *41*, 7589–7605, doi:10.1093/nar/gkt556.
197. Soni, A.; Murmann-Konda, T.; Siemann-Loekes, M.; Pantelias, G.E.; Iliakis, G. Chromosome Breaks Generated by Low Doses of Ionizing Radiation in G2-Phase Are Processed Exclusively by Gene Conversion. *DNA Repair (Amst)* **2020**, *89*, 102828, doi:10.1016/j.dnarep.2020.102828.
198. Iliakis, G.; Mladenov, E.; Mladenova, V. Necessities in the Processing of DNA Double Strand Breaks and Their Effects on Genomic Instability and Cancer. *Cancers (Basel)* **2019**, *11*, 1671, doi:10.3390/cancers11111671.
199. Hada, M.; Georgakilas, A.G. Formation of Clustered DNA Damage after High-LET Irradiation: A Review. *J Radiat Res (Tokyo)* **2008**, *49*, 203–210.
200. Georgakilas, A.G.; O'Neill, P.; Stewart, R.D. Induction and Repair of Clustered DNA Lesions: What Do We Know So Far? *Radiat Res* **2013**, *180*, 100–109, doi:10.1667/RR3041.1.
201. Stewart, R.D.; Yu, V.K.; Georgakilas, A.G.; Koumenis, C.; Park, J.H.; Carlson, D.J. Effects of Radiation Quality and Oxygen on Clustered DNA Lesions and Cell Death. *Radiat Res* **2011**, *176*, 587–602, doi:10.1667/RR2663.1.
202. Mavragani, I. V.; Nikitaki, Z.; Kalospyros, S.A.; Georgakilas, A.G. Ionizing Radiation and Complex DNA Damage: From Prediction to Detection Challenges and Biological Significance. *Cancers (Basel)* **2019**, *11*, 1789, doi:10.3390/cancers11111789.
203. Tsao, D.; Kalogerinis, P.; Tabrizi, I.; Dingfelder, M.; Stewart, R.D.; Georgakilas, A.G. Induction and Processing of Oxidative Clustered DNA Lesions in 56 Fe-Ion-Irradiated Human Monocytes. *Radiat Res* **2007**, *168*, 87–97, doi:10.1667/RR0865.1.
204. Saha, J.; Wilson, P.; Thieberger, P.; Lowenstein, D.; Wang, M.; Cucinotta, F.A. Biological Characterization of Low-Energy Ions with High-Energy Deposition on Human Cells. *Radiat Res* **2014**, *182*, 282, doi:10.1667/RR13747.1.
205. Mavragani, I.; Nikitaki, Z.; Souli, M.; Aziz, A.; Nowsheen, S.; Aziz, K.; Rogakou, E.; Georgakilas, A. Complex DNA Damage: A Route to Radiation-Induced Genomic Instability and Carcinogenesis. *Cancers (Basel)* **2017**, *9*, 91, doi:10.3390/cancers9070091.
206. Nasonova, E.; Fussel, K.; Berger, S.; Gudowska-Nowak, E.; Ritter, S. Cell Cycle Arrest and Aberration Yield in Normal Human Fibroblasts. I. Effects of X-Rays and 195 MeV u(-1) C Ions. *Int J Radiat Biol* **2004**, *80*, 621–634.
207. Tenhumberg, S.; Gudowska-Nowak, E.; Nasonova, E.; Ritter, S. Cell Cycle Arrest and Aberration Yield in Normal Human Fibroblasts. II: Effects of 11 MeV u −1 C Ions

and 9.9 MeV u −1 Ni Ions. *Int J Radiat Biol* **2007**, *83*, 501–513, doi:10.1080/09553000701436802.

208. Lücke-Huhle, C.; Blakely, E.A.; Chang, P.Y.; Tobias, C.A. Drastic G2 Arrest in Mammalian Cells after Irradiation with Heavy-Ion Beams. *Radiat Res* **1979**, *79*, 97–112.
209. Ochab-Marcinek, A.; Gudowska-Nowak, E.; Nasonova, E.; Ritter, S. Modeling Radiation-Induced Cell Cycle Delays. *Radiat Environ Biophys* **2009**, *48*, 361–370, doi:10.1007/s00411-009-0239-7.
210. Hagiwara, Y.; Oike, T.; Niimi, A.; Yamauchi, M.; Sato, H.; Limsirichaikul, S.; Held, K.D.; Nakano, T.; Shibata, A. Clustered DNA Double-Strand Break Formation and the Repair Pathway Following Heavy-Ion Irradiation. *J Radiat Res* **2019**, *60*, 69–79, doi:10.1093/jrr/rry096.
211. Hagiwara, Y.; Niimi, A.; Isono, M.; Yamauchi, M.; Yasuhara, T.; Limsirichaikul, S.; Oike, T.; Sato, H.; Held, K.D.; Nakano, T.; et al. 3D-Structured Illumination Microscopy Reveals Clustered DNA Double-Strand Break Formation in Widespread ΓH2AX Foci after High LET Heavy-Ion Particle Radiation. *Oncotarget* **2017**, *8*, 109370–109381, doi:10.18632/oncotarget.22679.
212. Timm, S.; Lorat, Y.; Jakob, B.; Taucher-Scholz, G.; Rübe, C.E. Clustered DNA Damage Concentrated in Particle Trajectories Causes Persistent Large-Scale Rearrangements in Chromatin Architecture. *Radiotherapy and Oncology* **2018**, *129*, 600–610, doi:10.1016/j.radonc.2018.07.003.
213. Ryan, T.L.; Pantelias, A.G.; Terzoudi, G.I.; Pantelias, G.E.; Balajee, A.S. Use of Human Lymphocyte G0 PCCs to Detect Intra- and Inter-Chromosomal Aberrations for Early Radiation Biodosimetry and Retrospective Assessment of Radiation-Induced Effects. *PLoS One* **2019**, *14*, e0216081, doi:10.1371/journal.pone.0216081.
214. Bedford, J.S.; Goodhead, D.T. Breakage of Human Interphase Chromosomes by Alpha Particles and X-Rays. *Int J Radiat Biol* **1989**, *55*, 211–216, doi:10.1080/09553008914550261.
215. Loucas, B.D.; Geard, C.R. Initial Damage in Human Interphase Chromosomes from Alpha Particles with Linear Energy Transfers Relevant to Radon Exposure. *Radiat Res* **1994**, *139*, 9–14.
216. Goodwin, E.H.; Blakely, E.A.; Tobias, C.A. Chromosomal Damage and Repair in G1-Phase Chinese Hamster Ovary Cells Exposed to Charged-Particle Beams. *Radiat Res* **1994**, *138*, 343–351.
217. Suzuki, M.; Kase, Y.; Kanai, T.; Yatagai, F.; Watanabe, M. LET Dependence of Cell Death and Chromatin-Break Induction in Normal Human Cells Irradiated by Neon-Ion Beams. *Int J Radiat Biol* **1997**, *72*, 497–503.
218. Durante, M.; Furusawa, Y.; George, K.; Gialanella, G.; Greco, O.; Grossi, G.; Matsufuji, N.; Pugliese, M.; Yang, T.C. Rejoining and Misrejoining of Radiation-Induced Chromatin Breaks. IV. Charged Particles. *Radiat Res* **1998**, *149*, 446–454.

219. Nasonova, E.; Gudowska-Nowak, E.; Ritter, S.; Kraft, G. Analysis of Ar-Ion and X-Ray-Induced Chromatin Breakage and Repair in V79 Plateau-Phase Cells by the Premature Chromosome Condensation Technique. *Int J Radiat Biol* **2001**, *77*, 59–70.
220. Gudowska-Nowak, E.; Nasonova, E.; Ritter, S.; Scholz, M. Chromosome Fragmentation after Irradiation with C Ions. *Radiotherapy and Oncology* **2004**, *73*, S123–S126, doi:10.1016/S0167-8140(04)80032-X.
221. Tsuruoka, C.; Suzuki, M.; Hande, M.P.; Furusawa, Y.; Anzai, K.; Okayasu, R. The Difference in LET and Ion Species Dependence for Induction of Initially Measured and Non-Rejoined Chromatin Breaks in Normal Human Fibroblasts. *Radiat Res* **2008**, *170*, 163–171, doi:10.1667/rr1279.1.
222. Sekine, E.; Okada, M.; Matsufuji, N.; Yu, D.; Furusawa, Y.; Okayasu, R. High LET Heavy Ion Radiation Induces Lower Numbers of Initial Chromosome Breaks with Minimal Repair than Low LET Radiation in Normal Human Cells. *Mutat Res Genet Toxicol Environ Mutagen* **2008**, *652*, 95–101, doi:10.1016/j.mrgentox.2008.01.003.
223. Vitti, E.T.; Parsons, J.L. The Radiobiological Effects of Proton Beam Therapy: Impact on DNA Damage and Repair. *Cancers (Basel)* **2019**, *11*, 946, doi:10.3390/cancers11070946.
224. Badie, C.; Iliakis, G.; Foray, N.; Alsbeih, G.; Cedervall, B.; Chavaudra, N.; Pantelias, G.; Arlett, C.; Malaise, E.P. Induction and Rejoining of DNA Double-Strand Breaks and Interphase Chromosome Breaks after Exposure to X Rays in One Normal and Two Hypersensitive Human Fibroblast Cell Lines. *Radiat Res* **1995**, *144*, 26–35.
225. Kodym, R.; Hoerth, E. Determination of the Radiation Sensitivity of the Stromal Cells in the Murine Long-Term Bone Marrow Culture by Measuring the Induction and Rejoining of Interphase Chromosome Breaks. *Int J Radiat Oncol Biol Phys* **1993**, *25*, 829–833, doi:10.1016/0360-3016(93)90312-J.
226. Hada, M.; Wu, H.; Cucinotta, F.A. MBAND Analysis for High- and Low-LET Radiation-Induced Chromosome Aberrations: A Review. *Mutation Research/Fundamental and Molecular Mechanisms of Mutagenesis* **2011**, *711*, 187–192, doi:10.1016/j.mrfmmm.2010.12.018.
227. Chatzipapas, K.P.; Papadimitroulas, P.; Emfietzoglou, D.; Kalospyros, S.A.; Hada, M.; Georgakilas, A.G.; Kagadis, G.C. Ionizing Radiation and Complex DNA Damage: Quantifying the Radiobiological Damage Using Monte Carlo Simulations. *Cancers (Basel)* **2020**, *12*, 799, doi:10.3390/cancers12040799.
228. Cornforth, M.N. Occam's Broom and the Dirty DSB: Cytogenetic Perspectives on Cellular Response to Changes in Track Structure and Ionization Density. *Int J Radiat Biol* **2020**, 1–10, doi:10.1080/09553002.2019.1704302.
229. Jakob, B.; Dubiak-Szepietowska, M.; Janiel, E.; Schmidt, A.; Durante, M.; Taucher-Scholz, G. Differential Repair Protein Recruitment at Sites of Clustered and Isolated DNA Double-Strand Breaks Produced by High-Energy Heavy Ions. *Sci Rep* **2020**, *10*, 1443, doi:10.1038/s41598-020-58084-6.

230. Sage, E.; Shikazono, N. Radiation-Induced Clustered DNA Lesions: Repair and Mutagenesis. *Free Radic Biol Med* **2017**, *107*, 125–135, doi:10.1016/j.freeradbiomed.2016.12.008.
231. Belli, M.; Cherubini, R.; Galeazzi, G.; Mazzucato, S.; Moschini, G.; Sapora, O.; Simone, G.; Tabocchini, M.A. Proton Irradiation Facility for Radiobiological Studies at a 7 MV Van de Graaff Accelerator. *Nucl Instrum Methods Phys Res A* **1987**, *256*, 576–580, doi:10.1016/0168-9002(87)90304-4.
232. CERA; F. A Radiobiological Facility Set up at LNL XTU-Tandem Accelerator for Irradiation in Air of Cultured Mammalian Cells with Heavy Ion Beams. *INFN-LNL Annual Report* **1993**.
233. Pantelias, G.E.; Terzoudi, G.I. A Standardized G2-Assay for the Prediction of Individual Radiosensitivity. *Radiother Oncol* **2011**, *101*, 28–34.
234. Terzoudi, G.I.; Manola, K.N.; Pantelias, G.E.; Iliakis, G. Checkpoint Abrogation in G2 Compromises Repair of Chromosomal Breaks in Ataxia Telangiectasia Cells. *Cancer Res* **2005**, *65*, 11292–11296.
235. Terzoudi, G.I.; Hatzi, V.I.; Barszczewska, K.; Manola, K.N.; Stavropoulou, C.; Angelakis, P.; Pantelias, G.E. G2-Checkpoint Abrogation in Irradiated Lymphocytes: A New Cytogenetic Approach to Assess Individual Radiosensitivity and Predisposition to Cancer. *Int J Oncol* **2009**, *35*, 1223–1230.
236. Nikolakopoulou, A.; Soni, A.; Habibi, M.; Karaiskos, P.; Pantelias, G.; Terzoudi, G.I.; Iliakis, G. G2/M Checkpoint Abrogation With Selective Inhibitors Results in Increased Chromatid Breaks and Radiosensitization of 82-6 HTERT and RPE Human Cells. *Front Public Health* **2021**, *9*, doi:10.3389/fpubh.2021.675095.